EXPERIMENTAL INVESTIGATION ON TWO BODY ABRASIVE WEAR BEHAVIOUR OF HYBRID Al-Mg-Si METAL MATRIX COMPOSITES

A dissertation work submitted in the partial fulfilment of the requirement for the award of the degree of

DOCTORATE OF PHILOSOPHY

in

MECHANICAL ENGINEERING

submitted by

N.Ch. Kaushik
(Roll. No. 701238)
Mechanical Engineering Department
National Institute of Technology-Warangal

under the guidance of

Dr. R. Narasimha Rao
Associate Professor
Mechanical Engineering Department
National Institute of Technology-Warangal

DEPARTMENT OF MECHANICAL ENGINEERING
NATIONAL INSTITUTE OF TECHNOLOGY
WARANGAL -506004, TELANGANA, INDIA.
2016

EXPERIMENTAL INVESTIGATION ON TWO BODY ABRASIVE WEAR BEHAVIOUR OF HYBRID Al-Mg-Si METAL MATRIX COMPOSITES

A dissertation work submitted in the partial fulfilment of the requirement for the award of the degree of

DOCTORATE OF PHILOSOPHY

in

MECHANICAL ENGINEERING

submitted by

N.Ch. Kaushik
(Roll. No. 701238)
Mechanical Engineering Department
National Institute of Technology-Warangal

under the guidance of

Dr. R. Narasimha Rao
Associate Professor
Mechanical Engineering Department
National Institute of Technology-Warangal

DEPARTMENT OF MECHANICAL ENGINEERING
NATIONAL INSTITUTE OF TECHNOLOGY
WARANGAL -506004, TELANGANA, INDIA.
2016

DEPARTMENT OF MECHANICAL ENGINEERING
NATIONAL INSTITUTE OF TECHNOLOGY
WARANGAL-506 004, INDIA.

CERTIFICATE

This is to certify that the work presented in the thesis entitled **"EXPERIMENTAL INVESTIGATION ON TWO BODY ABRASIVE WEAR BEHAVIOUR OF HYBRID Al-Mg-Si METAL MATRIX COMPOSITES"** which is being submitted by **Mr. N.Ch. Kaushik (Roll No. 701238),** is a bonafide work submitted to National Institute of Technology, Warangal in partial fulfillment of the requirement for the award of the degree of **Doctor of Philosophy** in **Mechanical Engineering**.

To the best of our knowledge, the work incorporated in the thesis has not been submitted to any other university or institute for the award of any other degree or diploma.

Dr. R. Narasimha Rao
Thesis Supervisor
Associate Professor
Department of Mechanical Engineering
National Institute of Technology
Warangal-506 004, Telangana, India.

Prof. S. Srinivasa Rao
Chairman - DSC
Professor and Head
Department of Mechanical Engineering
National Institute of Technology
Warangal-506 004, Telangana, India.

ACKNOWLEDGEMENT

I would firstly like to express my sincere gratitude and thanks to my research supervisor Dr. R. Narasimha Rao, Associate Professor, Department of Mechanical Engineering, National Institute of Technology, Warangal for the consistent supervision of my work, guidance and encouragement throughout my research.

The guidance, review and critical suggestions of the Doctoral Scrutiny Committee (DSC) during various review meetings comprising of Prof. S. Srinivasa Rao as DSC Chairman and members Prof. K.V. Sai Srinadh, Dr. A. Kumar and Dr. N. Narasaiah are acknowledged. I also express my sincere thanks to Prof. R.V. Chalam (Former Head, Design Section), Prof. L. Krishnanand (former Chairman, DSC) and Prof. C.S.P. Rao (former Chairman, DSC) Department of Mechanical Engineering, National Institute of Technology, Warangal for their motivation.

My heartful thanks go to my parents N.Ch. Krishnama Charyulu, N.Ch. Udaya Lakshmi and my brother N.Ch. Achyut and other family members for their encouragement, support, motivation and understanding. I would like to specially thank Portia Timothy for constant help/support in hard times to keep me focused. Their role is immeasurable, without which it would have been impossible for me to complete this project work and thesis.

I would like to thank my senior research scholars Dr. Srinvasu Gangisetti and Dr. T. Karthikeya Sharma for giving their valuable inputs and suggestions whenever required. It is my duty to acknowledge and thank my co-research scholars specially Krishna Kishore Mugada, P. Vayu Nandana Kishore, Sangamesh G., B. Durga Harikiran, V. Phaneendra, G. Mahanandeswara Gowd and R. Bheekya for their cooperation given during my course.

I would like to thank M.Tech students namely Durgesh Jha, Manish Kumar, Deepak Sahu, Karthik, A. Charan Reddy, J. Ramesh, Zechariah Timothy, Prasad Mahajan and also Ch. Sri Chaitanya for their technical support during project work.

Non-teaching staff of the Mechanical Engineering Department have been instrumental in making arrangements during DSC meetings, and their help is acknowledged. Finally, I am extremely thankful to my friends and well-wishers who helped me directly and indirectly during my entire course.

-N.Ch. Kaushik

LIST OF ABBREVIATIONS AND SYMBOLS

%	:	Percentage
μ	:	Microns
μm	:	micrometres
^{o}C	:	Degrees centigrade
ρ	:	Density
Δv	:	volume loss
Δw	:	weight loss
<	:	Less than
>	:	Greater than
±	:	Plus or minus
=	:	Equals to
+	:	Plus/ added to
-	:	Minus
×	:	Multiplication/ multiplied to
/	:	Division/ divided by
^	:	Power to
*	:	Multiplied by
&	:	And
Ø	:	diameter

2D	:	two dimensional
3D	:	three dimensional
A	:	Cross sectional area of the pin in mm^2
AC	:	As cast
ASTM	:	American Society for Testing Materials
Al	:	Aluminium
$Al(OH)_3$	:	Aluminium hydroxide
Al_2O_3	:	Aluminium oxide
Al-MMC	:	Aluminium metal matrix composite
Al-SiC	:	Aluminium reinforced with silicon carbide
Al-SiC-Gr	:	Aluminium reinforced with silicon carbide and graphite

ANOVA	:	Analysis of variance
B_4C	:	Boron Carbide
C	:	Carbon
cc	:	cubic centimetre
CCD	:	central composite design
C_f	:	Carbon fiber
CO	:	Carbon monoxide
CO_2	:	Carbon dioxide
Cr	:	Chromium
Cu	:	Copper
d	:	average diagonal length left by the indenter
DOF	:	Degrees of freedom
EDM	:	Electron discharge machining
F	:	Force
f.c.c	:	face centred cubic
Fe	:	Iron
Fig.	:	Figure
g	:	Grams
gm	:	Grams
GPa	:	Giga pascal
Gr	:	Graphite
H	:	Hardness of the pin sample
H_2O	:	Water
HCl	:	Hydrochloric acid
HF	:	Hydrofluoric acid
HNO_3	:	Nitric acid
HV	:	Vickers hardness
K	:	wear coefficient of the material
kg	:	Kilograms
kgf	:	Kilogram force
L	:	applied load
Li	:	Lithium
Ltd.	:	Limited

m	:	Meters
Mg	:	Magnesium
mm	:	Millimetres
MMC	:	Metal matrix composite
Mn	:	Manganese
MPa	:	Mega pascal
N	:	Newtons
Na_3AlF_6	:	Cryolite
$NaAlO_2$	:	sodium aluminate
NaOH	:	sodium hydroxide
O	:	Oxygen
psi	:	Pounds per square inch
RPM	:	Rotations per minute
RSM	:	response surface methodology
RWR	:	Relative wear resistance
S	:	sliding distance
SS	:	Stainless steel
SEM	:	Scanning electron microscopy
Si	:	Silicon
SiC	:	Silicon carbide
SiC_p	:	Silicon carbide particulate
SiC_w	:	Silicon carbide whisker
Sn	:	Tin
T6	:	T6 heat treated
Ti	:	Titanium
TiC	:	Titanium carbide
UTS	:	Ultimate Tensile Strength
Vol.	:	Volume
Vs	:	Versus
W1	:	weight of specimen in air
W2	:	weight of specimen in water
W_d	:	wear depth of the material
w_f	:	final weight of sample (after wear test)

w_i	:	initial weight of sample (before wear test)
W_s		specific wear rate
wt.	:	Weight
W_v	:	volumetric wear rate
XRD	:	X-ray diffraction
YS	:	Yield strength
Zn	:	Zinc

LIST OF FIGURES

LIST OF TABLES

ABSTRACT

The market demands for metal matrix composites (MMCs) has been substantially increased due to strength, stiffness, and wear properties etc. improvement over unreinforced matrix material. In automotive applications, the metal matrices generally used were observed to be aluminium, titanium, magnesium and their alloys. Aluminium and its alloys are observed to be vital in the aerospace industry and important in automotive, transportation and structural applications. However, to enhance the mechanical, tribological properties etc., of the aluminium matrix material, reinforcements either hard or soft type was added to cope up with stringent material requirements in different applications. The aluminium metal matrix composites (Al-MMCs) have been introduced in various engine components like piston, cylinder liners, push rods, connecting rods, brake rotors etc., by world reputed automobile companies. However, the tribological performance aspects of these developed Al-MMC parts still a major concern to have an effective combustion process, as it ultimately can affect the overall efficiency of the engine.

Since a few decades, the wear of Al-MMCs was extensively studied and particularly much attention has also been given on abrasive wear of fibre, whisker, and particle reinforced Al-MMCs. The effect of test parameters, characteristics of counter surface, the volume fraction, size and type of reinforcement on the wear process was studied extensively. It was proven that based on the test conditions adopted; these factors contribute either positively or negatively on the wear performance. The particle reinforced Al-MMCs were observed to be better due to the contribution of particle in an isotropic manner in wear process. The recent investigations reveal that the wear properties of Al-MMCs containing more than one reinforcement (i.e. hybrid composites) were observed to be beneficial compared to single particle reinforced ones.

The present study investigates on the two body abrasive wear behaviour Al-6082 alloy, Al 6082-10% SiC (Al-SiC) composites and Al 6082-5%SiC-5%Gr (Al-SiC-Gr) hybrid composites. The composites were prepared by stir casting process, a liquid metallurgy route. The wear experiments of these materials were conducted on pin-on-disc equipment at an applied load of 5-15N, sliding distance of 50-75m and grit size of 100-200μm. The wear response in terms of volumetric wear rate, relative wear resistance, wear coefficients and wear depth influenced by these parameters was analysed and compared with each other in as cast condition. Similarly this was done in T6 condition also. The wear

behaviour of developed hybrid composites was analysed and compared through developed power law and quadratic/polynomial equations. Later the worn surfaces of wear tested pin samples, emery papers and wear debris were captured by using field emission scanning electron microscope (SEM). The surface roughness of the materials was evaluated under non-contact optical profilometer. Finally, the ANOVA and regression modeling of the matrix alloy and its composite materials was done for understanding the nature and level of the contribution of each parameter in abrasive wear.

The wear rate increased with increase in the applied load, grit size and sliding distance in both as cast and T6 heat treated conditions seperately. But the wear rate of the materials reduced from as cast to T6 heat treated conditions. This could be due to matrix strengthening by precipitates formed. The hybrid composites yielded better wear resistance compared to unreinforced alloy and single SiC reinforced composites. At maximum conditions of applied load, grit size and sliding distance, the wear improvement of 16.4% and 27% for Al-SiC-Gr composite with respect to matrix alloy was observed in cast and T6 heat treated condition respectively. But at lower grit size, 19.6% and 26.9% wear improvement was observed by keeping others parametres as constant. The wear resistance plots indicate that it decreases with increase in applied pressure in both as cast and T6 conditions. In case of lower grit size and applied pressures, the improvement in wear resistance was 1.63 m/mm^3 (matrix alloy) to 3.29 m/mm^3 (Al-SiC-Gr). However, the marginal improvement of wear resistance was observed i.e. 0.67 m/mm^3 (matrix alloy) to 1.05 m/mm^3 (Al-SiC-Gr) at higher grit size and applied pressures. Relative wear resistance plots indicate that hybrid composites yielded better wear resistance properties compared to SiC reinforced composites.

The wear behaviour in the form of power law equation, $y = kx^n$ and quadratic equation, $y = ax^2+bx+c$ were presented. In this context, the x is applied load variable and y are wear rate variable; n is the power law exponent, k is a constant; and a, b & c are coefficients of equation. It was observed from the power law equations that, the change in abrasive wear mechanism was observed at 125µm grit size when traversed from alloy to hybrid composite as indicated in exponent terms in the power law equation. From the developed quadratic equations it was noted that ‘a’ coefficients were found to be near to zero irrespective of sign in both the conditions; ‘c’ term was decreasing in as cast condition and increasing in T6 condition when traversed from matrix alloy to composites; and no particular trend noticed in ‘b’ terms.

The effect on two body abrasive wear coefficients was noticed to be decreased and increased with increase in applied load and grit size respectively. At lower applied load, higher grit size and sliding distance, when compared matrix alloy to hybrid composite, the wear coefficient decreases from $0.771x10^{-3}$ to $0.547x10^{-3}$ in cast condition; $0.73x10^{-3}$ to $0.642X10^{-3}$ in T6 condition. But at higher load and higher grit size, the wear coefficient marginally decreased from $0.48x10^{-3}$ to 0.46×10^{-3} in cast condition; 0.497×10^{-3} to $0.42x10^{-3}$ in T6 condition. As sliding distance increased, the wear coefficients slightly increased for all the materials but when traversed from matrix alloy to hybrid composite, the wear coefficient decreases marginally.

Wear depth of materials increased with increase in applied load, grit size and sliding distance but it decreased from matrix alloy to hybrid composite. This trend was observed in both as cast and T6 condition. At lower applied load, higher grit size and sliding distance, when compared matrix alloy to hybrid composite, the percentage reduction in wear depth was 38.1 in cast condition; 25.1 in T6 condition. But at higher applied load, higher grit size and sliding distance, the percentage reduction in wear depth was around 16.4 in cast condition and 27 in T6 condition.

The worn surfaces of tested pin samples and emery papers was characterized and analysed though SEM to understand the wear mechanism involved. From the worn surfaces of alloy pin samples, the damaged portions on the surface, depth of grooves and roughness over the surface was found to be higher. But, the depth of grooves formed during wear process was observed to be narrow and shallower for hybrid composite pins compared to alloy pins. The worn surface images of emery papers contained the particle pick up, blunting of the abrasive grit particle, fracture of the abrasive grit particle and debris over the emery paper.

The ANOVA and regression equations were developed according to array generated in central composite design approach in response surface methodology. ANOVA results show that all individual factors are significant along with few interaction and square term effects. The order of contribution observed was applied load, abrasive grit size and sliding distance for all the materials. The adequacy of regression equations was done and it was observed to be below 10%.

TABLE OF CONTENTS

CHAPTER-1

INTRODUCTION

1.1 Introduction to Aluminium

1.1.1 Fundamental aspects of Aluminium

Aluminium is an element from the boron group represented with symbol Al has an atomic number of 13 and atomic weight of 27. This element is abundantly available in the Earth's crust and present around 8% of the crust mass after silicon and oxygen. It is silvery white in colour, relatively soft in nature, nonmagnetic type, ductile and malleable metal with face centred cubic (f.c.c) structure. It is having a density of ~2.7 g/cc and melting point of ~660◦C. It is noteworthy for its low density (i.e. one-third of the steel density) and corrosion resistance ability through the oxide layer passivation phenomenon. The yield strength of pure aluminium is in the range of 7–11 MPa, where as its alloys are observed to be in 200 - 600 MPa range. It has good electrical and thermal conductivity properties next to copper and can also act as superconductor. It is present in the form of bauxite ore and extraction of the pure aluminium is done in two stage process i.e. Bayer process and Hall-Heroult process. The Bayer process for refining the bauxite ore to get aluminium oxide, and the Hall-Heroult process for smelting the aluminium oxide to bring out pure aluminium (Totten *et al*., 2003).

The Bayer process was invented in the year 1888 AD by Russian chemist Carl Josef Bayer. In his process, the aluminium hydroxide compound is precipitated from the alkaline solution to have crystalline form for easy filtration/washing. In this process, the bauxite ore is heated in a pressure vessel along with a sodium hydroxide (NaOH) solution at a temperature of 150-200°C. The aluminium present in the bauxite ore gets dissolved as sodium aluminate ($NaAlO_2$) at these temperatures. The formed alkaline solution is cooled and treated with carbon dioxide bubbling, through which solution of supersaturated high-purity precipitates of aluminium hydroxide ($Al(OH)_3$) is formed. The $Al(OH)_3$ produced is converted into aluminium oxide (Al_2O_3) by heating in rotary kilns to a temperature greater than 1000 °C. The Hall–Héroult process was invented by the American chemist Charles Martin Hall and by the Frenchman Paul Héroult. In this

process alumina, Al_2O_3, is dissolved in molten synthetic cryolite (Na_3AlF_6) to lower its melting point for easier electrolysis (Totten *et al*., 2003).

1.1.2 Classification of Aluminium alloys

The alloying elements such as copper, manganese, silicon, magnesium, zinc etc. are added to pure aluminium to attain better properties such as mechanical strength, thermal conductivity, electrical conductivity etc. based on the application requirements (Totten *et al*., 2003). Table 1.1 shows the alloying elements and corresponding aluminium alloy nomenclature and designation.

Table 1.1: The alloying elements and corresponding aluminium alloy nomenclature and designation.

Sl. No	Principal alloying element	Nomenclature	Designation
1.	Unalloyed / pure aluminium	Al	1xxx
2.	Copper	Al-Cu	2xxx
3.	Manganese	Al-Mn	3xxx
4.	Silicon	Al-Si	4xxx
5.	Magnesium	Al-Mg	5xxx
6.	Magnesium and Silicon	Al-Mg-Si	6xxx
7.	Zinc and limited proportion of copper, magnesium, chromium and zirconium elements	Al-Zn	7xxx
8.	Tin and some Lithium compositions	Al-Sn & Al-Li	8xxx

1.1.3 Applications of Aluminium and its alloys

The applications of aluminium and its alloys with different weight percent combinations of alloying elements are observed in wide variety of applications. It was observed to be vital in the aerospace industry and important in automotive, transportation, energy, aerospace, defence and structural applications (Totten *et al*., 2003). Some of them have been reported as follows:

- Transportation applications such as bicycles, automobiles, trucks, railway cars, marine vessels, aircraft, spacecraft, etc. in the form of castings, sheets and tubes.
- Construction purposes such as doors, windows, roofing, etc.
- Electrical transmission lines for power distribution, used in high brightness LED lighting as substrate material of laminates.
- Thermite, solid rocket fuels and pyrotechnics.

- Beverage and food containers, packaging applications such as foil and beverage cans etc.
- A wide range of household items including cooking utensils
- The components in electronic appliances especially heat sinks for transistors, CPUs and other.
- Painting purposes and Light reflective surfaces.

1.2 Aluminium Metal Matrix Composites (Al-MMCs)

The demand in market for metal matrix composites (MMCs) has been substantially increased due to improvement in strength, stiffness, wear properties etc. over unreinforced matrix material. The metal matrices generally used were magnesium, titanium, aluminium and their alloys. The reinforcements which are generally used were broadly classified into carbides, oxides, nitrides and borides. Based on the application, a wide range of MMCs were developed for various components required in automotive, aerospace, naval, structural, sports etc. fields. In automotive application, the aluminium alloy reinforced with the hard particulate or fibre or whisker type reinforcement phases such as SiC, Al_2O_3, TiC, B_4C etc are generally being used. The aluminium as a matrix material with different reinforcements are termed as aluminium metal matrix composites (Al-MMCs). The characteristics such as low density and high specific mechanical properties of Al-MMCs, make these materials as alternatives for the lightweight parts of vehicles manufacturing. It was known that, these Al-MMCs are promising materials in manufacturing the lightweight automobile and other commercial parts. In many cases, the castings of Al-MMC are found to be economically feasible compared to ferrous castings. The production, advantages and applications of Al-MMCs was discussed briefly in below sections (Lloyd *et al.*, 1994, Clyne *et al*., 2000, Totten *et al*., 2003).

1.2.1 Manufacturing methods of Al-MMCs

The manufacturing or processing of Al-MMCs at an industrial scale can be categorized into primary processing and secondary processing. The primary processing of Al-MMCs is preparation of the composites and can be sub-classified into three main groups as mentioned below.

(1) Solid State Processing*:* In this type of processing, the following techniques come under this category

- ***Powder Metallurgical Processing:*** This process involved the initial blending of powdered metal and reinforcements, followed by consolidation i.e. compaction, degassing and pressing or extrusion. Figure 1.1 depicts the schematic process involved in powder metallurgical processing of Al-MMCs. It indicates the initial processing of powder, hot pressing and extrusion processing for MMCs fabrication reinforced with particulate or short fiber (Chawla *et al.*, 2006).

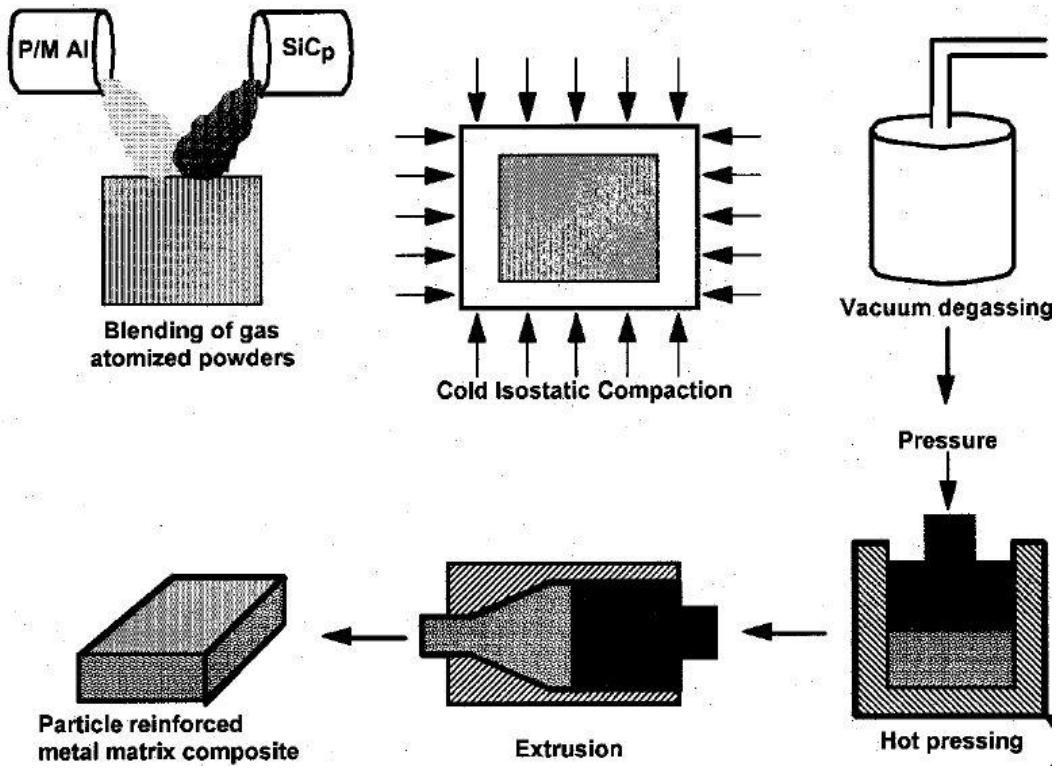

Figure 1.1: Processing of powder, hot pressing and extrusion processing for MMCs fabrication reinforced with particulate or short fiber (Chawla *et al.*, 2006).

- ***Diffusion Bonding:*** The metal layers are inserted with reinforcements like long fibers etc, and matrix formation through pressing action. Fig. 1.2 shows the schematic sketch of diffusion bonding of foil-fiber-foil. Fig. 1.2(a) depicts the applying of metal foil and cutting to required shape, Fig. 1.2 (b) indicates the desired plies lay-up, Fig. 1.2 (c) shows the vacuum encapsulation and heating to fabrication temperature, Fig. 1.2 (d) depicts the pressure application and hold for consolidation cycle, and Fig. 1.2 (e) indicates the cooling, removal and finished clean part (Chawla *et al.*, 2006).

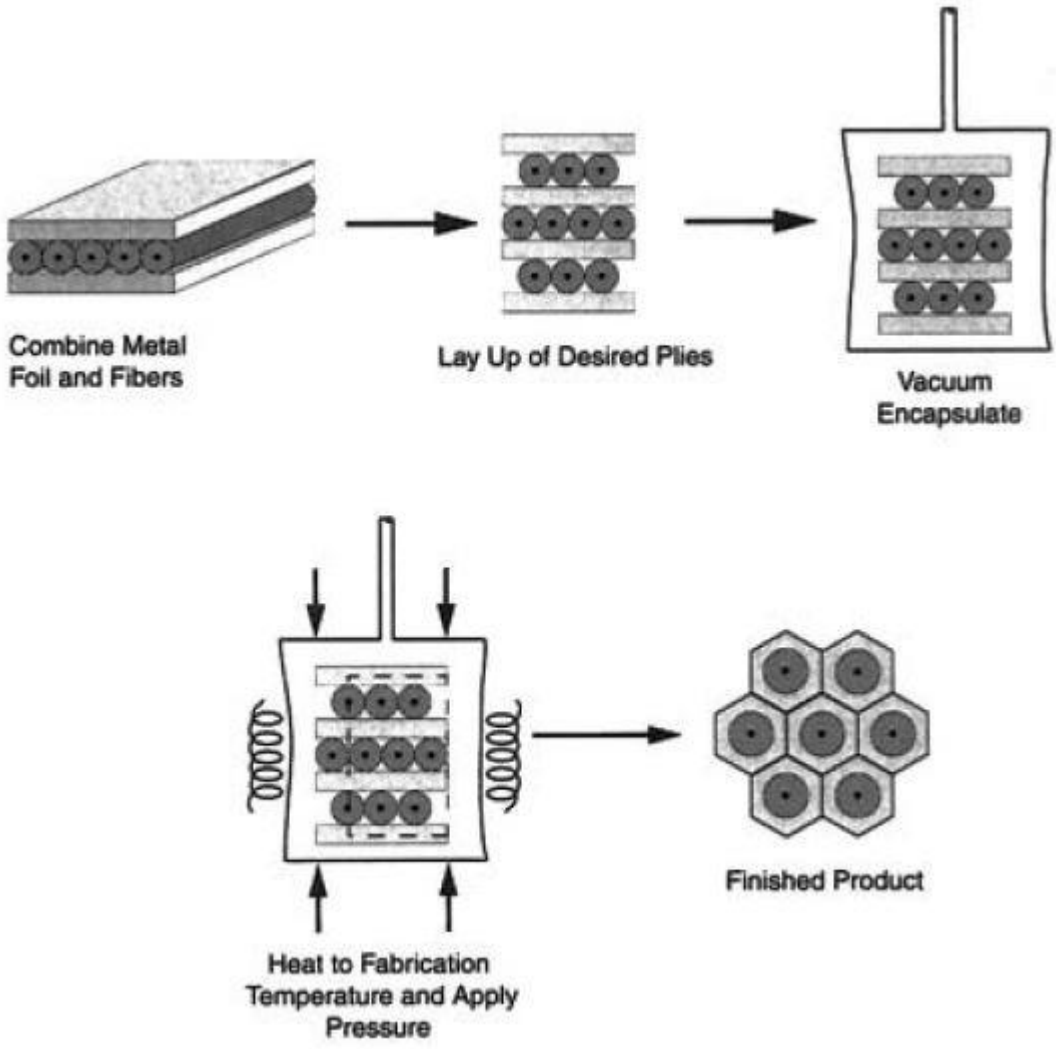

Figure 1.2: A schematic sketch of diffusion bonding of foil-fiber-foil: (a) apply metal foil and cut to shape, (b) desired plies lay-up, (c) vacuum encapsulation and heating to fabrication temperature, (d) pressure application and hold for consolidation cycle, and clean part (Chawla *et al.*, 2006).

- ***Vapor Deposition:*** The vaporized thick metal cloud coats the reinforcement especially fiber as it passes through.

(2) Liquid state processing: In the liquid state type of processing, the reinforcements are added to the metal matrix which is in molten state or semi-solid state. This route is one of the basic foundry technologies, which can be easily suited for the fabrication of Al-MMCs having reinforcements in discontinuous manner. This involves the inclusion of hard or soft reinforcement into a liquid state aluminium alloy (i.e. mixing the molten metal prior to casting) or the preform infiltration (e.g. pressure of vacuum infiltration, squeeze casting). These routes are found to be pleasing because they are cheap, simple and can be used for

the production of 3D compounds of complex nature. It is also capable to produce parts with local reinforcements. The main disadvantages of the liquid state routes are observed to be the improper wetting by liquid aluminium with the reinforcements (ceramics mainly); the development of defects during casting (i.e. shrinkage, entrapment of gases and blow holes) of the final product during solidification process; the insufficient bonding between the matrix and reinforcement and/or the reinforcement degradation due to excessive reaction. A typical reinforcement amount was found to be lower than 25 vol. %. The most commonly used liquid state techniques were briefly discussed below.

- ***Stir casting or Compo-casting****:* It is the vortex melt mixing or stirring process of molten alloy and reinforcement. It is an easy route for production of particle reinforced aluminium composites. The stirring action can be done by means of electromagnetic methods, mechanical or by gas injection. After vortex mixing, the slurry is poured into die and let to solidify. Fig. 1.3 shows the schematic sketch of the stirring action of composite slurry melt with ceramic particles. The problems associated with this technique are mainly the clustering or agglomeration of the particulates, the reinforcement expulsion by the liquid matrix. It can be noted that the particle distribution affects the desired properties (Chawla *et al.*, 2006).

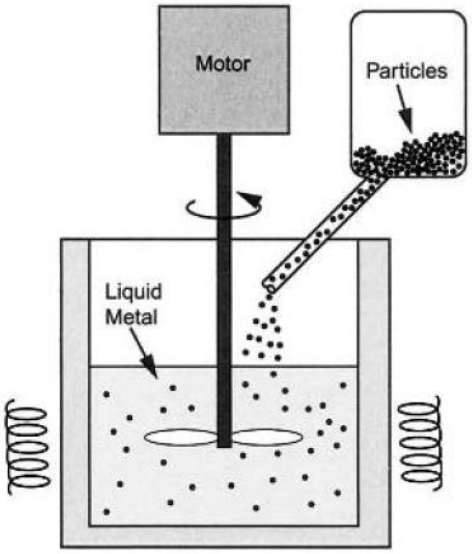

Figure 1.3: A schematic sketch of the stirring action of composite slurry melt with ceramic particles (Chawla *et al.*, 2006).

It was reported that these problems can be overcome by using several methods such as:

- the addition of the particles into the vortex, generated by an impeller,

- the surface treatment of reinforcement particulates
- the matrix alloying,
- preheating the reinforcement particles before introducing,
- the use of electromagnetic or ultrasonic vibrations,
- the addition of particulates and metal matrix powder as briquettes or pellets.

- ***Infiltration*:** In this technique, preform infiltration due to a pressure difference between the evacuated preform and the liquid melt is done. Al-MMCs having from 10 to 70% volume fraction of reinforcement can be produced using different infiltration techniques. The intensity of porosity and variations in the volume fractions of the reinforcement locally are often observed in the Al-MMCs components processed through infiltration technique (Chawla *et al.*, 2006).

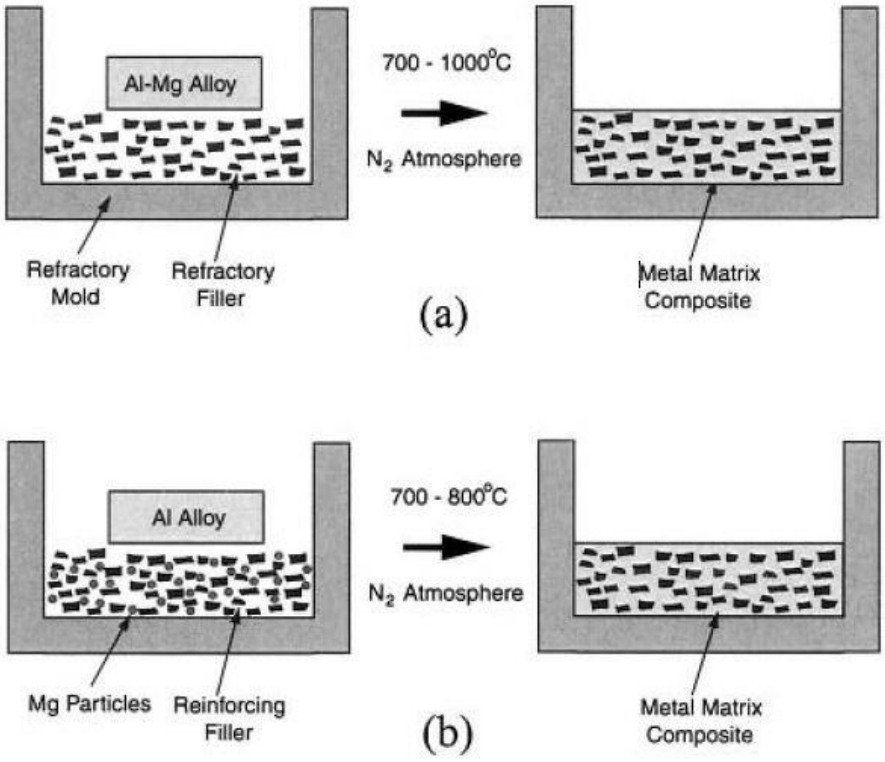

Figure 1.4: A schematic sketch of the pressureless infiltration technique of MMCs: (a) infiltration of alloy matrix with particulate preform and (b) infiltration of pure matrix with alloy and ceramic particulate preform (Chawla *et al.*, 2006).

- A pressureless metal infiltration process, called as Primex process, allows an alloy to infiltrate a reinforcement preform without pressure or vacuum exertion. The reinforcement level can be controlled by the noting the initial density of the preform being infiltrated. As long as interconnected porosity and appropriate infiltration conditions exist, the liquid aluminum will spontaneously infiltrate the

preform (Chawla *et al.*, 2006). Fig. 1.4 shows the schematic sketch of the pressureless infiltration technique of MMCs. Fig. 1.4 (a) shows the infiltration of alloy matrix with particulate preform and Fig. 1.4 (b) shows the infiltration of pure matrix with alloy and ceramic particulate preform.

- In pressure infiltration/ squeeze casting process, fibre preform with molten metal or an evacuated ones of particulate is subjected to applied pressure of 150–1500 psi range isostatic manner with inert gas. It is similar to that of squeeze infiltration process where mechanical pressure is applied whereas in this technique, an inert gas is used to promote consolidation. Fig. 1.5 shows the schematic sketch of pressure infiltration / squeeze casting process (Chawla *et al.*, 2006).

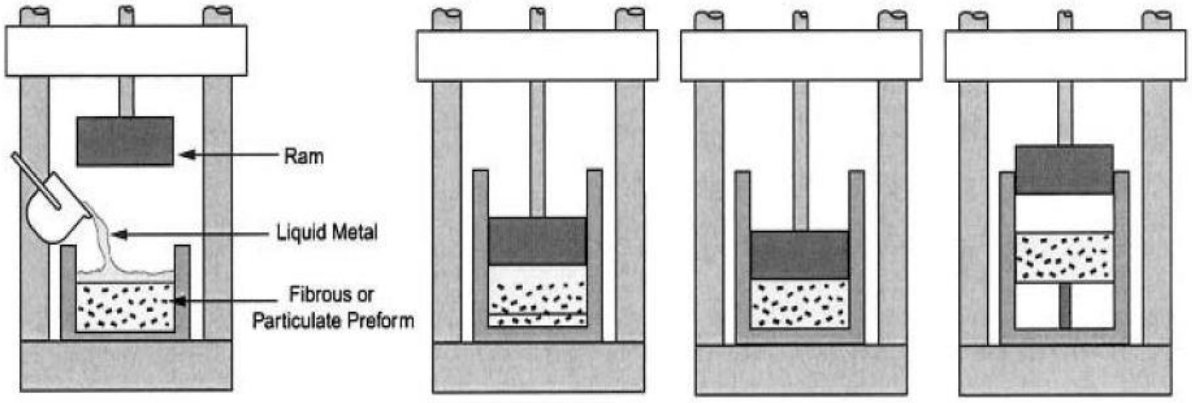

Figure 1.5: A schematic sketch of pressure infiltration / squeeze casting process (Chawla *et al.*, 2006).

- ***Spray Deposition****:* This technique was commercially developed by Osprey Ltd., a method where atomized molten metal stream with cold gas jets is used to build up a bulk material. It has been used to produce the particulate MMC by ceramic powder injection in the form of spray. The stages involved in this technique are (a) melting and dispensing (b) gas atomization (c) deposition and (d) manipulation of collector. This process has been extensively explored for the manufacturing of Al-MMCs by injecting ceramic whisker/particle/short fiber into the spray. The process parameters which are observed to be critical are the velocity, size distribution and initial temperature of the metal droplets; the feed rate, temperature, and velocity of the reinforcement; and also the substrate temperature. Al-MMCs produced in this method often have an inhomogeneous distribution of ceramic particles. The porosity is typically around 5–10% in sprayed state. Fig. 1.6 shows the schematic sketch of spray co-deposition

process of SiC reinforcement particles and a1uminium liquid droplets, to form composite particles. Al-MMCs processed by this technique is relatively lesser cost and with usually the cost is in between the stir cast and powder metallurgy processed components (Chawla *et al.*, 2006).

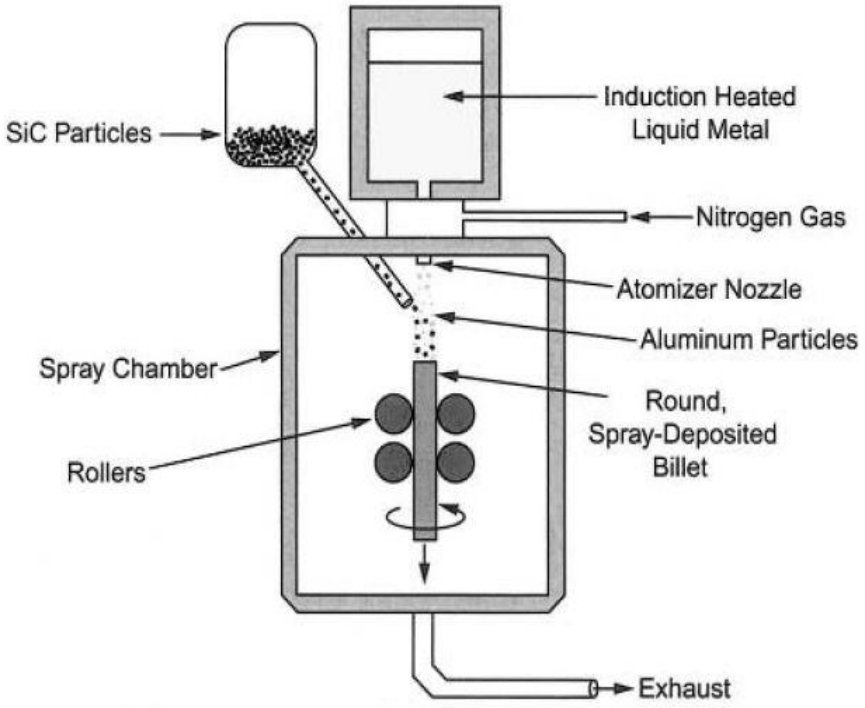

Figure 1.6: A schematic sketch of spray co-deposition process of SiC reinforcement particles and a1uminium liquid droplets, to form composite particles (Chawla *et al.*, 2006).

- ***Reactive/ In-situ type****:* The production of Al-MMCs, the reinforcements is formed through the chemical reaction within the metal matrix in a single step. The reactions may be occurred due to interactions of liquid-solid, liquid-liquid, liquid-gas and mixed salt. The advantages are
  - the interfaces between the matrix and the reinforcement are very clean,
  - better wetting and bonding between them (no oxidation, no gas adsorption and no other interface reactions which are detrimental).
  - safety hazards and costs are reduced.
  - the elimination of handling of the fine particulate reinforcement phases.

  A major disadvantage of in-situ processing technique is found to be in the thermodynamic restrictions on the nature of the reinforcement phase, its composition, and the kinetic restrictions on the size, shape and reinforcement volume fraction that can be attained through chemical reactions under the particular test conditions set.

(3) Two-phase Processing: It involves the mixing of ceramic and matrix in a region of the phase diagram where the matrix contains both solid and liquid phases. The phase methods also include spray deposition, compo casting/ rheocasting and variable code portion of multi-phase materials. In *compocasting or rheocasting* technique, inclusion of particulates or short fibers is done into partially solid aluminium slurry through vigorous agitation. The discontinuous ceramic phase is entrapped mechanically between the pro-eutectic phase present in the slurry state alloy, which is held in between its solidus and liquidus temperatures. This semi solid process allows fabrication of near net shape components, as the resistance to deformation is considerably improved due to the semi-fused state of the composite slurry.

Table 1.2: A comparison on different techniques used for Al-MMCs (Surappa *et al.,* 1997).

Processing Method	**Size and shape range**	**Yield of metal**	**Vol. % range**	**Reinforcement damage**	**Cost**
Liquid metallurgy (stir casting)	shapes of wide range, larger size, < 500 kg	Very high	< 0.3	No	Least
Squeeze casting	Limited by pre-form shape, < 2 cm height	Low	< 0.45	Severe	Moderate
Powder metallurgy	Wide range, restricted size	High	-	Fracture of reinforcement	Expensive
Spray casting	large size but limited shape	Medium	0.3 - 0.7	-	Expensive
Lanxide technique	restricted by preform shapes, size	-	-	-	Expensive

The secondary processing of Al-MMCs includes post mechanical processing such as forging, rolling, extrusion etc to achieve near net shape component. These additional deformation processing techniques are essential to enhance the mechanical properties and part shapes production. Further, it helps in breaking up the agglomerates of reinforcements,

porosity reduction or elimination, and enhances the bond between matrix and reinforcement (Chawla *et al.*, 2006).

Among these above mentioned processing techniques, it was noticed that each technique had its own advantages and disadvantages. It was found to be essential that a comparison is required for processing of Al-MMCs based on quality and quantity off requirement. Table 1.2 gives the comparison on different techniques used for Al-MMCs and it was noticed that the stir casting technique was found to advantageous in terms of yield of metal, no reinforcement damage and less expensive when compared to other manufacturing process (Surappa *et al.*, 1997). Hence the stir casting technique was chosen for the present research work for processing of Al-MMCs.

1.2.2 Advantages of Al-MMCs

It was noticed that Al-MMCs offered superior properties compared to monolithic materials such as ferrous, aluminium and titanium alloys. The following advantages of Al-MMCs were observed when compared to unreinforced matrix material:

1. Enhancement of strength
2. Stiffness and damping capability improvement
3. Density or weight reduction
4. Mass control (in reciprocatory motion applications)
5. Improvement of wear and abrasion resistance properties
6. Controlled thermal expansion coefficient
7. Better heat or thermal management properties
8. Enhancement of performance electrical applications

It can be noted that the above mentioned properties and their improvement depend on the reinforcing constituents' nature and interaction with the matrix material, volume or weight fraction of the reinforcement, composite preparation methodology adopted and heat or surface treatments if any. The property of a component can be tailored based the nature of working condition and its application (Surappa *et al.*, 2003).

1.2.3 Applications of Al-MMCs

Since decades, Al-MMCs have been utilized for high-tech structural and functional applications in aerospace, automotive, defence and also in sports and recreation. The reputed automotive companies like Chrysler, General motors, Honda, Nissan, and Toyota etc used Al-MMC components reinforced with SiC_p, SiC_w, Al_2O_3, saffil etc. Its automotive

applications, the aluminium metal matrix composites (Al-MMCs) have been used in brake motors, engine blocks, cylinder liners connecting rods, pistons, gears, valves, pulleys, suspension components etc. Table 1.3 shows the cast Al metal matrix composite components with proven automotive applications. The aerospace structural components including vertical tails, bulkheads, wing slat tracks, speed brakes, wheels, parts of landing gear, doors. For the present generation of jet engines, Al-MMCs were tested for high and low pressure compressor casings, stator rotor discs, vanes (Prasad *et al*., 2004, Miracle *et al*., 2005).

In electronics and communication applications, to give protection to the electronic circuits from moisture and other environmental risks, materials for hermetic package are developed. Therefore, materials with an adoptable thermal expansion coefficient are required. Al-based MMCs was found suitable, as it depends on the volume fraction of the particles or fibers (Rawal *et al*., 2001).

Table 1.3: The cast Al metal matrix composite components with proven automotive applications (Prasad *et al*., 2004).

Component	**Manufacturer**	**Composite type used**
Pistons	Duralcan, Lanxide	SiC_p /Al
	Martin Marietta	SiC_p / Al & TiC_p /Al
	Associated Engineering, Inc	Graphite/ Al
	Zollner	Fiberfrax/Al
Piston rings	Toyota	Al_2O_3/Al & $Boria_w$ /Al
Brake rotors	Duralcan, Lanxide, Lotus Elise, Volkswagen, Chrysler	SiCp /Al
Brake discs on ICE bogies	Knorr-Bremse, Kobenhavn	SiC/Al
Connecting rods	DuPont, Chrysler	Al_2O_3/Al
	Nissan	SiC_w / Al
Engine blocks	Honda	Al_2O_3–C_f /Al
Propeller shaft	GKN, Duralcan	SiC_p /Al
calipers, liners	Duralcan, Lanxide	SiC_p /Al
Driveshaft, Rear brake drum for EV-1, engine cradle	General Motors	SiC_p /Al
PCB heat sinks	Textron	B/Al
	Lanxide	SiC_p /Al
Multichip electronic module	Alcoa Innometalx	SiC_p /Al
Electronic packages	Cercast	graphite foam/ Al

The other typical applications of Al-based composites in sports and recreation are tennis and squash rackets, golf club heads, bicycle frames and fishing rods (Prasad *et al*., 2004, Miracle *et al*., 2005).

Fig. 1.7, Fig 1.8 and Fig. 1.9 show the images of different applications of Al-MMCs. Fig. 1.7 (a) indicate the engine with integrally cast Al-MMC cylinder liners; Fig. 1.7 (b) show the Al-MMC brake rotors [14]. Fig 1.8(a) show the Al-MMC driveshaft used in the Chevrolet Corvette [15]; Fig 1.8 (b) Brake rotors for German high speed train ICE-2. Fig. 1.9 shows the discontinuously reinforced Al-MMCs for electronic packaging applications. Fig. 1.9(a) SiC_p/Al electronic package for a remote power controller; Fig. 1.9 and (b) cast Gr_p/Al components.

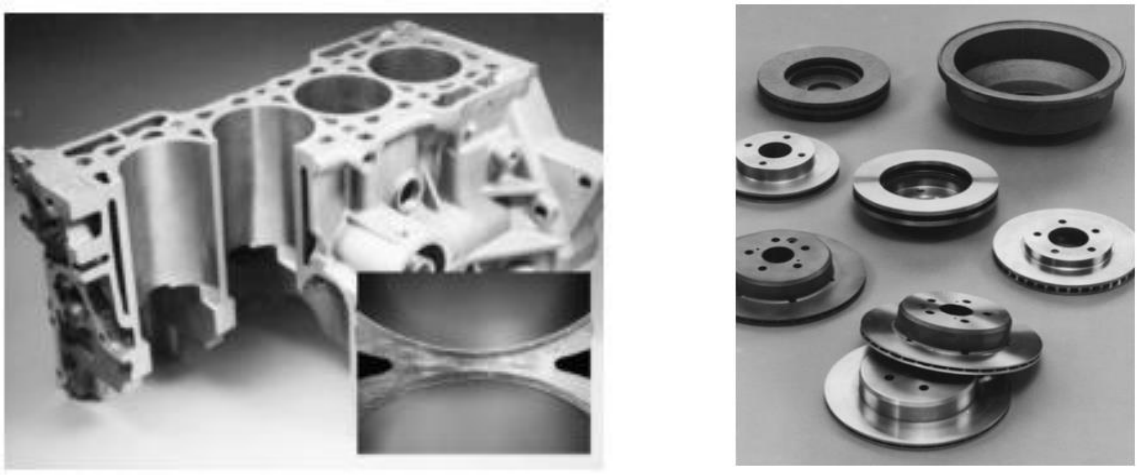

(a) (b)

Figure 1.7: (a) Engine with integrally cast aluminium MMC cylinder liners, (b) Aluminium MMC brake rotors.

(a) (b)

Figure 1.8: (a) Aluminium MMC driveshaft used in the Chevrolet Corvette. (Photo courtesy of Chevrolet), (b) Brake rotors for German high speed train ICE-2. (Photo courtesy of Knorr Bremse AG).

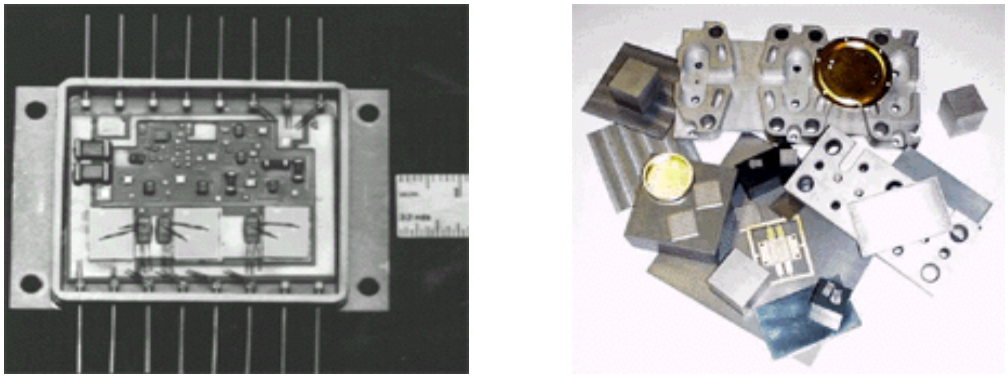

(a) (b)

Figure 1.9: Discontinuously reinforced aluminium MMCs for electronic packaging applications: (a) SiCp/Al electronic package for a remote power controller (photo courtesy of Lockheed Martin Corporation), and (b) cast Grp/Al components (photo courtesy of MMCC, Inc.).

1.3 Fundamental aspects on Wear and its types

The wear is the material removal and degradation over a surface as a result of mechanical action of the counter surface depending on type and intensity of the interactions between surfaces. The different wear phenomena which are commonly encountered are abrasive wear, adhesive wear, erosive wear, surface fatigue, fretting wear, corrosion and oxidation wear etc. It can be observed that these wear mechanisms, do not necessarily act independently and are not mutually exclusive. The sliding and abrasive wear properties of the above mentioned composite components were studied by several researchers since three to four decades with a wide variety of soft and hard reinforcements. It was noticed that the abrasive wear was severe compared to sliding wear as there would be rapid removal of material due to presence of hard asperities in between two surfaces. This can lead to inefficiency of the component system (Bharat Bhushan *et al*., 2013, Rabinowitz *et al*., 1995).

The wear of Al-MMCs was extensively studied since decades and particularly much attention has also been given on abrasive wear of fiber, whisker, and particle reinforced Al-MMCs. The effect of test parameters, characteristics of counter surface, the volume fraction, size and type of reinforcement was studied and it was proven that these factors contribute positively or negatively based on the test conditions adopted. The particle reinforced Al-MMCs was observed to be better due to the contribution of particle in isotropic manner.

- ***Adhesive Wear*:** The unwanted displacement and attachment of material and wear debris from one surface to another. The contact of two solid surfaces under high pressure and frictional heat, arise of atomic bonds takes place. Subsequently, the material from one surface will be detached and adhere to the opposite surface. In some cases, the process of adhesion can also be noted as cold welding. Fig. 1.10 shows the transfer of metal due to adhesive wear process.

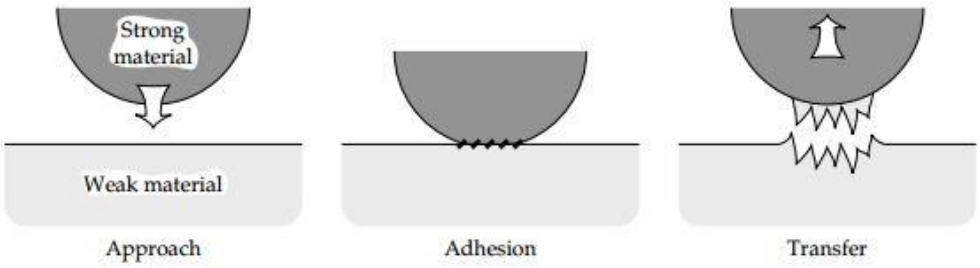

Figure 1.10: Transfer of metal due to adhesive wear (Stachowiak *et al*., 2013).

- ***Abrasive Wear*:** In this wear, the removal of material is due to hard asperities forced against moving solid surface. Fig. 1.11(a) shows the schematic sketch of surface mounted abrasive grits are sliding on a softer surface, and Fig. 1.11(b) shows the abrasive grits freely caught between the surfaces (abrasive grits harder than one of the surfaces). The wear process shown in Fig. 1.11(a) termed as two body abrasion and Fig. 1.11(b) termed as three body abrasion. The process of abrasive wear of material consists of diverse processes such as micro-ploughing, micro-cutting, micro-fracture and micro-fatigue, which usually occur simultaneously.
- ***Cavitation Wear*:** Cavitation wear is caused by the localized impact of fluid against a surface during the collapse of bubbles. Fig. 1.12 shows the schematic sketch of cavitation wear mechanism indicating the bubble collapse.
- ***Corrosion/Oxidation Wear*:** The wear due to chemical reaction between the worn material and the corroding medium is known as corrosive wear. Fig. 1.13 indicate the schematic interaction models showing a corrosive agent and a worn surface.
- ***Erosive Wear*:** This type of wear takes place when the impact of high velocity jet of solid or liquid particles against the object surface. Fig. 1.14 indicate the schematic sketch of a surface being hit by a high velocity jet of abrasive particles.
- ***Fretting Wear*:** The wear caused due to cyclical rubbing between two surfaces. Fig. 1.15 shows the schematic model in fretting wear indicating tribological transformed structure (TTS).

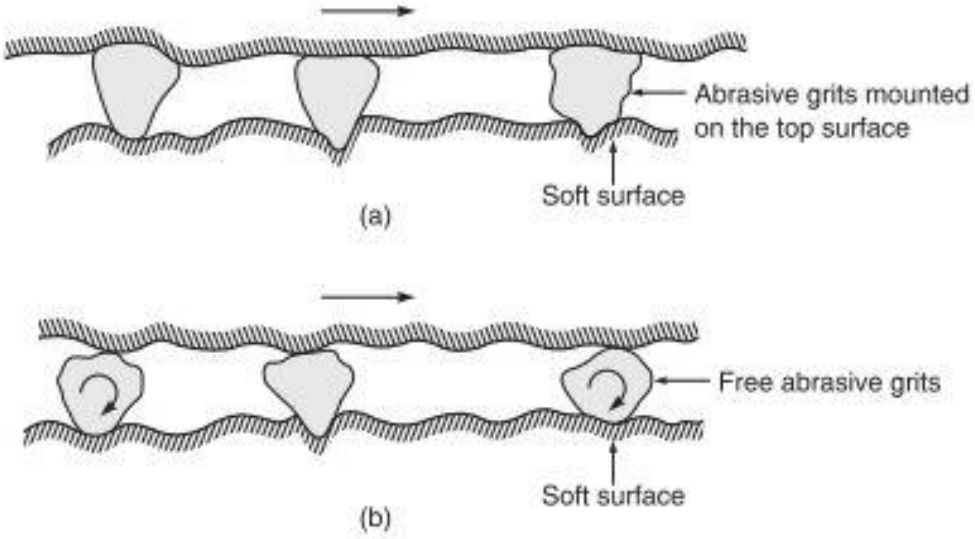

Figure 1.11: The schematic sketch of (a) surface mounted abrasive grits are sliding on a softer surface, and (b) abrasive grits freely caught between the surfaces (abrasive grits harder than one of the surfaces) (Bharat Bhushan, 2013).

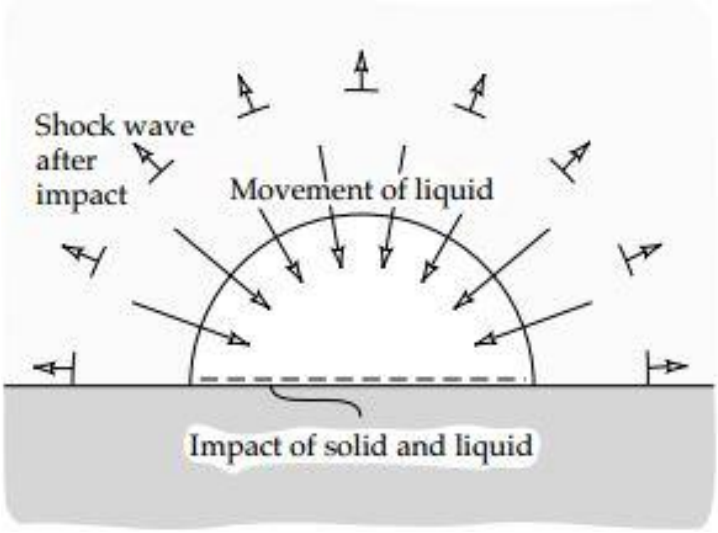

Figure 1.12: A schematic sketch of cavitation wear mechanism indicating the bubble collapse (Stachowiak *et al*., 2013).

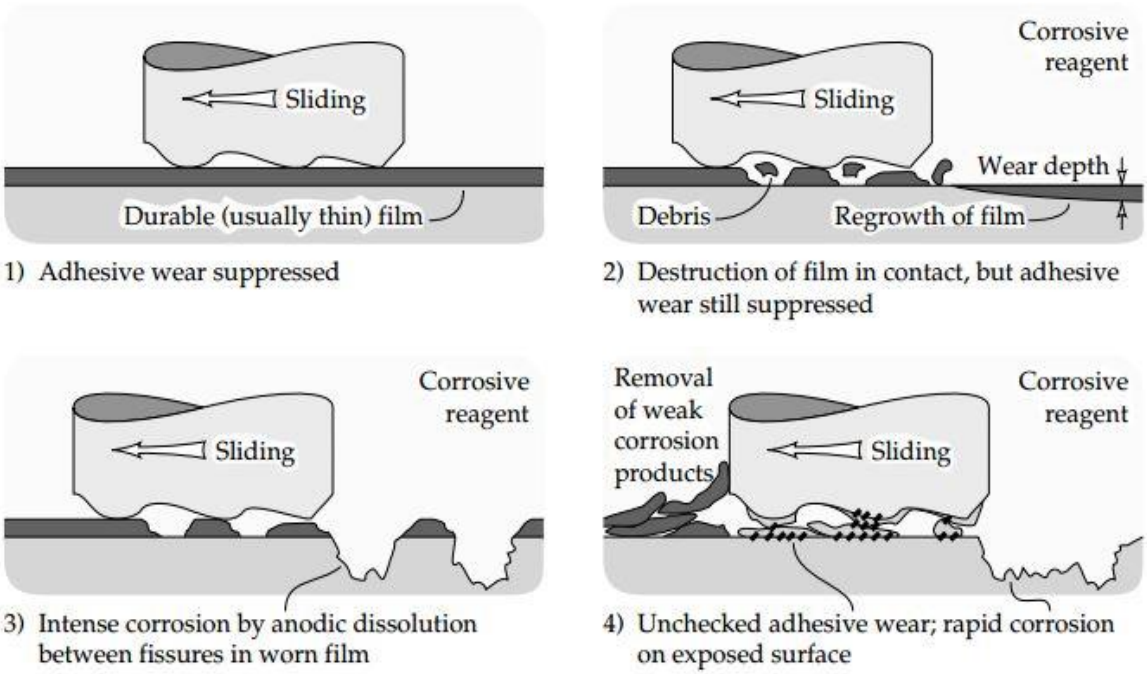

Figure 1.13: The schematic interaction models showing a corrosive agent and a worn surface (Stachowiak *et al*., 2013).

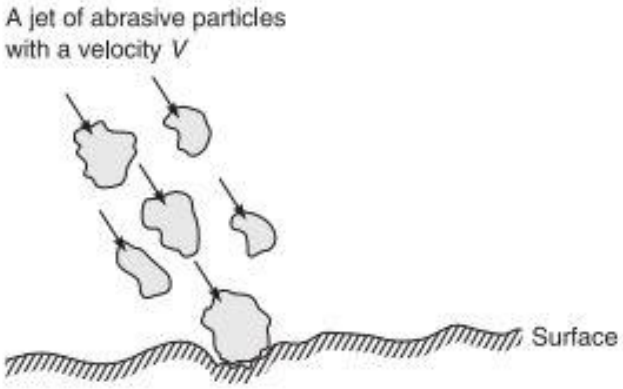

Figure 1.14: A schematic sketch of a surface being hit by a high velocity jet of abrasive particles (Bharat Bhushan, 2013).

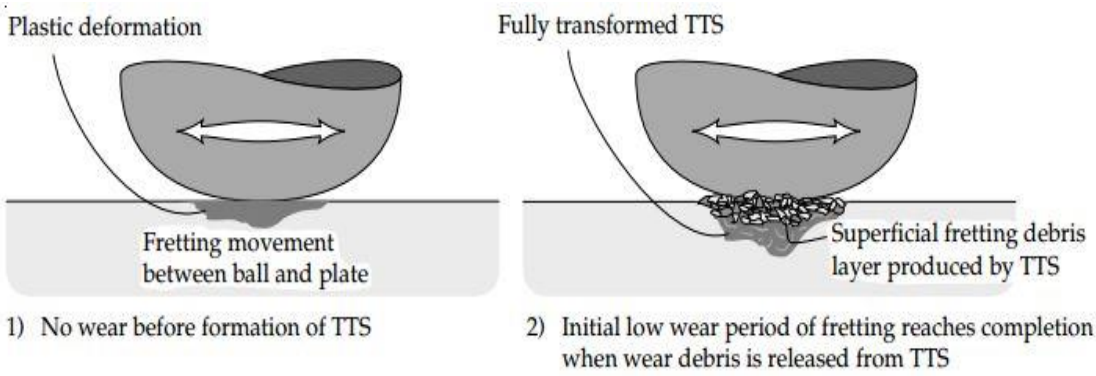

Figure 1.15 A schematic model in fretting wear indicating Tribological Transformed Structure (Stachowiak *et al*., 2013).

- ***Sliding wear*:** The wear occurs when two bodies slide i.e. move relative to each other. Fig. 1.16 shows the schematic sketch of two surfaces in sliding action indicating asperity contact and rupture. The material which is relatively softer will wear.

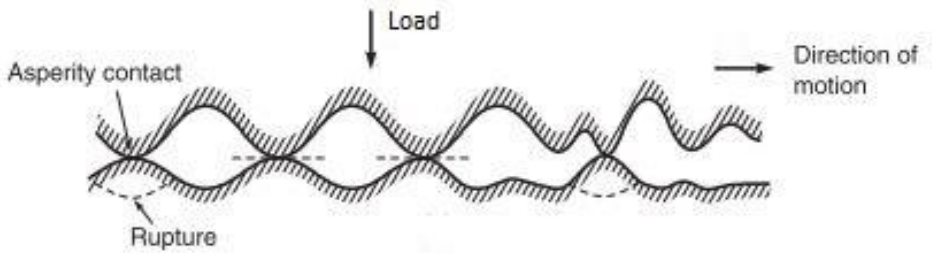

Figure 1.16: A schematic sketch of two surfaces in sliding action (Bharat Bhushan, 2013).

- ***Surface fatigue*:** In this wear process, the wear particles are detached by cyclic crack growth of micro-cracks on the surface. Fig. 1.17 shows the types of mechanical loading with respect to time. Fig. 1.18 shows the schematic sketch of surface fatigue process indicating crack initiation, crack propagation and detachment of wear particle from the surface.

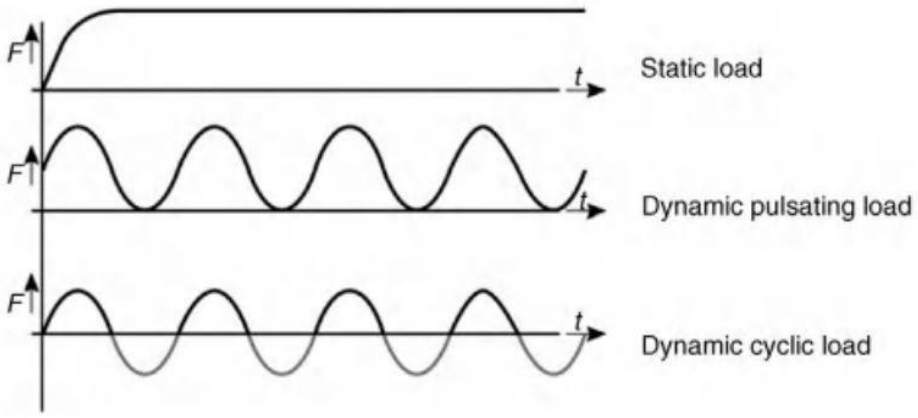

Figure 1.17: Types of mechanical loading with respect to time

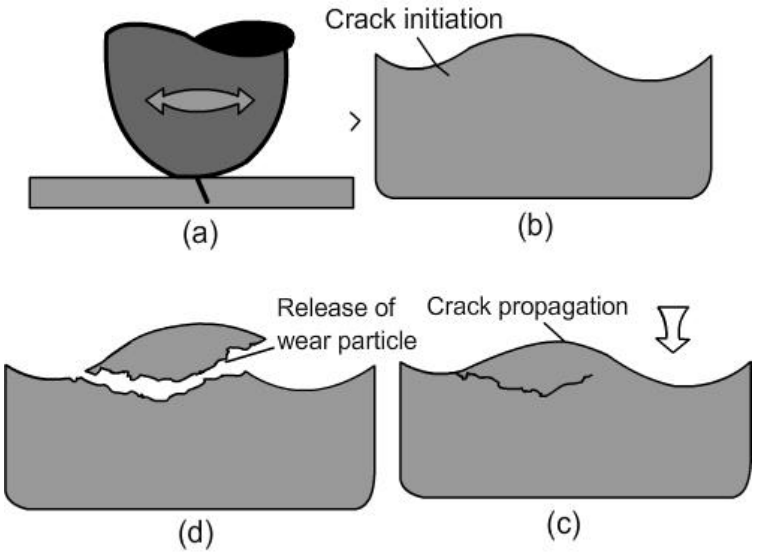

Figure 1.18: A schematic sketch of surface fatigue process (a) & (b) crack initiation, (c) crack propagation and (d) release of wear particle.

1.4 Organization of the Thesis

The whole thesis is organized into 7 chapters.

Chapter-1: This chapter briefly gives a brief introduction about the aluminium, its alloys and its metal matrix composites in general. This chapter also outlines the different types of wear and its mechanisms.

Chapter–2: This chapter briefly gives the comprehensive review of literature related to the present problem. Chapter outlines the research carried out by various investigators in similar and allied fields under separate headings.

Chapter–3: This chapter presents a description about the materials and methods used for the preparation of the metal matrix composites. The standards used for testing are also mentioned. Also a brief description about the ANOVA and regression modelling techniques that was used in this study were outlined in this chapter.

Chapter–4: This chapter describes the morphological/microstructural evaluation of reinforcements, composites and emery papers. The mechanical behaviour of materials is also discussed in the chapter.

Chapter–5: This chapter explains the two body abrasive wear behaviour of matrix alloy and its composites in as cast condition and T6 heat treated. The wear resistance characteristics, wear coefficients and wear depth at different wear parameters, worn surface observation of pin, emery paper and wear debris was also discussed.

Chapter–6: This chapter discusses on results of the ANOVA and regression equations generation of abrasive wear properties of the materials.

Chapter–7: Summarizes the overall conclusions of the present research work with possible remarks and the scope for future work.

References

List of Publications

CHAPTER-2

LITERATURE SURVEY

In this chapter, a brief discussion on the literature review on the research carried on Al-MMCs was done. The review consisting of mechanical, metallurgical, sliding and abrasive wear properties was reported. Finally, based on the understandings, factors affecting abrasive wear and the action plan of current research work was presented.

2.1 Metallurgical and Mechanical Properties of Al-MMCs

The metallurgical and mechanical properties of Al-MMCs basically will depend on the type of manufacturing / processing methodology and its corresponding parameters adopted for composite fabrication, solidification process and the technique used for distribution of particulate reinforcements.

Hashim *et al*., (1999) reported different types of stirrers as shown in Fig. 2.1. It can be noted that different stirrers create the vortex which helps in transfer of the particles into molten metal and maintaining the particles in suspension state. The improper or insufficient vortex mixing will sediment the reinforcements i.e. the particulates will settle down in the crucible. Surappa *et al*., (1997) discussed on the evolution of microstructure during solidification of metal matrix composites reinforced discontinuously. Fig. 2.2 indicate the vortex formation on the matrix melt surface. In Fig. 2.2 the line A shows the melt surface of the before stirring, line C indicate the shape of melt surface when rapid stirring forms a vortex, and line B is the surface level after stirring action is stopped. Fig. 2.3 indicate the schematic sketch indicating the various possible microstructures that can be obtained during composite casting. It was noticed that the interaction forces during solidification was evaluated and able to construct a map of particulate distribution, will give an idea of process parameters required for obtaining microstructures differently. The presence of reinforcing particles will affect the grain size of matrix, dendrite arm spacing etc. The segregation of solute and nucleation of matrix phase will be affected in the presence of particulates.

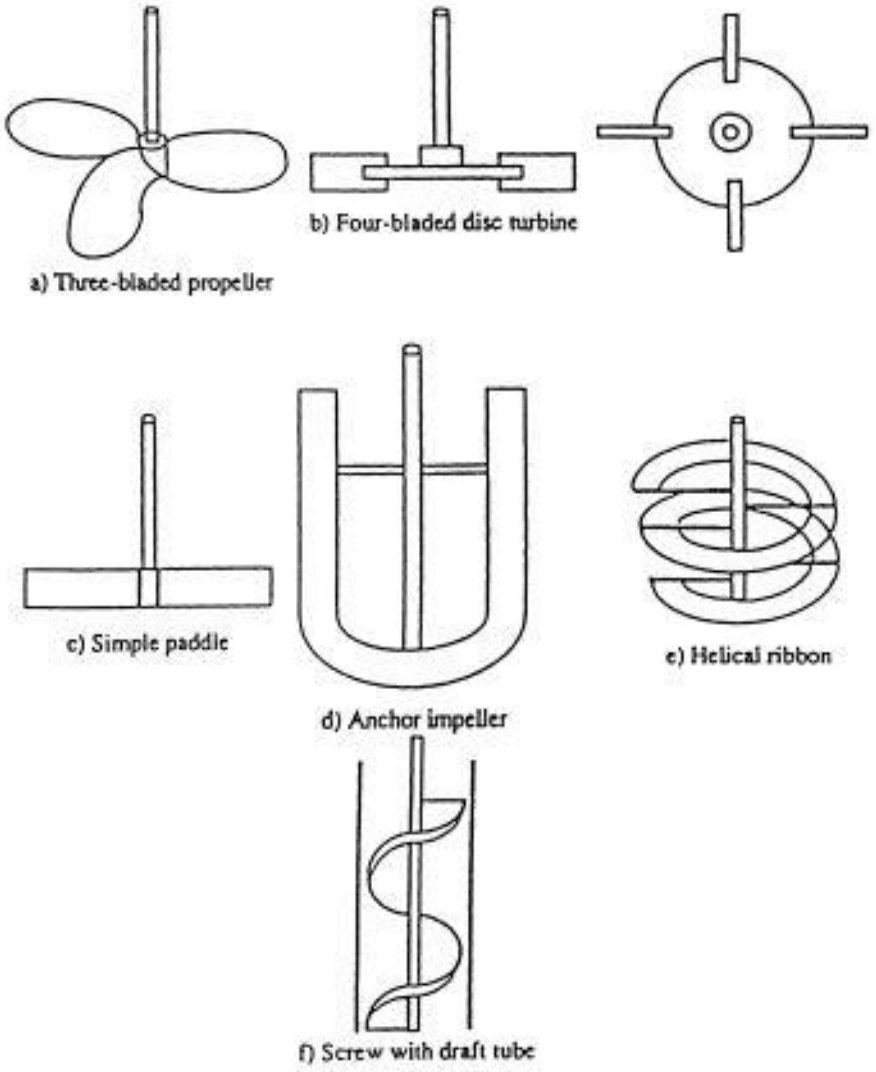

Figure 2.1 : Types of stirrer designs (Hashim et al., 1999).

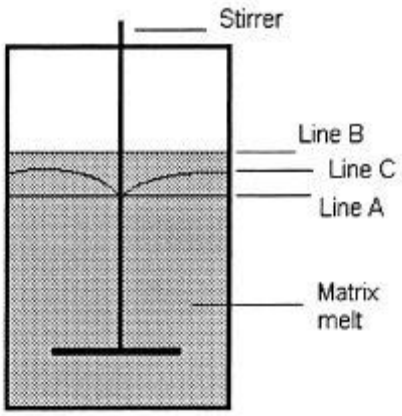

Figure 2.2: The vortex formation on the matrix melt surface (Surappa *et al*., 1997).

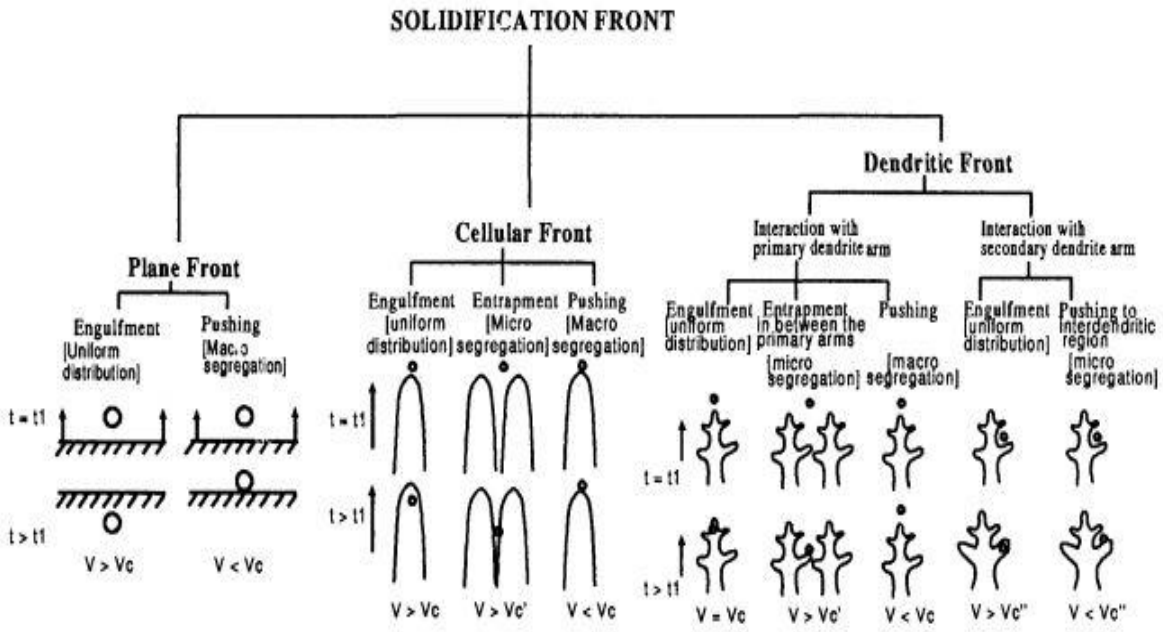

Figure 2.3: The schematic sketch indicating the various possible microstructures of the composite casting (Surappa *et al*., 1997).

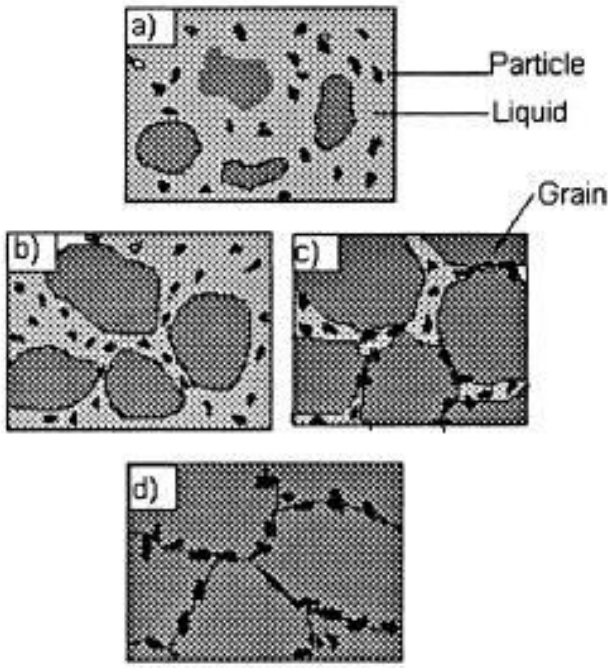

Figure 2.4: The schematic representation of the distribution of particle during process of solidification (a) grains freely growing in the liquid; (b) grain and particle interaction; (c) interface pushing few particles, while some others are being engulfed; (d) the particle final distribution in the matrix material (Hashim *et al*., 1999).

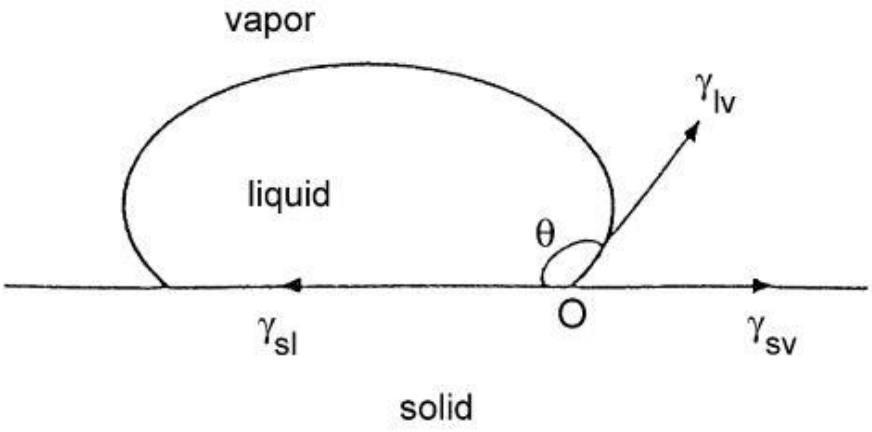

Figure 2.5: Measurement of contact angle in sessile drop experiment (Hashim *et al.*, 1999).

The wettability properties of liquid metal and solid reinforcement i.e. solid and liquid interaction is generally determined by sessile drop experiment and the contact angle, θ is determined by Young-Durpe equation (2.1).

$$\gamma_{sv}=\gamma_{sl}+\gamma_{lv}.\cos\theta \qquad (2.1)$$

where γ_{sv} is specific energy of the solid-vapour interface, γ_{sl} is specific energy of the solid-liquid interface and γ_{lv} is specific energy of the liquid-vapour interface. The $\theta = 0^o$ for perfect wetting, $\theta = 180^o$ for no wetting and $0^o < \theta < 180^o$ for partial wetting. It was noted that the bonding between the solid and liquid phase determines the strength at the interface.

As reported earlier, the mechanical properties of a composite material reinforced with ceramic particulates depend on the properties of matrix, mutual wetting at interface, and the amount and diameter of reinforcing phase. In Table 2.1, the mechanical properties of Al-MMCs are shown. It was noted that the increase of yield strength and ultimate tensile strength properties compared to matrix alloy (Kaczmar *et al*., 2000).

Table 2.1: The mechanical properties of Al-MMCs (Kaczmar *et al*., 2000)

Matrix	Reinforcement, content (vol.%)	Yield strength R_e (MPa)	Tensile strength R_m (MPa)	Elongation (%)
Al	–	64	90	21
Al	SiC, 20	117	200	10
2014-T6	–	429	476	7.5
2014-T6	SiC, 10	457	508	1.8
2014-T6	Al_2O_3, 20	495	515	1.2
6061-T6	–	275	290	18
6061-T6	SiC, 15	290	340	5.5
6061-T6	SiC, 20	345	410	4.9
6061-T6	SiC, 30	380	435	1.8
6061-T6	Al_2O_3, 20	307	349	5.3
7091-T6	–	520	590	10.2
7091-T6	SiC, 20	500	560	1.8

2.2 Wear of Al-MMCs

2.2.1 Sliding Wear Characteristics

The sliding wear characteristics of Al-MMCs with wide variety of fibre, whisker and particulate type reinforcements and its volume fraction with respect to alloy was studied extensively. Sannino *et al*., (1995) reviewed and discussed extensively on the tribological parameters effecting the dry sliding wear behaviour of aluminium composites reinforced in discontinuous fashion. It was reported that factors effecting wear are classified into two categories i.e. intrinsic and extrinsic to the material. The intrinsic factors consists of whereas extrinsic factors consists load, sliding velocity, sliding distance, orientation of reinforcement, the temperature and environment, the counterpart and its surface finish.

It was noted from Wang *et al*., (1991) work that, the wear rate linearly increased with sliding distance in steady state condition and also wear mechanisms changed with increase in sliding distance. It was also reported that orientation of reinforcement had a significant effect on wear rate. Alpas *et al*., (1990) observed that cracks of subsurface were nucleated at interface of aluminium matrix and SiC_p reinforcement. Cao *et al*., (1990) observed that below transition load, the wear rates of composites and alloy were similar whereas beyond the transition load, the wear rate dramatically increased. It was stated that the wear rate increased monotonically with load upto 10N under dry sliding condition by Hosking *et al*., (1982). Pramila Bai *et al*., (1992) noticed that A356 composites with SiC_p reinforcements showed better resistance to wear in 6-75N load range. Sato *et al*., (1976) noticed that wear rate of aluminium alloy and its SiC, SiO_2 reinforced composites increased with increase in sliding velocity whereas it was unaffected in case of Al_2O_3, TiC, Si_3N_4 reinforced composites. The type, size, shape, volume/weight fraction and spatial distribution of SiC, TiC, B_4C, TiB_2, Al_2O_3 etc reinforcements had significant role in enhancing the wear properties. It was proved that, based on such reinforcement characteristics, interface characteristics will vary (Lloyd *et al*., 1994). It was proved by Song *et al*. (1995) that effect of ageing had beneficial effect on wear properties.

Singh *et al*. (2001) studied on sliding wear of granite reinforced aluminium composites and stated that wear rate lowered when compared to matrix alloy. Acilar *et al*., (2004) noted that as sliding distance and load increased, the wear rate increased. Rao *et al*. (2010) studied on heat treatment effects on sliding wear of Al 7009 alloy composites reinforced with SiC and stated that the maximum hardness and minimum wear rate was

observed at 6 hours of aging treatment. Rao *et al*. (2011) evaluated on the effect of sliding distance on friction and wear behaviour of cast and heat treated SiC reinforced composites. It was concluded that, irrespective of material, as load and sliding distance increased, the wear rate increased.

Some researchers investigated on the wear behaviour of Al-MMCs containing multiple reinforcements and compared with single particle reinforced composites and unreinforced alloy. These works were focused to understand the combined effects of hard and soft type of reinforcements in the wear behaviour on the matrix material. It was revealed that the addition of secondary reinforcement found to have beneficial effect especially in terms of wear properties. It was noted that the graphite addition to Al-SiC composites was found to be advantageous in tribolayer formation, subsurface deformation and machining of Al-SiC composites.Ted Guo *et al*., (2000) studied on tribological behaviour of self-lubricating Al 6061-SiC-graphite hybrid composites produced by semi-solid powder densification method. It was stated that wear rate increased up to 5% vol. of graphite and then decreased. It was observed that wear becomes stabilized when the addition of graphite increases. Riahi *et al*. (2001) has done investigation on the role of the tribo-layers that are formed during the sliding wear of the A356 Al–SiC–Gr & A356 Al–Al_2O_3–Gr composites determined ultra-mild, mild and severe wear regimes. In his work, the change in wear mechanism was observed from micro-cutting to micro-cracking when abrasive size increased from 100 to 120 μm. Fig. 2.6 shows the wear rate versus load for A356 Al–10% SiC–4% Gr at different sliding speeds. Fig. 2.7 shows the schematic sketch indicating the tribolayer, iron oxide layer on the surface and fractured ceramics in graphitised MMCs. Basavarajappa *et al*. (2005) has done study on dry sliding wear behaviour of Al 2219-SiC–Gr hybrid metal matrix composites and proved that wear rates decreased due to addition of graphite. Aziz *et al*., (2006) studied on the effect of wear characteristics and heat treatment of TiC and Al_2O_3 reinforced Al 6063 hybrid composites. Suresha *et al*. (2010) parametrically studied on the sliding wear characteristics of SiC and graphite reinforced hybrid aluminium matrix composites. It was noted through mechanically mixed tribo-layer that speed reduced the wear, whereas load increases the wear of the composites. Radhika *et al*. (2012) studied on sliding wear of Al/Al_2O_3/graphite hybrid metal matrix composites and concluded that wear rate increased with increase in load and decreased with increasing reinforcements and sliding speed. Hence, from the above literature it was noticed from the above literature that

the sliding wear properties of hybrid composites was found to be advantageous in reducing the wear.

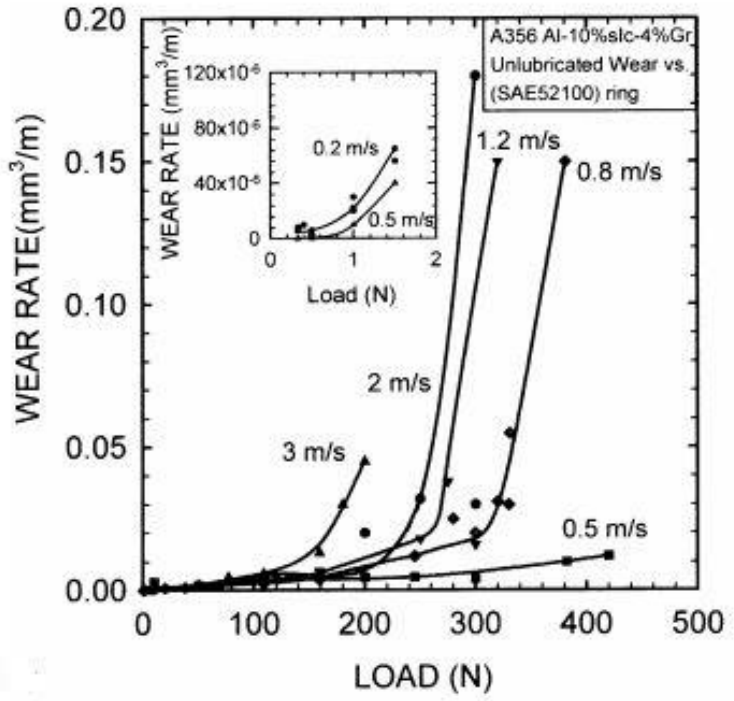

Figure 2.6: Wear rate versus load for A356 Al–10% SiC–4% Gr at different sliding speeds (Riahi *et al*., 2001)

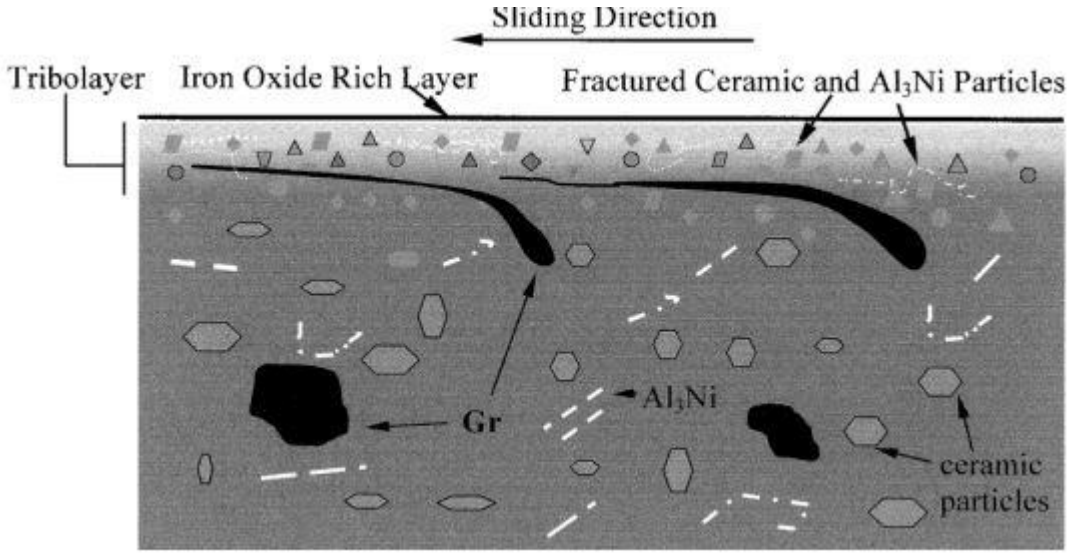

Figure 2.7: A schematic sketch indicating the tribolayer, iron oxide layer on the surface and fractured ceramics in graphitised MMCs (Riahi *et al*., 2001).

Zhang *et al*., (1995) identified the three wear mechanisms: abrasion in the running-in period, oxidation during steady wear at low load levels, and adhesion at high loads. It was stated that a higher particle volume fraction raised the transition load, but increased the wear rate in the abrasion and adhesion regimes.

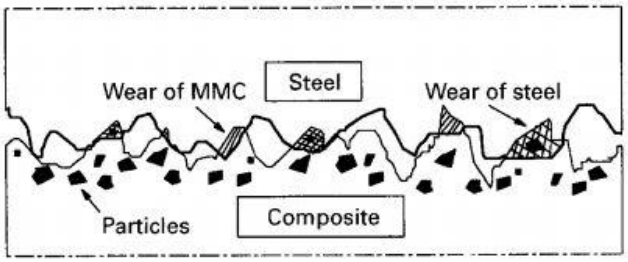

Figure 2.8. Illustration of scratch interactions

An investigation of indentation reported by Zhang *et al*., (1995) revealed that the tensile principal residual stress in the work material is almost perpendicular to the surface and the compressive one parallel to it, as indicated in Figure 2.9 (a). It was noticed that such a residual stress state can make the cracks propagate easily in the sliding direction. Later Zhang *et al*., (1998) illustrated on wear sheet formed by delamination as indicated in Fig 2.9 (b).

(a)

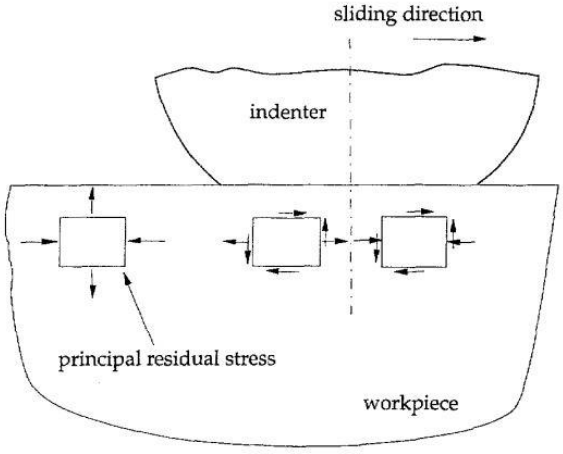

(b)

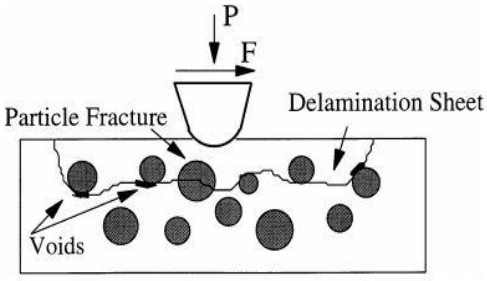

Figure 2.9: (a) Schematic stress distribution beneath a sliding contact (Zhang *et al*., (1995)) and (b) Illustration on wear sheet formed by delamination (Zhang *et al*., (1998))

2.2.2 Abrasive Wear Characteristics of Al-MMCs

The abrasive wear was classified as low stress and high stress condition depending on the extent of the abrasive grit particles fracture themselves under normally applied load. The low stress abrasive wear is otherwise can be termed as three body abrasion and high stress as two body abrasive wear. The wear studies on different materials were done by adopting various material processing techniques and varying the microstructural characteristics of materials. The test conditions like applied load, sliding distance, time duration etc.; counter surface properties like grit particle size (in abrasive wear); and also environmental conditions. Simon *et al.* (2004) reported that abrasive wear is generally considered to be a dominant wear mechanism for the cylinder bore and piston ring system. It was noticed that wear of these components can affect the efficiency of combustion process. It was noticed that when compared to sliding wear, the abrasive wear was found to be severe as there would be removal of material takes place rapidly due to presence of hard asperities and this can lead to inefficiency of the wear critical component in the tribo-system.

The abrasive wear behaviour of Al-MMCs was reviewed comprehensively by Deuis *et al*. (1996). Later Hutchings *et al*. (2000) reviewed on sliding wear and abrasive wear of Al-MMCs and also reported on wear mechanism maps. Rohatgi *et al*. (1979) reported that abrasive wear resistance of 5% quartz reinforced Al-MMC was three times that of matrix material. Banerji *et al*. (1982) investigated on abrasive wear of zircon particle reinforced Al-Si-Mg composites produced by liquid metallurgy route and reported that wear resistance increased with zircon volume fraction. Lin *et al*. (1988) demonstrated the effect of ageing temperature and time duration on SiC reinforced Al-Zn-Mg composites. Wang and Hutchings *et al*. (1989) examined on the influence of volume fraction of fiber, grit size on the two body abrasive wear behavior of alumina fiber reinforced Al-MMCs and observed that change in wear behavior for different size of abrasive grits. It was noted that abrasive particles of smaller size offered increased wear resistance with increase in fiber volume fraction. Alpas and Embury (1990) showed that abrasive wear resistance of SiCp reinforced Al 2014 alloy increased with increased sliding distance. Wilson *et al*. (1990) studied on two body abrasive wear of Al6061-20 vol.% SiC_p and reported on transition of wear behavior. It stated that the state of abrasive wear changed when the size of abrasive grit was reduced as finer grits promotes low stress abrasion i.e. the chipping and reinforcement removal to more plastic smearing of the matrix metal. Turenne *et al*. (1990) investigated

and proved that the wear resistance of Al6061-20% SiC composites and proved that it increases with decreased size of abrasive grit particle.

Zongyi *et al*. (1991) experimentally investigated on the abrasive wear of Al 6061 and its SiCw, SiCp reinforced composites against P400 and P600 grit papers. It was noted that the wear rate of composite with SiCw reinforcement was higher compared to SiCp reinforced composites. This was due to greater tendency of agglomeration of ceramic in former composite. Wang *et al*. (1991) reported on abrasive wear behaviour of Al 7091 composites reinforced with particulate and whisker type reinforcements. It was stated that for normally oriented whisker type reinforcements and smaller abrasive sizes, the wear resistance was observed to be higher. Huei-Long *et al*. (1992) studied on the effects of volume fraction, reinforcement size on abrasive wear resistance properties of SiCp reinforced Al 6061 composites processed by powder metallurgy method concluded that as the vol. % of SiCp increases, the wear rate of composite decreases. Axen *et al*. (1994) worked on alumina reinforced aluminium composites and revealed that abrasive wear resistance improved in mild abrasion conditions, i.e. low applied loads, soft and small abrasives. He also stated that in severe abrasion cases, the abrasive wear resistance was equal to or lower than that of unreinforced material. Gurcan *et al*. (1995) investigated on abrasive wear behaviour of saffil and SiCp reinforced Al 6061 composites over P400 SiC grit. It was reported that wear resistance increased for saffil and SiCp reinforced hybrid composites when compared to SiCp reinforced composites. Song *et al*. (1995) reported on thermal ageing effects on abrasive wear of age-hardened Al 2014 and Al 6061 composites reinforced with SiC. It was noticed that at 200^{o}C i.e. peak ageing temperature, the hardness and abrasion resistance observed was higher compared to under aged and over aged composites. Hamblin *et al*. (1996) described on shape of abrasive particle and its relation to abrasive wear in two body condition. It was reported that wear rates are linear proportional to developed spike parameter. It was noticed that wear rates increases linearly with speed, with partial decrease in friction due to lubrication effect caused by fine wear particles. Garcia-Cordovilla *et al*. (1996) conducted abrasive wear experiments on A357, A339, AA 6061 composites reinforced with SiC and Al_2O_3 produced by stir casting method. It was stated that specific wear rate of the composites decreases with increase in size and volume percentage of particulates. Mondal *et al*. (1998) studied on the two body abrasive wear behaviour of 10% wt. Al_2O_3 particle reinforced aluminium alloy composite and deduced that applied load effect was severe on wear rate. Zum Gahr *et al*. (1998)

reported on wear by hard particles and stated that abrasive wear resistance can also be improved through second phases present in matrix which is either soft or hard. Al-Rubaie *et al*. (1999) concluded that resistance to abrasion of Al-SiC composites increased with increase in size of reinforcement i.e. within 40μm range.

Yilmaz *et al*. (2001) investigated on Al_2O_3 reinforced Al-MMCs under different abrasive conditions and noticed that the composites having larger reinforcement particles were more effective compared to smaller ones. It has been proven that wear rate of composites decreased rapidly with increase in Al_2O_3 volume fraction, when performed under SiC emery paper of 80 grade than in 220 grade. Sahin *et al*. (2003) proved that abrasive grit size is major significant factor followed by reinforcement weight fraction for SiC reinforced Al-Cu alloy composites. This was due to the greater fragmentation and fracturing of hard particulate reinforcements in composites. This was case when the SiC emery paper was used for experimentation. Sawla *et al*. (2004) studied on abrasive wear properties of 15% SiC reinforced LM 13 alloy composites in as cast and heat treated condition. It was reported that wear constant, K decreased with increase in applied load. Wear constant of heat treated alloy and composite was lower compared to cast alloy due to heat treatment. Mondal *et al*. (2006) focused on high stress abrasive wear behaviour of ADC-12-SiCp reinforced composites and compared with unreinforced matrix alloy. Sahin *et al*. (2008) demonstrated the abrasive wear rate of SiC_p reinforced Al MMCs with models and concluded through developed equations that wear rate increased with increase in load applied, size of abrasive and decreased with sliding distance. Das *et al*. (2008) conducted study on the heat treatment and reinforcement effects on abrasive wear of Al–Si alloy composites under different abrasive sizes and loads.

Canakci *et al*. (2012) investigated on the effects of sliding time, reinforcement size of B4C on abrasive wear properties of B_4C reinforced Al-MMCs. It was shown that larger size of reinforcement is more effective than smaller size of reinforcement. Tofigh *et al*. (2013) reported that as the particle size of B_4C increases the surface roughness of the composites decreases. Yigezu *et al.* (2013) done experimental investigation on wear parameters such as applied load, sliding distance and wt.% of reinforcement on abrasive wear performance of in situ TiC reinforced Al-Si composites. It was noted that the wear increased with increase in applied load and sliding distance, it decreased with increase in wt.% TiC reinforcement. Canakci *et al*. (2014) used artificial neural network approach to estimate the volume loss, specific wear rate and surface roughness of Al 2014/B_4C

composites with respect to sliding time and volume fraction. Rahimipour *et al.* (2014) experimentally investigated on the effects of applied load, abrasive grit size and weight fraction of B_4C on abrasive wear behaviour reinforced Al MMCs. It was stated that composites with finer particle size, the wear rate linked with hardness of matrix whereas composites with large particle size, wear rate was connected with both hardness of matrix and particle fracture.

2.3 Research Problem Identification

2.3.1 Motivation and Scope of the present work

It was observed that, in order to meet the stringent government regulations and have advantage in tough competition, the better performance materials for efficient engine components have been developed according to demand within the automotive industry. In an internal combustion engine, the tribological performance of the piston ring/engine cylinder bore system has long been recognised as important in achieving desired efficiency and durability in terms of power loss, fuel consumption and even harmful exhaust emissions.

Tung *et al.* (2004), a researcher from General Motors Research and Development Centre, Michigan, USA, reported that the wear rate of piston ring/cylinder bore system is high initially, decreasing thereafter, then reaches to steady state. The ring/bore wear ultimately results in poor performance and decreased oil economy, eventually requiring an engine over haul. Similar to any other complicated physical system, several wear mechanisms would contribute to the progression of wear for piston ring/cylinder bore system. Becker *et al.* (1999) reviewed and Tung *et al.* (2004) reported that three important wear mechanisms mentioned over the years are corrosion, abrasion and adhesion. The corrosion is dominant mechanism when the engine runs either cold shut or very hot. Generally this can be reduced by the use of thermostats and also by the addition of corrosion inhibitors to engine oils. The abrasion caused from the cutting and ploughing action of hard particles (as indicated in Fig. 2.10) whereas adhesion occurs when the oil film between the ring and the bore is so thin that metal to metal contact happens. These are common during the running-in period because of the surface roughness of both the ring and the bore. These are common wear mechanisms for this tribo-system during steady state period. The other wear mechanisms, such as oxidation and splat delamination have also been reported by Becker *et al.* (1999).

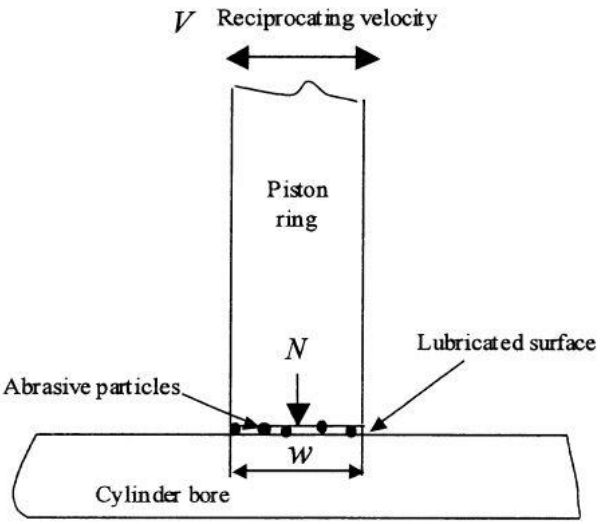

Figure 2.10: Schematic of the piston ring/cylinder bore tribo-system (Tung *et al*., 2004)

The total wear volume loss of both ring and bore tribo-system is the sum of the contribution from each wear mechanism that is observed. The real wear progression is quite complex, as it is a function of several factors ranging from metallurgy of contacting materials to operating conditions and lubricant properties. The use of real engine tests for the evaluation of the tribological performance of these tribo-components is very costly and time consuming. One way to speed up the process, while maintaining standard and accuracy in the evaluation of wear, is to develop the wear mechanisms of newly developed materials. In researching the piston ring/cylinder bore wear progression due to abrasion dominated wear mechanism, the pin on disc equipment has been used by several researchers in their wear related works mentioned in the above literature. But from the literature review mentioned above, it was noticed that the wear behaviour of single particle reinforced composites against different abrasive media, and the sliding wear of single particle reinforced and hybrid composites was understood well. As the wear behaviour of hybrid composites studied by few researchers was limited to dry sliding condition only, a gap was noticed in the abrasive wear case. Hence it was observed that, an investigation is necessary in studying abrasive wear behaviour of hybrid composites.

It can be understood that there will be number of parameters contribute for a wear process in a tribo-system. The level and type of contribution of each independent and variable parameters vary from application to application depending on interactions in the tribo-system. In this scenario, a broad outline of the independent and dependent variables

which are contributing the abrasive wear process of materials was chalked out and was indicated in Fig. 2.11.

From the flow chart Fig. 2.11, it was observed that input parameters that are majorly contributing abrasive wear process are broadly classified into machine parameters, material parameters, counter surface parameters and environmental parameters. The machine parameters include applied loads, sliding speed, time, sliding distance, wear track diameter etc. The type, size, % content and orientation of reinforcement, matrix composition, hardness, strength, toughness and microstructure etc comes under material characteristics. The counter surface characteristics include grit type, size, shape, hardness and its orientation, interface strength to which it is bonded, surface roughness/ texture and also lubrication condition if existing. The environmental parameters include the medium of operation (air, argon etc.), operating temperature, the relative humidity etc.

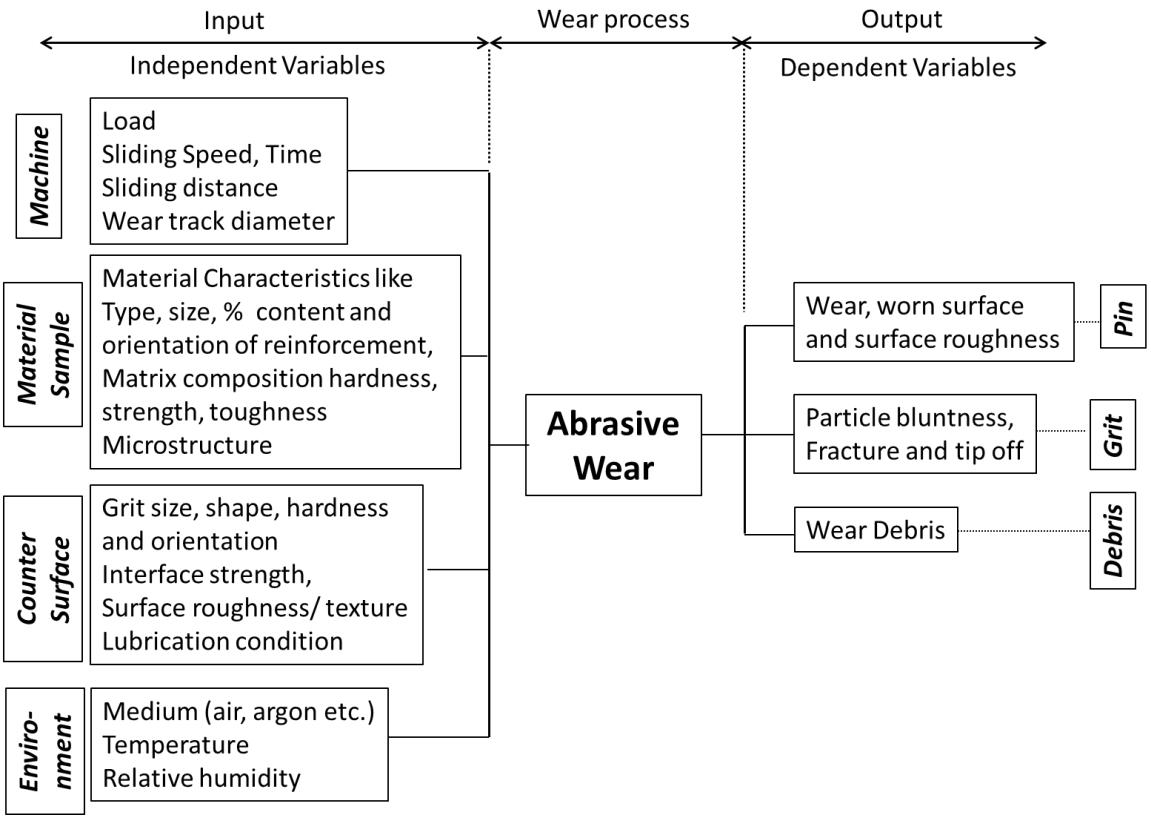

Figure 2.11: Independent and dependent variables in the abrasive wear process

The abrasive wear characteristics can be well explained through tested pin sample, grit paper and the wear debris. The pin sample characteristics include the amount of wear has happened after wear process, the worn surface observation through SEM and surface texture/roughness evaluation through advanced microscopy techniques. The grit particle

bluntness, fracture and tip off characteristics are related to counter surface characteristics after abrasive wear process. The wear debris formed can be understood similar to chips formed during machining process of a material.

2.3.2 Objectives and Work plan of the present work

The following objectives of the current research were adopted:

- Synthesis of hybrid metal matrix composites by liquid metallurgy route.
- Evaluation of microstructural, density, hardness and tensile properties of hybrid aluminium metal matrix composites.
- Influence of wear parameters such as applied load, grit size and sliding distance on abrasive wear properties.
- Effect of T6 heat treatment on abrasive wear behaviour.
- Understanding wear mechanisms through worn surface analysis of pin samples, emery paper and wear debris; and surface texture measurement like surface roughness, R_a after wear experimentation.
- ANOVA and Regression equations generation.

The detailed action plan adopted in the present research was represented in flow chart as indicated in Fig. 2.12.

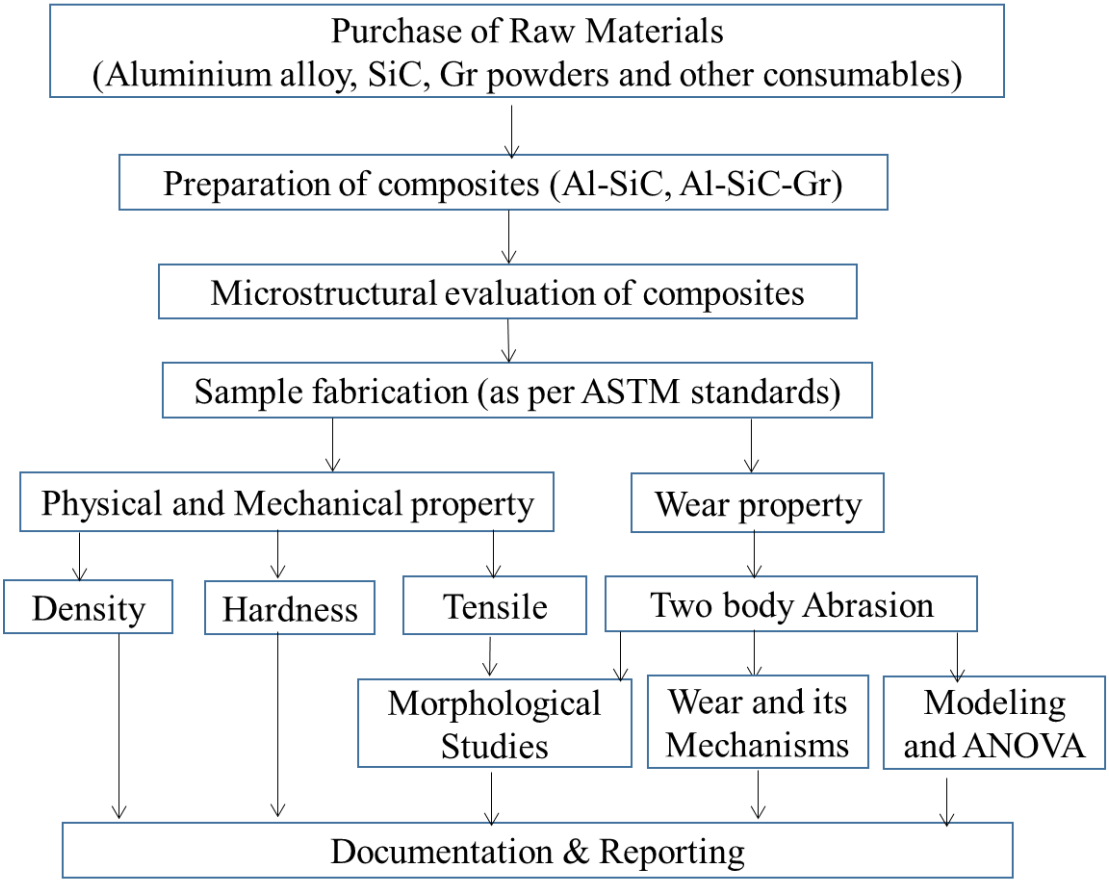

Figure 2.12: The flow chart of action plan

CHAPTER-3

MATERIALS AND METHODS

In this chapter, the detailed description on the process of material selection and composite preparation; microstructural/morphological characterization, density, hardness and tensile properties evaluation; experimentation of two body abrasive wear of materials; surface roughness evaluation and characterization of the worn surface of pin sample, emery paper and wear debris was reported. Finally the brief explaination of ANOVA and regression modelling of wear results was given.

3.1 Material Selection and Composite Preparation

In this present study, Al 6082 alloy, an alloy from Al-Mg-Si series having magnesium and silicon as major alloying elements was chosen as matrix material. The chemical composition of Al 6082 alloy was done by using Optical Emission Spectrometer, BAIRD-DV6. The details of chemical composition of the chosen matrix material was given in Table 3.1. The silicon carbide (SiC) and graphite (Gr) particulate type reinforcement were chosen for the preparation of composites. The details of SiC and graphite reinforcements was shown in Table 3.2. Fig 3.1 (a) and (b) shows the photographic images of graphite and silicon carbide respectively.

Table 3.1: Chemical composition of Al 6082 alloy

Material	**Element** (wt.%)								
	Cu	**Mg**	**Si**	**Fe**	**Mn**	**Zn**	**Ti**	**Cr**	**Al**
Al 6082 alloy	0.058	0.768	0.951	0.316	0.532	0.016	0.037	0.038	Balance

Table 3.2: Details of SiC and Graphite reinforcements.

Reinforcement	**Hardness (GPa)**	**Grain size (µm)**	**Density (g/cc)**
SiC	24.5–29	~32	3.22
Gr	0.25	~40	2.09–2.23

The Al 6082-10%SiC (Al-SiC) and Al 6082-5% SiC-5% Gr (Al-SiC-Gr) composites were synthesized by stir casting method. The amount of reinforcement content considered was in wt.% with respect to alloy wt.%. The alloy ingots were first melted in a crucible of graphite made by using a coal fired furnace. The reinforcement particles were subjected to preheating to ~500^{o}C. These particles were added to the molten alloy during vortex action created by mechanical stirrer initially set at 200 RPM. Later the rotational speed was increased to 400 RPM and left for a time duration of 10 minutes for proper mixing. This was done due to increase in viscosity of the melt due to addition of reinforcements. After thorough mixing, the slurry in molten form was made poured into stainless steel mould of dimensions length of 170 mm and Ø40 mm. After solidification, the cast ones were removed from the die and flat end sample pins of length 27mm, and Ø8 mm were prepared by wire cut electron discharge machining (EDM) process. After samples preparation through EDM, first half set of samples were separated to do respective tests in as cast (AC) condition and second half set of samples were separated for T6 heat treatments (T6).

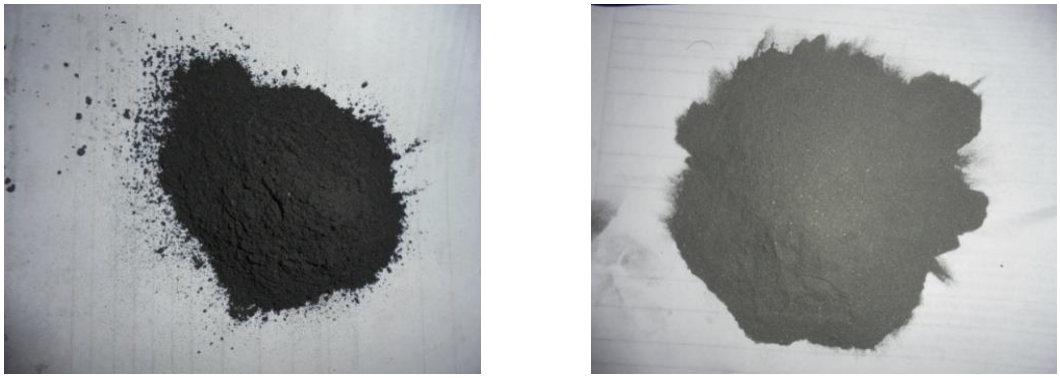

(a) (b)

Figure 3.1: The photographic images of (a) Graphite and (b) Silicon carbide

Fig 3.2 show the photographic images of the accessories used in the composite preparation by stir casting process. Fig 3.2 (a) indicate the chuck attached to variable speed motor, Fig 3.2 (b) show the SS304 stirrer rod used to create stirring action which was coated with Zirconia, Fig 3.2 (c) show the K type Inconel thermocouple used in measuring temperatures of molten slurry, Fig 3.2 (d) show the graphite crucible and Fig 3.2 (e) show the stainless steel die used for pouring molten slurry and left for solidification.

Fig.3.3 (a) indicate the snapshot taking during stir casting process, Fig. 3.3 (b) indicate the pouring of molten slurry into die, Fig. 3.3 (c) casting during solidification and Fig. 3.3 (d)-(e) indicate the schematic sketch of stir casting technique.

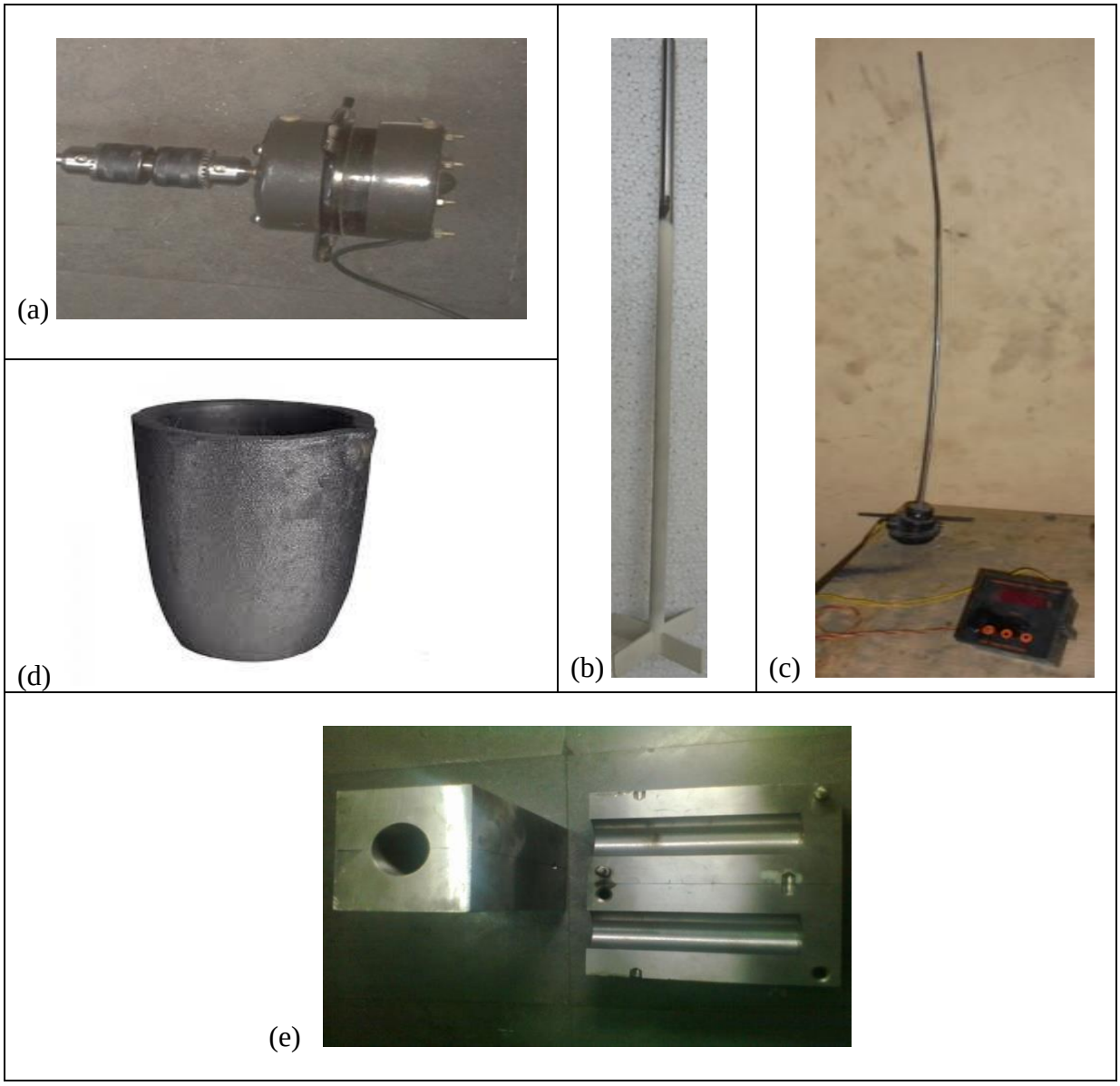

Figure 3.2: The photograph image of (a) Chuck attached to motor (b) SS 304 stirrer rod coated with Zirconia (c) K type Inconel temperature thermocouple (d) graphite crucible (e) stainless steel die

Fig. 3.4 (a), (b), (c) and (d) indicate the photograph snapshot of cast samples after solidification, samples after turning by lathe, electric discharge machining of samples and pin samples obtained for wear testing respectively.

Fig. 3.5 shows the line diagram for T6 heat treatment cycle adopted for materials. It depicts that samples were solutionized at 500 °C for time duration of 2hours and later these were subjected to 200 °C for time duration 6 hours to obtain T6 heat treatment condition.

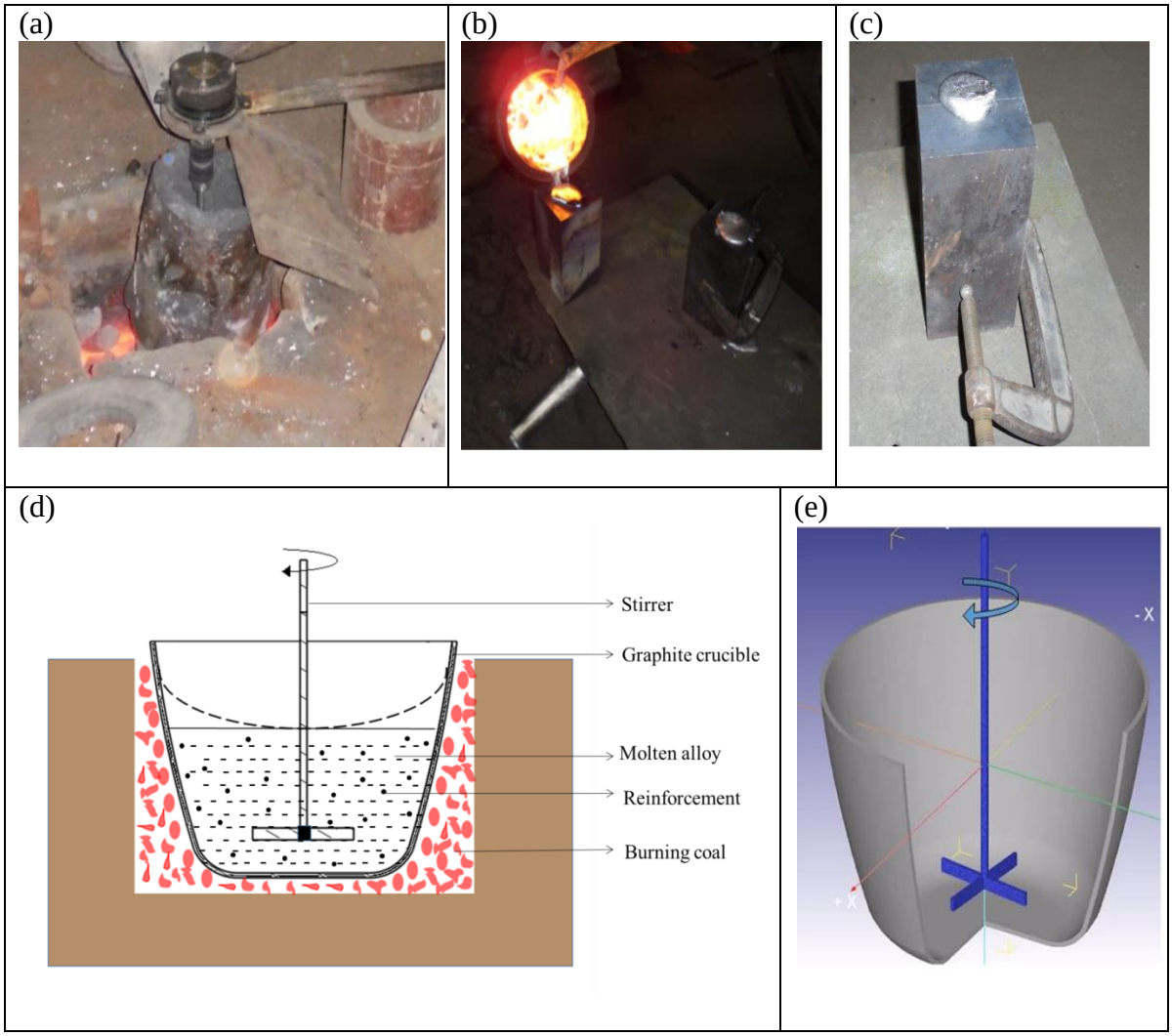

Figure 3.3: A snapshot taking during (a) casting process (b) pouring into die (c) casting during solidification and (d) & (e) A schematic sketch of stir casting technique

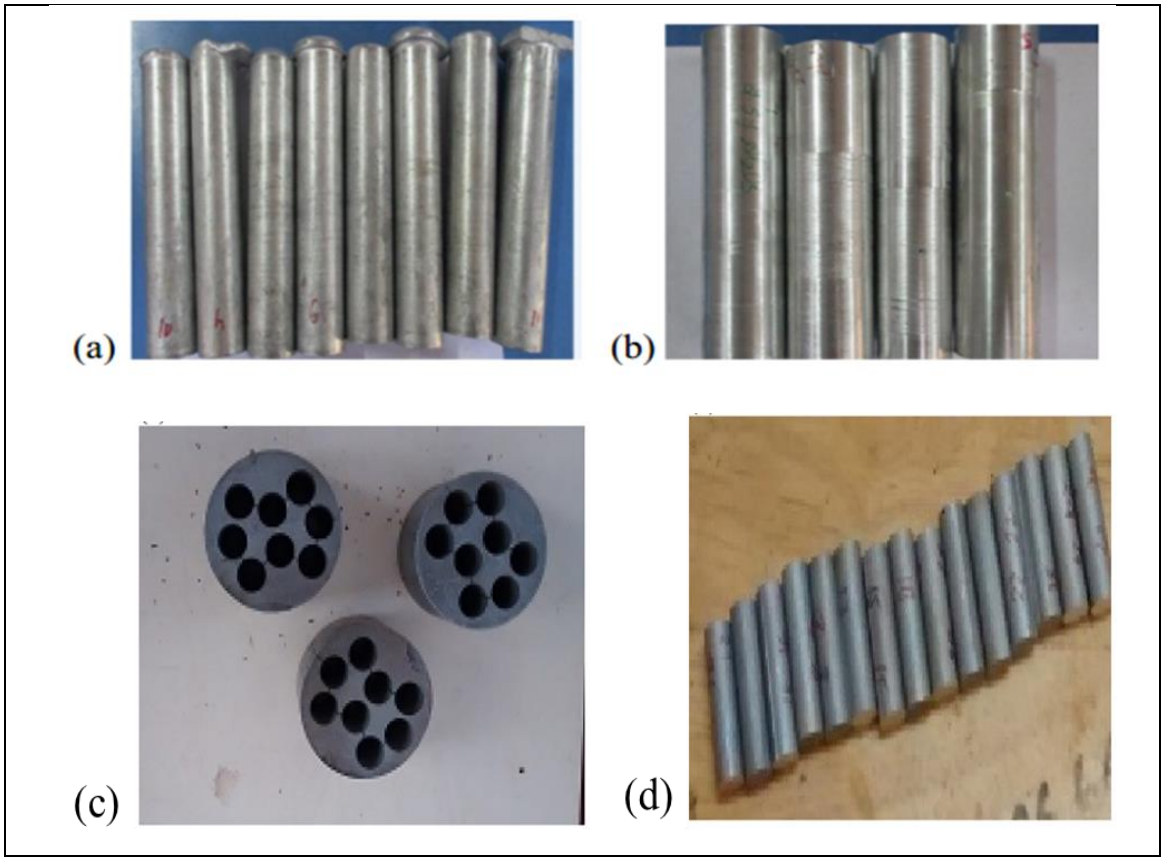

Figure 3.4: The photograph snapshot of (a) cast samples (b) after turning operation by lathe machine (c) electric discharge machining of samples (d) pins for wear testing

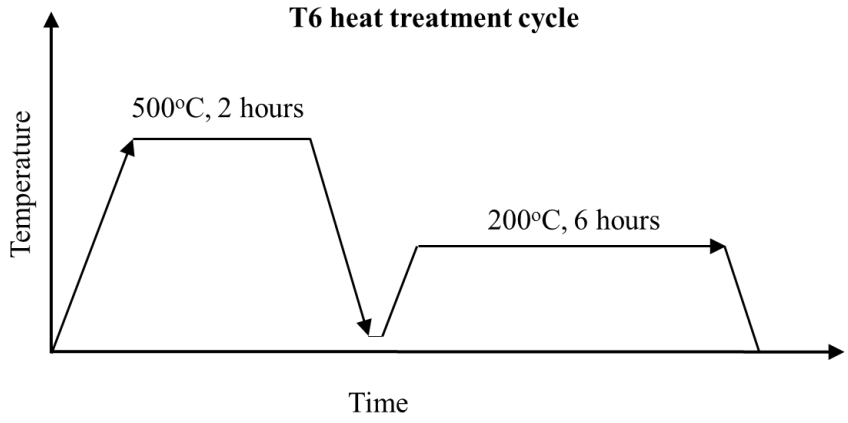

Figure 3.5: T6 heat treatment cycle adopted for materials

3.2 Microstructure Evaluation and Phase Identification

The morphology of powders, emery papers and composites were observed by under scanning electron microscopy (SEM). Fig 3.6 shows the image of SEM of TESCAN make, Model: Vega LMU 3 used in the study. The images were captured in secondary electron mode at different magnifications.

The composite samples were polished and etched with Keller's reagent (consisting of 1% HCl, 1% HF, 2.5% HNO_3 and remaining water) to know and understand the microstructural features. The emery papers before and after abrasion testing were subjected to gold sputtering prior to the SEM observation. After wear testing, the worn surfaces of pins, emery papers and wear debris were observed and presented in the results and discussion chapter.

Figure 3.6: A photograph image of Field Emission Scanning Electron Microscope

Figure 3.7: A photograph image of X-ray Diffraction machine

The following characterization activities were done by SEM namely:

- Morphology of SiC and graphite reinforcements
- Morphology of emery papers
- Microstructures of composites
- Worn surfaces evaluation of pin samples
- Worn surfaces evaluation of emery papers
- Wear debris analysis

Figure 3.7 represents the photograph image of X-ray Diffraction (XRD) machine of PANalytical make, Model: X'pert powder, adopted in this study. The XRD study of the samples was done at scan speed of 0.1°/s, using Cu Kα radiation for phase identification. The samples were cleaned with acetone prior to evaluation.

3.3 Density Measurement

The methodology for density measurement was adopted from the reference (Seah *et al*., 1995). The density measurement of the materials was done by using Archimedean method at 27°C room temperature. The initial weight of samples which are freely suspended in air were initially noted by electronic balance. Then the specimens were immersed in water filled in a beaker (pre-set to zero) and corresponding volume rise of water indicated the volume of the specimen. As the specific gravity of water is 1, it can be used as weight of specimen in water. The ratio of initial weight to final weight gives the density of specimen.

$$\rho_{\text{specimen}} = \frac{W1}{W2} = \frac{\text{weight of specimen in air}}{\text{weight of specimen in water}} \tag{3.1}$$

Weight of specimen in water = volume of the specimen

= volume of the displaced water

3.4 Hardness Measurement

The hardness of alloy and composite materials in both as cast and T6 condition was measured by utilizing Vickers hardness tester. The sample surfaces were polished and were made flat prior to testing. The measurements were done at an indentation load of 0.5 kgf for dwell time of 10 seconds and average readings were represented.

$$HV = 1.854\frac{F}{d^2} \tag{3.2}$$

Where, F is force in kgf and d is average length of the diagonal left by the indenter in millimetres.

The importance of the hardness measurement lies not only in the type and level of support between matrix and reinforcement but also the resistance offered to surface deterioration.

3.5 Tensile Test

The universal testing machine (UTM) of Dak system Inc., Model no. UTB9253, Maximum load capacity of 250 kN was used for tensile testing of the materials chosen for the present study. The ASTM B557 is the standard test method of tensile testing of wrought as well as cast aluminium and magnesium alloy products. Fig. 3.8 shows image of tensile test equipment used in this study. Fig. 3.9 (a) shows the schematic sketch of a tensile specimen and Fig. 3.9 (b) shows the photographic image of prepared tensile specimen. The yield strength and ultimate tensile strength was noted.

Figure 3.8: A photograph image of tensile test equipment

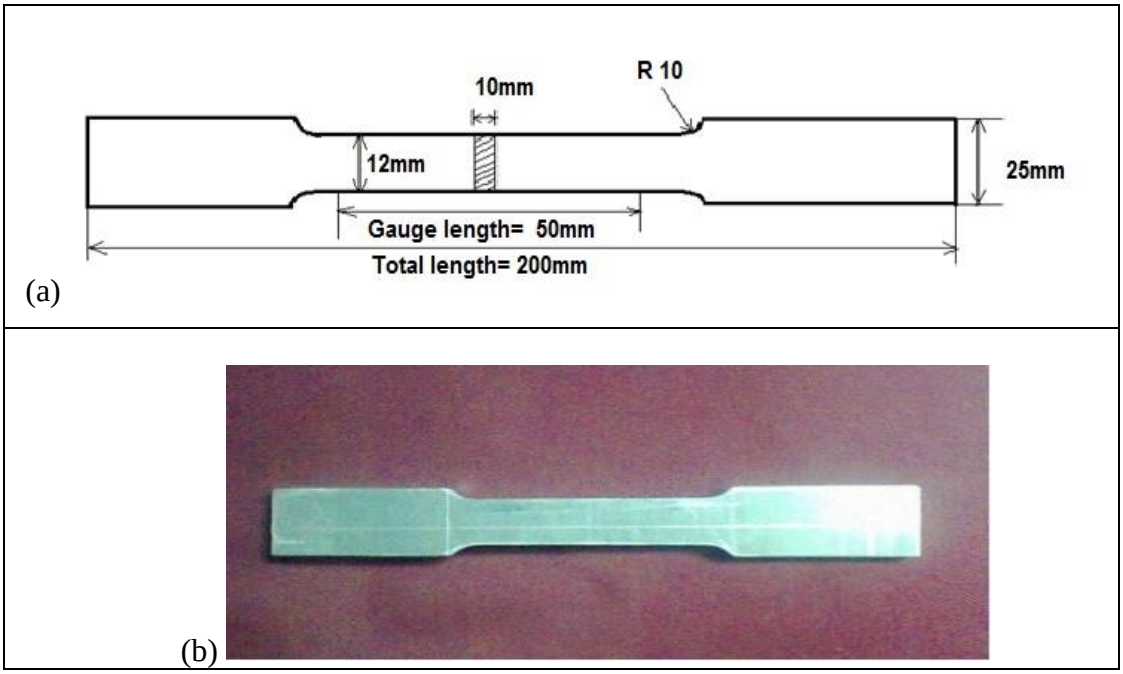

Figure 3.9: (a) A schematic sketch of a tensile specimen (b) A photographic image of tensile specimen

3.6 Two Body Abrasive Wear

The two body abrasive wear tests were done on a pin-on-disc equipment (Magnum make, model: TE-165-SPOD, Bangalore) at applied load of 5-15N, grit size of 100-200µm and 50-75m sliding distance. The wear tests were conducted as per ASTM D6037 standard. The emery paper of silicon carbide type (CUMI make, Muragappa Group, India) was used in the present study. Fig. 3.10 (a) shows the abrasive wear testing of sample, Fig. 3.10 (b) indicate the wear tracks over emery paper and Fig. 3.10 indicate the front view of schematic sketch of pin on disc. The emery paper was sized and bonded over wheel of 70 mm radius, 12 mm thickness. The cleaning of specimens was done with acetone before and after wear tests. The difference in weights of the sample i.e. before and after abrasion testing gives the weight loss of the corresponding pin sample. Fig. 3.11 depicts the two body abrasive wear testing of a pin sample. After abrasion testing, from the measured weight loss, volume loss, the volumetric wear rates, the specific wear rates, wear coefficients and wear depth of material were calculated by using Eq. (3.3), (3.4), (3.5), (3.6), (3.7) and (3.8) respectively.

$$\Delta w = w_i - w_f \tag{3.3}$$

$$\Delta v = \frac{\Delta w}{\rho} \tag{3.4}$$

$$W_v = \frac{\Delta w}{\rho \times S} \tag{3.5}$$

$$W_s = \frac{\Delta w}{\rho \times L \times S} \quad (3.6)$$

$$K = \frac{\Delta w \times H}{\rho \times L \times S} \quad (3.7)$$

$$W_d = \frac{K \times L \times S}{A \times H} \quad (3.8)$$

Where, w_i= initial weight of sample in gm, w_f = final weight of sample in gm, Δw = weight loss in gm, Δv= volume loss in mm^3, ρ = density of material in g/cc, A = cross sectional area of the pin in mm^2, L = applied load in N, S = sliding distance in m, H = hardness of the pin sample in N/mm^2, W_v = volumetric wear rate in mm^3/m, W_s = specific wear rate in mm^3/Nm, K = wear coefficient of the material and W_d= wear depth of the material.

(a)

(b)

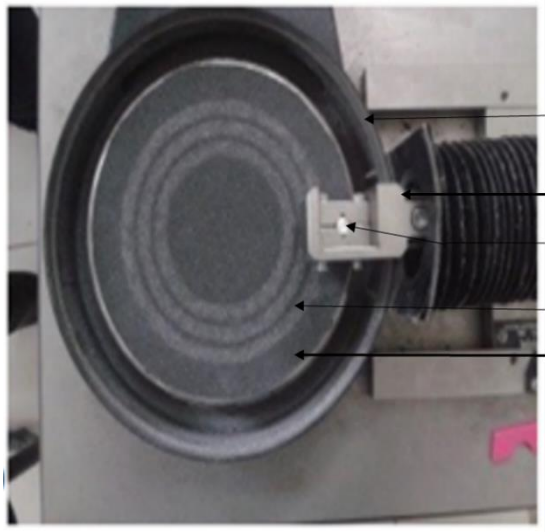

Figure 3.10: (a) A snapshot of abrasive wear testing of sample (b) Wear tracks indication on the emery paper

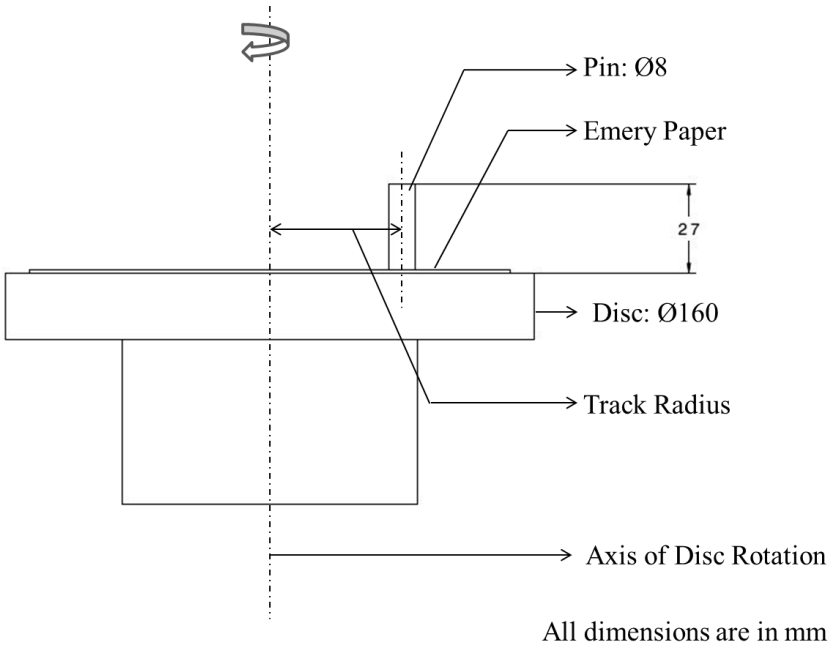

Figure 3.11: A schematic sketch of pin over the disc (in front view).

3.7 Surface Roughness Evaluation

The surface roughness evaluation was done by Taylor Hobson optical profilometer, shown in Fig. 3.12. The lens with 10x magnification and Mirau interferometry method was adopted. Three readings of Ra parameter values were noted at three random surfaces on the wear tested pin sample and the average values were being tabulated. The two dimensional (2D) and three dimensional (3D) surface profiles were also captured and reported.

Figure 3.12: A snapshot of optical profilometer

A brief working principle of non-contact type profilometer is as follows:

- A light beam is split, reflecting from reference and test material.
- Constructive and destructive interference occurs.
- This forms the light and dark bands known as interference fringes.
- The optical path differences are due to height variations in the test surface.
- Constructive interference areas are lighter and the destructive interference areas are darker.

3.8 ANOVA and Regression Equations

The ANOVA and regression equations generation was done from the experimental array generated randomly in coded terms by central composite design (CCD) approach in response surface methodology (RSM) using Design Expert v9 software. Table 3.3 represent the parameters with its corresponding coded terms and levels.

Table 3.3: Parameters with corresponding coded terms and levels

Parameter (units)	Coded term	Level-1	Level-2	Level-3
Load (N)	A	5	10	15
Grit Size (µm)	B	100	125	200
Sliding Distance (m)	C	50	63	75

Table 3.4: Adopted list of experiments in coded terms and uncoded terms without repetition.

Run order	A	B	C	A-Load (N)	B-Grit Size (µm)	C-Sliding Distance (m)
1	-1	-1	-1	5	100	50
2	-1	1	1	5	200	75
3	1	-1	-1	15	100	50
4	1	-1	1	15	100	75
5	-1	0	0	5	125	63
6	1	1	-1	15	200	50
7	-1	-1	1	5	100	75
8	0	0	-1	10	125	50
9	1	1	1	15	200	75
10	0	0	0	10	125	63
11	0	1	0	10	200	63
12	0	0	1	10	125	75
13	0	-1	0	10	100	63
14	1	0	0	15	125	63
15	-1	1	-1	5	200	50

Table 3.4 indicate list of run order experiments in coded terms and uncoded terms without repetition was adopted in this study. The contour and surface plots of the interaction terms were represented for all the materials. The ANOVA was done to know the significance, the percentage influence of each individual parameter and other interaction effects if any contributing in the abrasion wear process. The regression equations indicate the type and level of contribution in wear rate.

CHAPTER-4

RESULTS & DISCUSSION: MORPHOLOGY, MICROSTRUCTURAL AND MECHANICAL PROPERTIES OF MATERIALS

In this chapter, the morphological, microstructural and mechanical properties of matrix alloy and its composites was studied and discussed briefly. The morphological or microstructural studies include the morphology of reinforcements and emery papers, microstructures of matrix alloy and composite materials. The mechanical properties include the density, hardness and tensile characteristics of matrix alloy and its composites.

4.1 Morphology of reinforcements and emery papers

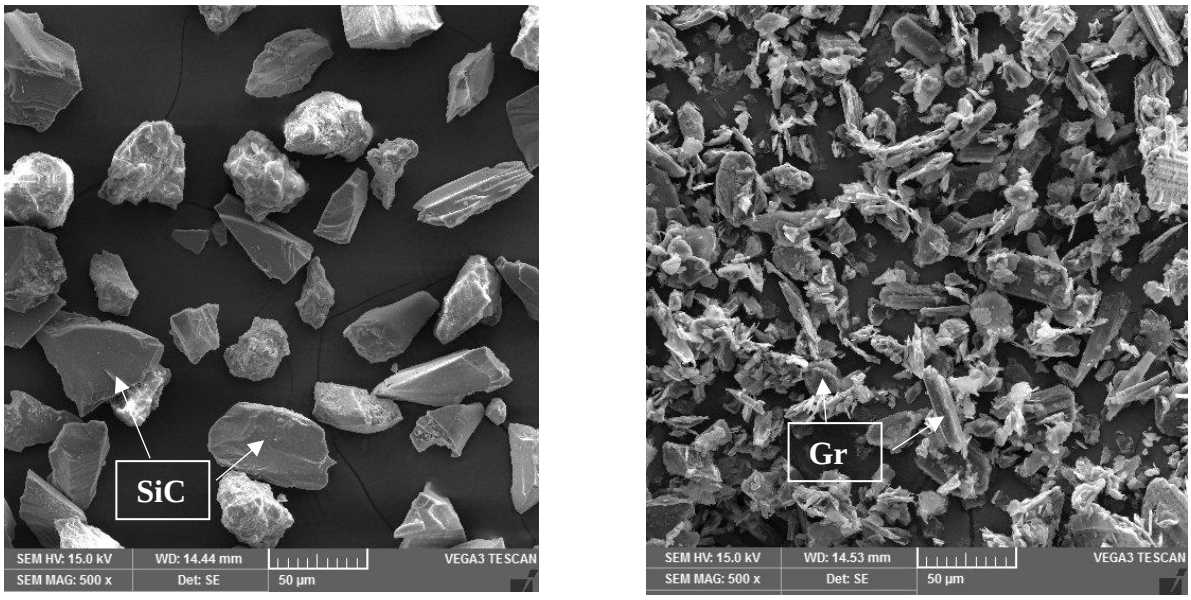

(a) (b)

Figure 4.1: Morphology of reinforcements (a) SiC and (b) Graphite

The morphology of the silicon carbide reinforcement was represented as 'SiC' in Fig. 4.1 (a) and the graphite reinforcement was represented as 'Gr' Fig. 4.1 (b). From the SEM images, it was observed that SiC particles had sharp edges, granular type shape whereas for graphite particle is flaky shaped. As noted from literature review and Fig. 2.8, the type, shape and size of the reinforcements would directly affect the properties of the composite materials. Hence, it was found necessary to understand the basic structure of the reinforcements.

The morphology of emery papers indicating SiC abrasives was shown in Fig. 4.2. Fig. 4.2 (a), (b) and (c) indicate the morphology of 100µm, 125µm and 200µm abrasive grit size emery paper respectively. It was observed that grits on all the emery papers are arranged in discontinuous fashion and are not aligned or oriented in one particular direction. It was noticed that the grits on 100µm grit size emery paper are closer to each other whereas the grits on 200µm grit size emery paper are not closer as compared to earlier. It was understood that the number of grits come in contact with pin surface will be more in 100µm grit size emery paper compared to other two grit size emery papers.

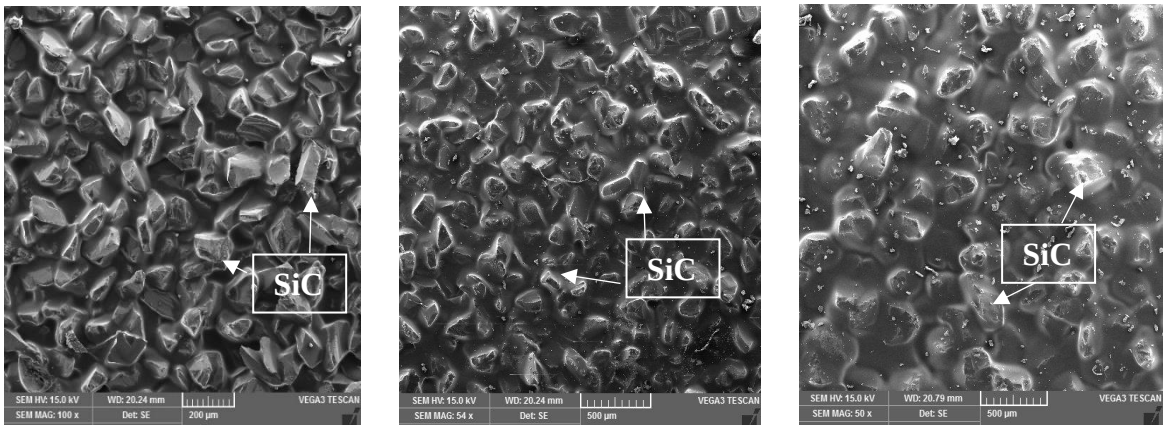

(a) (b) (c)

Figure 4.2: Morphology of (a) 100µm, (b) 125µm and (c) 200µm abrasive grit size emery paper indicating SiC abrasives

4.2 Microstructures of composites and Phase Evaluation

The microstructures of Al 6082 alloy, Al 6082-SiC composite and Al 6082-SiC-Gr hybrid composite was shown in Fig. 4.3.

(a) (b)

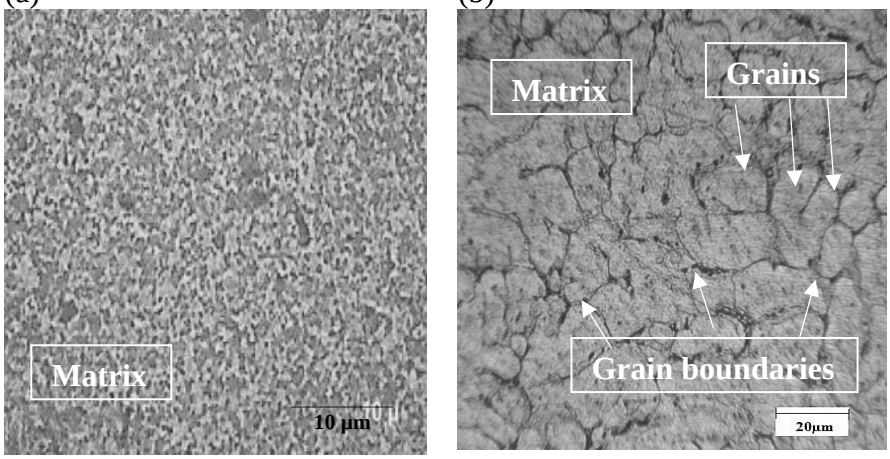

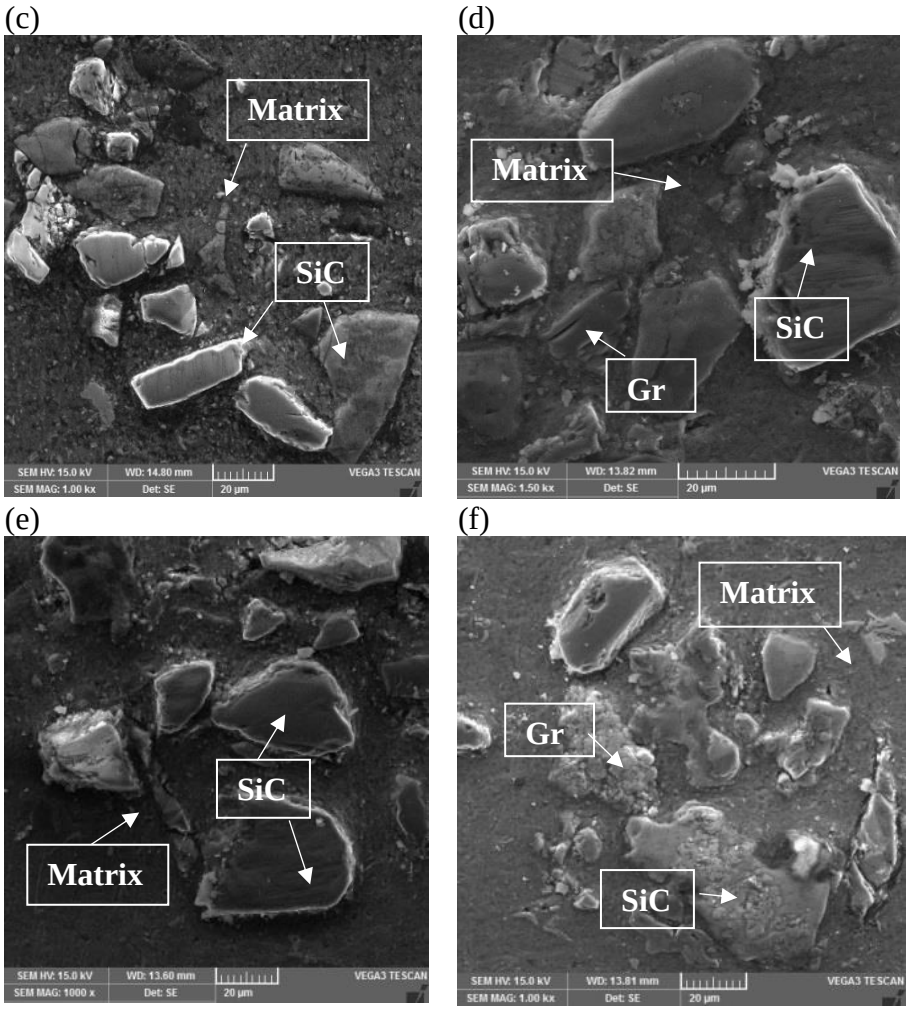

Figure 4.3: Microstructures of (a) Al 6082 alloy in as cast condition (b) Al 6082 alloy in T6 heat treated condition (c) Al 6082-SiC composite in as cast condition (d) Al 6082-SiC-Gr hybrid composite in as cast condition (e) Al 6082-SiC composite in T6 condition (f) Al 6082-SiC-Gr composite in T6 heat treated condition.

Fig. 4.3 (a) and (b) represent the microstructures of matrix alloy with grains and grain boundaries indicated with arrow marks. Fig. 4.3 (c) and (e) represent the microstructures of Al-SiC composite (the SiC reinforcements are indicated with arrow marks). Fig. 4.3 (d) and (f) indicate the microstructures of Al-SiC-Gr hybrid composite (the SiC and Gr reinforcements indicated in arrow marks). It was also observed that some SiC and Gr reinforcements are in angular in shape, some are spherical in shape in the matrix. It was noticed from the preliminary observation that reinforcement particles arranged in random manner and also had a good bond with matrix material.

(a) 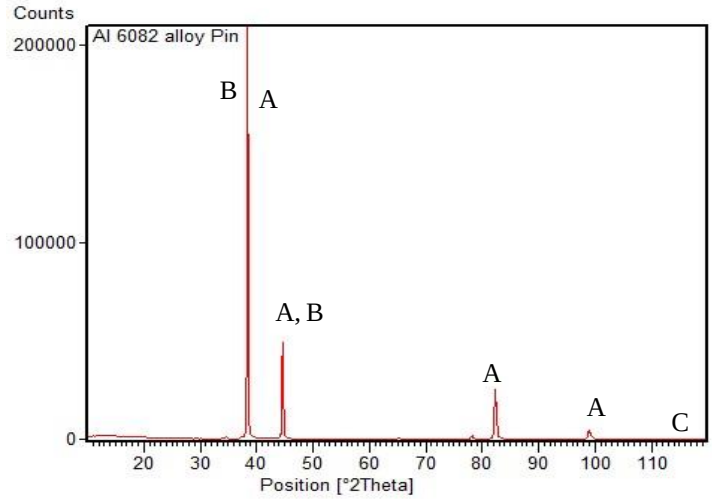 	*Phases identified:* [2θº (d Å)] A: Al:- 38.35º (2.34), 44.5º (2.03), 82.5º (1.17), 99.2º (1.01), 111.8º (0.93) B: Mg_2Si:- 37º (2.42), 44.5º (2.03) C: AlFeSi:- 116.4º (0.9)
(b) 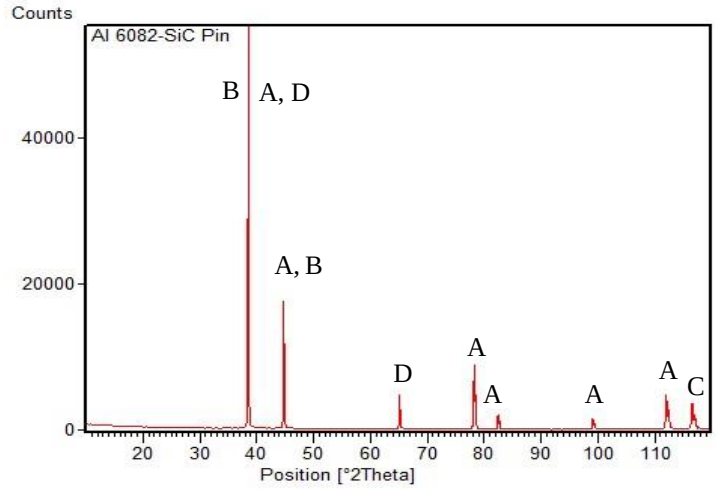 	*Phases identified:* [2θº (d Å)] A: Al:- 38.5º (2.33), 44.7º (2.02), 82.4º (1.17), 99.1º (1.01), 112º (0.93) B: Mg_2Si:- 37.2º (2.41) 44.8º (2.02), C: AlFeSi:- 116.6º (0.9) D: SiC:- 38.5º (2.33), 65.3º (1.43)
(c) 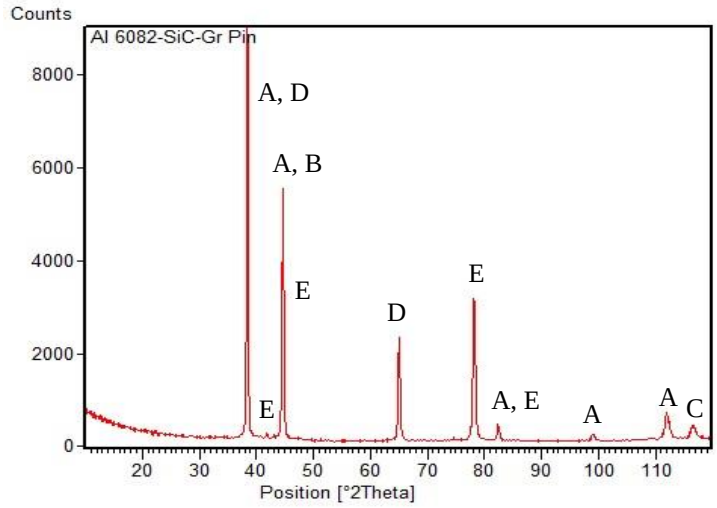 	*Phases identified:* [2θº (d (Å)] A: Al:- 38.4º(2.34), 44.7º (2.02), 82.4º (1.17), 99.1º (1.01) 111.9º (0.93) B: Mg_2Si:- 44.7º (2.02) C: AlFeSi:- 116.5º (0.9) D: SiC:- 38.4º (2.34), 64.9º (1.43) E: Gr :- 41.8º (2.15), 44.6º(2.02), 78.1º(1.22), 82.4º (1.16)

Figure 4.4. XRD images of (a) Al 6082 alloy, (b) Al 6082-SiC and (c) hybrid Al 6082-SiC-Gr composites

Figure 4.4 (a), (b) and (c) shows the XRD images with phase representation for matrix alloy, Al-SiC and hybrid Al-SiC-Gr composites respectively. The peaks for different phases at '2θ' (i.e. diffracted angle) with 'd' (i.e. inter-planar spacing) in brackets was reported. It was noticed that, for matrix alloy the Al, Mg_2Si, AlFeSi (represented with A, B, C respectively in Fig. 4.4 (a)) phases were observed; for Al-SiC composite the Al, Mg_2Si, AlFeSi, SiC (represented with A, B, C, D respectively in Fig. 4.4(b)) phases were observed; and for Al-SiC-Gr hybrid composite the Al, Mg_2Si, AlFeSi, SiC, Gr (represented with A, B, C, D, E respectively in Fig. 4.4(c)) phases were observed.

4.3 Density and Hardness properties of the materials

The density and Vickers hardness of the matrix alloy and its composites were indicated in Table 4.1. The density of the alloy, Al-SiC and Al-SiC-Gr was noted to be 2.7, 2.79 and 2.74 gm/cc respectively. The density of graphite (~2.2 g/cc) is less than that of density of matrix alloy (~2.7 g/cc) and SiC particles (~3.2 g/cc). Consequently the density of hybrid composites will tend to be lower than hard particle reinforced composites.

Table 4.1: Density, Hardness of materials in as cast and T6 condition

Material	**Density** (g/cc)	**Hardness** (HV)	
		AC condition	**T6 condition**
Al6082 alloy	2.7	48±5	57±6
Al6082-10% SiC composite	2.79	61±8	78±7
Al6082-5% SiC-5%Gr composite	2.74	55±6	67±8

From Table 4.1 and Fig. 4.5, in cast condition, the Vickers hardness of matrix alloy with 48HV increased to 61HV and 55HV for Al-SiC composites and Al-SiC-Gr hybrid composites respectively. In T6 heat treated condition, hardness of matrix alloy with 57HV increased to 78HV and 67HV for Al-SiC composites and Al-SiC-Gr hybrid composites respectively. The hardness of the reinforced composites was found to be higher than matrix material. It was observed that due to T6 heat treatment, the hardness improved by 18-30%. This could be generally due to the formation of intermetallic precipitates. But there was 9.8% and 14.1% hardness drop from SiC reinforced composite to hybrid composite in cast and T6 condition respectively. This shows that the graphite addition could not positively contribute to the Al-SiC-Gr hybrid composite. Seah *et al*., (1995) noted that graphite being the soft dispersoid and effective solid lubricant, will ease the grain movement along the slip

planes. Hence this would lead to more deformation of the material during indentation process.

In wear process, the digging out or cracking of the reinforcing phase will depend on the hardness of the matrix. The effect of the reinforcement in wear process gets improved when the matrix becomes harder. The matrix hardness should act not only as an agent to decrease the depth of penetration of abrasive grits on counter surface but also it should provide better support to reinforcing phase. It can observed that in case of Al-MMCs, the hardness in peak aged composites was higher compared to the hardness of under aged and over aged composites (Axen *et al.*, 1994).

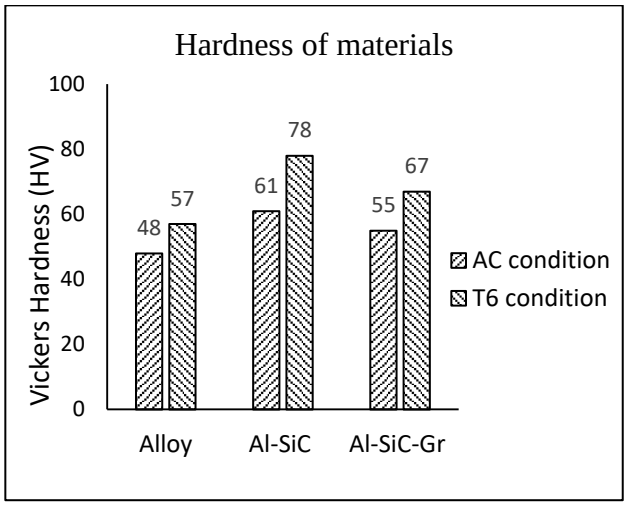

Figure 4.5: The Vickers hardness comparison of materials in as cast and T6 condition

4.4 Tensile properties of the materials

The tensile properties of the materials such as 0.2% proof stress, yield stress, ultimate tensile stress and % elongation was reported and discussed briefly. Fig. 4.6 (a), (c) and (e) shows the stress vs strain curves of Al 6082 alloy, Al 6082-SiC composite and Al 6082-SiC-Gr hybrid composite respectively in cast condition; whereas Fig. 4.6 (b), (d) and (f) shows the stress vs strain curves of Al 6082 alloy, Al 6082-SiC composite and Al 6082-SiC-Gr hybrid composite respectively in T6 condition. Table 4.2 indicate the tensile properties of the materials and a bar chart showing the yield stress and ultimate tensile stress of the materials was represented Fig. 4.7(a) and (b). It was noticed that the addition of SiC reinforcement led to increase in yield strength and ultimate tensile strength. But due to addition of graphite to matrix material reduced the strength property. This could be due to easy movement of grains during plastic flow, attributing to hexagonal rings formed by carbon atoms in graphite (Seah *et al*., 1995).

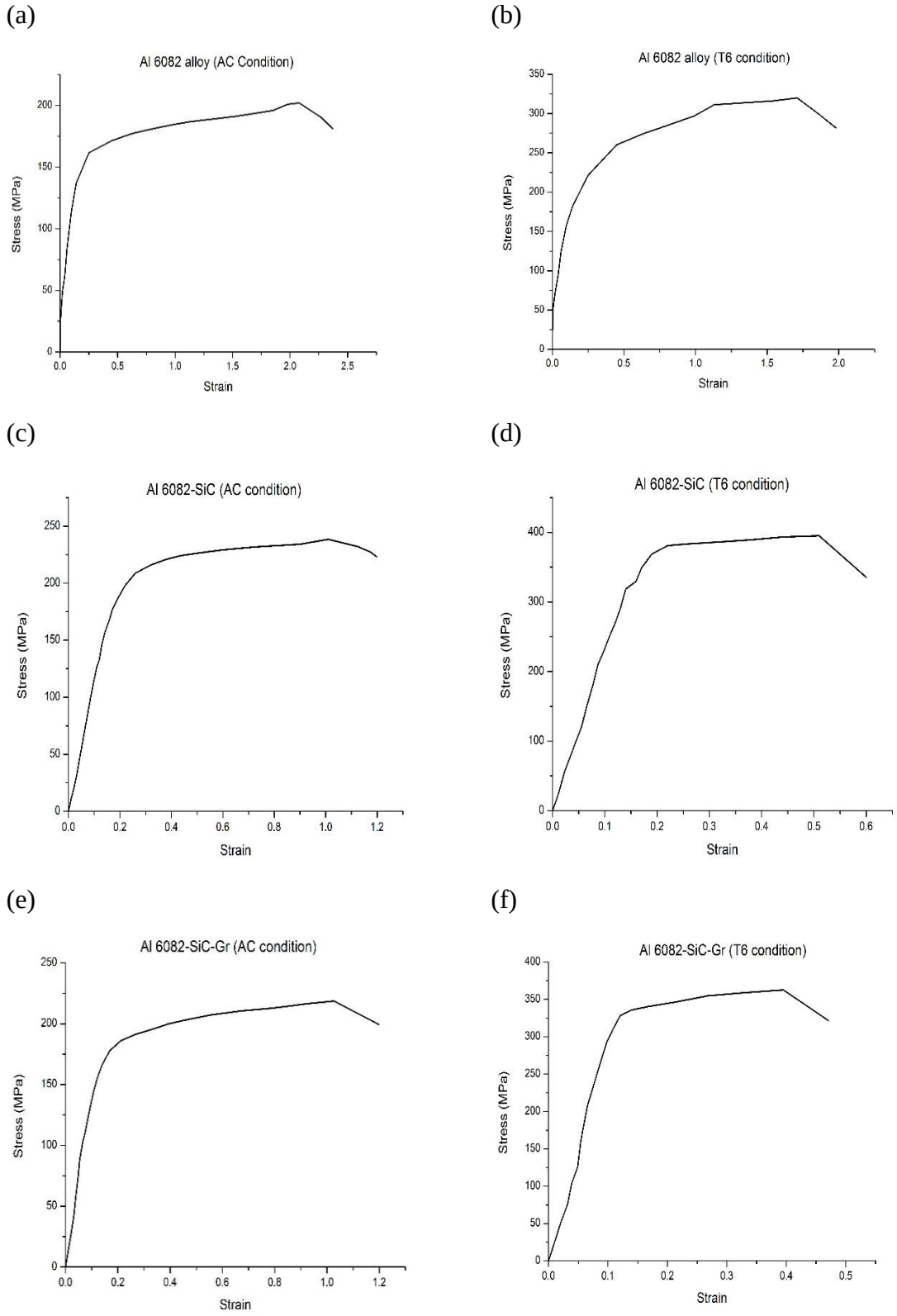

Figure 4.6: Stress Vs strain curves of (a) Al 6082 alloy (AC condition), (b) Al 6082 alloy (T6 condition), (c) Al 6082-SiC composite (AC condition) (d) Al 6082-SiC composite (T6

condition), (e) Al 6082-SiC-Gr composite (AC condition) and (f) Al 6082-SiC-Gr composite (T6 condition)

Table 4.2: Tensile properties of Al 6082 alloy, Al 6082-SiC composite and Al 6082-SiC-Gr hybrid composite in as cast condition and T6 condition.

Material		0.2% Proof stress (MPa)	Yield stress (MPa)	Ultimate tensile stress (MPa)	% Elongation
AC	Al 6082 alloy	120	124	203	10.6
	Al-SiC composite	222	226	239	8
	Al-SiC-Gr hybrid composite	195	204	220	8.2
T6	Al 6082 alloy	268	273	320	9.1
	Al-SiC composite	375	378	395	7.6
	Al-SiC-Gr hybrid composite	335	341	363	8.1

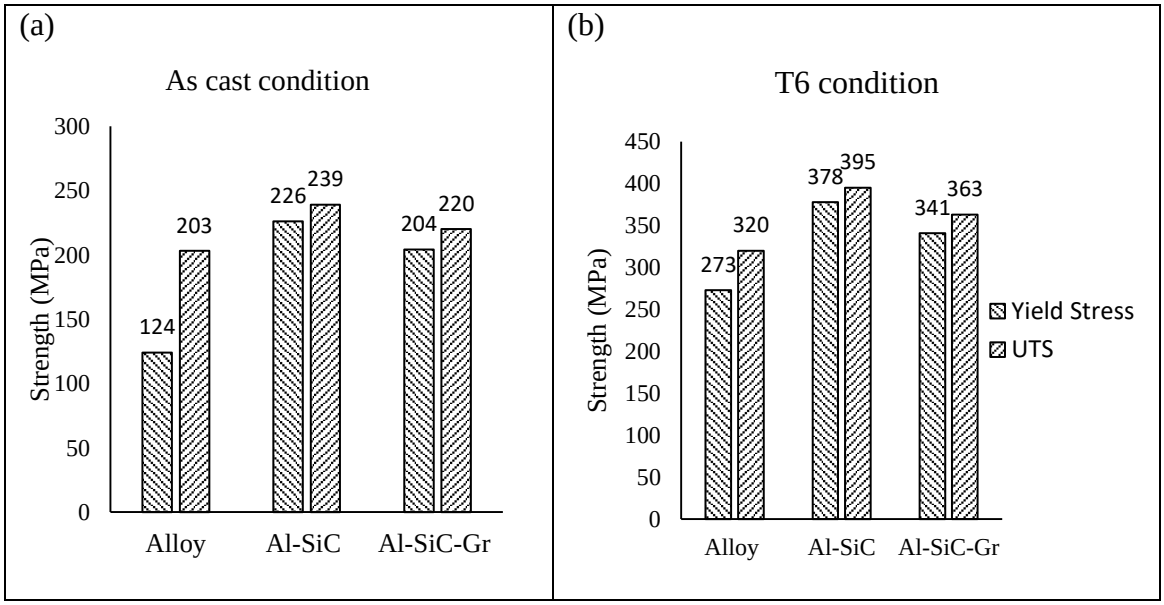

Figure 4.7: The tensile property comparison of matrix alloy and its composite materials in (a) as cast condition (b) T6 condition

The SEM analysis of the fracture surfaces of the tensile samples of matrix alloy had small dimples and tear ridges associated with ductile type failure. These tear ridges are fine, near featureless and non-circular type dimples. Fig. 4.8 shows the morphology of tensile fracture surfaces of matrix alloy and composites. Fig. 4.8 (a) and (b) indicate the morphology of tensile fracture surfaces Al 6082 alloy; Fig. 4.8 (c) and (d) indicate the morphology of tensile fracture surfaces of Al 6082-SiC composites; Fig. 4.8 (e) and (f) indicate the morphology of tensile fracture surfaces Al 6082-SiC-Gr composites. In case of

composites, the cracked or fractured reinforcing particles are often present on the surface (as noted in Fig. 4.8 (c)-(f) and Fig. 4.9), especially when the high intensity of load transfer from plastically deforming matrix material. Sometimes, the fracture surfaces showed the debonding of matrix phase and reinforced particles, indicating that weak interfacial bond strength during casting process. This can be attributed when the low matrix flow stresses are persisting, the matrix will try accommodate itself the local strains formed.

Fig. 4.9 (a) shows the crack propagation through SiC particle (indicated with arrow marks) after tensile testing whereas Fig. 4.9 (b) indicate the fracture and debonding with matrix material at the interface (as indicated with arrow marks). The defects and cracks that are originated during casting process will be often present on the fracture surfaces of the samples, but these were rarely observed on the fracture surfaces. These defects could be formed during casting or solidification or cooling from the higher temperature.

(a) (b)

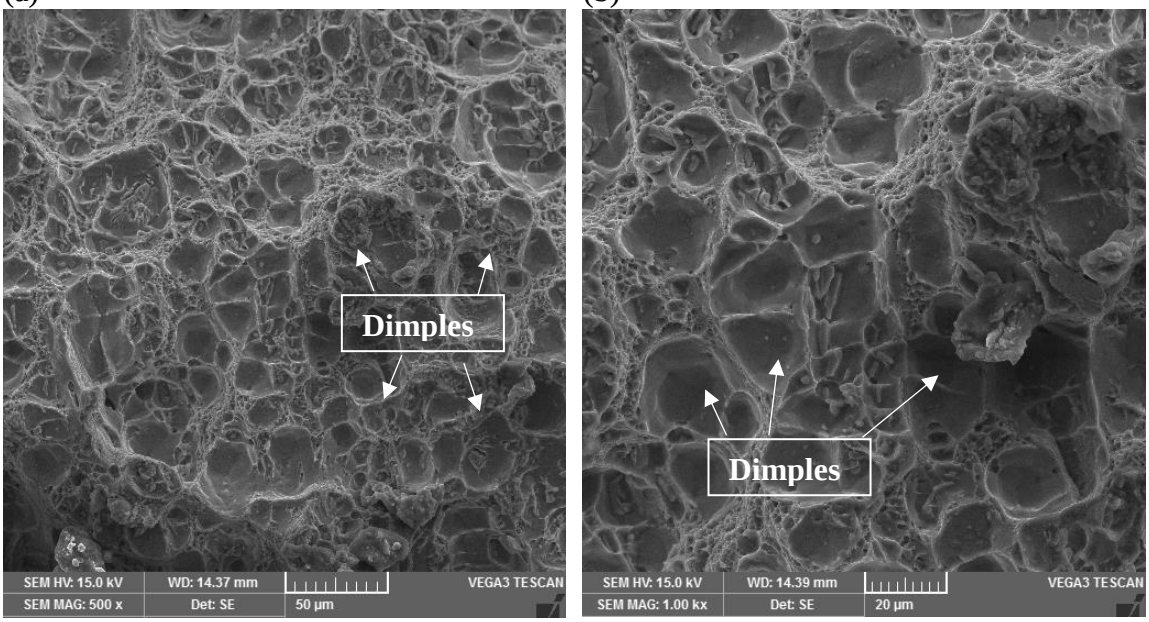

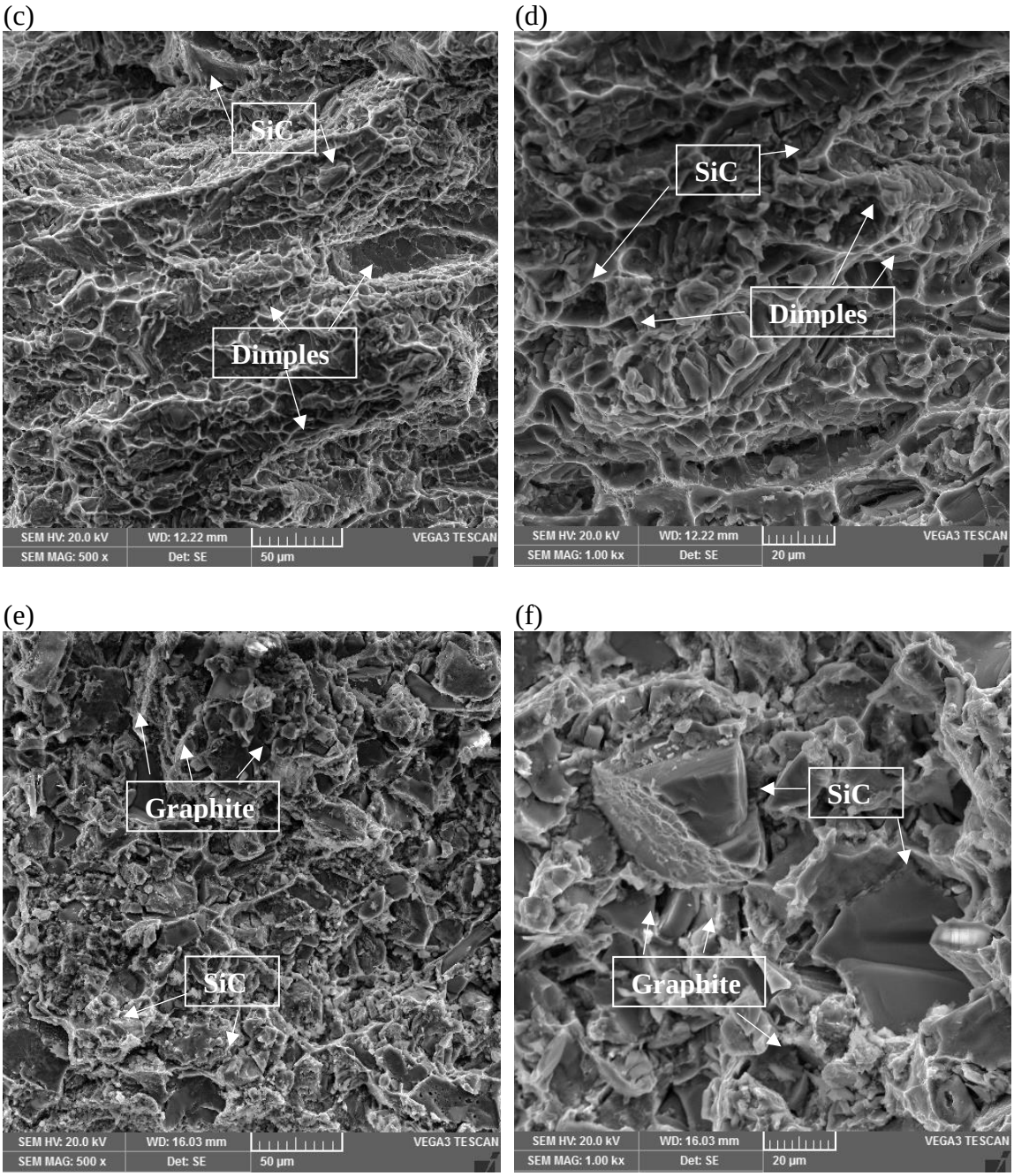

Figure 4.8: Morphology of tensile fracture surfaces of (a) and (b) Al 6082 alloy; (c) and (d) Al 6082-SiC composite; (e) and (f) Al 6082-SiC-Gr composite

(a)

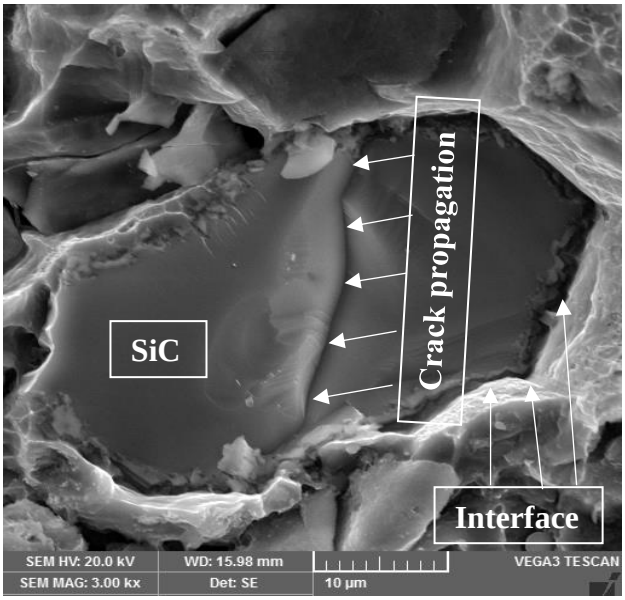

(b)

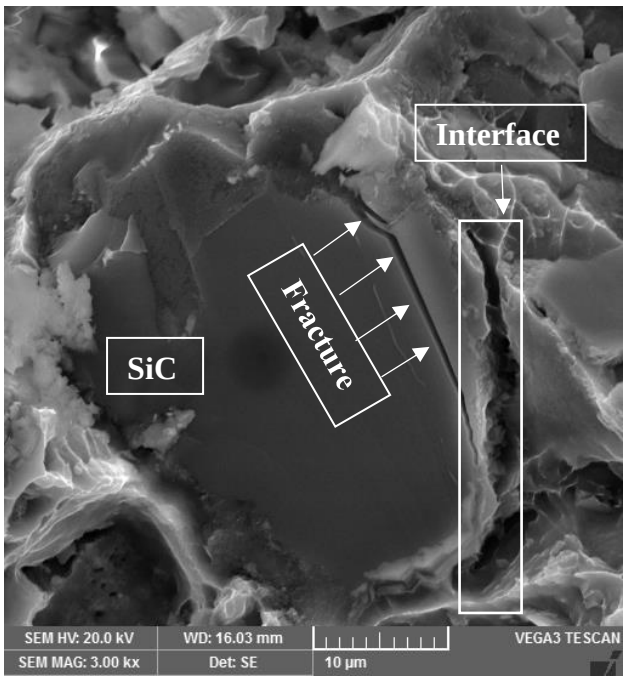

Figure 4.9: Morphology of SiC particle after tensile testing (a) Crack propagation, (b) Fracture and debonding with matrix material at the interface.

CHAPTER-5

RESULTS & DISCUSSION: TWO BODY ABRASIVE WEAR CHARACTERISTICS OF MATERIALS

In this chapter, the two body abrasive wear characteristics of the materials in as cast and T6 conditions were studied as a function of applied load, grit size and sliding distance. The effect of wear parameters on wear rate, relative wear resistance, wear coefficients and wear depth was also studied and presented. Finally, in this chapter the investigation on worn surfaces of pin samples, emery papers and wear debris was done to understand the possible wear mechanisms in abrasive wear process and the same was represented.

5.1 Wear Rate

The volumetric wear rate of the materials in as cast condition and T6 condition was calculated from wear (or weight loss) data after the tests and the same reported in the following Table 5.1. The effect of applied load, grit size and sliding distance on volumetric wear rate was discussed briefly and separately in following sub sections.

Table 5.1: The details of test combinations and corresponding volumetric wear rate of the materials obtained.

Load (N)	Grit size (µm)	Sliding distance (m)	Vol. Wear rate, W_v (mm^3/m)					
			As cast condition			T6 heat treated condition		
			Alloy	Al-10SiC	Al-5SiC-5Gr	Alloy	Al-10SiC	Al-5SiC-5Gr
5	200	50	0.7370	0.5362	0.3964	0.5393	0.4552	0.3066
5	200	63	0.7743	0.6048	0.4663	0.6238	0.5194	0.3621
5	200	75	0.8035	0.6208	0.4968	0.6405	0.5496	0.4793
5	125	50	0.6622	0.5211	0.4445	0.4504	0.3749	0.2540
5	125	63	0.6755	0.5706	0.5092	0.4703	0.4159	0.3995
5	125	75	0.6899	0.5916	0.5217	0.5081	0.4655	0.4151
5	100	50	0.5889	0.4409	0.3818	0.3748	0.3047	0.2715
5	100	63	0.6099	0.4990	0.4389	0.4650	0.3402	0.2624
5	100	75	0.6133	0.5166	0.4496	0.4800	0.3565	0.3066
10	200	50	1.1933	1.0349	0.8956	0.9778	0.7312	0.4892
10	200	63	1.1899	1.0633	0.9877	1.0494	0.7487	0.5550
10	200	75	1.2025	1.1360	1.0511	1.0810	0.8225	0.6297
10	125	50	0.9615	0.8502	0.7438	0.7859	0.6373	0.4328
10	125	63	0.9865	0.8904	0.8551	0.8083	0.6571	0.5202

10	125	75	1.0874	0.9128	0.8934	0.8286	0.6925	0.5669
10	100	50	0.8615	0.6803	0.6599	0.6919	0.5720	0.3321
10	100	63	0.9189	0.7322	0.6674	0.7061	0.5888	0.4061
10	100	75	0.9378	0.7570	0.6759	0.7348	0.6022	0.4803
15	200	50	1.4615	1.2789	1.1774	1.2178	0.9784	0.7686
15	200	63	1.4703	1.3045	1.2247	1.2422	0.9928	0.7601
15	200	75	1.4998	1.3257	1.2535	1.3072	1.1069	0.9539
15	125	50	1.1681	1.0559	0.9993	1.0341	0.8867	0.6934
15	125	63	1.1728	1.0747	1.0057	1.0635	0.9279	0.7108
15	125	75	1.2474	1.0925	1.0263	1.0854	0.9462	0.7338
15	100	50	1.0415	0.8817	0.7803	0.9081	0.7785	0.6263
15	100	63	1.0658	0.9171	0.8348	0.9218	0.7937	0.5498
15	100	75	1.0825	0.9429	0.8696	0.9422	0.8582	0.6889

5.1.1 Effect of applied load

Fig. 5.1 shows the two body abrasive wear rate of the cast materials plotted as a function of applied load at different sliding distance of 50-75m and constant grit size of 200 µm. Fig. 5.1 (a) shows the wear rate of Al 6082 alloy, Al 6082-SiC composite and Al 6082-SiC-Gr hybrid composite was found to be 0.737 mm^3/m, 0.5362 mm^3/m and 0.3964 mm^3/m respectively, at an applied load of 5N and 50 m sliding distance. The percentage improvement of wear rate is around 27.2 and 46.2 for Al-SiC and Al-SiC-Gr respectively. At 15N load, the wear rate of Al 6082 alloy, Al 6082-SiC hybrid composite and Al 6082-SiC-Gr composite was found to be 1.4615 mm^3/m, 1.2789 mm^3/m and 1.1774 mm^3/m respectively. The wear rate decreased around 12.5% and 19.4% for Al-SiC and Al-SiC-Gr respectively. Fig. 5.1 (b) shows at an applied load of 5N and sliding distance of 63m, the wear rate of Al 6082 alloy, Al 6082-SiC composite and Al 6082-SiC-Gr hybrid composite was found to be 0.7743 mm^3/m, 0.6048 mm^3/m and 0.4663 mm^3/m respectively. The wear rate improvement was around 21.9% and 39.8% for Al-SiC and Al-SiC-Gr respectively. The wear rate of Al 6082 alloy, Al 6082-SiC composite and Al 6082-SiC-Gr hybrid composite was found to be 1.4703 mm^3/m, 1.3045 mm^3/m and 1.2247 mm^3/m respectively at 15N load. The improvement in wear rate of Al-SiC and Al-SiC-Gr composites was around 11.3% and 16.7% respectively. Fig. 5.1 (c) shows that at 5N load and 75m sliding distance, the wear rate of Al 6082 alloy, Al 6082-SiC composite and Al 6082-SiC-Gr hybrid composite was found to be 0.8035 mm^3/m, 0.6208 mm^3/m and 0.4968 mm^3/m respectively. The percentage improvement of wear rate is around 22.7 and 38.2 for Al-SiC and Al-SiC-Gr respectively. But at 15N load, the wear rate of Al 6082 alloy, Al 6082-SiC composite and Al 6082-SiC-Gr hybrid composite was found to be 1.4998 mm^3/m, 1.3257 mm^3/m and

1.2535 mm^3/m respectively. The percentage decrease in wear rate of Al-SiC and Al-SiC-Gr composites was around 11.6 and 16.4 respectively.

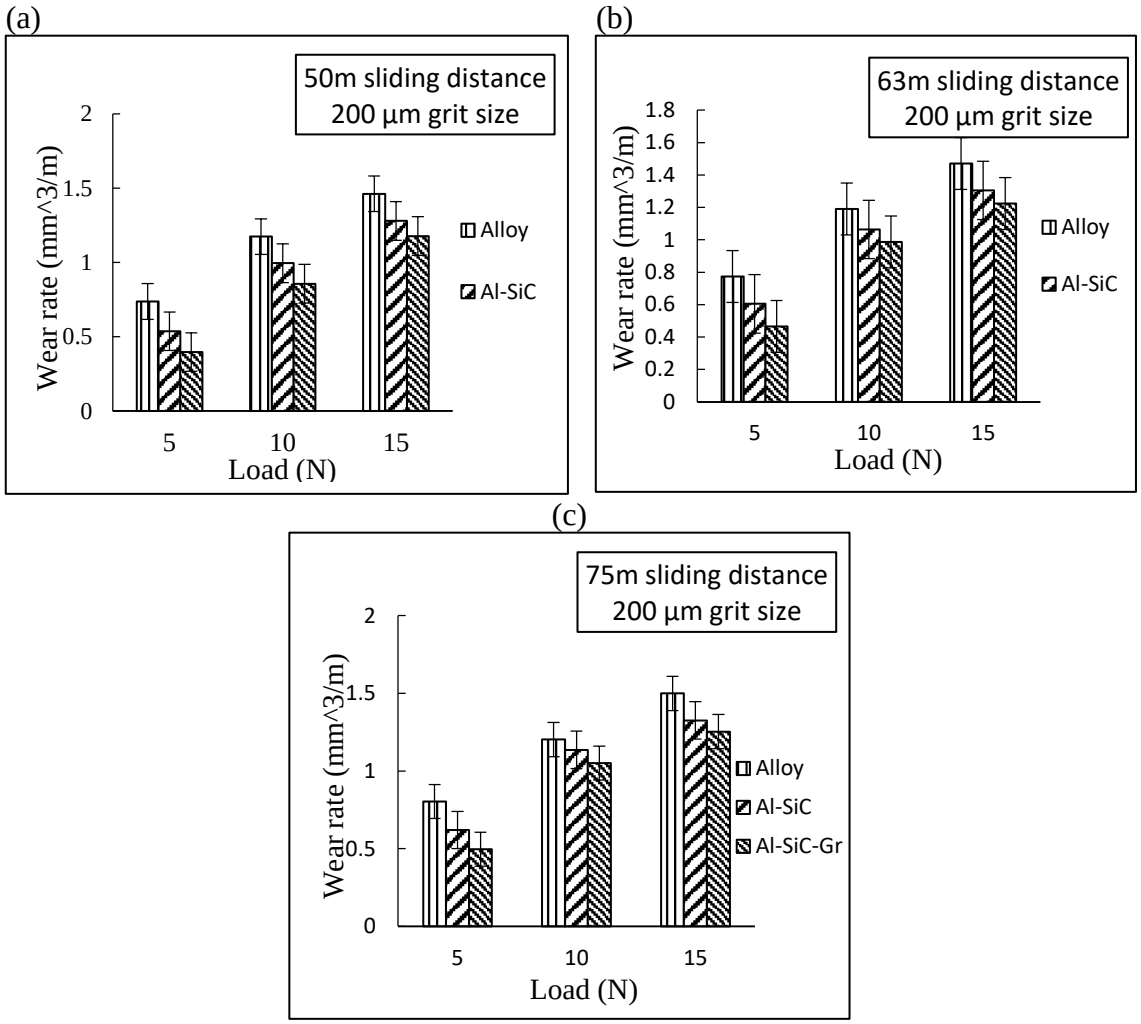

Figure 5.1: Variation of wear rate of cast alloy and its composites at an applied load of 5N-15N, abrasive grit size of 200µm and sliding distance of (a) 50m (b) 63m and (c) 75m.

Fig. 5.2 shows the two body abrasive wear rate of the T6 heat treated materials plotted as a function of applied loads at different sliding distances of 50-75m at constant grit size of 200µm. The wear rate of Al 6082 alloy, Al 6082-SiC composite and Al 6082-SiC-Gr hybrid composite was found to be 0.5393 mm^3/m, 0.4552 mm^3/m and 0.3066 mm^3/m respectively in Fig. 5.2 (a) at an applied load of 5N load and sliding distance of 50m. The percentage improvement of wear rate was around 15.6 and 43.1 for Al-SiC and Al-SiC-Gr composite respectively. At 15N load, the wear rate of Al 6082 alloy, Al 6082-SiC composite and Al 6082-SiC-Gr hybrid composite was found to be 1.2178 mm^3/m, 0.9784 mm^3/m and 0.7686 mm^3/m respectively. The percentage improvement of wear rate is around 19.6 and 36.9 for Al-SiC and Al-SiC-Gr respectively. Fig. 5.2 (b) shows that at 5N

load and 63m sliding distance, the wear rate of Al 6082 alloy, Al 6082-SiC composite and Al 6082-SiC-Gr hybrid composite was found to be 0.6238 mm^3/m, 0.5194 mm^3/m and 0.3621 mm^3/m respectively. The decrease in wear rate was around 16.7% and 41.9% for Al-SiC and Al-SiC-Gr composites respectively. The wear rate of Al 6082 alloy, Al 6082-SiC composite and Al 6082-SiC-Gr hybrid composite was found to be 1.2422 mm^3/m, 0.9928 mm^3/m and 0.7601 mm^3/m respectively at 15N load. The percentage decrease of wear rate of Al-SiC and Al-SiC-Gr composites was around 20.1 and 38.8 respectively.

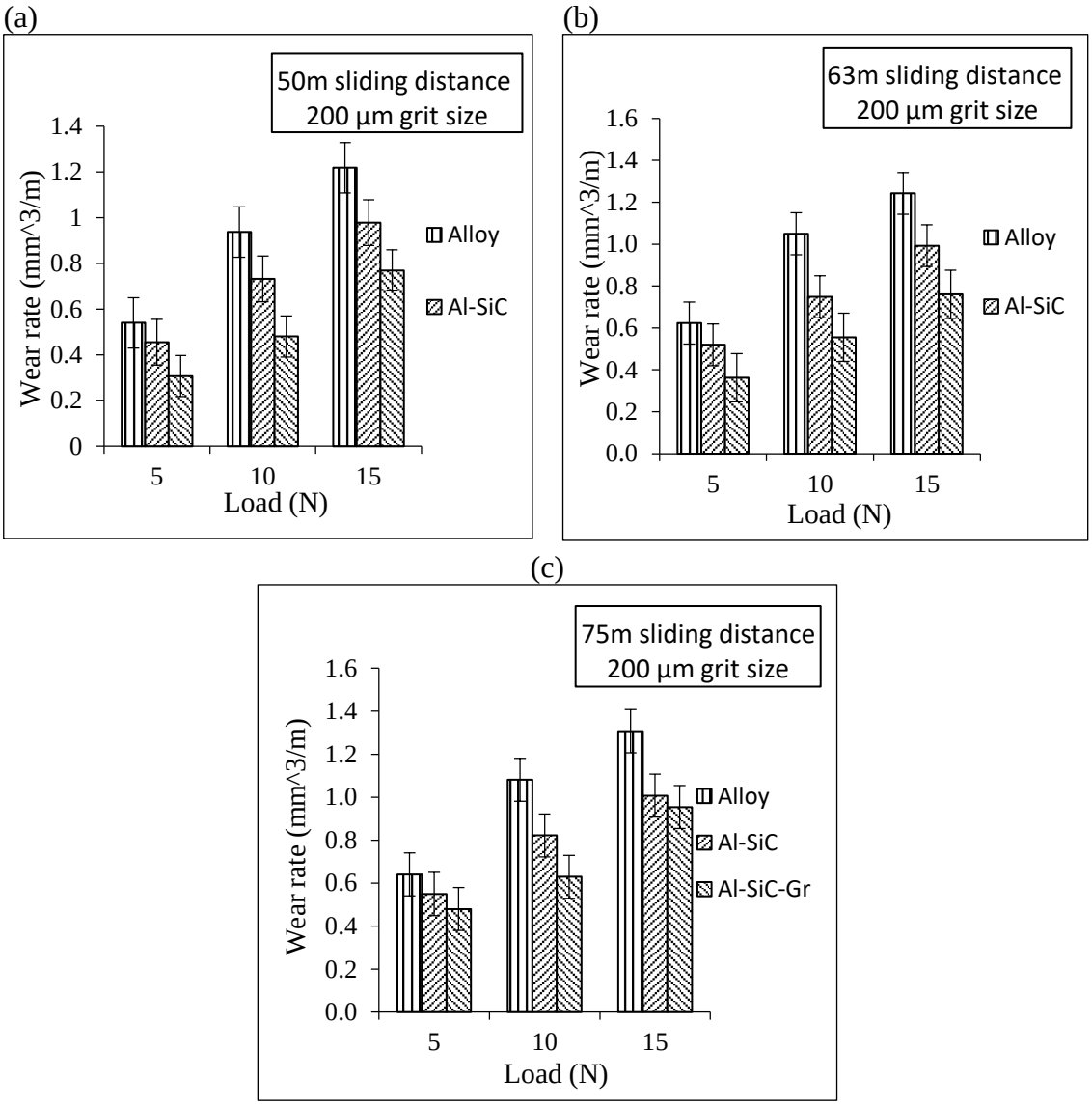

Figure 5.2: Variation of wear rate of T6 heat treated alloy and its composites at an applied load of 5N-15N and abrasive grit size of 200µm and sliding distance of (a) 50m (b) 63m and (c) 75m.

The rate of wear is for Al 6082 alloy, Al 6082-SiC composite and Al 6082-SiC-Gr hybrid composite was found to be 0.6405 mm^3/m, 0.5496 mm^3/m and 0.4793 mm^3/m respectively

at an applied load of 5N and sliding distance of 75m in Fig. 5.2 (c). The percentage decrease in wear rate was around 14.2 and 25.2 for Al-SiC and Al-SiC-Gr respectively. At 15N load, the wear rate of Al 6082 alloy, Al 6082-SiC composite and Al 6082-SiC-Gr hybrid composite was found to be 1.3072 mm^3/m, 1.0069 mm^3/m and 0.9539 mm^3/m respectively. The percentage improvement of wear rate is around 22.9 and 27 for Al-SiC and Al-SiC-Gr respectively.

Banerji *et al*., (1982) evaluated the wear rate with respect to load at different passes and stated that wear rate increased with load for all passes. In the present case, it was understood that, as applied load increases, the pressure in between the pin sample and grits on emery paper increases, leading to increase in the wear rate for all the materials in both as cast and T6 conditions. Similar trends were also observed in research work carried by Zyongi *et al*., (1991), Aziz *et al*., (2006) and Yigezu *et al*., (2013). The addition of SiC to matrix alloy enhanced the resistance to wear compared to matrix alloy. But the hybrid Al-SiC-Gr composites exhibited superior resistance to wear compared to matrix alloy and Al-SiC composites. Due to T6 condition, the wear of the materials was lowered when compared to as cast condition due to formation of intermetallic precipitates and stronger bond between reinforcement and matrix material. The effect of T6 heat treatment proved to be beneficial in improvement of wear properties (Lin *et al*., 1988). The effect of applied load on the pin samples and emery papers was also discussed through worn surface examination as represented in Fig. 5.20 and Fig. 5.22.

5.1.2 Effect of grit size

Fig.5.3 shows the two body abrasive wear rate of the cast materials was plotted as a function of grit size at different applied loads and constant sliding distance of 75m. Fig. 5.3 (a) shows that at 5N load and 200µm grit size, the wear rate of Al 6082 alloy, Al 6082-SiC composite and Al 6082-SiC-Gr hybrid composite was found to be 0.8036 mm^3/m, 0.6608 mm^3/m and 0.5684 mm^3/m respectively. The percentage improvement of wear rate is around 17.7 and 29.3 for Al-SiC and Al-SiC-Gr respectively. At 100µm grit size, the wear rate of Al 6082 alloy, Al 6082-SiC composite and Al 6082-SiC-Gr hybrid composite was found to be 0.6133 mm^3/m, 0.5166 mm^3/m and 0.4496 mm^3/m respectively. The decrease in wear rate was around 15.8% and 26.7% for Al-SiC and Al-SiC-Gr respectively. Fig. 5.3 (b) depicts that at 10N load and 200µm grit size, the wear rate of Al 6082 alloy, Al 6082-SiC composite and Al 6082-SiC-Gr hybrid composite was found to be 1.2025 mm^3/m, 1.1359 mm^3/m and 1.0511 mm^3/m respectively. The percentage decrease in wear rate for

Al-SiC and Al-SiC-Gr was around 5.5 and 12.6 respectively. It is to be noted (Fig. 5.3 (b)) that for 100µm grit size, the wear rate of Al 6082 alloy, Al 6082-SiC hybrid composite and Al 6082-SiC-Gr composite was found to be 0.9378 mm^3/m, 0.7570 mm^3/m and 0.6759 mm^3/m respectively. The percentage improvement of wear rate is around 19.3 and 27.9 for Al-SiC and Al-SiC-Gr respectively.

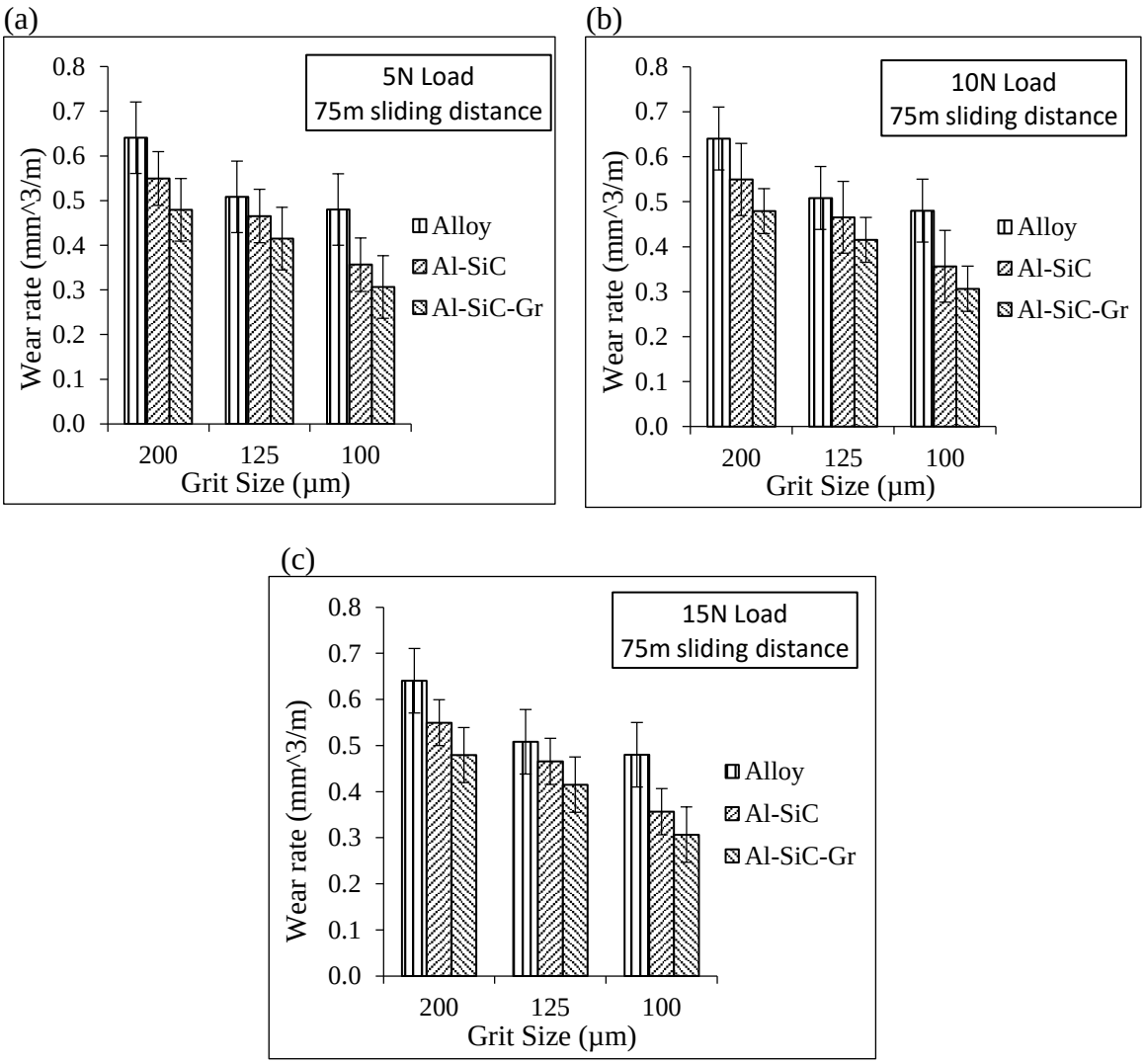

Figure 5.3: Variation of wear rate of cast alloy and its composites at abrasive grit size 100µm to 200µm, 75m sliding distance and applied load of (a) 5N (b) 10N and (c) 15N.

At an applied load of 15N and 200µm grit size, the wear rate of Al 6082 alloy, Al 6082-SiC composite and Al 6082-SiC-Gr hybrid composite was found to be 1.4998 mm^3/m, 1.3257 mm^3/m and 1.2539 mm^3/m respectively (Fig. 5.3 (c)). The percentage improvement of wear rate is around 11.6 and 16.4 for Al-SiC and Al-SiC-Gr respectively. The wear rate of Al 6082 alloy, Al 6082-SiC composite and Al 6082-SiC-Gr hybrid composite was found to be 1.0825 mm^3/m, 0.9429 mm^3/m and 0.8696 mm^3/m respectively when tested on 100µm

grit size. The wear rate improvement of Al-SiC and Al-SiC-Gr composites around 12.9% and 19.6% respectively.

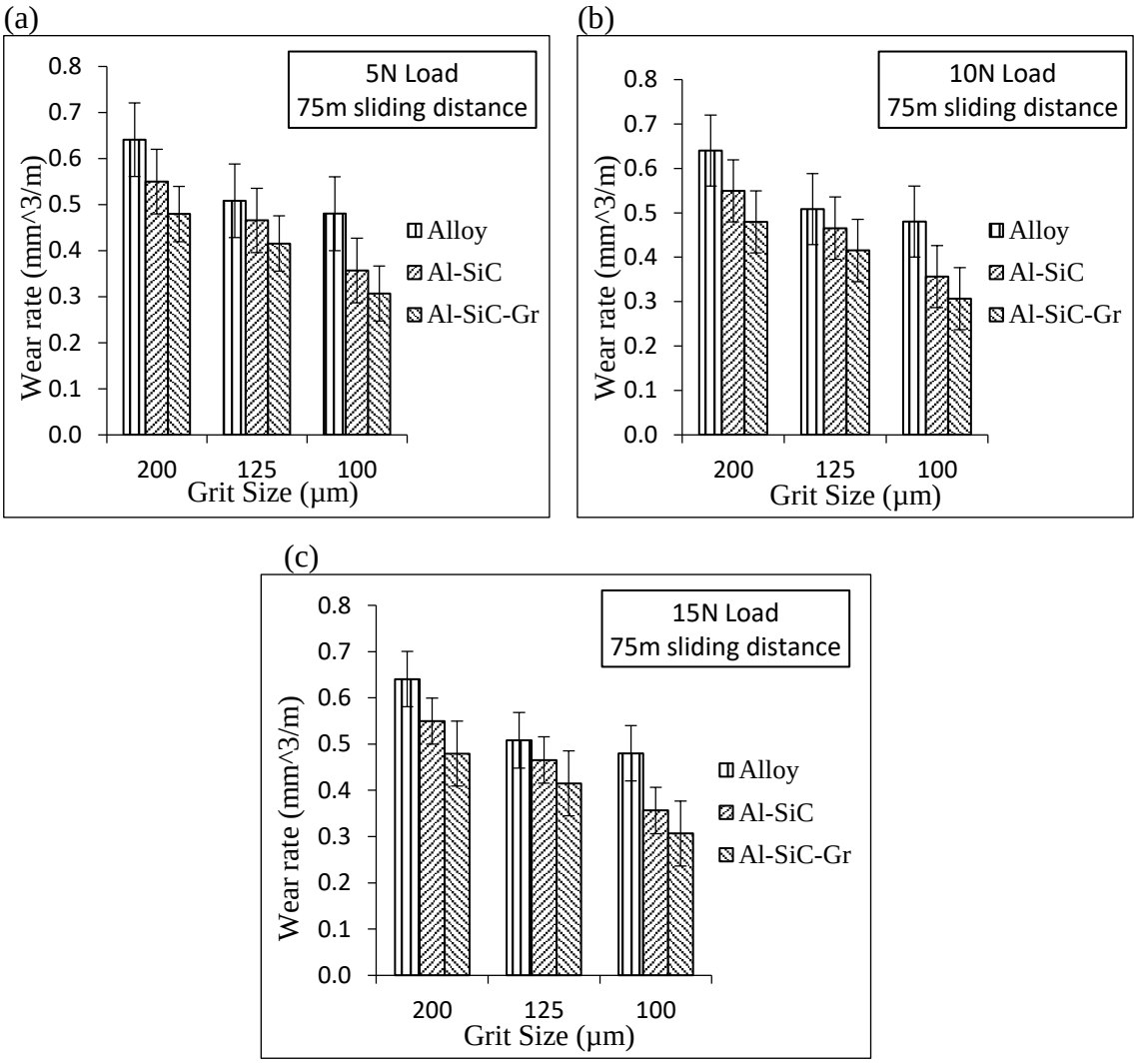

Figure 5.4: Variation of wear rate of T6 heat treated alloy and its composites at abrasive grit size of 100µm to 200µm, 75m sliding distance and applied load of (a) 5N (b) 10N and (c) 15N.

Fig. 5.4 shows the two body abrasive wear rate of the T6 heat treated materials was plotted as a function of grit size at different loads and constant sliding distance of 75m. It is to be noted from the Fig. 5.4 (a) that at 5N load and 200µm grit size, the wear rate of Al 6082 alloy, Al 6082-SiC composite and Al 6082-SiC-Gr hybrid composite was found to be 0.6405 mm^3/m, 0.5496 mm^3/m and 0.4793 mm^3/m respectively. The percentage improvement of wear rate was around 12.6 and 25.2 for Al-SiC and Al-SiC-Gr respectively. It was observed from (Fig. 5.4 (a)), the wear rate of Al 6082 alloy, Al 6082-SiC composite and Al 6082-SiC-Gr hybrid composite was found to be 0.48 mm^3/m, 0.3565 mm^3/m and

0.3066 mm^3/m respectively when tested on 100 µm grit size. The wear rate improved around 25.7% and 36.1% for Al-SiC and Al-SiC-Gr composites respectively. It is to be observed from the Fig. 5.4 (b) that at 10N load and 200µm grit size, the wear rate of Al 6082 alloy, Al 6082-SiC composite and Al 6082-SiC-Gr composite was found to be 1.0810 mm^3/m, 0.8225 mm^3/m and 0.6297 mm^3/m respectively. The improvement of wear rate for Al-SiC and Al-SiC-Gr composites was around 23.9% and 41.7% respectively. At 100µm grit size, the wear rate of Al 6082 alloy, Al 6082-SiC composite and Al 6082-SiC-Gr hybrid composite was found to be 0.7348 mm^3/m, 0.6022 mm^3/m and 0.4803 mm^3/m respectively. The percentage decrease in wear rate was around 18 and 34.6 for Al-SiC and Al-SiC-Gr respectively. At 15N load and 200µ grit size, the wear rate of Al 6082 alloy, Al 6082-SiC composite and Al 6082-SiC-Gr hybrid composite was found to be 1.3072 mm^3/m, 1.0069 mm^3/m and 0.9539 mm^3/m respectively (indicated in Fig. 5.4 (c)). The improvement of wear rate in percentage was around 22.9 and 27 for Al-SiC and Al-SiC-Gr respectively. The wear rate of Al 6082 alloy, Al 6082-SiC composite and Al 6082-SiC-Gr hybrid composite was found to be 0.9422 mm^3/m, 0.8582 mm^3/m and 0.6889 mm^3/m respectively at 100µm grit size. The decrease in wear rate for Al-SiC and Al-SiC-Gr composites was around 8.9% and 26.9% respectively.

From the above results it was noticed that, as grit size increases, the penetration into the pin sample increases, the wear rate of both as cast and T6 condition materials increased (Banerji *et al.*, 1988, Wang *et al.*, 1989, Wang *et al.*, 1991 and Sahin *et al.*, 2003). It can be noticed that, the Al-SiC composites showed higher resistance to wear compared to matrix alloy, whereas the addition of both SiC and Gr reinforcement to matrix alloy enhanced the wear resistance further compared to matrix alloy and Al-SiC composites. As reported earlier, the wear rate of the materials in T6 condition was improved further compared to materials in as cast condition, due to interface bond between reinforcement and matrix strengthening through intermetallic precipitation in the matrix material (Zyongi *et al.*, 1991, Lin *et al.*, 1988). The grit size effect on the emery papers and pins can be well understood through SEM evaluation of worn surfaces. This was presented in Fig. 5.21 and Fig. 5.22 and related discussion was briefly reported.

5.1.3 Effect of sliding distance

Fig. 5.5 shows the two body abrasive wear rate of the as cast materials was plotted as a function of sliding distance at different loads and constant grit size of 200µm. Fig. 5.5 (a) shows that at 5N load and 50m sliding distance, the wear rate of Al 6082 alloy, Al 6082-

SiC composite and Al 6082-SiC-Gr hybrid composite was found to be 0.7370 mm^3/m, 0.5262 mm^3/m and 0.3964 mm^3/m respectively. The percentage improvement of wear rate is around 28.6 and 46.2 for Al-SiC and Al-SiC-Gr respectively. At 75m sliding distance, the wear rate of Al 6082 alloy, Al 6082-SiC composite and Al 6082-SiC-Gr hybrid composite was found to be 0.8035 mm^3/m, 0.6208 mm^3/m and 0.4968 mm^3/m respectively. The wear rate improvement was around 22.7% and 38.2% for Al-SiC and Al-SiC-Gr composites respectively.

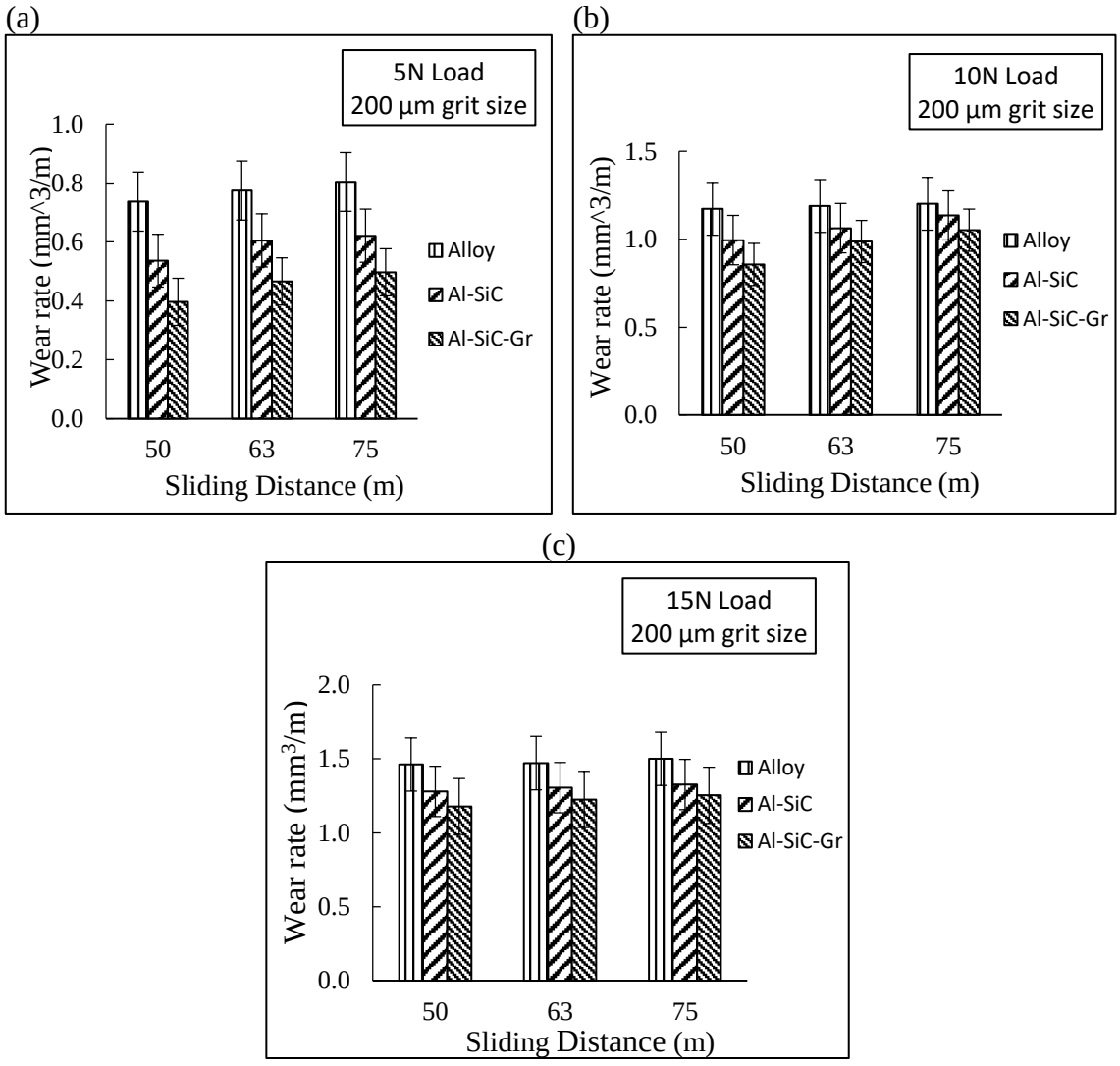

Figure 5.5: Variation of wear rate versus sliding distance of as cast alloy and its composites at abrasive grit size of 200µm and applied load of (a) 5N (b) 10N and (c) 15N

At 10N load and 50m sliding distance, the wear rate of Al 6082 alloy, Al 6082-SiC composite and Al 6082-SiC-Gr hybrid composite was found to be 1.1933 mm^3/m, 1.0349 mm^3/m and 0.8956 mm^3/m respectively as indicated in Fig. 5.5 (b). The percentage decrease in wear rate for Al-SiC and Al-SiC-Gr is around 13.3 and 24.9 respectively. The

wear rate of Al 6082 alloy, Al 6082-SiC composite and Al 6082-SiC-Gr hybrid composite at 75m sliding distance was found to be 1.2025 mm^3/m, 1.1360 mm^3/m and 1.0511 mm^3/m respectively. The wear rate decreased around 5.5% and 12.6% for Al-SiC and Al-SiC-Gr composites respectively. Fig. 5.5 (c) shows that at 50m sliding distance and applied load of 15N, the wear rate of Al 6082 alloy, Al 6082-SiC composite and Al 6082-SiC-Gr hybrid composite was found to be 1.4615 mm^3/m, 1.2789 mm^3/m and 1.1773 mm^3/m respectively. The percentage improvement of wear rate is around 12.5 and 19.4 for Al-SiC and Al-SiC-Gr respectively. The wear rate of Al 6082 alloy, Al 6082-SiC composite and Al 6082-SiC-Gr hybrid composite was found to be 1.4998 mm_3/m, 1.3257 mm^3/m and 1.2535 mm^3/m respectively at 75m sliding distance. The wear rate of Al-SiC and Al-SiC-Gr composites improved around 11.6% and 16.4% respectively.

Fig. 5.6 shows the two body abrasive wear rate of the T6 heat treated materials was plotted as a function of sliding distance at different loads and constant grit size of 200µm. Fig. 5.6 (a) shows that at 5N load and 50m sliding distance, the wear rate of Al 6082 alloy, Al 6082-SiC composite and Al 6082-SiC-Gr hybrid composite was found to be 0.5393 mm^3/m, 0.4552 mm^3/m and 0.3066 mm^3/m respectively. The percentage improvement of wear rate for Al-SiC and Al-SiC-Gr was around 15.6 and 44 respectively. The wear rate of Al 6082 alloy, Al 6082-SiC composite and Al 6082-SiC-Gr composite was found to be 0.6405 mm^3/m, 0.5496 mm^3/m and 0.4793 mm^3/m respectively for a sliding distance of 75m. The wear rate improved around 14.2% and 25.2% for Al-SiC composite and Al-SiC-Gr hybrid composite respectively. At 10N load and 50m sliding distance, the wear rate of Al 6082 alloy, Al 6082-SiC composite and Al 6082-SiC-Gr hybrid composite was found to be 0.9778 mm^3/m, 0.7312 mm^3/m and 0.4892 mm^3/m respectively in Fig. 5.6 (b). The improvement of wear rate for Al-SiC and Al-SiC-Gr composites was around 25.2% and 49.9% respectively. But at 75m sliding distance, the wear rate of Al 6082 alloy, Al 6082-SiC composite and Al 6082-SiC-Gr hybrid composite was found to be 1.0810 mm^3/m, 0.8225 mm^3/m and 0.6297 mm^3/m respectively. The wear rate improved around 23.9% and 41.7% for Al-SiC and Al-SiC-Gr respectively. It is to be noted from the Fig. 5.6 (c) that at 15N load and 50m sliding distance, the wear rate of Al 6082 alloy, Al 6082-SiC composite and Al 6082-SiC-Gr hybrid composite was found to be 1.2178 mm^3/m, 0.9784 mm^3/m and 0.7686 mm^3/m respectively. The wear rate improvement for Al-SiC and Al-SiC-Gr composites was 19.7% and 36.9% respectively. It is to be observed from the Fig. 5.6 (c) that the wear rate of Al 6082 alloy, Al 6082-SiC composite and Al 6082-SiC-Gr hybrid

composite was found to be 1.3072 mm^3/m, 1.0069 mm^3/m and 0.9539 mm^3/m respectively for sliding distance of 75m. The percentage improvement of wear rate is around 22.9 and 27 for Al-SiC and Al-SiC-Gr respectively.

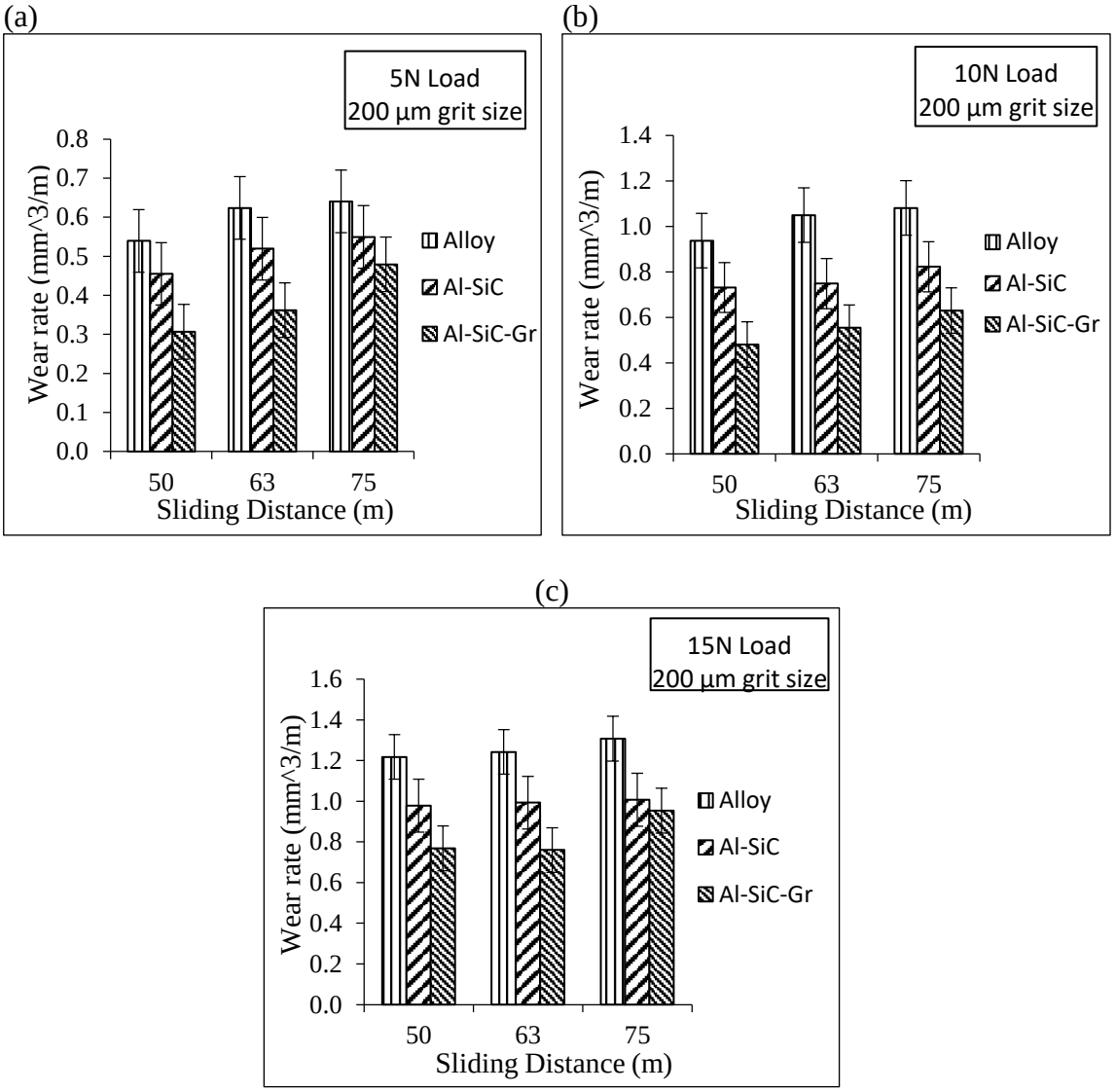

Figure 5.6: Variation of wear rate versus sliding distance of T6 heat treated alloy and its composites, at abrasive grit size of 200µm and applied load of (a) 5N (b) 10N and (c) 15N.

From the above results it was noticed that, as sliding distance increases, the wear rate increases for all the materials in both as cast and T6 condition (Lee *et al.*, 1992). Due to T6 condition, the wear rate of the materials was reduced further compared to as cast condition (Lin et al., 1988). It can be found that the addition of SiC reinforcement to matrix alloy exhibited superior resistance to wear compared to matrix alloy whereas the simultaneous addition of SiC and Gr reinforcement to matrix alloy reduced wear compared to matrix alloy and Al-SiC composites.

As time progresses, the sliding of pin on the emery paper releases the wear debris and tends to stay in between the valleys of pin sample and the emery paper. The abrasive wear tests of longer sliding distance will lead to deterioration of abrasive grits on the emery paper which are in interaction with pin. The deterioration of abrasive grits could be of blunting, fracture and even pick up. Hence it was noted that first few minutes of sliding on fresh emery paper decides the abrasive wear mechanism of material (Wang *et al*., 1989). Hence, the time duration of sliding should be and was adopted till the steady state condition is obtained.

5.2 Relative Wear Resistance (RWR)

The reduction in abrasive wear rate can also be qualitatively described in terms of relative wear resistance (RWR). It is defined as the ratio of wear rate of unreinforced matrix alloy and wear rate of composite under the similar conditions. The RWR values of composites that are subjected to abrasion can generally vary from 1 (or even less than 1 in special circumstances) to 10 (or even greater in few cases). In this present study, relative wear resistance of Al-SiC composite w.r.t unreinforced alloy was represented as RWR1 and relative wear resistance of Al-SiC-Gr hybrid composite w.r.t unreinforced alloy was represented as RWR2. The formulae used for RWR calculation was represented in Eq. (5.1) and Eq. (5.2). The effect of wear parameters such as applied load, grit size and sliding distance on RWR was investigated separately and presented individually in following sub-sections.

$$\text{RWR1} = \frac{\text{wear rate of alloy}}{\text{wear rate of Al}-\text{SiC composite}} = \frac{W_v\ (\text{Alloy})}{W_v(\text{Al}-\text{SiC})} \tag{5.1}$$

$$\text{RWR2} = \frac{\text{wear rate of alloy}}{\text{wear rate of Al}-\text{SiC}-\text{Gr hybrid composite}} = \frac{W_v\ (\text{Alloy})}{W_v(\text{Al}-\text{SiC}-\text{Gr})} \tag{5.2}$$

5.2.1 Effect of applied load

The relative wear resistance of as cast and T6 heat treated Al-SiC and Al-SiC-Gr composites with respect to matrix alloy was plotted as a function of applied loads at different sliding distances and constant 200µm grit size were represented in Table 5.2., Fig. 5.7 (a) - (c) and Fig. 5.8 (a) - (c). Fig. 5.7 (a), (b) and (c) represent relative wear resistance behaviour tested at 50m, 63m and 75m sliding distance respectively. Fig. 5.7 (a) indicates that the relative wear resistance of Al-SiC/Alloy and Al-SiC-Gr/Alloy was 1.3746 and 1.8596 respectively at 5N applied load and 50m sliding distance. But at 15N applied load,

the relative wear resistance of Al-SiC/Alloy and Al-SiC-Gr/Alloy was 1.1428 and 1.2413 respectively. Fig. 5.7 (b) indicates that the relative wear resistance of Al-SiC/Alloy and Al-SiC-Gr/Alloy was 1.2802 and 1.6603 respectively at 5N applied load and 63m sliding distance. At an applied load of 15N, the relative wear resistance was 1.1271 and 1.2006 for Al-SiC/Alloy and Al-SiC-Gr/Alloy respectively. Fig. 5.7 (c) indicates the relative wear resistance of Al-SiC/Alloy and Al-SiC-Gr/Alloy was 1.2943 and 1.6171 respectively 5N applied load and 75m sliding distance. The relative wear resistance of Al-SiC/Alloy and Al-SiC-Gr/Alloy was 1.1313 and 1.1964 respectively at 15N applied load.

Table 5.2: Effect of load on RWR of materials in as cast and T6 heat treated condition.

S.No	**Condition**	**Grit size (µm)**	**Sliding Distance (m)**	**Load (N)**	**RWR1 (W_v (alloy):W_v(Al-SiC))**	**RWR2 (W_v (alloy):W_v(Al-SiC-Gr))**
1	As cast	200	50	5	1.3746	1.8596
2				10	1.153	1.3324
3				15	1.1428	1.2413
4			63	5	1.2802	1.6603
5				10	1.119	1.2047
6				15	1.1271	1.2006
7			75	5	1.2943	1.6171
8				10	1.0585	1.1440
9				15	1.1313	1.1964
10	T6 heat treated		50	5	1.1847	1.759
11				10	1.3372	1.9987
12				15	1.2447	1.5843
13			63	5	1.2008	1.7228
14				10	1.4016	1.8909
15				15	1.2512	1.6344
16			75	5	1.1654	1.3363
17				10	1.3143	1.7167
18				15	1.2982	1.3703

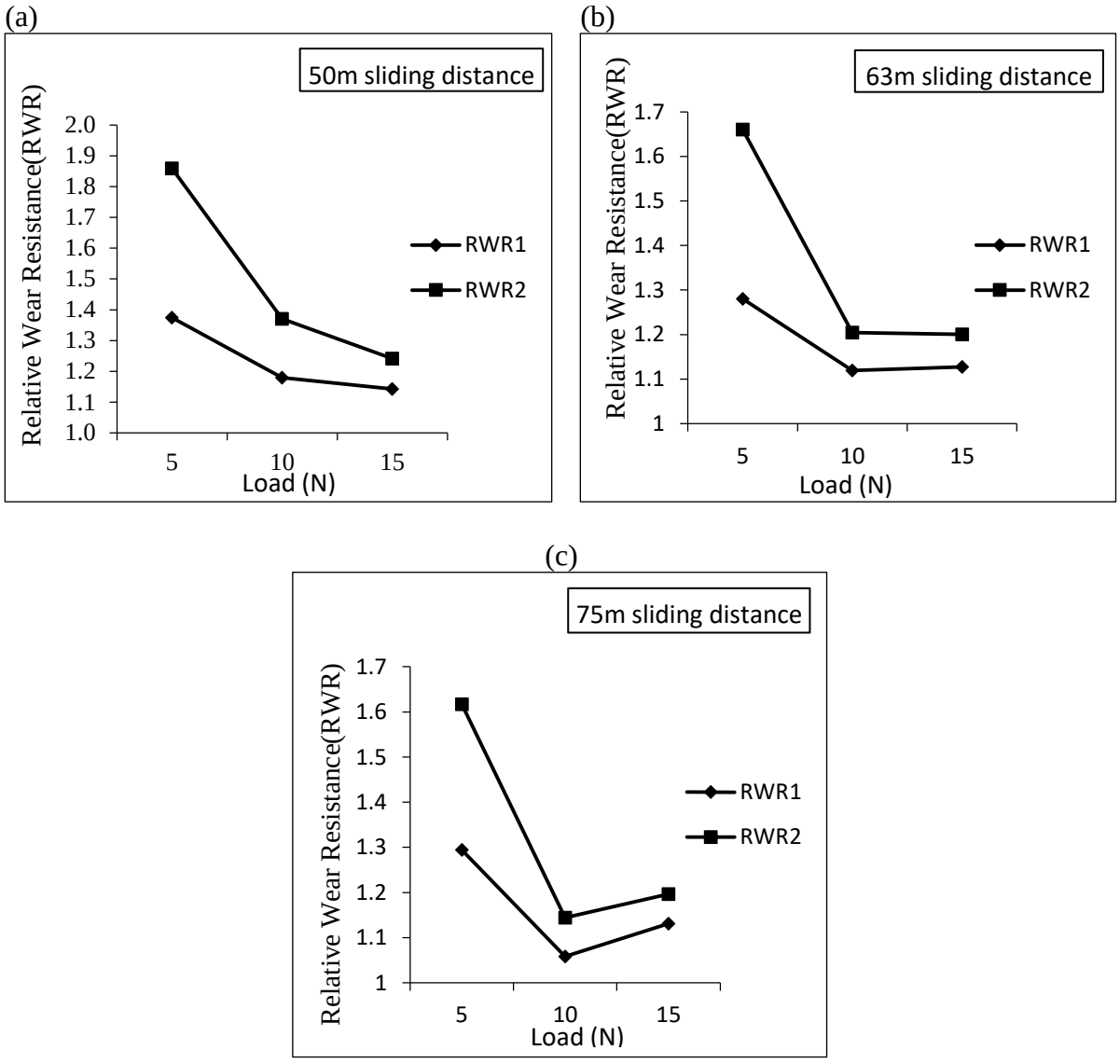

Figure 5.7: Relative wear resistance (RWR) Vs Load in as cast condition at 200µm grit size and sliding distance of (a) 50m (b) 63m and (c) 75m.

The relative wear resistance of T6 heat treated Al-SiC and Al-SiC-Gr composites with respect to matrix alloy was plotted as a function of applied loads at different sliding distances and constant 200µm grit size were represented in Fig. 5.8 (a) - (c). Fig. 5.8 (a), (b) and (c) represent relative wear resistance behaviour tested at 50m, 63m and 75m sliding distance respectively. Fig. 5.8 (a) indicates, the relative wear resistance of Al-SiC/Alloy and Al-SiC-Gr/Alloy was 1.1847 and 1.759 respectively at 5N applied load and 50m sliding distance. At 15N applied load, the relative wear resistance of Al-SiC/Alloy and Al-SiC-Gr/Alloy was 1.2447 and 1.5843 respectively. From the Fig. 5.8 (b), the relative wear resistance of Al-SiC/Alloy and Al-SiC-Gr/Alloy was 1.2008 and 1.7228 respectively at 5N applied load and 63m sliding distance. The relative wear resistance of Al-SiC/Alloy and

Al-SiC-Gr/Alloy was 1.2512 and 1.6344 respectively at 15N applied load. Fig. 5.8 (c) represents the relative wear resistance of Al-SiC/Alloy and Al-SiC-Gr/Alloy was 1.1654 and 1.3363 respectively 5N applied load and 75m sliding distance. The relative wear resistance was 1.2982 and 1.3703 for Al-SiC/Alloy and Al-SiC-Gr/Alloy respectively at 15N applied load.

It was noticed that from Fig. 5.7 that RWR was higher at lower loads and lower at higher loads. This was noticed in the as cast condition of materials. In T6 condition of materials, the RWR was higher at intermediate loads as noticed from Fig. 5.8. Axen *et al*., (1994) reported that at higher loads, the wear resistance is independent of reinforcement and lower loads, the wear resistance enhances with reinforcement, when the materials tested on 75 µm grit size of SiC emery paper. The present observed range of RWR was in the range of 1-2, similar to that of previous work carried out by Axen *et al*., (1994). The improvement of RWR was found to be higher in case of hybrid composites.

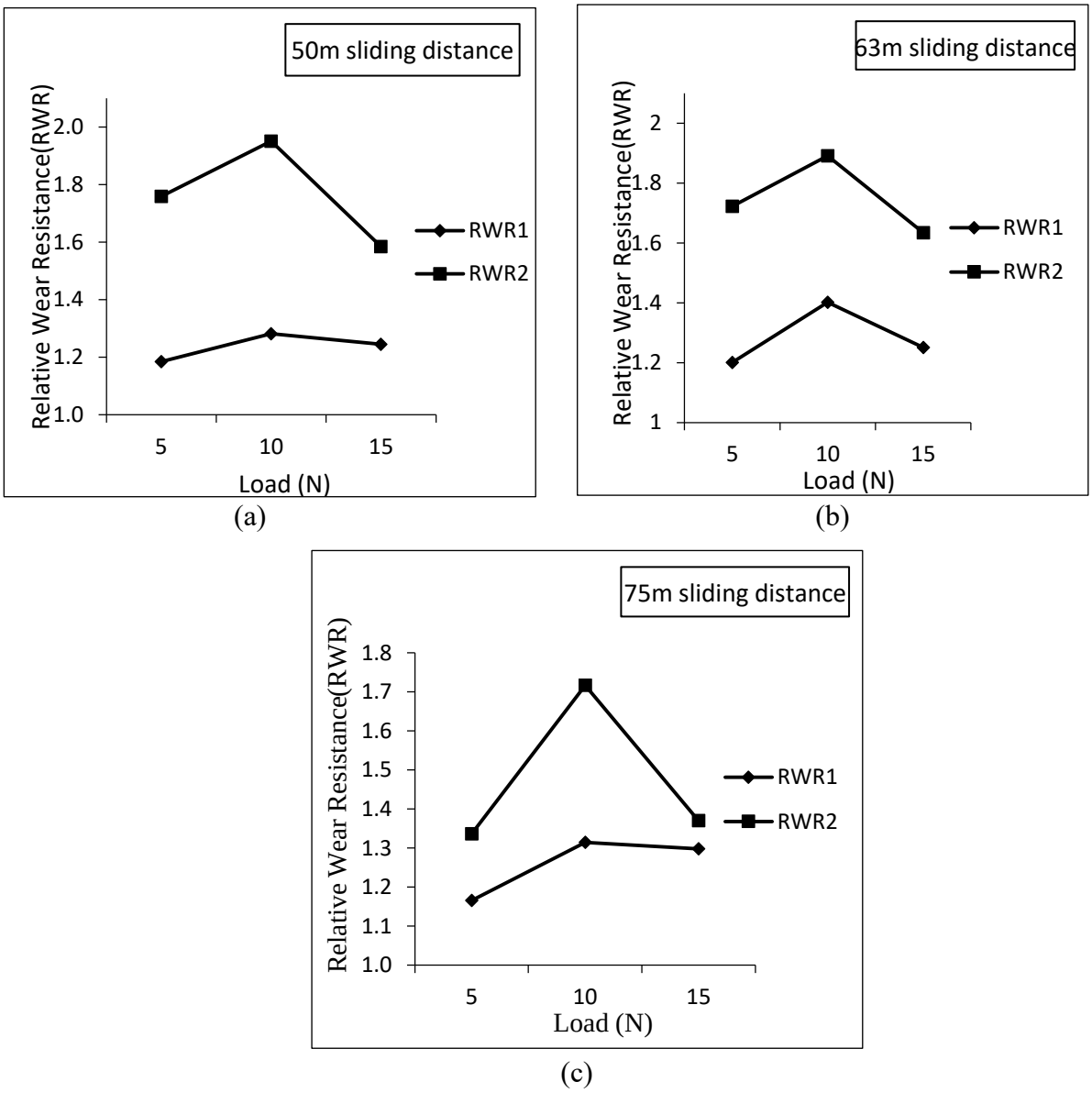

Figure 5.8: Relative wear resistance (RWR) Vs Load in T6 condition at 200µm grit size and sliding distance of (a) 50m (b) 63m and (c) 75m.

5.2.2 Effect of grit size

The relative wear resistance of as cast and T6 heat treated Al-SiC and Al-SiC-Gr composites with respect to matrix alloy was plotted as a function of grit size at different applied loads and constant sliding distance of 75m was represented in Fig. 5.9, Fig. 5.10 and Table 5.3. Fig. 5.9 (a), (b) and (c) represent relative wear resistance behaviour tested at 5N, 10N and 15N applied loads respectively. Fig. 5.9 (a) indicates that the relative wear resistance was 1.1872 and 1.3641 for Al-SiC/Alloy and Al-SiC-Gr/Alloy respectively at 5N applied load and 100µm grit size. But at 200µm grit size, the relative wear resistance

of Al-SiC/Alloy and Al-SiC-Gr/Alloy was 1.2159 and 1.4136 respectively. In Fig. 5.9 (b), the relative wear resistance of Al-SiC/Alloy and Al-SiC-Gr/Alloy was 1.2338 and 1.3874 respectively at 10N applied load and 100µm grit size. At 200µm grit size, the relative wear resistance of Al-SiC/Alloy and Al-SiC-Gr/Alloy was 1.0585 and 1.1440 respectively. It is to be observed from Fig. 5.9 (c), the relative wear resistance of Al-SiC/Alloy and Al-SiC-Gr/Alloy was 1.148 and 1.2448 respectively at 15N applied load and 100µm grit size. The relative wear resistance was 1.1313 and 1.1964 for Al-SiC/Alloy and Al-SiC-Gr/Alloy respectively at 200µm grit size.

Table 5.3: Effect of grit size on RWR of materials in as cast and T6 heat treated condition.

S.No	Condition	Sliding Distance (m)	Load (N)	Grit size (µm)	RWR1 (Al-SiC : Alloy)	RWR2 (Al-SiC-Gr : Alloy)
1	As cast	75	5	100	1.1872	1.3641
2				125	1.1660	1.3225
3				200	1.2159	1.4136
4			10	100	1.2338	1.3874
5				125	1.1913	1.2171
6				200	1.0585	1.1440
7			15	100	1.1480	1.2448
8				125	1.1418	1.2155
9				200	1.1313	1.1964
10	T6 heat treated		5	100	1.3463	1.5657
11				125	1.0917	1.2242
12				200	1.1654	1.3363
13			10	100	1.2203	1.5299
14				125	1.1966	1.4617
15				200	1.3143	1.7169
16			15	100	1.0979	1.3676
17				125	1.1471	1.4791
18				200	1.2981	1.3703

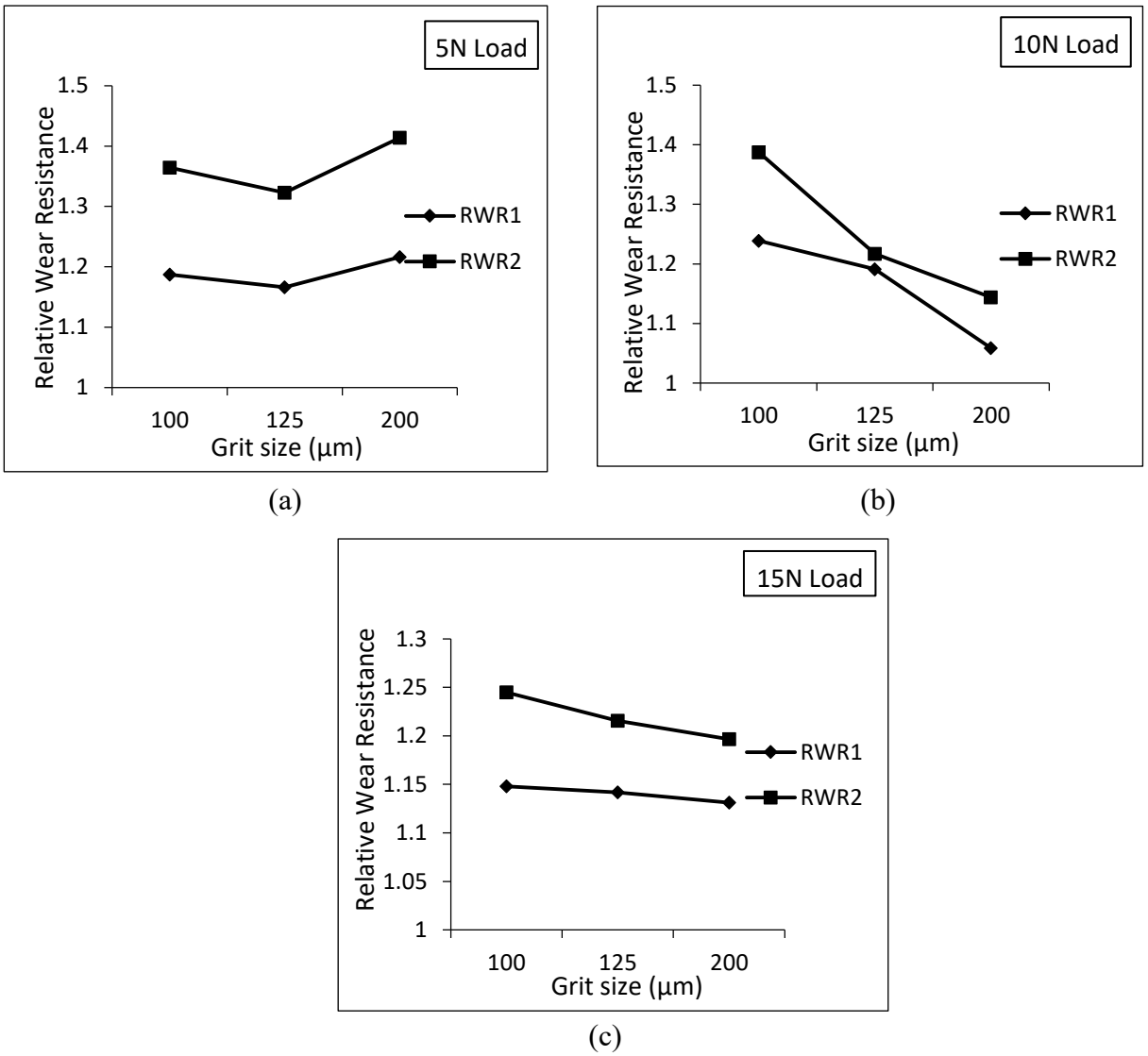

Figure 5.9: Relative wear resistance (RWR) Vs Grit size in as cast condition at 75m sliding distance and applied load of (a) 5N (b) 10N and (c) 15N.

The relative wear resistance of T6 heat treated Al-SiC and Al-SiC-Gr composites with respect to matrix alloy was plotted as a function of grit size at different applied loads and constant sliding distances of 75m was represented in Fig. 5.10 (a) - (c). Fig. 5.10 (a), (b) and (c) represent relative wear resistance behaviour tested at 5N, 10N and 15N applied loads respectively. The relative wear resistance of Al-SiC/Alloy and Al-SiC-Gr/Alloy was 1.3463 and 1.5657 respectively at 5N applied load and 100µm grit size in Fig. 5.10 (a). At 200µm grit size, the relative wear resistance was 1.1654 and 1.3363 for Al-SiC/Alloy and Al-SiC-Gr/Alloy respectively. Fig. 5.10 (b) indicates that the relative wear resistance of Al-SiC/Alloy and Al-SiC-Gr/Alloy was 1.2203 and 1.5299 respectively at 10N applied load and 100µm grit size. The relative wear resistance of Al-SiC/Alloy and Al-SiC-Gr/Alloy

was 1.3143 and 1.7169 respectively at 200µm grit size. From the Fig. 5.10 (c), the relative wear resistance of Al-SiC/Alloy and Al-SiC-Gr/Alloy was 1.0979 and 1.3676 respectively at 15N applied load and 100µm grit size. But at 200µm grit size, the relative wear resistance was 1.2981 and 1.3703 for Al-SiC/Alloy and Al-SiC-Gr/Alloy respectively.

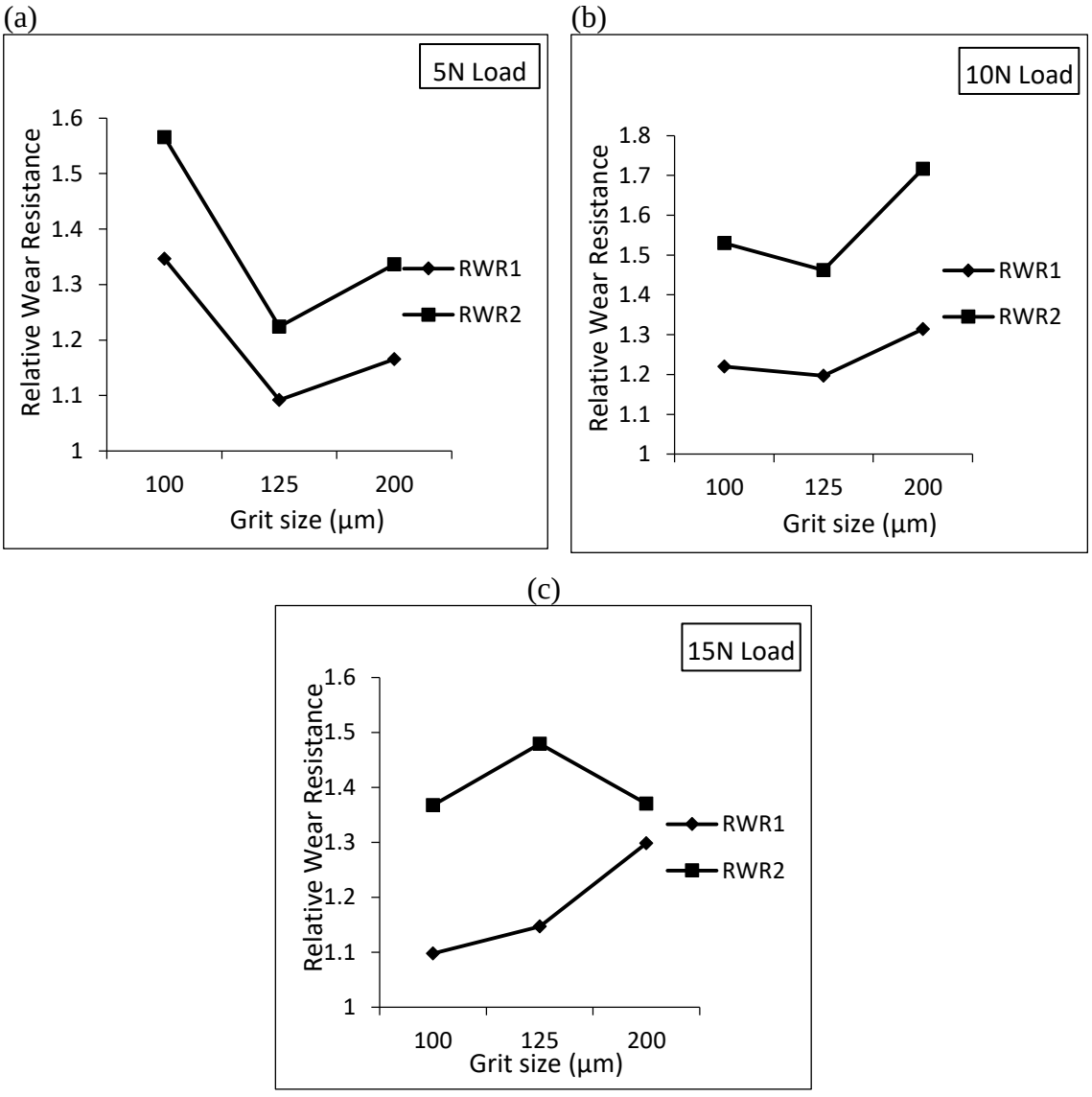

Figure 5.10: Relative wear resistance (RWR) Vs Grit size in T6 condition at 75m sliding distance and applied load of (a) 5N (b) 10N and (c) 15N.

Axen *et al*., (1994) stated that abrasion against SiC grits, the wear resistance increased with decrease in abrasive grit size i.e. below 75 µm. In this study, the similar observations were noted at 100µm grit size, at all loads and in as cast condition. In T6 condition, at lower loads, relative wear resistance was higher at lower grit size. But the reverse in trends was observed at intermediate and higher loads. The enhancement of RWR was noticed in case of hybrid composites.

5.2.3 Effect of sliding distance

The relative wear resistance of as cast and T6 heat treated Al-SiC and Al-SiC-Gr composites with respect to matrix alloy was plotted as a function of sliding distance at different applied loads and constant grit size of 200 µm was represented in Fig. 5.11, 5.12 and Table 5.4.

Table 5.4: Effect of sliding distance on RWR of materials in as cast and T6 condition.

S.No	Condition	Grit size (µm)	Load (N)	Sliding Distance (m)	RWR1 (Al-SiC : Alloy)	RWR2 (Al-SiC-Gr : Alloy)
1	As cast	200	5	50	1.374487	1.859233
2				63	1.280258	1.660519
3				75	1.294298	1.617351
4			10	50	1.153058	1.332403
5				63	1.119063	1.204718
6				75	1.058539	1.14404
7			15	50	1.142779	1.241294
8				63	1.127099	1.200539
9				75	1.131327	1.19649
10	T6 heat treated		5	50	1.184754	1.758969
11				63	1.201001	1.722729
12				75	1.165393	1.336324
13			10	50	1.337254	1.998774
14				63	1.401629	1.890811
15				75	1.314286	1.71669
16			15	50	1.244685	1.584439
17				63	1.251209	1.634259
18				75	1.180956	1.370374

Fig. 5.11 (a), (b) and (c) represent relative wear resistance behaviour tested at 5N, 10N and 15N applied loads respectively. Fig. 5.11 (a) shows the relative wear resistance of Al-SiC/Alloy and Al-SiC-Gr/Alloy was 1.374 and 1.8592 respectively at 5N applied load and 50m sliding distance. At 75m sliding distance, the relative wear resistance of Al-SiC/Alloy and Al-SiC-Gr/Alloy was 1.2943 and 1.6173 respectively.

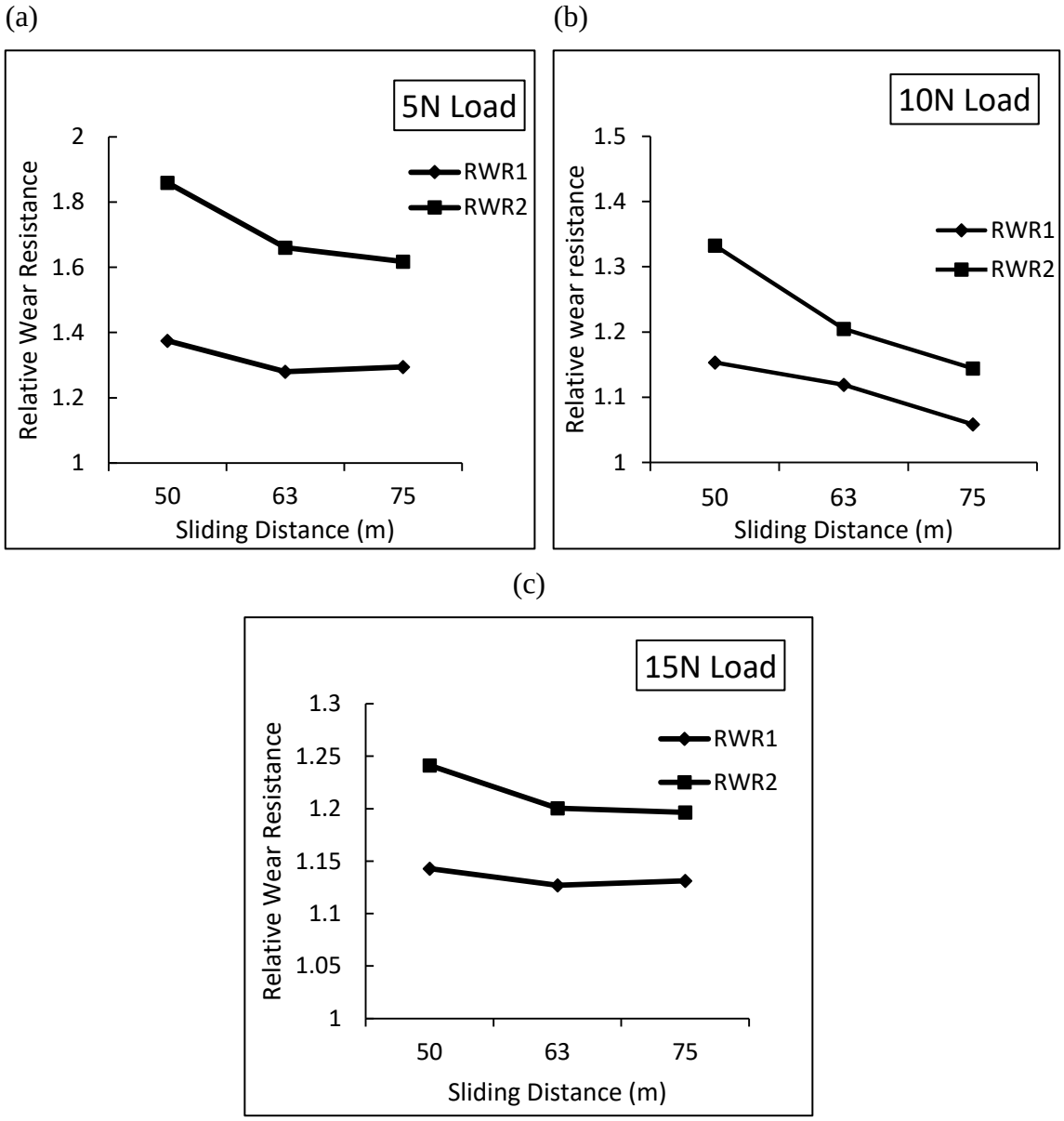

Figure 5.11: Relative wear resistance (RWR) Vs Sliding distance in as cast condition at an applied load of (a) 5N (b) 10N and (c) 15N.

Fig. 5.11 (b) indicates that the relative wear resistance of Al-SiC/Alloy and Al-SiC-Gr/Alloy was 1.153 and 1.3324 respectively at 10N applied load and 50m sliding distance. But at 75m sliding distance, the relative wear resistance was 1.0585 and 1.144 for Al-SiC/Alloy and Al-SiC-Gr/Alloy respectively. The relative wear resistance of Al-SiC/Alloy and Al-SiC-Gr/Alloy was 1.1428 and 1.24123 respectively at 15N applied load and 50m sliding distance as noted from Fig. 5.11 (c). The relative wear resistance of Al-SiC/Alloy and Al-SiC-Gr/Alloy was 1.1313 and 1.1965 respectively at 75m sliding distance.

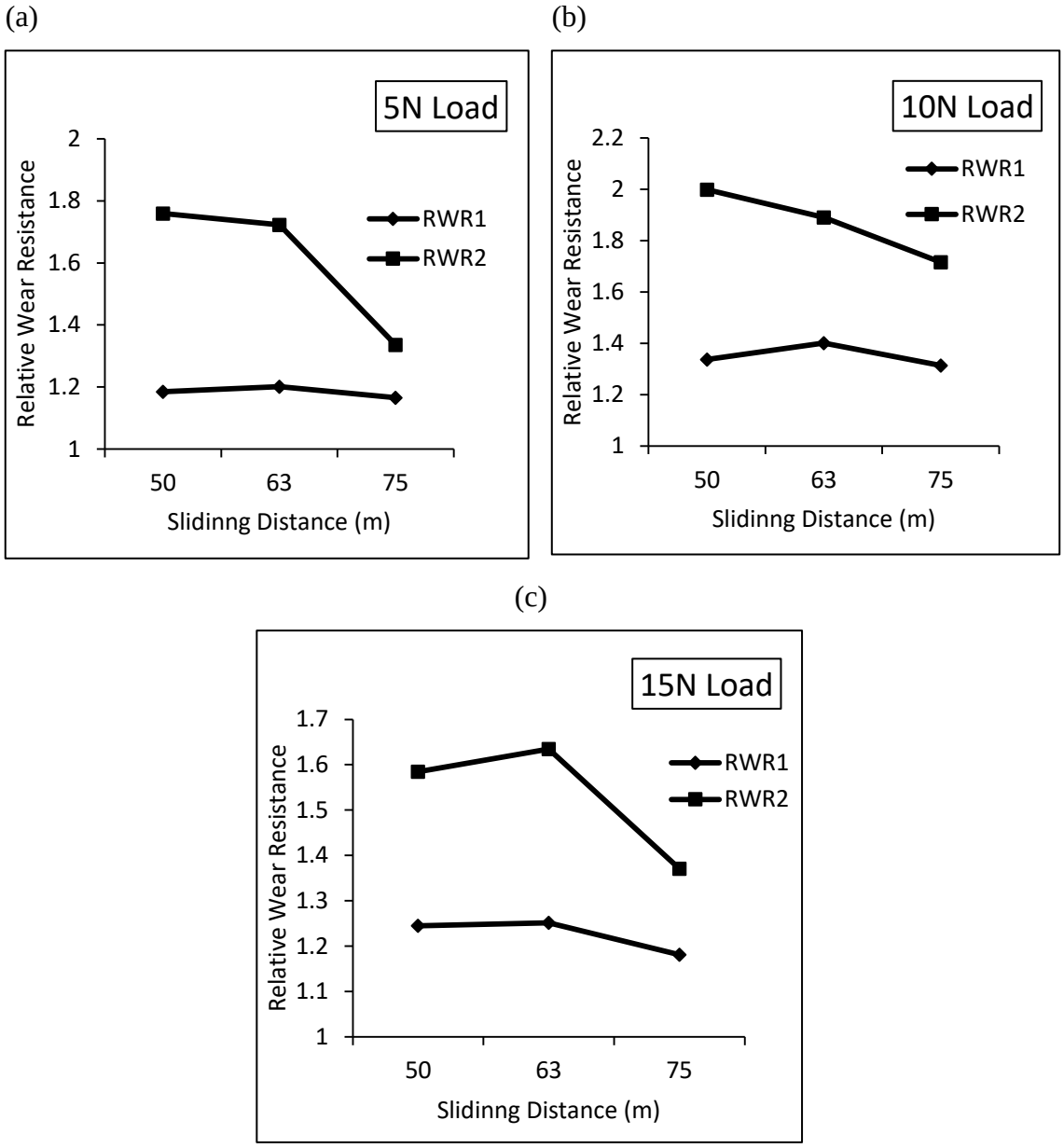

Figure 5.12: Relative wear resistance (RWR) Vs Sliding distance in T6 condition at an applied load of (a) 5N (b) 10N and (c) 15N.

The relative wear resistance of T6 heat treated Al-SiC and Al-SiC-Gr composites with respect to matrix alloy was plotted as a function of sliding distance at different applied loads and constant grit size of 200 µm was represented in Fig. 5.12 (a) - (c). Fig. 5.12 (a), (b) and (c) represent relative wear resistance behaviour tested at 5N, 10N and 15N applied loads respectively. Fig. 5.12 (a) represents the relative wear resistance of Al-SiC/Alloy and Al-SiC-Gr/Alloy was 1.1847 and 1.759 respectively at 5N applied load and 50m sliding distance. But at 75m sliding distance, the relative wear resistance of Al-SiC/Alloy and Al-SiC-Gr/Alloy was 1.1654 and 1.3363 respectively. Fig. 5.12 (b) shows the relative wear

resistance of Al-SiC/Alloy and Al-SiC-Gr/Alloy was 1.3373 and 1.9988 respectively at 10N applied load and 50m sliding distance. But at 75m sliding distance, the relative wear resistance of Al-SiC/Alloy and Al-SiC-Gr/Alloy was 1.3143 and 1.7167 respectively. It is to be noted from the Fig. 5.12 (c) that the relative wear resistance of Al-SiC/Alloy and Al-SiC-Gr/Alloy was 1.2447 and 1.5844 respectively at 15N applied load and 50m sliding distance. The relative wear resistance was 1.181 and 1.3704 for Al-SiC/Alloy and Al-SiC-Gr/Alloy respectively at 75m sliding distance. As noted earlier, as sliding distance, the cutting efficiency of the abrasive grit reduces due to its deterioration during abrasion process. This can be attributed for decrease of RWR as sliding distance increases. However the RWR improved further due to T6 heat treated condition.

5.3 Power law and Polynomial equations of abrasive wear rate of materials

The wear behaviour in the form of power law equation, $y = kx^n$ (where x, y are variables, n is the power law exponent and k is a constant) and second order polynomial equation i.e. quadratic equation in the form of $y = ax^2+bx+c$ (where x, y are variables and a, b & c are coefficients of equation) were presented to understand the empirical relationship between the wear and its affecting parameters. In the present context, y can be termed as wear rate which is represented on y axis and x can be termed as applied load.

Fig. 5.13 (a), (b) and (c) shows the volumetric wear rate as a function of load applied, abrasive grit size for Al 6082 matrix alloy, Al 6082-SiC composites and Al 6082-SiC-Gr hybrid composites respectively in as cast condition. It was observed that as load and size of abrasive grit increases, the wear rate increases for all the materials. However the substantial improvement in abrasive wear resistance can be observed due to the addition of SiC and graphite reinforcements. Table 5.5 show the power law and polynomial wear equations of cast Al 6082 alloy, Al 6082-SiC, Al 6082-SiC-Gr materials when tested on 100 µm, 125 µm and 200 µm abrasive grit size emery papers. It was observed from the power law equations that the exponent component was increasing from 0.57 to 0.75 and 0.55 to 0.64 from alloy to hybrid composite for the materials tested on 200 µm and 125 µm abrasive grit sizes respectively. But for 100 µm abrasive grit size, the exponent component was decreasing from 0.66 to 0.6. From the developed quadratic equations it was noted that 'a' coefficients before square terms were found to be near to zero irrespective of sign. It was noted that 'c' intercept term was found to be decreasing from alloy to composites i.e. 0.3027 to -0.19 for 200 µm grit size and 0.058 to -0.08 for 125 µm grit size. But for 100 µm grit size, the 'c' term slightly decreased from 0.1091 to 0.18. There was no particular

trend noticed in case of 'b' coefficient terms. The values of R^2 were observed in the range of 0.97 and 0.99.

Table 5.5: Power law and polynomial wear equations of cast materials tested on (a) 200 µm (b) 125 µm and (c) 100 µm abrasive grit size

Material	**Power law equation**	**Polynomial equation**	**R^2**
(a) 200 µm			
Al 6082 alloy	$y= 0.32x^{0.57}$	$y= -0.002x^2+0.1103x+0.3027$	0.9997
Al 6082-10% SiC	$y= 0.24x^{0.65}$	$y= -0.0057x^2+0.1807x-0.0998$	0.9744
Al 6082-5% SiC-5% Gr	$y= 0.18x^{0.75}$	$y= -0.0056x^2+0.18x-0.19$	0.9741
(b) 125 µm			
Al 6082 alloy	$y= 0.29x^{0.55}$	$y= -0.0048x^2+0.1508x+0.058$	0.9776
Al 6082-10% SiC	$y= 0.24x^{0.57}$	$y= -0.0028x^2+0.1067x+0.129$	0.9929
Al 6082-5% SiC-5% Gr	$y= 0.19x^{0.64}$	$y= -0.0046x^2+0.143x-0.08$	0.9716
(c) 100 µm			
Al 6082 alloy	$y= 0.27x^{0.66}$	$y= -0.0036x^2+0.1188x+0.1091$	0.9836
Al 6082-10% SiC	$y= 0.21x^{0.56}$	$y= -0.0011x^2+0.\ 0644x+0.2217$	0.9998
Al 6082-5% SiC-5% Gr	$y= 0.17x^{0.6}$	$y= -0.008x^2+0.058x+0.18$	0.9999

Figure 5.14 (a), (b) and (c) shows the volumetric wear rate as a function of load applied, abrasive grit size for Al 6082 matrix alloy, Al 6082-SiC composites and Al 6082-SiC-Gr hybrid composites respectively in T6 heat treated condition. The trends noticed were found to be similar to cast condition. Table 5.6 shows the power law and polynomial wear equations of T6 heat treated Al 6082 alloy, Al 6082-SiC, Al 6082-SiC-Gr materials tested on 100 µm, 125 µm and 200 µm abrasive grit size emery papers. It was observed from the power law equations that the exponent component was decreasing from 0.66 to 0.6 and 0.69 to 0.51 from alloy to hybrid composite for the materials tested on 200 µm and 125 µm abrasive grit sizes respectively. But for 100 µm abrasive grit size, the exponent component was increasing from 0.61 to 0.73. From the developed quadratic equations it was noted that 'a' coefficients before square terms were found to be near to zero irrespective of sign. It was noted that 'c' intercept term was found to be increasing from alloy to composites i.e. -0.0143 to 0.5028 for 200 µm grit size and 0.124 to 0.2783 for 125 µm grit size. But for 100 µm grit size, the 'c' term slightly decreased from 0.1776 to 0.1678.

In this condition also, there was no particular trend noticed in case of 'b' coefficient terms. The values of R^2 were observed in the range of 0.98 and 0.99.

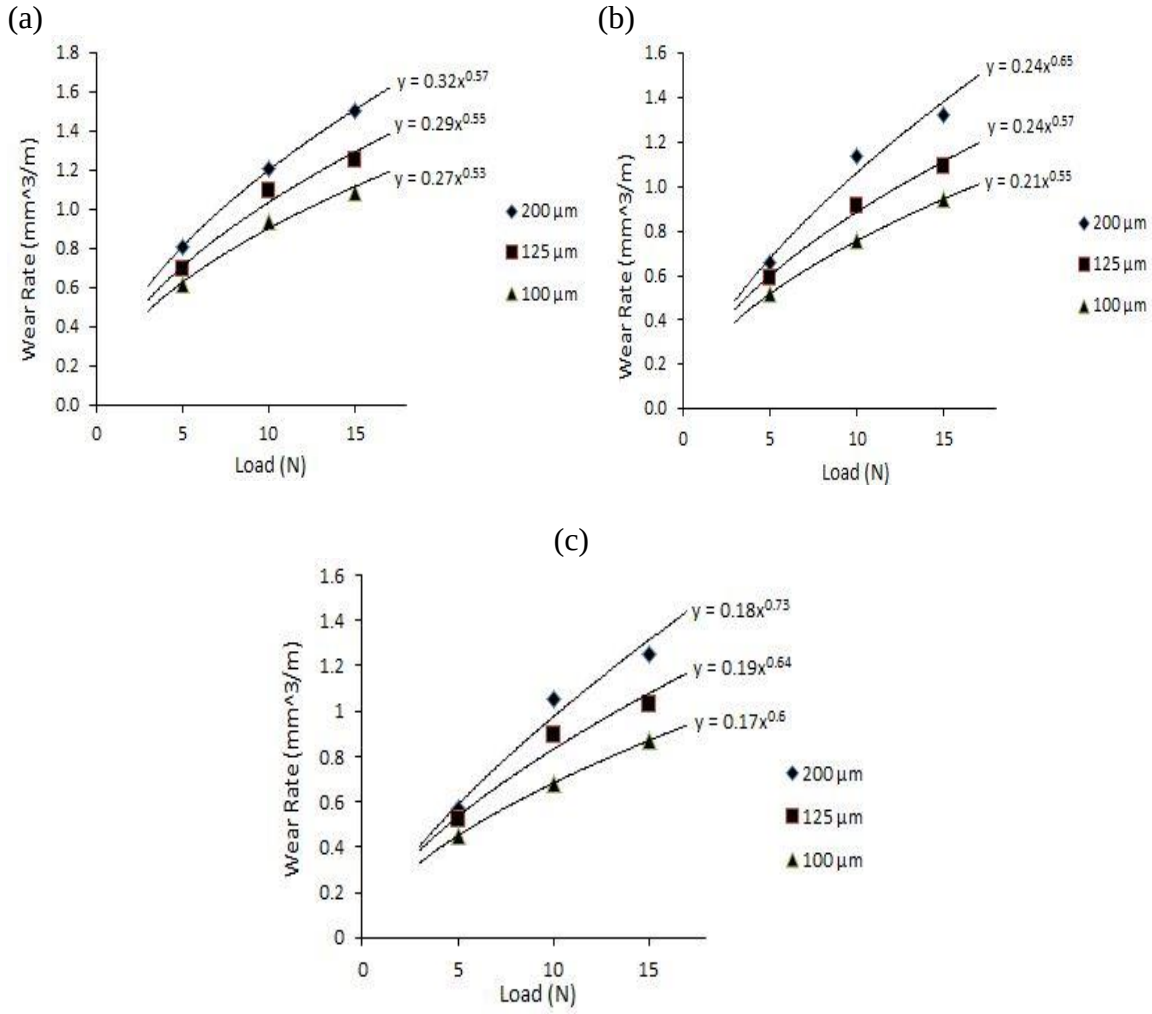

Figure 5.13: Volumetric wear rate as a function of load applied and abrasive grit size for (a) Al 6082 matrix alloy, (b) Al 6082-10% SiC composites and (c) Al 6082-5%SiC-5%Gr hybrid composites in cast condition.

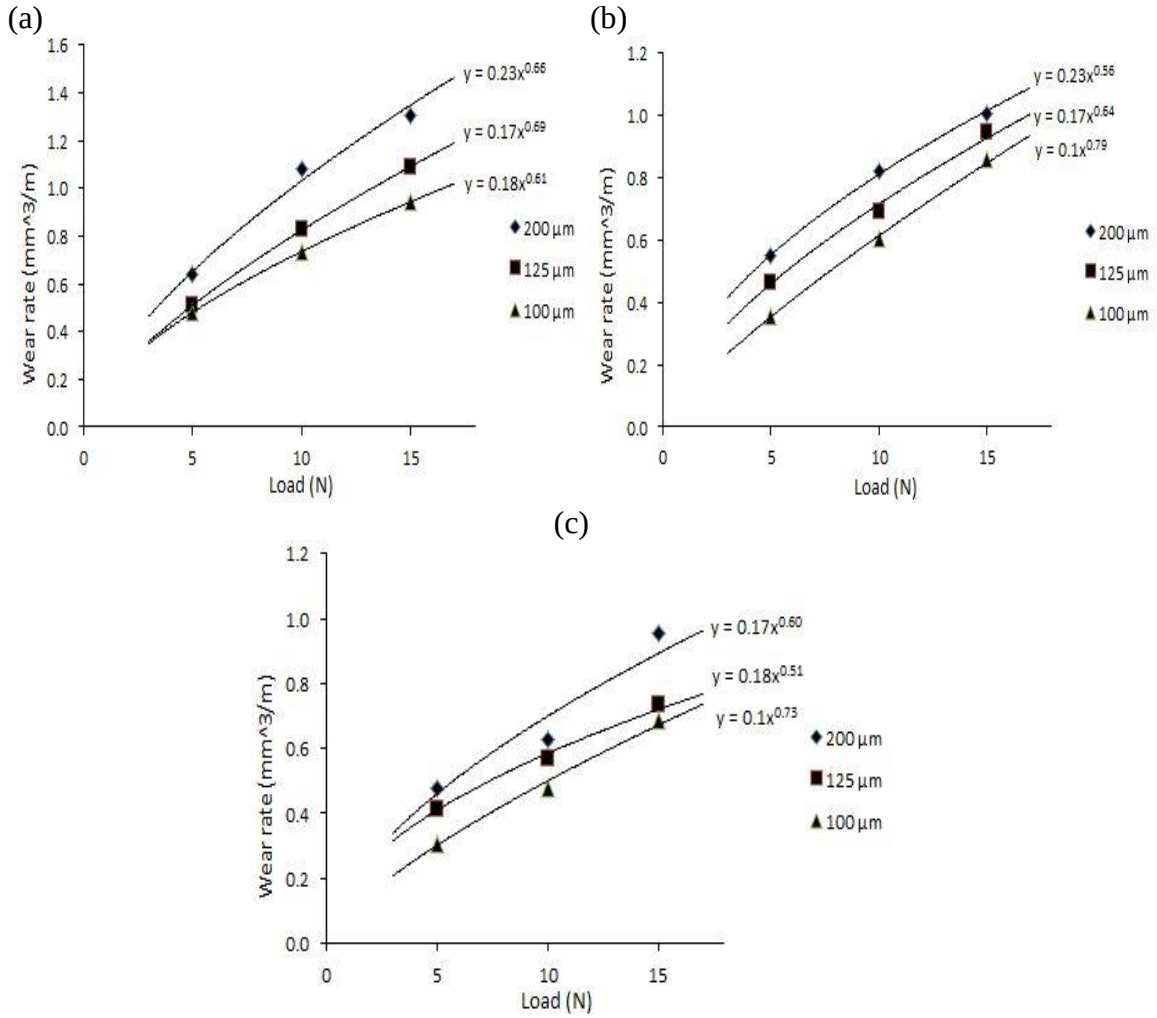

Figure 5.14: Volumetric wear rate as a function of load applied and abrasive grit size for (a) Al 6082 matrix alloy, (b) Al 6082-10% SiC composites and (c) Al 6082- 5% SiC- 5% Gr hybrid composites in T6 heat treated condition.

It was pointed out that the wear rate increases monotonically with increase in load applied and follows nearly a linear relationship. This trend was noticed when the materials were tested against all abrasive sizes chosen in this study. There was a transition in abrasive wear rates (i.e. sudden increase in wear rate) when abrasive size changes from 100 to 125 µm (Mondal *et al.*, 2005). It was evident in this present study also for both as cast and T6 conditions of materials.

Table 5.6: Power law and polynomial wear equations of T6 heat treated materials tested on (a) 200 µm, (b) 125 µm and (c) 100 µm abrasive grit size emery paper.

Material	**Power law equation**	**Polynomial equation**	**R^2**
(a) 200 µm			
Al 6082 alloy	$y= 0.23x^{0.66}$	$y= -0.0043x^2+0.1524x-0.0143$	0.9872
Al 6082-10% SiC	$y= 0.23x^{0.56}$	$y= -0.0018x^2+0.811x+0.1883$	0.9985
Al 6082-5% SiC-5% Gr	$y= 0.17x^{0.6}$	$y= 0.0035x^2-0.0221x+0.5028$	0.9294
(b) 125 µm			
Al 6082 alloy	$y= 0.17x^{0.69}$	$y= -0.0013x^2+0.0832x+0.124$	0.9998
Al 6082-10% SiC	$y= 0.17x^{0.64}$	$y= 0.0005x^2+0.0374x+0.2652$	0.9935
Al 6082-5% SiC-5% Gr	$y= 0.18x^{0.51}$	$y= 0.0003x^2+0.0258x+0.2783$	0.9909
(c) 100 µm			
Al 6082 alloy	$y= 0.18x^{0.61}$	$y= -0.0009x^2+0.0652x+0.1776$	0.9999
Al 6082-10% SiC	$y= 0.18x^{0.79}$	$y= 0.0002x^2+0.0046x+0.1213$	0.9985
Al 6082-5% SiC-5% Gr	$y= 0.1x^{0.73}$	$y= 0.0007x^2+0.0243x+0.1678$	0.9924

5.4 Wear Coefficients

Table 5.7 shows the wear coefficients of Al 6082 alloy, Al 6082- 10% SiC composites and Al 6082- 5% SiC- 5% Gr hybrid composites in cast and T6 heat treated conditions. The effect of applied load, grit size and sliding distance on wear coefficients was discussed briefly.

Table 5.7: Wear coefficients of Al 6082 alloy, Al 6082- 10% SiC composite and Al 6082- 5% SiC- 5% Gr composite in cast and T6 heat treated conditions.

Load (N)	**Grit size (µm)**	**Sliding distance (m)**	**Wear coefficient , K (x 10^{-3})**					
			As cast condition			**T6 condition**		
			Alloy	**Al-10SiC**	**Al-5SiC-5Gr**	**Alloy**	**Al-10SiC**	**Al-5SiC-5Gr**
5	200	50	0.708	0.665	0.436	0.615	0.674	0.417
5	200	63	0.743	0.750	0.513	0.711	0.769	0.492
5	200	75	0.771	0.770	0.584	0.730	0.813	0.641
5	125	50	0.636	0.646	0.489	0.513	0.555	0.345
5	125	63	0.648	0.708	0.560	0.536	0.616	0.543
5	125	75	0.662	0.734	0.520	0.579	0.689	0.565
5	100	50	0.565	0.547	0.420	0.427	0.451	0.369
5	100	63	0.575	0.564	0.438	0.530	0.504	0.357
5	100	75	0.589	0.641	0.495	0.547	0.528	0.417
10	200	50	0.563	0.617	0.471	0.534	0.541	0.327
10	200	63	0.571	0.659	0.543	0.598	0.554	0.377
10	200	75	0.577	0.704	0.543	0.616	0.609	0.428
10	125	50	0.462	0.527	0.409	0.448	0.472	0.294
10	125	63	0.474	0.552	0.470	0.461	0.486	0.354
10	125	75	0.522	0.566	0.491	0.472	0.512	0.385
10	100	50	0.414	0.422	0.363	0.394	0.423	0.226
10	100	63	0.441	0.454	0.367	0.402	0.436	0.276
10	100	75	0.450	0.469	0.372	0.419	0.446	0.327
15	200	50	0.468	0.529	0.432	0.463	0.482	0.348
15	200	63	0.470	0.539	0.449	0.472	0.490	0.345
15	200	75	0.480	0.548	0.460	0.497	0.546	0.432
15	125	50	0.374	0.436	0.366	0.393	0.437	0.314
15	125	63	0.375	0.444	0.369	0.404	0.458	0.322
15	125	75	0.399	0.452	0.376	0.412	0.467	0.333
15	100	50	0.333	0.364	0.286	0.345	0.384	0.284
15	100	63	0.341	0.379	0.306	0.350	0.392	0.249
15	100	75	0.346	0.390	0.319	0.358	0.423	0.312

(a) (b)

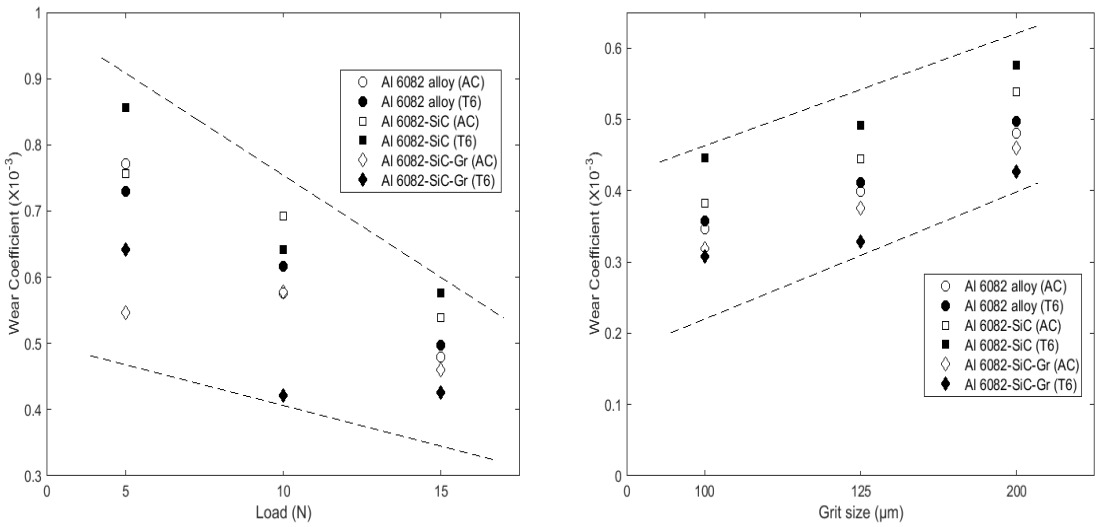

(c)

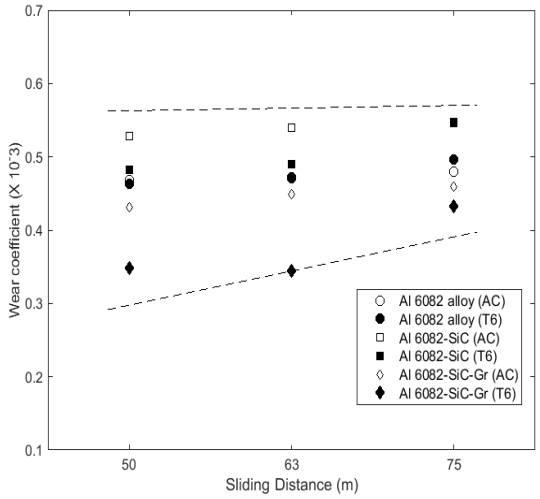

Figure 5.15: Wear coefficients as a function of (a) load (b) grit size and (c) sliding distance for alloy and its composite materials (The discontinuous lines are guide to eye)

It was noticed from Fig. 5.15 (a) that at 200 µm grit size and 75 m sliding distance as applied load increases from 5N to 15N, the wear coefficients of alloy, Al 6082-SiC composite and Al 6082-SiC-Gr composite decreased from 0.771 x 10^{-3} to 0.48 x 10^{-3}, 0.757 x 10^{-3} to 0.539 x 10^{-3} and 0.547 x 10^{-3} to 0.46 x 10^{-3} respectively. At 5N load the decrease in wear coefficient from matrix alloy to hybrid composite observed was 0.771x10^{-3} to 0.547x10^{-3} and at 15N load it was 0.48 X 10^{-3} to 0.46 X 10^{-3} correspondingly. This was the case when materials were tested in as cast condition. The wear coefficients of alloy, Al 6082-SiC composite and Al 6082-SiC-Gr composite decreased from 0.73 x10^{-3} to 0.497 x 10^{-3}, 0.857 x 10^{-3} to 0.576 x 10^{-3} and 0.642 x 10^{-3} to 0.426 x 10^{-3} respectively in T6

condition. At 5N applied load, the decrease in wear coefficient from matrix alloy to hybrid composite was 0.73 x 10^{-3} to 0.642 x 10^{-3} and at 15N load it was 0.497 x 10^{-3} to 0.426 x 10^{-3} correspondingly.

Fig. 5.15(b) shows that at 15N load and 75 m sliding distance, as grit size increases 100 µm from 200 µm, the wear coefficients of matrix alloy, Al 6082-SiC composite and Al 6082-SiC-Gr composite increased from 0.346 x 10^{-3} to 0.48 x 10^{-3}, 0.383 x 10^{-3} to 0.539 x 10^{-3} and 0.319 x 10^{-3} to 0.46 x 10^{-3} respectively. At 100 µm grit size, the decrease in wear coefficient from matrix alloy to hybrid composite observed was 0.346 x 10^{-3} to 0.319x10^{-3} and at 200 µm grit size it was 0.48x10^{-3} to 0.46x10^{-3} correspondingly. This was the case when materials were tested in as cast condition. The wear coefficients of alloy, Al 6082-SiC composite and Al 6082-SiC-Gr composite increased from 0.358 x 10^{-3} to 0.497 x 10^{-3}, 0.446 x 10^{-3} to 0.576 x 10^{-3} and 0.308 x 10^{-3} to 0.426 x 10^{-3} respectively in T6 condition. At 100 µm grit size, the decrease in wear coefficient from matrix alloy to hybrid composite was 0.346 x 10^{-3} to 0.319 x 10^{-3} and at 200 µm grit size it was 0.497 x 10^{-3} to 0.426 x 10^{-3} correspondingly.

Fig. 5.15(c) depicts that at 15N load and 200 µm grit size, as sliding distance increases from 50 m to 75 m, the wear coefficients of matrix alloy, Al 6082-SiC composite and Al 6082-SiC-Gr composite increased from 0.468 x 10^{-3} to 0.48 x 10^{-3}, 0.529 x 10^{-3} to 0.548 x 10^{-3} and 0.432 x 10^{-3} to 0.46 x 10^{-3} respectively. At 50 m sliding distance, the decrease in wear coefficient from matrix alloy to hybrid composite observed was 0.468 x 10^{-3} to 0.432 x 10^{-3} and at 75 m sliding distance it was 0.48 x 10^{-3} to 0.46 x 10^{-3} correspondingly. This was the case when materials were tested in as cast condition. In T6 condition, as sliding distance increases from 50 m to 75 m, the wear coefficients of alloy, Al 6082-SiC composite and Al 6082-SiC-Gr composite increased from 0.463 x 10^{-3} to 0.497 x 10^{-3}, 0.482 x 10^{-3} to 0.547 x 10^{-3} and 0.348 x 10^{-3} to 0.432 x 10^{-3} respectively. At 50 m sliding distance, the decrease in wear coefficient from matrix alloy to hybrid composite was 0.463 x 10^{-3} to 0.348 × 10^{-3} and at 75 m sliding distance it was 0.497 x 10^{-3} to 0.432 x 10^{-3} correspondingly.

It was observed that the wear coefficient K of the matrix alloy and composite materials decreased with increase in the loads applied. The similar trends were observed in cast and T6 heat treated conditions (Sawla *et al.*, 2004, Rao *et al.*, 2010). But the wear coefficient K increased with increase in abrasive grit size for all materials in both the conditions. It was noted that the wear coefficients of the alloy and composites were more

or less same irrespective of the load and grit size. It was deduced that the hardness of the SiC reinforced composite materials dominated the abrasive wear coefficients. The observed trend was according to Archard's wear equation given in Eq. (5.3) where Q= volume loss per unit sliding distance, H= hardness of the material surface, W= applied pressure and K is the dimensionless wear coefficient less than unity (Archard *et al.*, 1953).

$$K= QH/W \tag{5.3}$$

But in case of the hardness of the hybrid composites was lower in both conditions when compared to SiC reinforced composites. It was further noticed that the wear coefficients of the hybrid composites i.e. formation probability of wear particle was found to be lower than matrix alloy. This can be attributed to composite surface being protected by reducing the material plastic flow by SiC reinforcement and self-lubricating layer formed by graphite reinforcement (Riahi *et al.*, 2001, Ted Guo *et al.*, 2000, Basavarajappa *et al.*, 2005, Suresha *et al.*, 2010, Prasad *et al.*, 1987).

At lower loads, the higher wear coefficients indicate that the probability formation of wear particle could be mainly due to crack nucleation and its propagation into micro-level crack even though the level of depth penetration of abrasive grit is low. But at higher loads it can be observed that penetration level of the grit particle will be more and the material is subjected to deform plastically (Wang *et al.*, 1989, Al-Rubaie *et al.*, 1999, Yılmaz *et al.*, 2001, Sawla *et al.*, 2004, Lin *et al.*, 1988). At higher loads, it can be noted that the asperities formed during wear process could be due to fragmentation either from the pin surface or counter surface. It was known that the hard asperities mainly consisting of grit particles, present on the counter surface penetrate deeper into the softer pin material in the very initial stages of the wear. The grit particle itself acting as a micro cutting tool where its rake angle may be positive, negative or orthogonal when it approaches the pin material. This depends on the orientation of abrasive grits bonded over the emery paper.

5.5 Wear Depth

Table 5.8 shows the wear depth of Al 6082 alloy, Al 6082- 10% SiC composites and Al 6082- 5% SiC- 5% Gr hybrid composites in cast and T6 heat treated conditions. The effect of applied load, grit size and sliding distance on wear depth was discussed briefly and separately in following sub sections.

Table 5.8: Wear depth of Al 6082 alloy, Al 6082- 10% SiC composite and Al 6082- 5% SiC- 5% Gr composite in cast and T6 heat treated conditions.

Load (N)	Grit size (µm)	Sliding distance (m)	Wear Depth , W_d (mm)					
			As cast condition			T6 condition		
			Alloy	Al-10SiC	Al-5SiC-5Gr	Alloy	Al-10SiC	Al-5SiC-5Gr
5	200	50	0.0734	0.0534	0.0394	0.0537	0.0453	0.0305
5	200	63	0.0971	0.0758	0.0585	0.0782	0.0651	0.0454
5	200	75	0.1199	0.0927	0.0742	0.0956	0.0820	0.0716
5	125	50	0.0659	0.0519	0.0442	0.0448	0.0373	0.0253
5	125	63	0.0847	0.0716	0.0639	0.0590	0.0522	0.0501
5	125	75	0.1030	0.0883	0.0706	0.0759	0.0695	0.0620
5	100	50	0.0586	0.0439	0.0380	0.0373	0.0303	0.0270
5	100	63	0.0750	0.0570	0.0500	0.0583	0.0427	0.0329
5	100	75	0.0916	0.0771	0.0671	0.0717	0.0532	0.0458
10	200	50	0.1168	0.0990	0.0852	0.0933	0.0728	0.0478
10	200	63	0.1492	0.1333	0.1239	0.1316	0.0939	0.0696
10	200	75	0.1795	0.1696	0.1569	0.1614	0.1228	0.0940
10	125	50	0.0957	0.0846	0.0740	0.0782	0.0634	0.0431
10	125	63	0.1237	0.1117	0.1072	0.1014	0.0824	0.0652
10	125	75	0.1623	0.1363	0.1334	0.1237	0.1034	0.0846
10	100	50	0.0857	0.0677	0.0657	0.0689	0.0569	0.0331
10	100	63	0.1152	0.0918	0.0837	0.0885	0.0738	0.0509
10	100	75	0.1400	0.1130	0.1009	0.1097	0.0899	0.0717
15	200	50	0.1454	0.1273	0.1172	0.1212	0.0973	0.0764
15	200	63	0.1844	0.1636	0.1536	0.1558	0.1245	0.0953
15	200	75	0.2239	0.1979	0.1871	0.1951	0.1652	0.1424
15	125	50	0.1163	0.1051	0.0994	0.1029	0.0883	0.0690
15	125	63	0.1471	0.1348	0.1261	0.1334	0.1164	0.0891
15	125	75	0.1862	0.1631	0.1532	0.1620	0.1413	0.1095
15	100	50	0.1037	0.0878	0.0777	0.0904	0.0775	0.0623
15	100	63	0.1337	0.1150	0.1047	0.1156	0.0995	0.0689
15	100	75	0.1616	0.1408	0.1298	0.1407	0.1281	0.1029

5.5.1 Effect of applied load

Fig. 5.16 shows the wear depth of alloy and composite materials plotted as a function of applied load at different grit size i.e. 100 µm-200 µm and constant 75m sliding distance in both as cast and T6 condition. It was noticed that the wear depth of the materials increases as applied load increases in as cast condition. It found to be reduced in T6 heat treatment condition from as cast condition. Fig. 5.16 (a) shows that in as cast condition, at 100 µm grit size and 5N load, the wear depth of Al 6082 alloy, Al 6082-SiC composite and Al 6082-SiC-Gr composite was found to be 0.0916 mm, 0.0771 mm and 0.0671 mm respectively. The wear depth of Al-SiC and Al-SiC-Gr reduced 15.8% and 26.7% respectively. At 15N load the wear depth of Al 6082 alloy, Al 6082-SiC hybrid composite and Al 6082-SiC-Gr hybrid composite was found to be 0.1616 mm, 0.1408 mm and 0.1298 mm respectively. The wear depth reduced around 12.9% and 19.7% for Al-SiC and Al-SiC-Gr composites respectively. In T6 condition and at 5N load, the wear depth of Al 6082 alloy, Al 6082-SiC composite and Al 6082-SiC-Gr hybrid composite was found to be 0.0717 mm, 0.0532 mm and 0.0458 mm respectively. The decrease in wear depth was 25.8% and 36.1% for Al-SiC and Al-SiC-Gr respectively. At 15N load, the wear depth of Al 6082 alloy, Al 6082-SiC composite and Al 6082-SiC-Gr hybrid composite was found to be 0.1407 mm, 0.1281mm and 0.1029 mm respectively. The percentage reduction of wear depth was around 9 and 26.9 for Al-SiC and Al-SiC-Gr composites respectively.

Fig. 5.16 (b) shows that in as cast condition, at 125 µm grit size and 5N load, the wear depth of Al 6082 alloy, Al 6082-SiC composite and Al 6082-SiC-Gr composite was found to be 0.103 mm, 0.0883 mm and 0.0706 mm respectively. The wear depth reduction for Al-SiC and Al-SiC-Gr composites was around 14.3% and 31.4% respectively. At 15N load the wear depth of Al 6082 alloy, Al 6082-SiC hybrid composite and Al 6082-SiC-Gr hybrid composite was found to be 0.1862 mm, 0.1631mm and 0.1532 mm respectively. The percentage reduction of wear depth is around 12.4 and 17.7 for Al-SiC and Al-SiC-Gr respectively. In T6 condition and at 5N load, the wear depth of Al 6082 alloy, Al 6082-SiC composite and Al 6082-SiC-Gr hybrid composite was found to be 0.0756 mm, 0.0695 mm and 0.0619 mm respectively. The decrease in wear depth is around 8% and 18.1% for Al-SiC and Al-SiC-Gr composites respectively. At 15N load, the wear depth of Al 6082 alloy, Al 6082-SiC composite and Al 6082-SiC-Gr hybrid composite was found to be 0.162 mm, 0.1412 mm and 0.1095 mm respectively. The percentage reduction of wear depth is around 12.8 and 47.9 for Al-SiC and Al-SiC-Gr respectively.

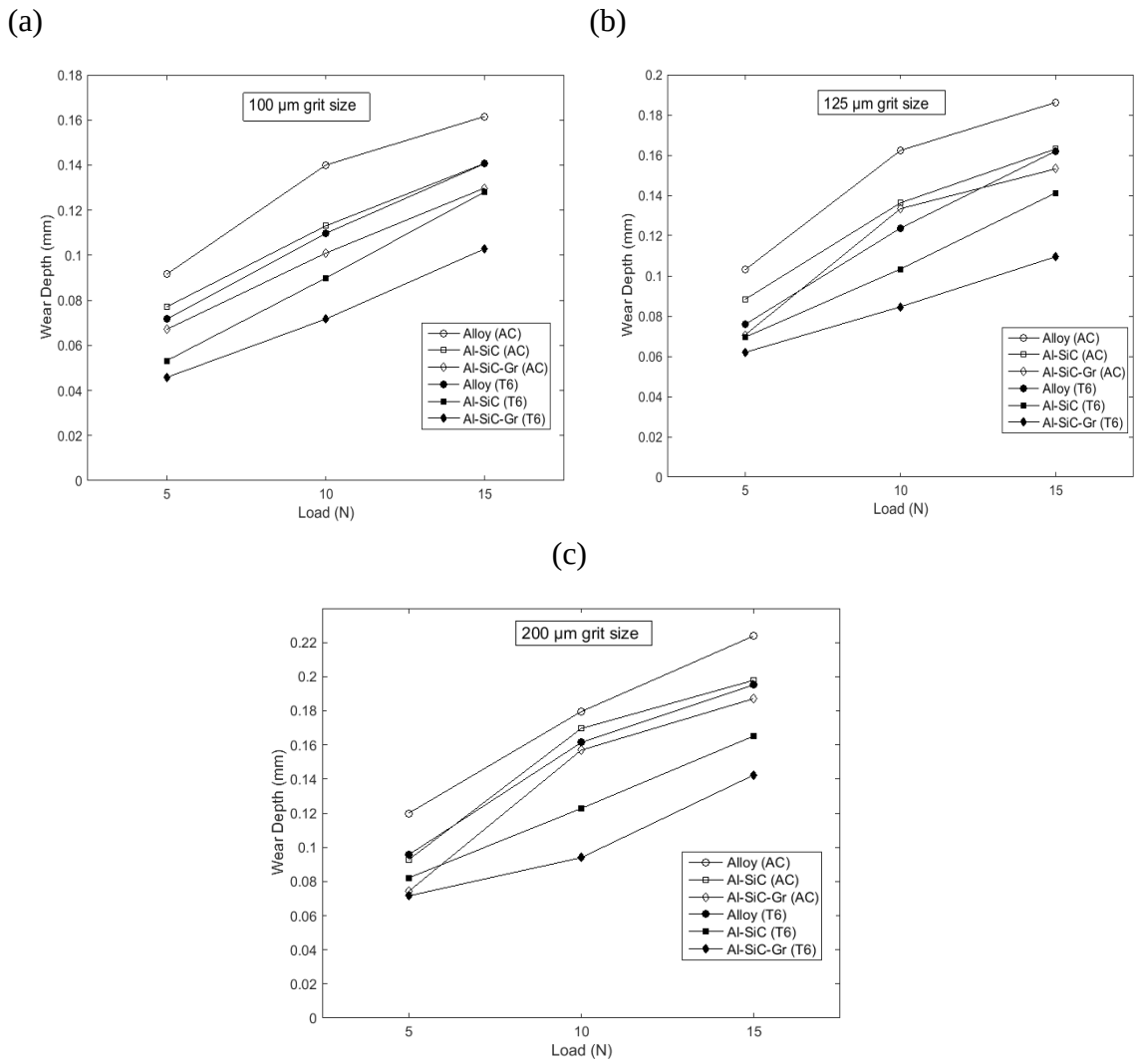

Figure 5.16: Wear Depth vs Load of unreinforced alloy and its composites at sliding distance of 75m and grit size of (a) 100 µm, (b) 125 µm and (c) 200 µm

Fig. 5.16 (c) shows that in as cast condition, at 200 µm grit size and 5N load, the wear depth of Al 6082 alloy, Al 6082-SiC composite and Al 6082-SiC-Gr composite was found to be 0.1199 mm, 0.0927 mm and 0.0742 mm respectively. The reduction of wear depth for Al-SiC and Al-SiC-Gr composites was around 22.7% and 38.1% respectively. At 15N load the wear depth of Al 6082 alloy, Al 6082-SiC hybrid composite and Al 6082-SiC-Gr hybrid composite was found to be 0.2234 mm, 0.1979 mm and 0.1871 mm respectively. The decrease in wear depth was around 11.4% and 16.2% for Al-SiC and Al-SiC-Gr respectively. In T6 heat treated condition and at 5N load, the wear depth of Al 6082 alloy, Al 6082-SiC composite and Al 6082-SiC-Gr hybrid composite was found to be 0.0956 mm, 0.082 mm and 0.0716 mm respectively. The percentage reduction of wear depth is around 14.2 and 25.1 for Al-SiC and Al-SiC-Gr respectively. At 15N load, the wear depth of Al 6082 alloy, Al 6082-SiC composite and Al 6082-SiC-Gr hybrid composite

was found to be 0.1951mm, 0.1652 mm and 0.1424 mm respectively. The wear depth of Al-SiC and Al-SiC-Gr reduced 15.3% and 27% respectively.

5.5.2 Effect of grit size

Fig. 5.17 shows the wear depth of alloy and composite materials plotted as a function of grit size at different applied loads i.e. 5N-15N and constant 75m sliding distance in both as cast and T6 condition. It was noted that as abrasive grit size increases, the wear depth of the materials increases in both condition whereas it reduced to addition of reinforcements and T6 heat treatment. Fig. 5.17 (a) shows that in as cast condition, at 5N load and 100 µm grit size, the wear depth of Al 6082 alloy, Al 6082-SiC composite and Al 6082-SiC-Gr composite was found to be 0.0916 mm, 0.0771 mm and 0.0671 mm respectively. The wear depth reduced 15.8% and 26.7% for Al-SiC and Al-SiC-Gr respectively. At 200 µm grit size the wear depth of Al 6082 alloy, Al 6082-SiC hybrid composite and Al 6082-SiC-Gr hybrid composite was found to be 0.1199 mm, 0.0927 mm and 0.0742 mm respectively. The percentage reduction of wear depth is around 22.7 and 38.1 for Al-SiC and Al-SiC-Gr respectively. In T6 condition and at 100 µm grit size, the wear depth of Al 6082 alloy, Al 6082-SiC composite and Al 6082-SiC-Gr hybrid composite was found to be 0.0717 mm, 0.0532 mm and 0.0458 mm respectively. The reduction percentage of wear depth was noted to be 25.8 and 36.1 for Al-SiC and Al-SiC-Gr respectively. At 200 µm grit size, the wear depth of Al 6082 alloy, Al 6082-SiC composite and Al 6082-SiC-Gr hybrid composite was found to be 0.0956 mm, 0.082 mm and 0.0716 mm respectively. The decrease in wear depth for Al-SiC and Al-SiC-Gr composites was around 14.2% and 25.1% respectively.

Fig. 5.17 (b) shows that in as cast condition, at 10N load and 100 µm grit size, the wear depth of Al 6082 alloy, Al 6082-SiC composite and Al 6082-SiC-Gr composite was found to be 0.1399 mm, 0.113 mm and 0.1009 mm respectively. The decrease in wear depth was around 19.2% and 27.9% for Al-SiC and Al-SiC-Gr respectively. At 200 µm grit size, the wear depth of Al 6082 alloy, Al 6082-SiC hybrid composite and Al 6082-SiC-Gr hybrid composite was found to be 0.1795 mm, 0.1696 mm and 0.1569 mm respectively. The percentage reduction of wear depth for Al-SiC and Al-SiC-Gr was 5.5 and 12.6 respectively. In T6 condition and at 100 µm grit size, the wear depth of Al 6082 alloy, Al 6082-SiC composite and Al 6082-SiC-Gr hybrid composite was found to be 0.1097 mm, 0.0899 mm and 0.0717 mm respectively. The wear depth reduced 18% and 34.6% for Al-SiC and Al-SiC-Gr respectively. At 200 µm grit size, the wear depth of Al 6082 alloy, Al

6082-SiC composite and Al 6082-SiC-Gr hybrid composite was found to be 0.1614 mm, 0.1228 mm and 0.094 mm respectively. The reduction of wear depth for Al-SiC and Al-SiC-Gr was around 23.9% and 41.8% respectively.

(a) (b)

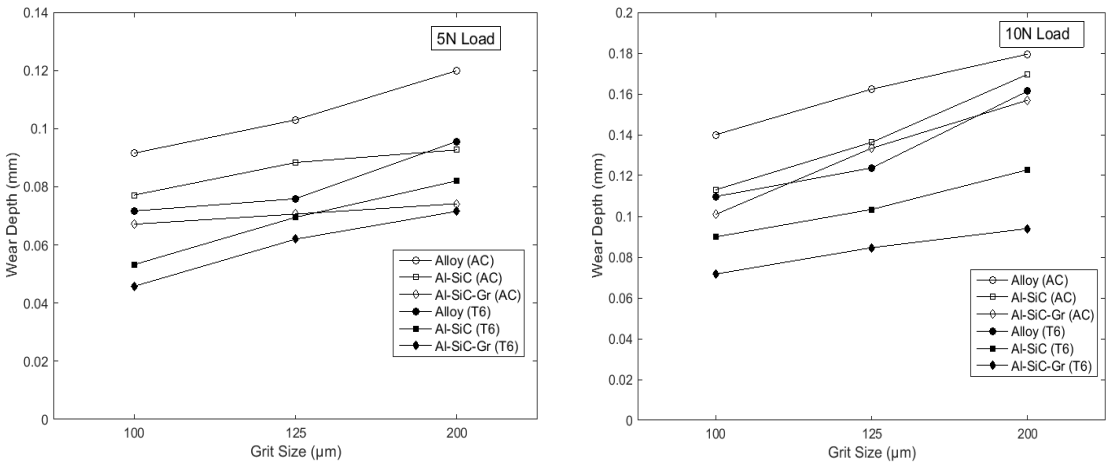

(c)

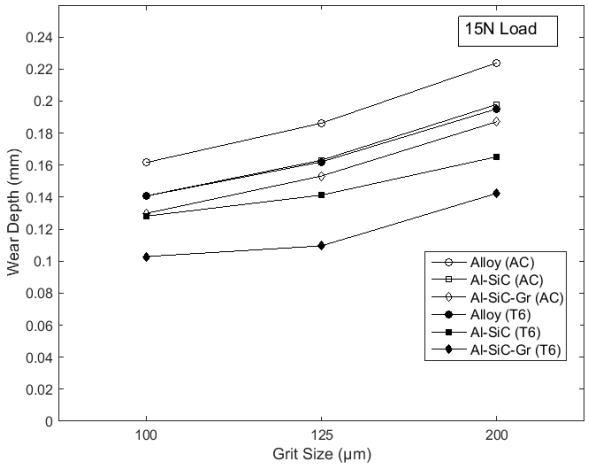

Figure 5.17: Wear Depth vs grit size of unreinforced alloy and its composites at sliding distance of 75m and applied loads of (a) 5N, (b) 10N and (c) 15N

Fig. 5.17 (c) shows that in as cast condition, at 15N load and 100 µm grit size, the wear depth of Al 6082 alloy, Al 6082-SiC composite and Al 6082-SiC-Gr composite was found to be 0.1616 mm, 0.1408 mm and 0.1298 mm respectively. The percentage reduction of wear depth is around 12.9 and 19.6 for Al-SiC and Al-SiC-Gr respectively. At 200 µm grit size the wear depth of Al 6082 alloy, Al 6082-SiC hybrid composite and Al 6082-SiC-Gr hybrid composite was found to be 0.2239 mm, 0.1979 mm and 0.1871mm respectively. The percentage reduction of wear depth is around 11.6 and 16.4 for Al-SiC and Al-SiC-Gr respectively. But in T6 condition and at 100 µm grit size, the wear depth of Al 6082 alloy,

Al 6082-SiC composite and Al 6082-SiC-Gr hybrid composite was found to be 0.1406 mm, 0.1281 mm and 0.1028 mm respectively. The percentage reduction of wear depth is around 8.9 and 26.9 for Al-SiC and Al-SiC-Gr respectively. At 200 µm grit size, the wear depth of Al 6082 alloy, Al 6082-SiC composite and Al 6082-SiC-Gr hybrid composite was found to be 0.1951 mm, 0.1652 mm and 0.1424 mm respectively. The reduction of wear depth is around 15.3% and 27% for Al-SiC and Al-SiC-Gr respectively.

5.5.3 Effect of sliding distance

Fig. 5.18 shows the wear depth of alloy and composite materials plotted as a function of sliding distance at different applied loads i.e. 5N-15N and constant 200 µm grit size in both as cast and T6 condition. It was observed that as sliding distance increases, the depth of wear of the materials in both conditions increased. But it improved due to T6 heat treatment and addition of reinforcements. Fig. 5.18 (a) shows that in as cast condition, at 5N load and 50 m sliding distance, the wear depth of Al 6082 alloy, Al 6082-SiC composite and Al 6082-SiC-Gr composite was found to be 0.0733 mm, 0.0534 mm and 0.0394 mm respectively. The reduction in wear depth was around 27.1% and 46. 2% for Al-SiC and Al-SiC-Gr respectively. At 75 m sliding distance the wear depth of Al 6082 alloy, Al 6082-SiC hybrid composite and Al 6082-SiC-Gr hybrid composite was found to be 0.1199 mm, 0.0927 mm and 0.0742 mm respectively. The percentage reduction of wear depth is around 22.7 and 38.1 for Al-SiC and Al-SiC-Gr respectively. But in T6 condition and at 50 m sliding distance, the wear depth of Al 6082 alloy, Al 6082-SiC composite and Al 6082-SiC-Gr hybrid composite was found to be 0.0537 mm, 0.0453 mm and 0.0305 mm respectively. The wear depth reduction percentage was around 15.6 and 43.2 for Al-SiC and Al-SiC-Gr respectively. At 75 m sliding distance, the wear depth of Al 6082 alloy, Al 6082-SiC composite and Al 6082-SiC-Gr hybrid composite was found to be 0.0956 mm, 0.082 mm and 0.0715 mm respectively. The percentage decrease in wear depth for Al-SiC and Al-SiC-Gr was around 14.2 and 25.1 respectively.

Fig. 5.18 (b) shows that in as cast condition, at 10N load and 50 m sliding distance, the wear depth of Al 6082 alloy, Al 6082-SiC composite and Al 6082-SiC-Gr composite was found to be 0.1168 mm, 0.099 mm and 0.0852 mm respectively. The percentage reduction in wear depth of Al-SiC and Al-SiC-Gr is around 15.2 and 27 respectively. The wear depth of Al 6082 alloy, Al 6082-SiC hybrid composite and Al 6082-SiC-Gr hybrid composite was found to be 0.1795 mm, 0.1696 mm and 0.1569 mm respectively at 75 m sliding distance. The reduction in wear depth for Al-SiC and Al-SiC-Gr was around 5.5%

and 12.6% respectively. But in T6 condition and at 50 m sliding distance, the wear depth of Al 6082 alloy, Al 6082-SiC composite and Al 6082-SiC-Gr hybrid composite was found to be 0.0932 mm, 0.0728 mm and 0.0478 mm respectively. The percentage reduction of wear depth is around 21.9 and 48.7 for Al-SiC and Al-SiC-Gr respectively. At 75 m sliding distance, the wear depth of Al 6082 alloy, Al 6082-SiC composite and Al 6082-SiC-Gr hybrid composite was found to be 0.1614 mm, 0.1228 mm and 0.094 mm respectively. The wear depth reduction for Al-SiC and Al-SiC-Gr was 23.9% and 41.8% respectively.

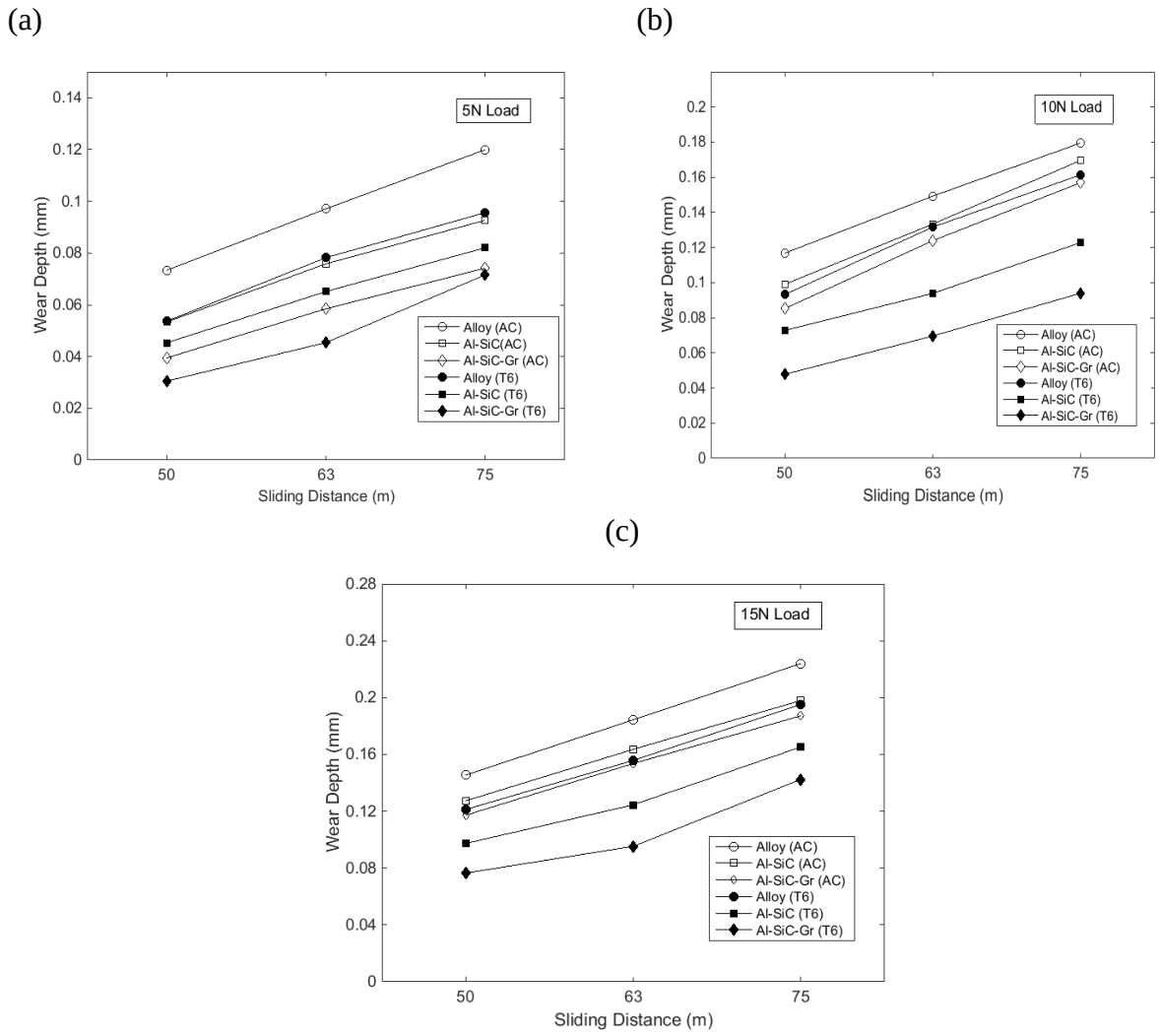

Figure 5.18: Wear Depth vs sliding distance of unreinforced alloy and its composites at grit size of 200 µm and applied loads of (a) 5N, (b) 10N and (c) 15N

Fig. 5.18 (c) shows that in as cast condition, at 15N load and 50 m sliding distance, the wear depth of Al 6082 alloy, Al 6082-SiC composite and Al 6082-SiC-Gr composite was found to be 0.1454 mm, 0.1272 mm and 0.1172 mm respectively. The wear depth reduced 12.5% and 19.4% for Al-SiC and Al-SiC-Gr respectively. At 75 m sliding distance the wear depth of Al 6082 alloy, Al 6082-SiC hybrid composite and Al 6082-SiC-Gr hybrid

composite was found to be 0.2239 mm, 0.1979 mm and 0.1871 mm respectively. The percentage reduction of wear depth is around 11.6 and 16.4 for Al-SiC and Al-SiC-Gr respectively. In T6 condition and at 50 m sliding distance, the wear depth of Al 6082 alloy, Al 6082-SiC composite and Al 6082-SiC-Gr hybrid composite was found to be 0.1212 mm, 0.0973mm and 0.0764 mm respectively. The wear depth decreased 19.7% and 36.9% for Al-SiC and Al-SiC-Gr composites respectively. At 75 m sliding distance, the wear depth of Al 6082 alloy, Al 6082-SiC composite and Al 6082-SiC-Gr hybrid composite was found to be 0.1951 mm, 0.1652 mm and 0.1424 mm respectively. The reduction in wear depth was 15.3% and 27% for Al-SiC and Al-SiC-Gr respectively.

5.6 Surface Profilometry

The surface roughness was evaluated and represented in 3D surface profiles of all the materials in both the conditions. This was represented in Table 5.9 and Fig. 5.19.

Table 5.9: Surface roughness of alloy and composites

Sl. No	Load (N)	Grit (µm)	Sliding Distance (m)	Surface Roughness, Ra (µm)					
				Alloy (AC)	Alloy (T6)	Al-SiC (AC)	Al-SiC (T6)	Al-SiC-Gr (AC)	Al-SiC-Gr (T6)
1	5	200	75	16.9	12.9	12.6	10	4.7	2.8
2	10			20.2	13.6	18.4	11.2	5.4	3.1
3	15			28.8	21.7	24	15.4	7.8	4.7
4	5	125		14.9	11.6	13.3	9.1	6	1.9
5	10			21.8	12.8	16.7	10.9	6.7	2.7
6	15			25.9	20	21.9	16.1	8.1	3.9
7	5	100		12.1	10.7	9.5	7.5	3.7	1.8
8	10			13.2	11.4	8.3	6.4	4.2	2.2
9	15			14.5	12.5	7.8	5.9	4.6	2.9

It was noticed that surface roughness was found to be lower in hybrid composites when compared to matrix material and SiC alone reinforced composites. From the Table 5.9, the results show that the surface roughness increased with increase in load and abrasive grit size for matrix alloy and its composites in both the conditions. It was observed that the effect of T6 heat treatment reduced the surface roughness. The addition of hard SiC reinforcement to the matrix material reduced the surface roughness. It can be expected that SiC reinforcement reduced the deformation zones by hindering the plastic flow of the matrix material. It was observed that the addition of both SiC and graphite reinforcements to the matrix material, the surface roughness further reduced. The addition of reinforcements to matrix material lead to reduction in surface roughness of the materials as

reported by Yilmaz et al., (2001) and Suresh et al., (2014). This could be due to SiC addition arrests the material flow and reduces the deformed zones whereas graphite acted as a polishing or lubricating agent in between pin sample and grit paper during abrasion process.

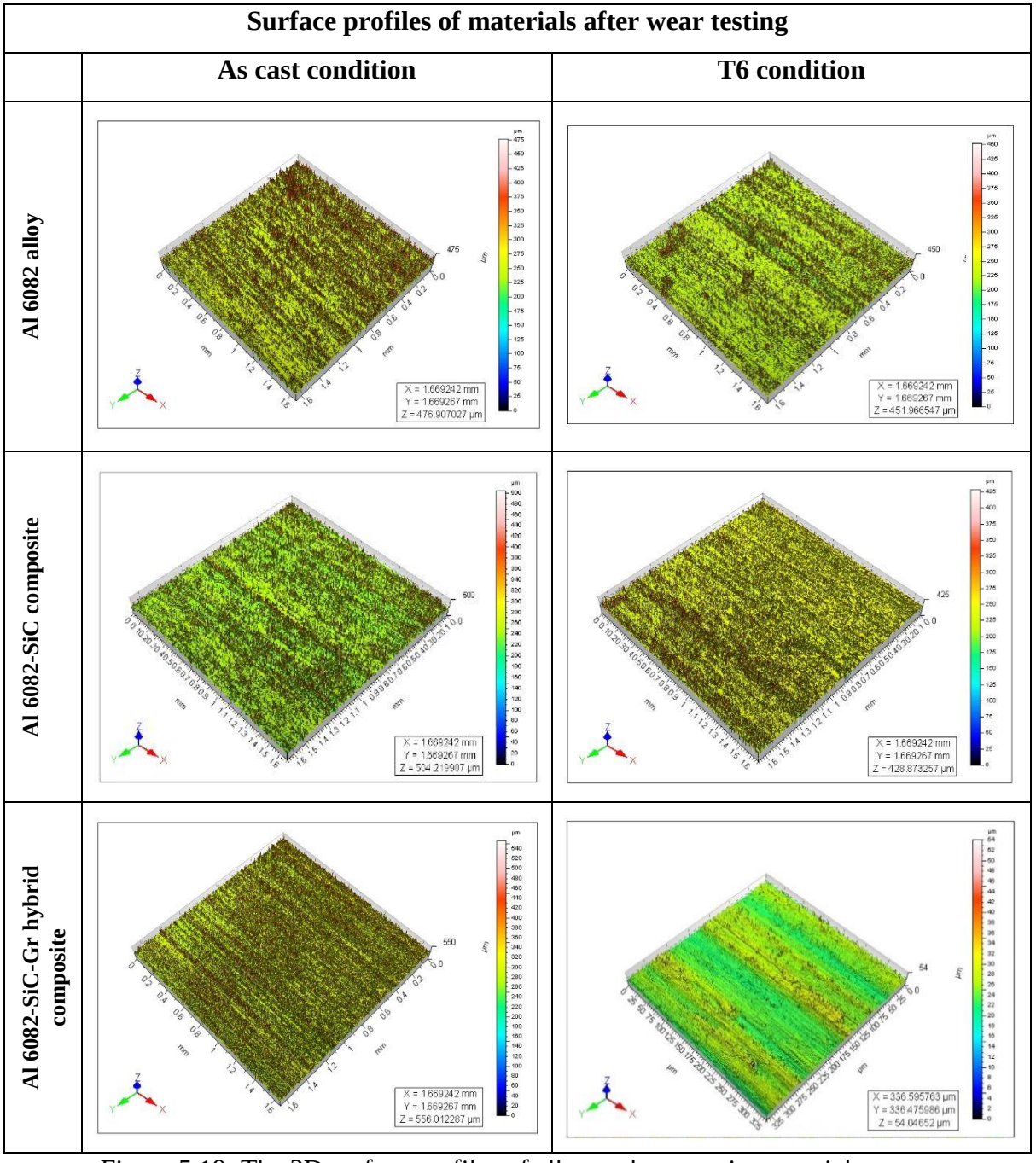

Figure 5.19: The 3D surface profiles of alloy and composite materials

5.7 Worn Surface Analysis

5.7.1 Pin Sample

The worn surface examination of Al 6082 alloy, Al-SiC composites and Al-SiC-Gr hybrid composites pin samples was done to understand the possible material removal mechanism in the wear process. Fig 5.20 indicates the worn surface topographies of wear tested pins at different applied loads, grit size of 200 µm and sliding distance of 75m. Fig. 5.20 (a), (c) and (e) were the abrasive worn surface topographies of Al 6082 alloy, Al-SiC, Al-SiC-Gr tested at lower loads respectively. Fig. 5.20 (b), (d) and (f) were the abrasive worn surface topographies of Al 6082 alloy, Al-SiC, Al-SiC-Gr tested at higher loads respectively. Fig 5.20 (a) shows the worn surface of Al 6082 alloy at 5N applied load; Fig 5.20 (b) Al 6082 alloy at 15N applied load; Fig 5.20 (c) Al 6082-SiC composite at 5N applied load; Fig 5.20 (d) Al 6082-SiC composite at 15N applied load; Fig 5.20 (e) Al 6082-SiC-Gr composite at 5N applied load; Fig 5.20 (f) Al 6082-SiC-Gr composite at 15N applied load.

Fig. 5.20 (a)-(f) show the parallel continuous long grooves in sliding direction were marked with white arrows and the damaged portions formed during wear process were indicated with A. In the case of alloy, the damaged portions on pin surface was found severe as represented in Fig. 5.20 (a) & (b). It can be noticed that these portions will act as nucleating sites for material removal in wear process. Hence, the plastic type removal of material from the alloy pin surface takes place. Similarly, the long continuous grooves were observed in Al-SiC composites (Fig. 5.20 (c) & (d)), but the damaged portions were found to be reduced when compared with matrix alloy. In case of Al-SiC-Gr hybrid composites, partial surface deformation can be observed in the Fig. 5.20 (e)-(f). The worn surfaces were found to be comparable to matrix alloy and Al-SiC composites. This could be due to presence of hard SiC reinforcement arrested plastic flow of matrix material and soft graphite reinforcement formed self-lubricant and sacrificial layer over the counter surface.

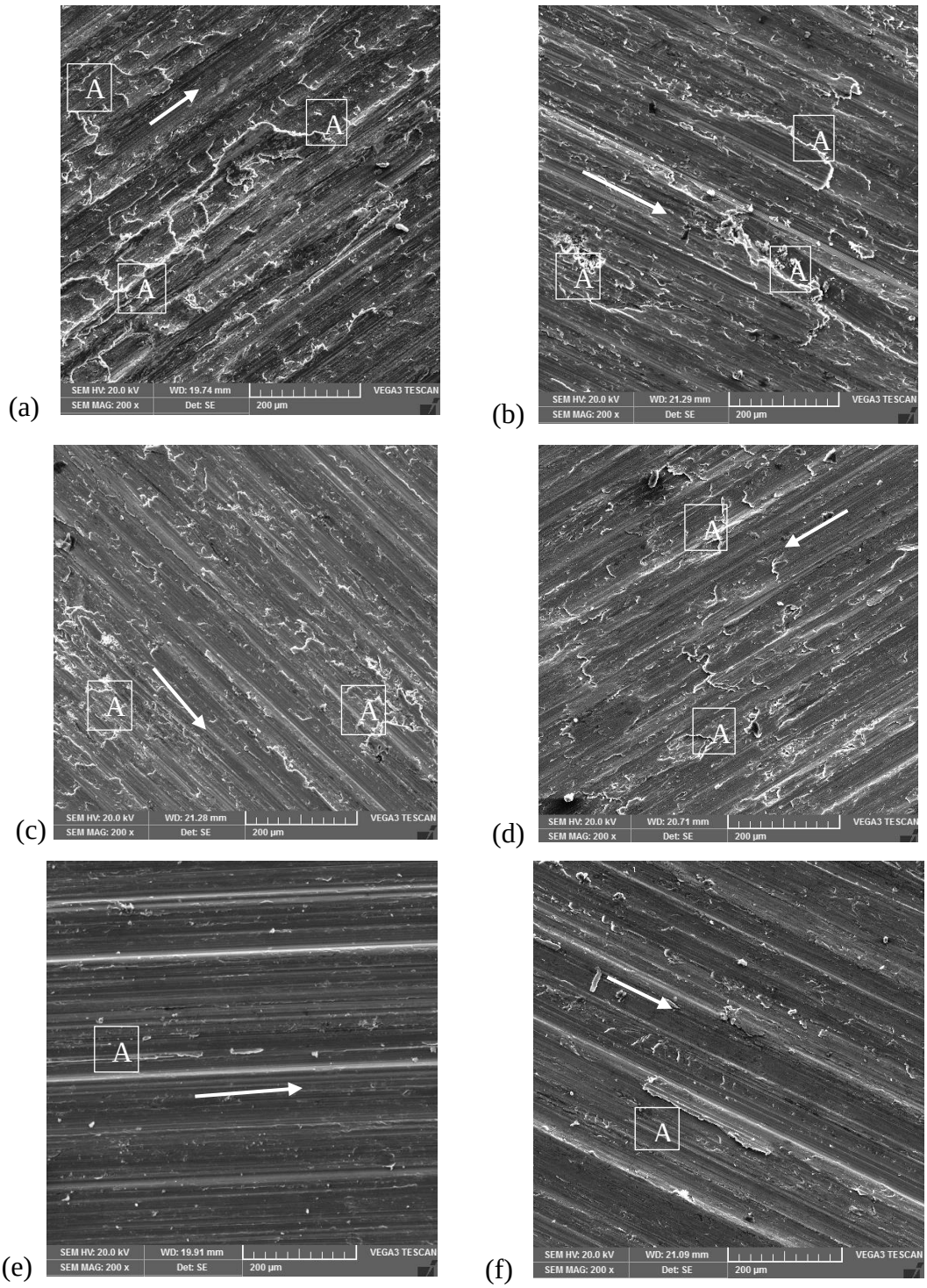

Figure 5.20: Worn surface topographies of wear tested pins of (a) Al 6082 alloy at 5N load and 200 µm grit size (b) Al 6082 alloy at 15N load and 200 µm grit size (c) Al 6082-SiC composite at 5N load and 200 µm grit size (d) Al 6082-SiC composite at 15N load and 200

μm grit size (e) Al 6082-SiC-Gr composite at 5N load and 200 μm grit size (f) Al 6082-SiC-Gr composite at 15N load and 200 μm grit size.

Fig. 5.21 (a)-(f) show the worn surface images of Al 6082 matrix alloy and Al 6082-SiC-Gr hybrid composite pins tested at 15N applied load, 75m sliding distance and different grit size conditions. Fig. 5.21 (a) indicate the worn surface of Al 6082 matrix alloy pin tested at 15N applied load and 200 μm grit size; Fig. 5.21 (b) indicate the worn surface of Al 6082 matrix alloy pin tested at 15N applied load and 125 μm grit size; Fig. 5.21 (c) indicate the worn surface of Al 6082 matrix alloy pin tested at 15N applied load and 100μm grit size; Fig. 5.21 (d) indicate the worn surface of Al 6082-SiC-Gr hybrid composite pin tested at 15N applied load and 200 μm grit size; Fig. 5.21 (e) indicate the worn surface of Al 6082-SiC-Gr hybrid composite pin tested at 15N applied load and 125 μm grit size and Fig. 5.21 (f) indicates the worn surface of Al 6082-SiC-Gr hybrid composite pin tested at 15N applied load and 100 μm grit size.

The plastic flow of the material on the pin happened due to abrasion and the wear tracks were clearly shown in Fig. 5.21 (a)-(f). The arrow marks in the Fig. 5.21 indicate the continuous parallel grooves formed over pin surface in the direction of the sliding during the abrasive wear process. In some areas (represented with A) indicate the deformed zones i.e. craters, extended lips. From the Fig. 5.21 (a)-(c) to Fig. 5.21 (d)-(f), it was noticed that the worn surfaces of matrix alloy pins and hybrid composite pins can be differentiated. The damaged portions on the surface, depth of grooves and roughness over the surface of alloy pin was found to be higher due to more material deterioration shown in Fig. 5.21 (a)-(c). But, the depth of grooves formed during wear was observed to be shallower for hybrid composite pin compared to alloy. The addition of SiC reinforcement to the matrix material reduced the surface roughness as reported earlier was observed. It can be expected that hard reinforcement reduced the deformation zones by hindering the plastic flow of the matrix material during abrasive action of grit (Yilmaz *et al.*, 2001, Riahi *et al.*, 2001, Ted Guo *et al.*, 2000, Prasad *et al.*, 1987). The reduction in the deformation zones was observed in Fig. 5.21 (d)-(f). It can be regarded that from the worn surfaces, the groove plays an important role, as wear process is progressed by its formation and growth. The groove formation takes place at locally fractured area of matrix or reinforcement. But due to non-uniform surface of counter material and defective areas of pin surface, localization of frictional forces arise and aggravate to the fracture over the surface along with groove (Lee *et al*., 1992).

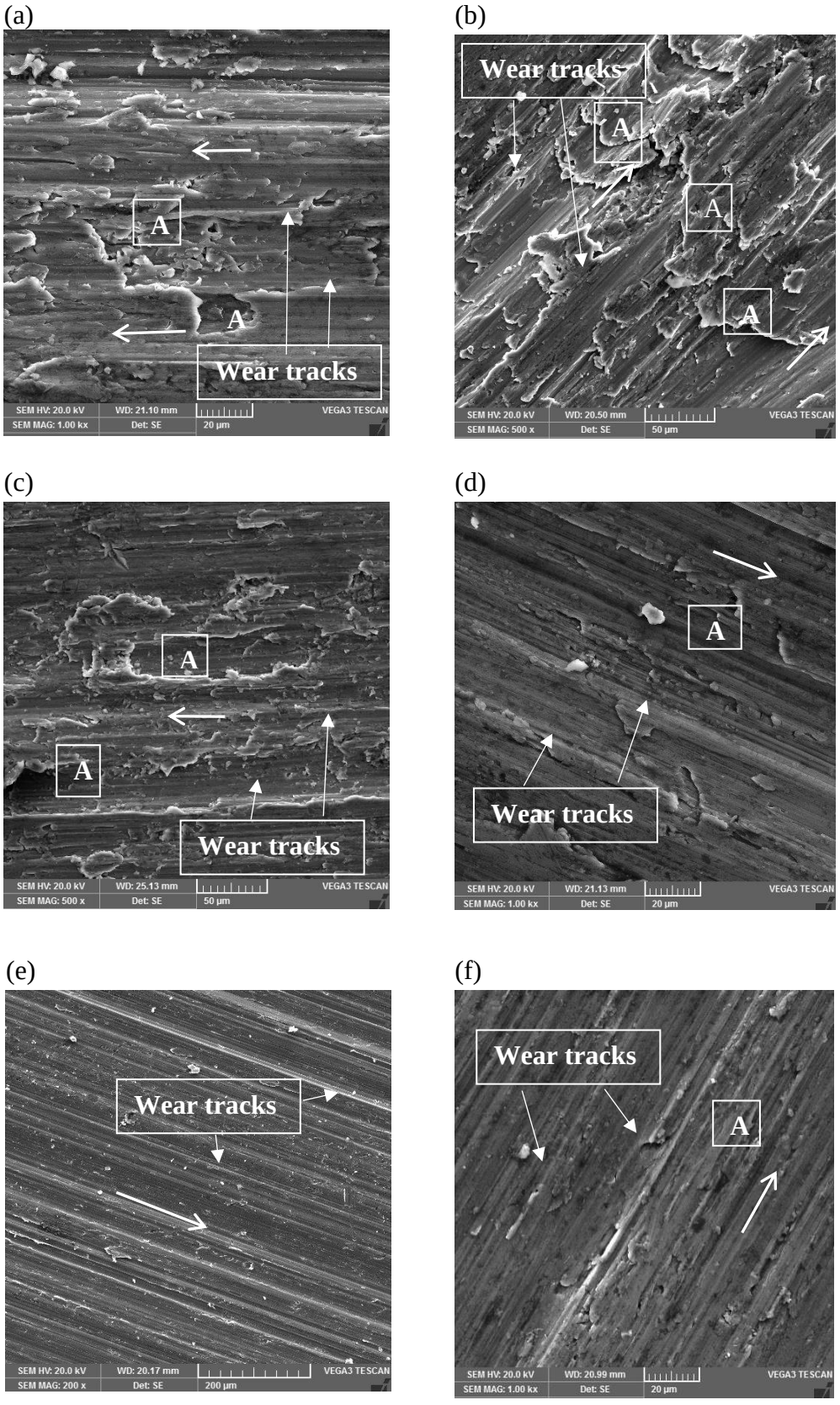

Figure 5.21: The worn surface images of (a) Al 6082 matrix alloy pin tested at 15N load and 200 µm grit size (b) Al 6082 matrix alloy pin tested at 15N load and 125 µm grit size (c) Al 6082 matrix alloy pin tested at 15N load and 100 µm grit size (d) Al 6082-SiC-Gr

hybrid composite pin tested at 15N load and 200 µm grit size (e) Al 6082-SiC-Gr hybrid composite pin tested at 15N load and 125 µm grit size (f) Al 6082-SiC-Gr hybrid composite pin tested at 15N load and 100 µm grit size.

5.7.2 Emery Paper

Fig. 5.22 (a)-(f) represent the worn surfaces of emery paper on which Al 6082 matrix alloy and Al 6082-SiC-Gr hybrid composite pins were tested at different load and grit size conditions. Fig. 5.22 (a) indicate the worn surface of emery paper on which Al 6082 matrix alloy pin was tested at 5N load and 200µm grit size; Fig. 5.22 (b) shows the worn surface of emery paper on which Al 6082 matrix alloy pin was tested at 15N load and 200 µm grit size; Fig. 5.22 (c) depicts the worn surface of emery paper on which Al 6082 matrix alloy pin was tested at 15N load and 100 µm grit size; Fig. 5.22 (d) indicate the worn surface of Al 6082-SiC-Gr hybrid composite pin was tested at 5N load and 200 µm grit size; Fig. 5.22 (e) represents the worn surface of emery paper on which Al 6082-SiC-Gr hybrid composite pin was tested at 15N load and 200 µm grit size and Fig. 5.22 (f) indicate the worn surface of emery paper on which Al 6082-SiC-Gr hybrid composite pin was tested at 15N load and 100 µm grit size.

The worn surface images of emery papers contained (i) the particle pick up i.e. debonded from the emery paper, (ii) blunting of the abrasive grit particle, (iii) fracture of the abrasive grit particle and (iv) debris (indicated with D) over the emery paper. The particle pick up (indicated with P) and blunting of abrasive grit particle (indicated with B) or fracture of abrasive grit particle (indicated with F) depend on the intensity of the applied pressures acted upon each abrasive grit. At lower applied pressures and higher abrasive grit size, the blunting of grit particle was observed along with grit particle pickup. This was indicated in Fig. 5.22 (a) and (d). At higher applied pressures and lower abrasive grit size, the pickup and fracture of grit particle was observed to be higher as observed in Fig. 5.22 (c) and (f). It was also noticed that few areas had debris over the emery paper. This can be observed in Fig. 5.22 (b)-(f). The debris formed could be mainly of the fragments which are detached or released either from the pin surface or the emery paper.

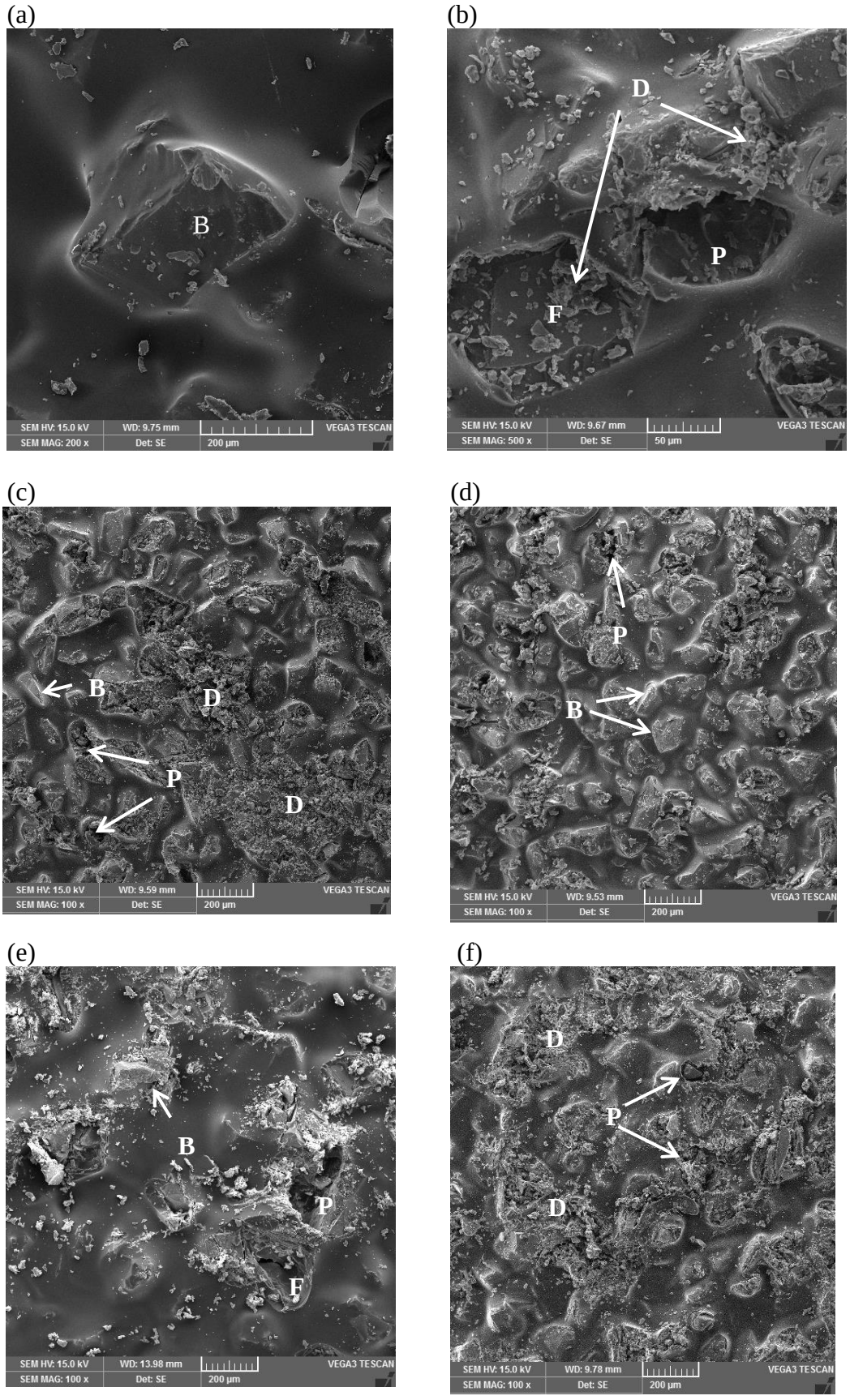

Figure 5.22: The worn surfaces of emery paper tested on (a) Al 6082 matrix alloy pin tested at 5N load and 200 µm grit size (b) Al 6082 matrix alloy pin tested at 15N load and 200

μm grit size (c) Al 6082 matrix alloy pin tested at 15N load and 100 μm grit si ze (d) Al 6082-SiC-Gr hybrid composite pin tested at 5N load and 200 μm grit size (e) Al 6082-SiC-Gr hybrid composite pin tested at 15N load and 200 μm grit size (f) Al 6082-SiC-Gr hybrid composite pin tested at 15N load and 100 μm grit size.

Larsen-Basse *et al*., (1972) reported that abrasives with finer grit size would deteriorate severely than that of coarser grits for given load and sliding distance. The particle pick-up (marked as B) depends on the level of interface bond of grit particle to the emery paper. Johnson *et al*., (1970) observed that the pick-up of abrasive grit particle will be higher for finer ones than coarser grits. This was due to deterioration of finer grits rapidly in operating condition. It was also expected that the wear rate will be lesser for finer grits. Hence the finer grits would ruin easily and ability of material removal comes down. It was noticed that as the applied load increases, the stress levels increase at the contact interface of pin specimen and counter emery paper. For higher grit particle size and applied load, it was deduced that the penetration depth would be more and even it can cause intense damage to the material surface.

5.7.3 Wear Debris

The SEM images of wear debris of pin samples in Fig. 5.23. Fig. 5.23 (a) indicate the wear debris of Al 6082 matrix alloy pin tested at lower load and lower grit size; Fig. 5.23 (b) represents the wear debris of Al 6082-SiC-Gr hybrid composite pin tested at lower load and grit size; Fig. 5.23 (c) shows the wear debris of Al 6082 matrix alloy pin tested at higher load and higher grit size; Fig. 5.23 (d) depicts the wear debris of Al 6082-SiC-Gr hybrid composite pin tested at higher load and higher grit size. In Fig. 5.23, the region marked as ‘C’ indicates the chips and the region ‘G’ represents the grit particle that was fractured or debonded from the emery paper. The chips formed in debris are of short, long discontinuous and fragmented in case alloy as indicated in Fig. Fig. 5.23 (a)-(b). But in Fig. Fig. 5.23 (c)-(d) the grit particle along with discontinuous chips was also evident. This could be due to higher applied stresses developed during abrasion process (Sawla *et al.*, 2004, Lin *et al.*, 1988).

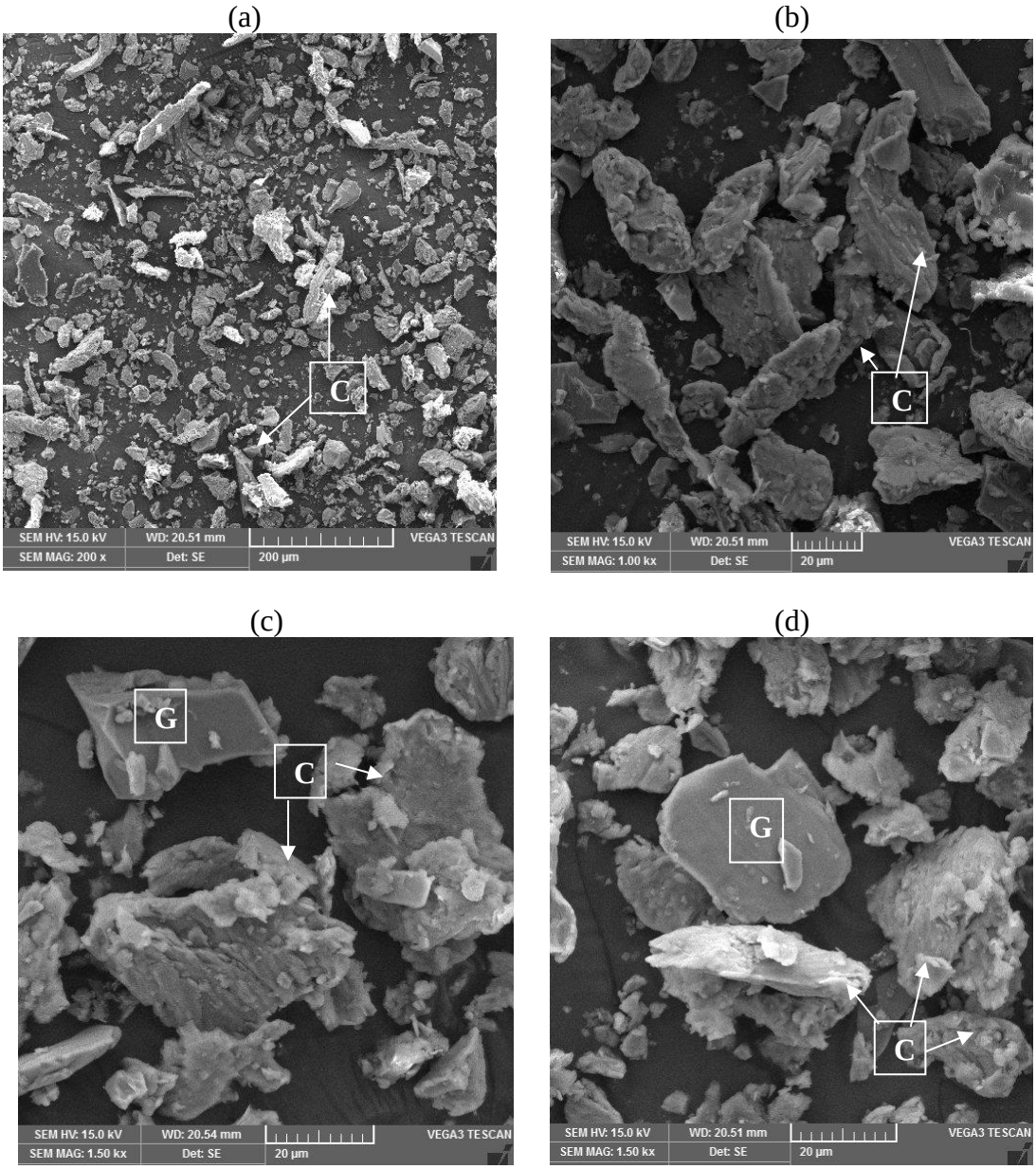

Figure 5.23: The SEM images of wear debris removed from (a) Al 6082 matrix alloy pin tested at lower load and lower grit size (b) Al-SiC-Gr hybrid composite pin tested at lower load and grit size (c) Al 6082 matrix alloy pin tested at higher load and higher grit size (d) Al-SiC-Gr hybrid composite pin tested at higher load and higher grit size

(a) 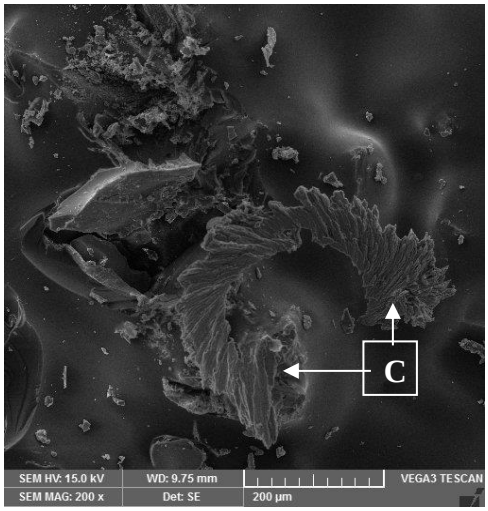

(b) 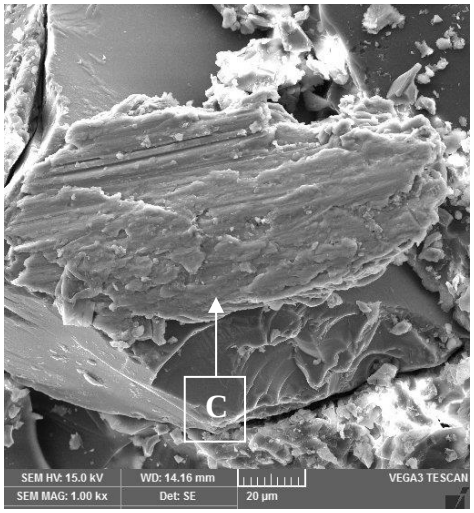

Figure 5.24: Type of chip temporarily bonded over grit particle in abrasive wear process (a) plastically flowed chip formed for alloy pin (b) discontinuous chip formed for hybrid composite pin.

Fig. 5.24 indicates the type of chips which are temporarily bonded over grit particle during abrasive wear process of alloy and hybrid composite pin. The formation of chip represented with 'C' is observed to be different from matrix alloy and composite material. The chip formed was found to be temporarily bonded over the emery paper. Fig. 5.24 (a) and Fig. 5.24 (b) represent the plastically flow chip (ribbon type) of alloy pin and discontinuous chip of hybrid composite pin adhered to the abrasive grit of the emery paper.

5.8 Wear Mechanisms

In this section, a brief understanding on the possible wear mechanisms was discussed. Fig. 5.25 shows the schematic diagram of abrasion process of pin sample, which is over the emery paper bonded disc. The arrow marks longitudinal direction indicates the applied load and lateral direction indicates the sliding direction.

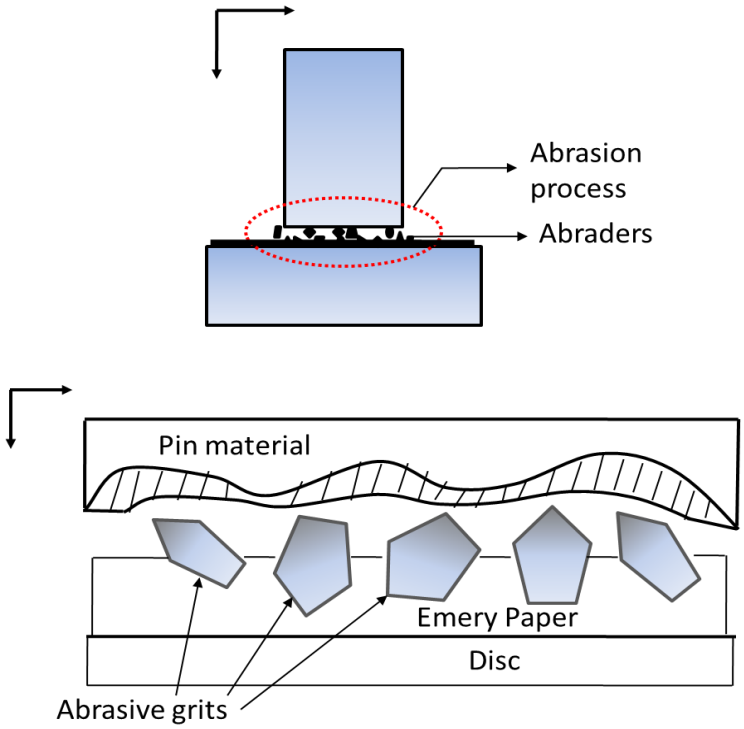

Figure 5.25 : A schematic diagram of abrasion process

Fig. 5.26 shows the possible interaction between abrasive grit and material surface. It was illustrated through the rake angle of the abrasive grit. As studied in machining process, the abrasive grit can be assumed as a cutting tool. The process of abrasive wear process can be understood similar to that grinding process. The rake angle of a cutting tool, one of the major significant parameter in tool nomenclature, decides the characteristics of machining process. The type of rake angle and its effects was reported below.

(i) Negative rake angle

- Rake face ahead the radial line
- Make the tool more blunt
- Increases the strength of the cutting edge.
- Increase the cutting forces.

- Can increase friction, resulting in higher temperatures.
- Can improve surface finish.

(ii) Zero rake angle

- Rake face and the radial line coincide each other.
- It has a larger crater wear when compared to positive rake angle as the chip slides over the rake face.

(iii) Positive rake angle

- Rake face trials the radial line
- Make the tool more sharp and pointed.
- This reduces the strength of the tool, as the small included angle in the tip may cause it to chip away.
- Reduce cutting forces and power requirements.
- Helps in the formation of continuous chips in ductile materials.

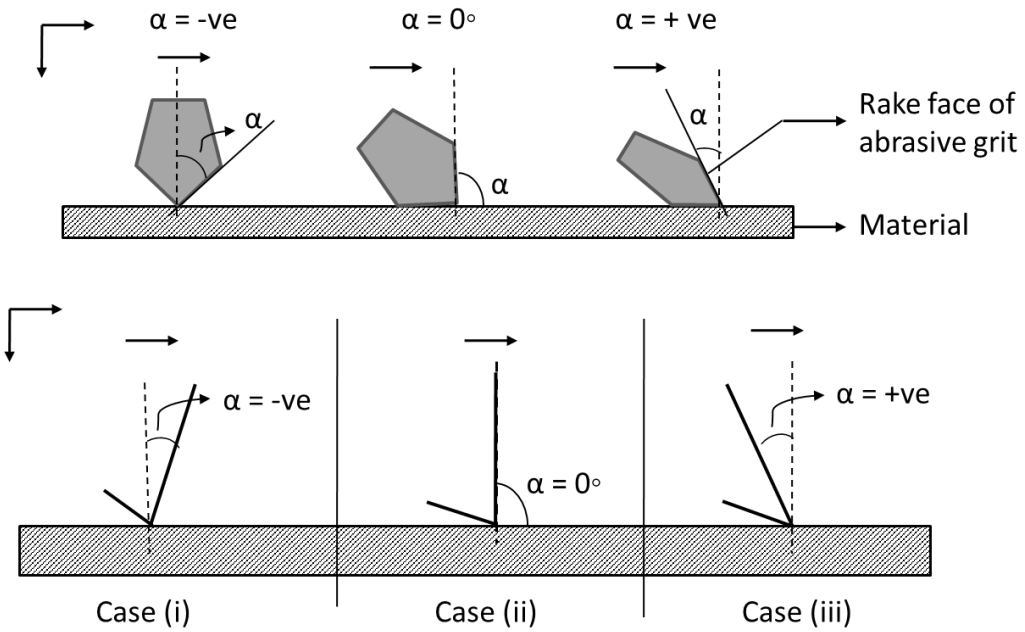

Figure 5.26: Abrasive grit and material surface interaction: Illustration through the effect of rake angle

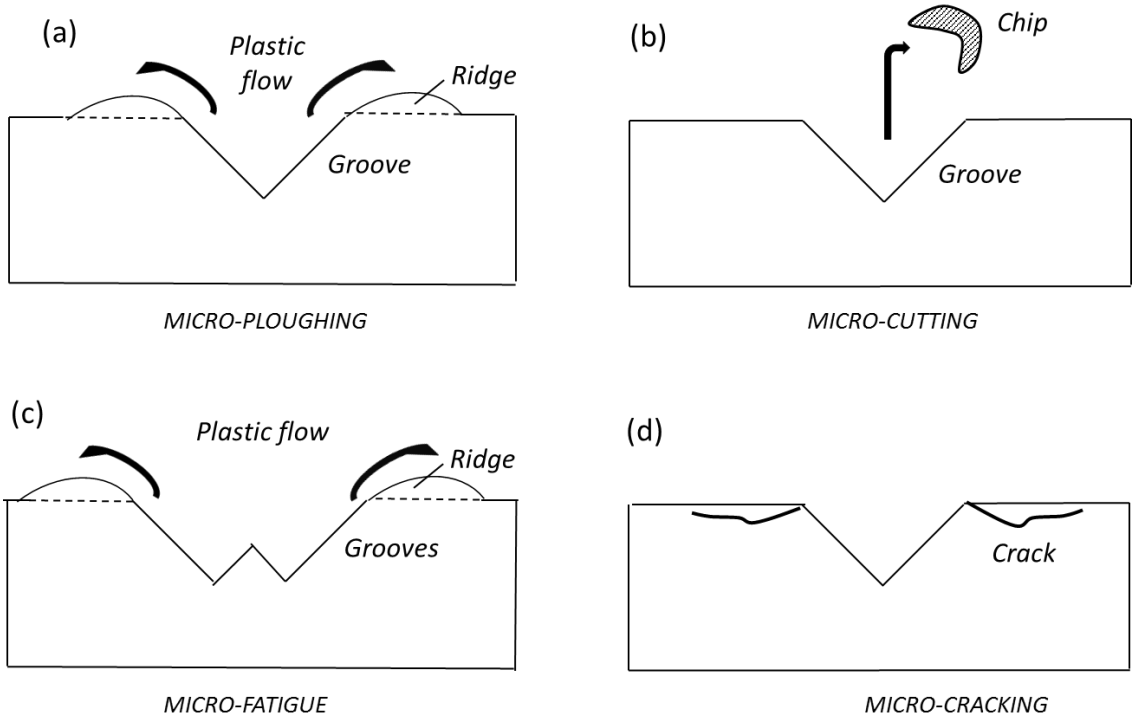

Figure 5.27 : A schematic sketch showing four mechanisms of groove formation in wear of matrix alloy

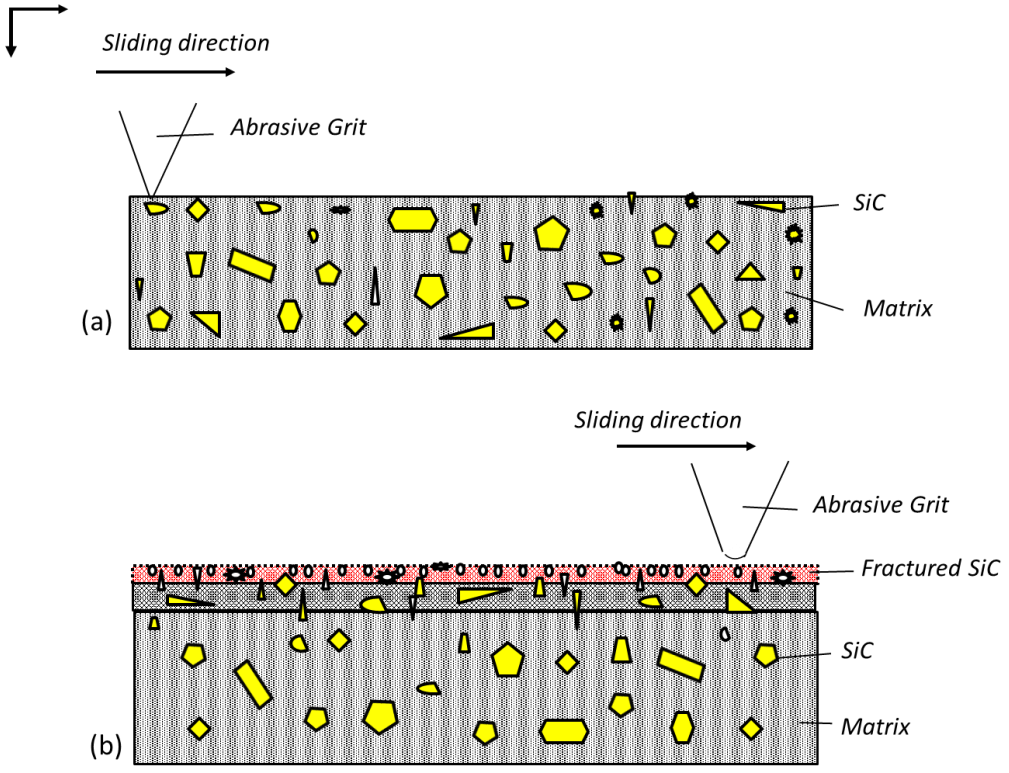

Figure 5.28: A schematic diagram showing possible wear mechanism of Al 6082-SiC composites.

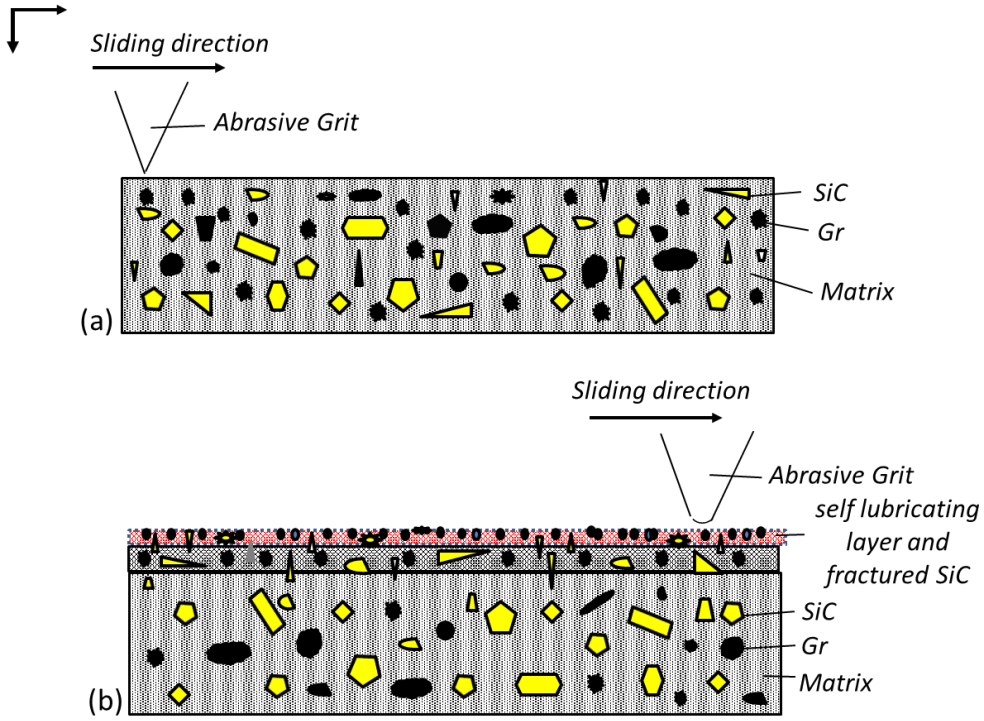

Figure 5.29: A schematic diagram showing possible mechanism of Al 6082-SiC-Gr hybrid composites

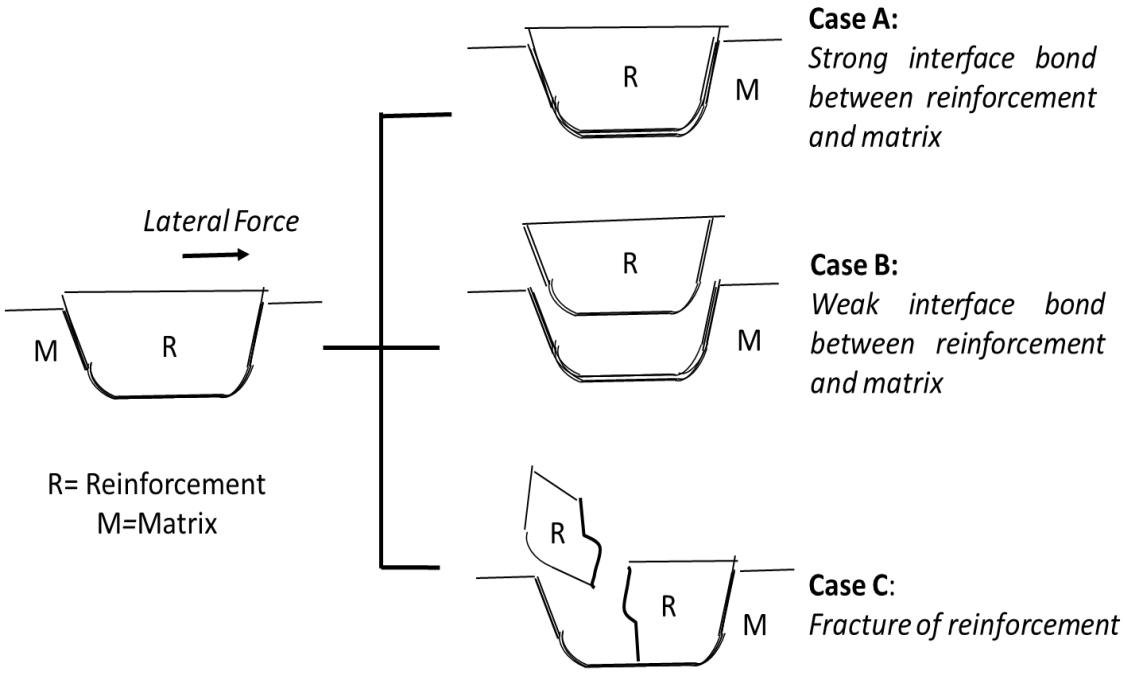

Figure 5.30: Interface characteristics between reinforcement and matrix

Fig. 5.27 shows the schematic sketch of four mechanisms of groove formation in abrasive wear of matrix material. The digging of softer material surface takes place due to

interaction of the hard reinforcements present on the counter body surface. The material removal of ductile aluminium matrix would be due to indentation, ploughing and cutting action created by abraders on the counter surface. In this present case, apart from size and shape of the abrasive grit, the wear rate of the material from the ploughed groove depends on the hardness, toughness and work hardening of the material. The repeated action of ploughing created by series of abraders generates the cracks on surface and the fatigue will be created over the surface of the material (Murray *et al.*, 1982, Norton *et al.*, 2009).

Fig. 5.28 shows the schematic diagram showing possible wear mechanism of Al 6082-SiC composites. In this case, the sharp abraders try to dig the matrix material initially and if an abrasive grit encounter the SiC reinforcement which is relatively harder than matrix material, then one phenomenon among the three cases takes place between the reinforcement and matrix. This was pictorially depicted in Fig. 5.30, representing the interface characteristics of between the reinforcement and matrix. Case A indicates the reinforcement remain intact within matrix due to strong interface bond; Case B indicates the reinforcement removal from matrix creating a cavity/pit due to weak interface bond and existence of higher stresses; Case C indicates the fracture of the reinforcement due to existence of higher stresses and partial interfacial bond. If case A happens, the reinforcement will try to obstruct the plastic flow of the matrix material, reducing the wear. But due to repeated digging/ ploughing and cutting action, the removal of matrix material surrounding the reinforcement takes place, exposing the protrusions of the reinforcement for next engagement with abrasive grit. The probability of blunting or fracture or tip off of an abrasive grit present on the counter surface increases in this scenario. The fracture or tip off of abrasive grits and detachment of reinforcement from the matrix (as indicated in case B) will try stay in between valleys of pin and emery paper, leading to third body abrasion. In case C, the fracture of reinforcement causes the formation of micron and sub-micron abrader chips in between the pin and counter surface, thereby promoting the three body abrasive wear condition. (Zhang *et al.,* (1995), Zhang *et al.,* (1998))

Fig. 5.29 shows the schematic diagram showing possible mechanism of Al 6082-SiC-Gr hybrid composites. In the case of hybrid composites, the effect of both hard SiC and soft graphite reinforcement has to be observed individually and combinedly. As reported earlier, the effect of hard reinforcement was noted, but the soft graphite reinforcement cannot restrict the plastic flow caused by abrasive grit, instead it offers lubrication in the wear process. The fracture of graphite reinforcement (i.e. case C in Fig. 5.30), which was

expected during wear process, tend to stay in between the valleys of pin and emery paper. A schematic sketch of an abrasive surface before and after wear, showing blunting (as indicated in Fig. 5.31(a)) and wear debris clogged on abrasive surface (as indicated in Fig. 5.31(b)) (Rabinowitz *et al*., 1995). This will lead to formation of graphite layer, as it is self-lubricant in nature, it tries to reduce the surface deterioration of the pin sample. It was evident in the worn surface of pin sample depicted in Fig. 5.20 (e), Fig. 5.20 (f), Fig. 5.21 (e) and Fig. 5.21 (f). Hence, the addition of graphite reinforcement found to be advantageous along with hard SiC reinforcement, in improving the wear resistance of hybrid composites (Ted Guo *et al.*, 2000, Riahi *et al.*, 2001, Basavarajappa *et al.*, 2005).

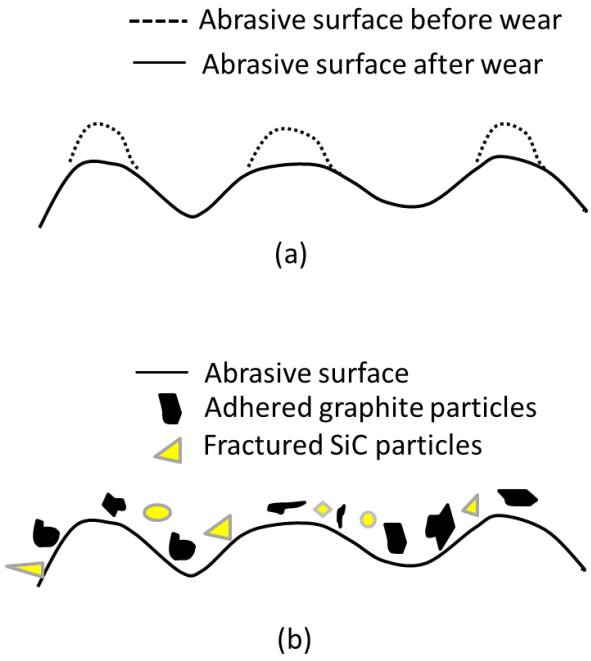

Figure 5.31 A schematic sketch of (a) an abrasive surface before and after wear, showing blunting, and (b) wear debris clogged on abrasive surface (Bharat Bhushan *et al*., 2013).

CHAPTER - 6

RESULTS & DISCUSSION: ANOVA AND REGRESSION EQUATIONS

In this chapter, the analysis of variance (ANOVA) and regression equations of two body abrasive wear rate of Al 6082 alloy, Al 6082-SiC composites and Al 6082-SiC-Gr hybrid composites for both as cast and T6 conditions of the materials was investigated. The results obtained were reported and was discussed briefly.

6.1 ANOVA of two body abrasive wear of materials

The experimental matrix and corresponding results obtained of all materials at different conditions were consolidated for as shown in Table 6.1. This was done by adopting central composite design approach in response surface methodology (RSM) using Design Expert 9 software. ANOVA reveals the significance (% contribution) of parameters and regression analysis shows the correlation between the parameters involved in the present set of experiments.

Table 6.1: Details of test combinations in actual values of factors and corresponding experimental results.

Run order	Load (N)	Grit Size (µm)	Sliding Distance (m)	Wear rate (mm^3/m) in as cast condition			Wear rate (mm^3/m) in T6 condition		
				Al alloy	Al-SiC	Al-SiC-Gr	Al alloy	Al-SiC	Al-SiC-Gr
1	5	100	50	0.5889	0.4409	0.3818	0.3748	0.3047	0.2715
2	5	200	75	0.8035	0.6208	0.4968	0.6405	0.5496	0.4793
3	15	100	50	1.0415	0.8817	0.7803	0.9081	0.7785	0.6263
4	15	100	75	1.0825	0.9428	0.8696	0.9422	0.8582	0.6889
5	5	125	63	0.6755	0.5706	0.5092	0.4703	0.4159	0.3995
6	15	200	50	1.4615	1.2789	1.1774	1.2178	0.9784	0.7686
7	5	100	75	0.6133	0.5166	0.4496	0.48	0.3565	0.3066
8	10	125	50	0.9615	0.8502	0.7438	0.7859	0.6373	0.4328
9	15	200	75	1.4998	1.3257	1.2535	1.3072	1.1069	0.9539
10	10	125	63	0.9865	0.8904	0.8551	0.8083	0.6571	0.5202
11	10	200	63	1.1899	1.0633	0.9877	1.0494	0.7487	0.555
12	10	125	75	1.0874	0.9128	0.8934	0.8286	0.6925	0.5669
13	10	100	63	0.9189	0.7322	0.6674	0.7061	0.5888	0.4061
14	15	125	63	1.1728	1.0747	1.0057	1.0635	0.9279	0.7108
15	5	200	50	0.737	0.5362	0.3964	0.5393	0.4552	0.3066

6.1.1 ANOVA of Al 6082 alloy: As cast condition

Table 6.2 shows the significant model terms of cast Al 6082 alloy were A, B, C, AB, A^2. The major significant terms were found to be load with 77.1 %, grit size with 19.4 %, sliding distance with ~1% and load-grit interaction with 3.2 %. The Pred R-Squared of 0.9668 is found to be in reasonable agreement with the Adj R-Squared of 0.9892. Fig. 6.1 (a) show the normal plot of residuals whereas Fig. 6.1 (b) and (c) represent the contour and surface plots respectively with load and grit size parameters tested on Al 6082 alloy in as cast condition. It was noticed that as the load increased from 5N to 15N the wear rate increased from 0.8035 mm^3/m to 1.4998 mm^3/m at higher grit size and sliding distance but as grit size increases from 100µm to 200µm the wear rate increased from 1.0825 mm^3/m to 1.4998 mm^3/m at higher load and sliding distance.

Table 6.2: ANOVA for Al 6082 alloy in as cast condition

Source	DOF	Sum of Squares	Mean Square	F Value	p-value Prob > F
A-Load	1	0.833128	0.833128	1002.287	5.9E-07
B-Grit size	1	0.209234	0.209234	251.717	1.81E-05
C-Sliding Distance	1	0.008703	0.008703	10.46985	0.023059
AB	1	3.40E-02	3.40E-02	40.8836	0.001386
AC	1	1.92E-05	1.92E-05	0.023084	0.885179
BC	1	3.61E-06	3.61E-06	0.004347	0.949986
A^2	1	1.87E-02	1.87E-02	2.25E+01	0.005147
B^2	1	0.001804	0.001804	2.170024	0.200716
C^2	1	6.78E-04	6.78E-04	0.815618	0.407866
Error	5	4.16E-03	8.31E-04		
Total	14	1.08			
R-Squared = 0.9961 Adj-R-Squared= 0.9892 Pred R-Squared=0.9668					

(a)

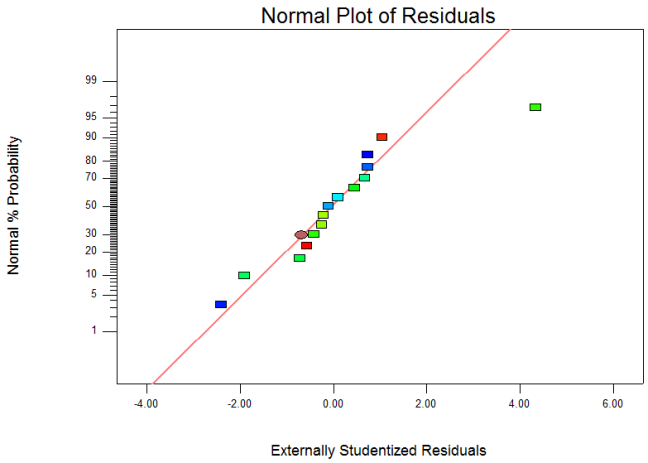

(b)

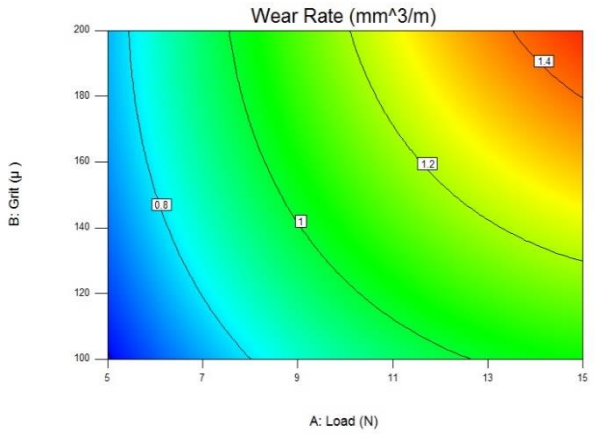

(c)

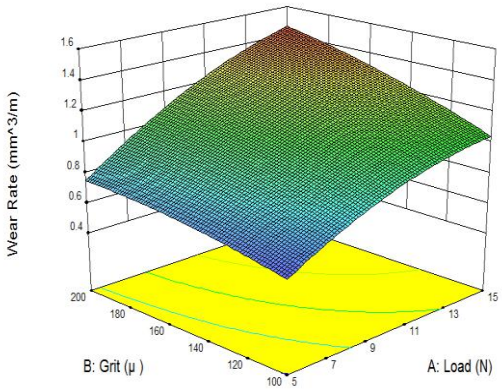

Figure 6.1: (a) Normal plot of residuals, (b) contour plot and (c) surface plot of Al 6082 alloy in as cast condition.

6.1.2 ANOVA of Al 6082 alloy: T6 condition

In T6 heat treated Al 6082 alloy the significant model terms are A, B, C, AB, A^2 as shown in Table 6.3. The major significant terms were found to be load with 80.3%, grit size with 16.5%, sliding distance with 1.3% and load-grit interaction with 1.3%. The Pred R-Squared of 0.9857 is found to be in reasonable agreement with the Adj R-Squared of 0.9478. Fig. 6.2 (a) show the normal plot of residuals whereas Fig. 6.2 (b) and (c) represent the contour and surface plots respectively with load and grit size parameters tested on Al 6082 alloy in T6 condition. It was noticed that as the load increased from 5N to 15N, the wear rate increased from 0.6405 mm^3/m to 1.3072 mm^3/m at higher grit size and sliding distance but as grit size increases from 100µm to 200µm the wear rate increased from 0.9422 mm^3/m to 1.3072 mm^3/m at higher load and sliding distance.

Table 6.3: ANOVA for Al 6082 alloy in T6 condition

Source	DOF	Sum of Squares	Mean Square	F Value	p-value Prob > F
A-Load	1	0.87513	0.87513	787.1252	1.08E-06
B-Grit size	1	0.180171	0.180171	162.053	5.32E-05
C-Sliding Distance	1	0.014343	0.014343	12.90065	0.015679
AB	1	1.43E-02	1.43E-02	12.83072	0.015841
AC	1	0.000826	0.000826	0.743324	0.428003
BC	1	5.88E-04	5.88E-04	0.529301	0.499526
A^2	1	8.20E-03	8.20E-03	7.37E+00	0.042002
B^2	1	0.000402	0.000402	0.361537	0.573872
C^2	1	5.60E-04	5.60E-04	0.503518	0.509669
Error	5	5.56E-03	1.11E-03		
Total	14	1.09			
R-Squared = 0.9948	Adj-R-Squared= 0.9857		Pred R-Squared=0.9478		

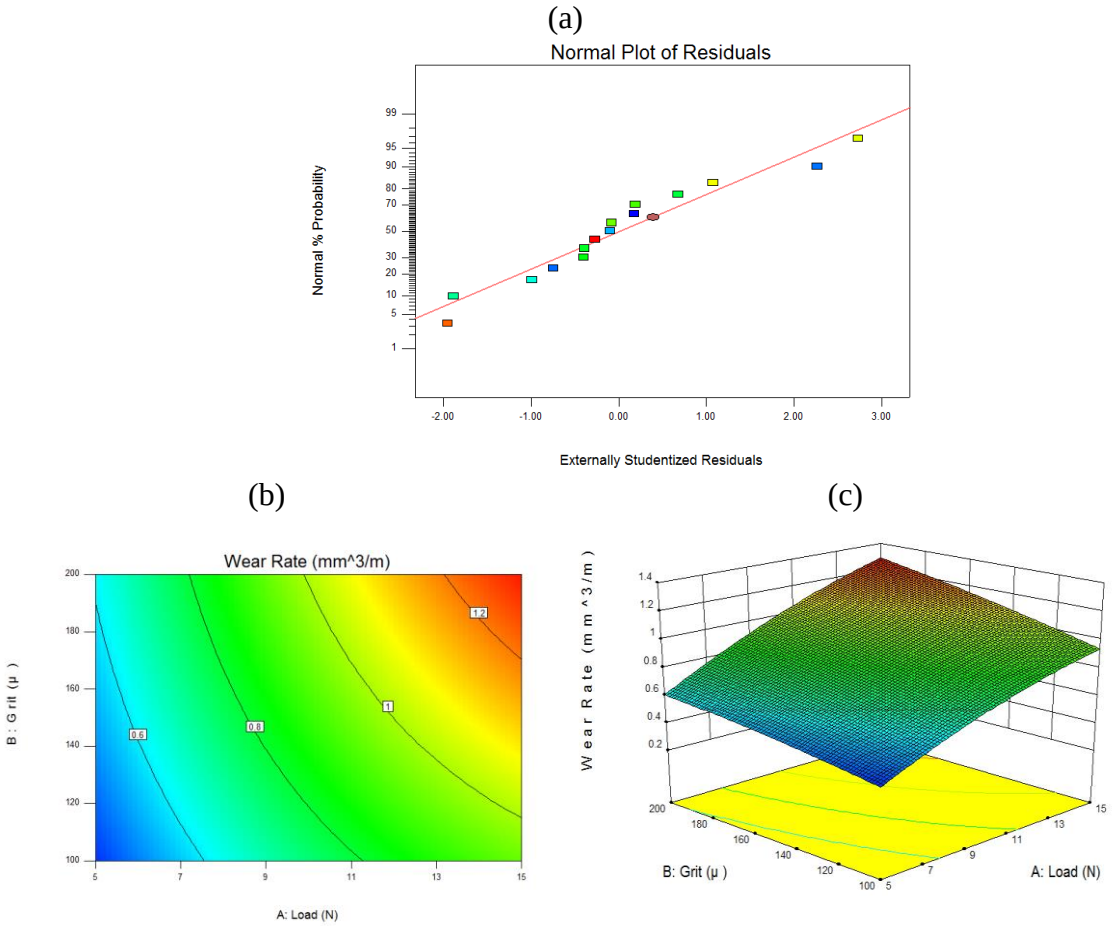

Figure 6.2: (a) Normal plot of residuals, (b) contour plot and (c) surface plot of Al 6082 alloy in T6 heat treated condition.

6.1.3 ANOVA of Al 6082-10% SiC composite: As cast condition

The significant model terms for cast Al 6082-SiC composite were found to be A, B, C, AB, A^2, B^2 as shown in Table 6.4. The major significant terms were found to be load with 79.5%, grit size with 16.5%, sliding distance with 1% and load-grit interaction with 4.3%. The Pred R-Squared of 0.9719 was found to be in reasonable agreement with the Adj R-Squared of 0.9918.

Table 6.4: ANOVA for Al-SiC composite in as cast condition

Source	DOF	Sum of Squares	Mean Square	F Value	p-value Prob > F
A-Load	1	0.826392	0.826392	1353.188	2.8E-07
B-Grit size	1	0.171782	0.171782	281.2877	1.38E-05
C-Sliding Distance	1	0.010808	0.010808	17.69697	0.008434
AB	1	4.43E-02	4.43E-02	72.58468	0.000367
AC	1	0.000344	0.000344	0.563131	0.486792
BC	1	8.61E-08	8.61E-08	0.000141	0.990987
A^2	1	1.23E-02	1.23E-02	2.01E+01	0.006476
B^2	1	0.008578	0.008578	14.04575	0.013324
C^2	1	2.07E-04	2.07E-04	0.339103	0.585617
Error	5	3.05E-03	6.11E-04		
Total	14	1.04			
R-Squared = 0.9970 Adj-R-Squared= 0.9917 Pred R-Squared=0.9719					

Fig. 6.3(a) show the normal plot of residuals whereas Fig. 6.3(b) and (c) indicate the contour and surface plots respectively with load and grit size parameters tested on Al 6082-SiC composite in cast condition. It was noticed that as the load increased from 5N to 15N, the wear rate increased from 0.6208 mm^3/m to 1.3257 mm^3/m at higher grit size and sliding distance but as grit size increases from 100µm to 200µm the wear rate increased from 0.9428 mm^3/m to 1.3257 mm^3/m at higher load and sliding distance.

(a)

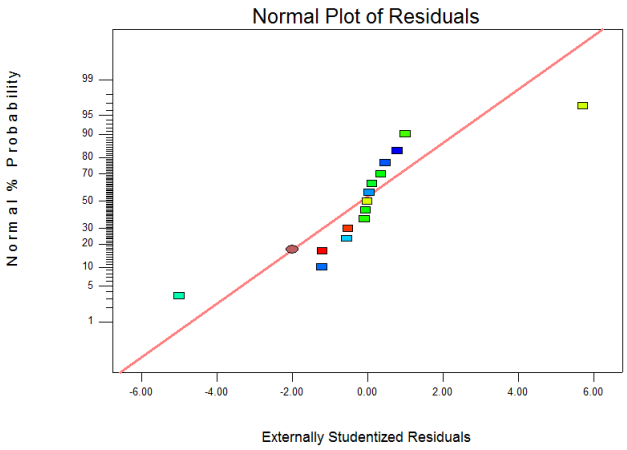

(b) (c)

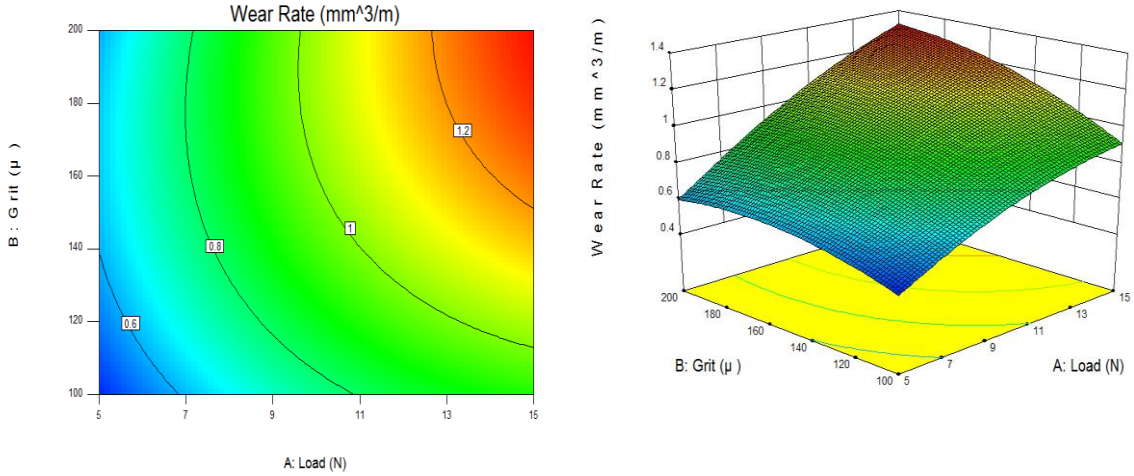

Figure 6.3: (a) Normal plot of residuals, (b) contour plot and (c) surface plot of Al-SiC composite in as cast condition.

6.1.4 ANOVA of Al 6082-10% SiC composite: T6 condition

In T6 heat treated Al 6082-SiC composite the significant model terms are A, B, C, AB, BC, B^2 as shown in Table 6.5. The major significant terms were found to be load with 85.3%, grit size with 11.7%, sliding distance with 2.3% and load-grit interaction with 0.2%. The Pred R-Squared of 0.9902 was found to be in reasonable agreement with the Adj R-Squared of 0.9967. Fig. 6.4 (a) show the normal plot of residuals, Fig. 6.4 (b) and (c) depict the contour and surface plots respectively with load and grit size parameters whereas Fig. 6.4 (d) and (e) represent the contour and surface plots respectively with sliding distance and grit parameters tested on Al 6082-SiC composite in T6 condition. It was noticed that as the load increased from 5N to 15N, the wear rate increased from 0.5496 mm^3/m to 1.1069 mm^3/m at higher grit size and sliding distance but as grit size increases from 100µm to 200µm the wear rate increased from 0.8582 mm^3/m to 1.1069 mm^3/m at higher load and sliding distance.

Table 6.5: ANOVA for Al-SiC composite in T6 condition

Source	DOF	Sum of Squares	Mean Square	F Value	p-value Prob > F
A-Load	1	0.657763	0.657763	3659.461	2.34E-08
B-Grit size	1	0.090455	0.090455	503.2452	3.27E-06
C-Sliding Distance	1	0.017593	0.017593	97.87916	0.00018
AB	1	1.34E-03	1.34E-03	7.448648	0.041319
AC	1	0.000486	0.000486	2.701755	0.161159
BC	1	1.28E-03	1.28E-03	7.106806	0.044569
A^2	1	1.25E-04	1.25E-04	6.96E-01	0.442079
B^2	1	0.004672	0.004672	25.99498	0.003775
C^2	1	6.16E-06	6.16E-06	0.028729	0.872051
Error	5	8.99E-04	1.80E-04		
Total	14	7.71E-01			
R-Squared = 0.9988 Adj-R-Squared= 0.9967 Pred R-Squared= 0.9902					

(a)

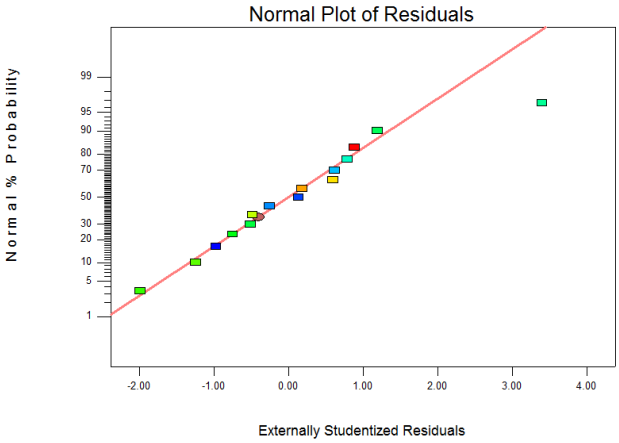

(b) (c)

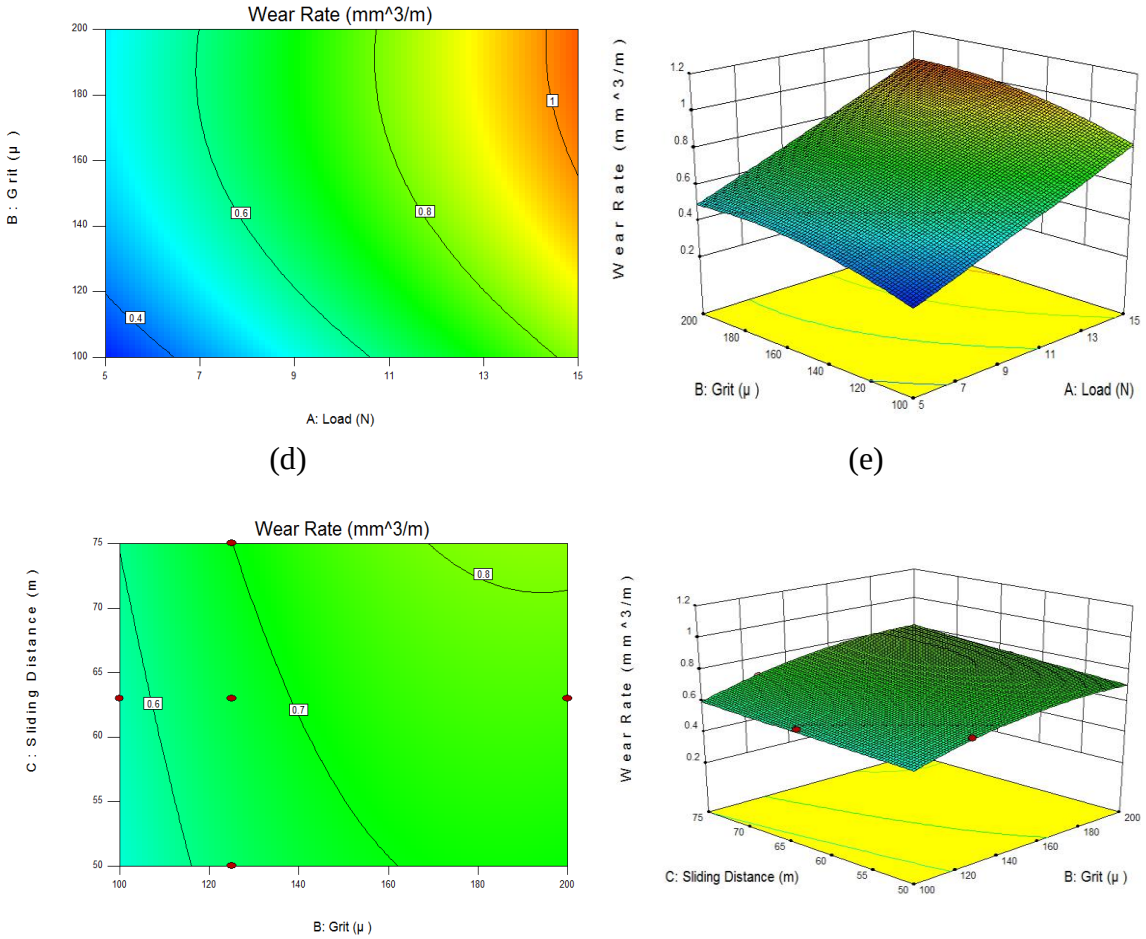

(d) (e)

Figure 6.4: (a) Normal plot of residuals, (b) & (d) contour plot and (c) & (e) surface plot of Al-SiC composite in T6 condition.

6.1.5 ANOVA of Al 6082-5% SiC-5%Gr hybrid composite: As cast condition

From Table 6.6 the significant model terms for cast Al 6082-SiC-Gr hybrid composite were observed to be A, B, C, AB, A^2, B^2. The major significant terms were found to be load with 79.2%, grit size with 14.3%, sliding distance with 2.1% and load-grit interaction with 3.5%. The Pred R-Squared of 0.9396 was found to be in reasonable agreement with the Adj R-Squared of 0.9817. Fig. 6.5 (a) show the normal plot of residuals whereas Fig. 6.5 (b) and (c) indicate the contour and surface plots respectively with load and grit size parameters tested on Al 6082-SiC-Gr hybrid composite in as cast condition. It was noticed that as the load increased from 5N to 15N, the wear rate increased from 0.4968 mm^3/m to 1.2535 mm^3/m at higher grit size and sliding distance but as grit size increases from 100µm to 200µm the wear rate increased from 0.8696 mm^3/m to 1.2535 mm^3/m at higher load and sliding distance.

Table 6.6: ANOVA for Al-SiC-Gr hybrid composite in as cast condition

Source	DOF	Sum of Squares	Mean Square	F Value	p-value Prob > F
A-Load	1	0.855731	0.855731	606.6192	2.06E-06
B-Grit size	1	0.155278	0.155278	95.89729	0.000189
C-Sliding Distance	1	0.023032	0.023032	16.32697	0.009916
AB	1	3.81E-02	3.81E-02	48.25877	0.000949
AC	1	1.04E-06	1.04E-06	0.000735	0.979418
BC	1	1.62E-06	1.62E-06	0.001147	0.974291
A^2	1	1.78E-02	1.78E-02	1.27E+01	0.016269
B^2	1	0.012302	0.012302	8.721024	0.03177
C^2	1	1.05E-03	1.05E-03	0.744929	0.427537
Error	5	7.05E-03	1.41E-03		
Total	14	1.08			
R-Squared = 0.9934 Adj-R-Squared= 0.9817 Pred R-Squared= 0.9396					

(a)

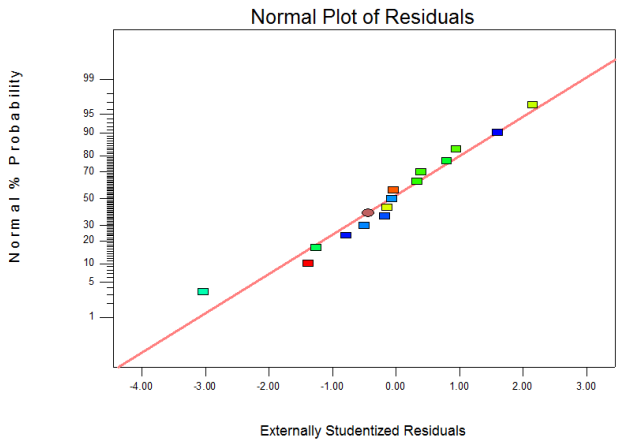

(b)

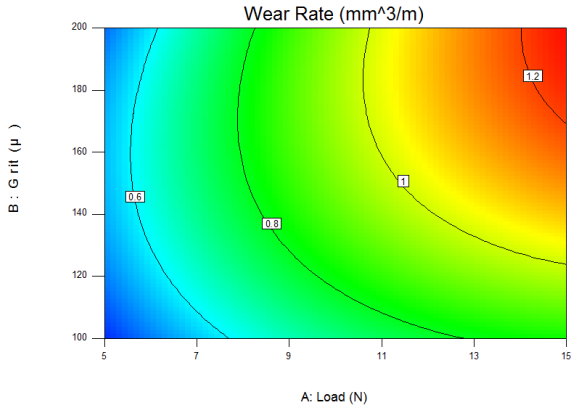

(c)

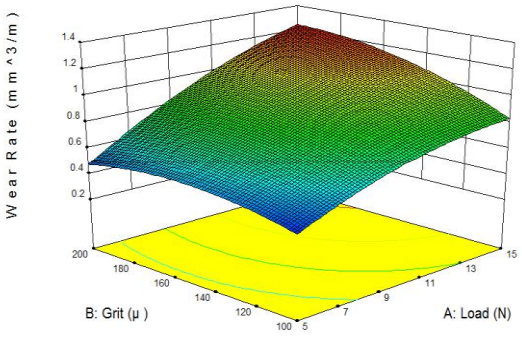

Figure 6.5: (a) Normal plot of residuals, (b) contour plot and (c) surface plot of Al-SiC-Gr hybrid composite in as cast condition.

6.1.6 ANOVA of Al 6082-5% SiC-5%Gr hybrid composite: T6 condition

In T6 heat treated Al 6082-SiC-Gr hybrid composite the significant model terms are A, B, C, AB, BC, A^2, B^2 as shown in Table 6.7. The major significant terms were found to be load with 79.5%, grit size with 12.3%, sliding distance with 2.5% and load-grit interaction with 1.1%. The Pred R-Squared of 0.9360 was found to be in reasonable agreement with the Adj R-Squared of 0.9769. Fig. 6.6 (a) represent the normal plot of residuals, Fig. 6.6 (b) and (c) show the contour and surface plots respectively with load and grit size parameters whereas Fig. 6.6 (d) and (e) indicate the contour and surface plots respectively with sliding distance and grit parameters, tested on Al 6082-SiC-Gr hybrid composite in T6 condition. It was noticed that as the load increased from 5N to 15N, the wear rate increased from 0.4793 mm^3/m to 0.9539 mm^3/m at higher grit size and sliding distance but as grit size increases from 100µm to 200µm the wear rate increased from 0.6889 mm^3/m to 0.9539 mm^3/m at higher load and sliding distance.

Table 6.7: ANOVA for Al-SiC-Gr hybrid composite in T6 condition

Source	DOF	Sum of Squares	Mean Square	F Value	p-value Prob > F
A-Load	1	0.490617	0.400617	470.6628	3.86E-06
B-Grit size	1	0.075999	0.075999	68.14018	0.000425
C-Sliding Distance	1	0.01596	0.01596	44.59765	0.001138
AB	1	7.00E-03	7.00E-03	8.224682	0.035082
AC	1	0.000177	0.000177	0.207503	0.667831
BC	1	7.55E-03	7.55E-03	8.870463	0.030859
A^2	1	9.16E-03	9.16E-03	1.08E+01	0.021938
B^2	1	0.006939	0.006939	8.152166	0.035606
C^2	1	1.01E-04	1.01E-04	0.118649	0.744519
Error	5	4.26E-03	8.51E-04		
Total	14	6.17E-01			
R-Squared = 0.9918 Adj-R-Squared= 0.9769 Pred R-Squared=0.9360					

(a)

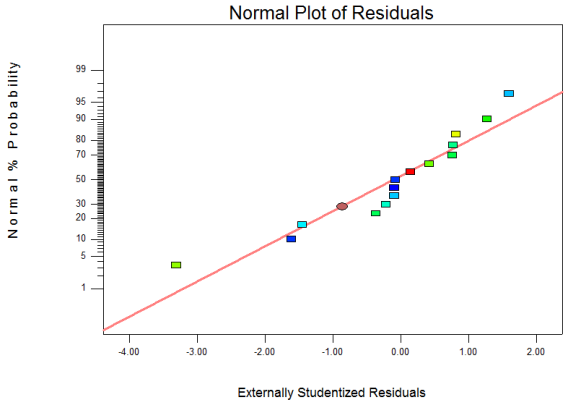

(b) (c)

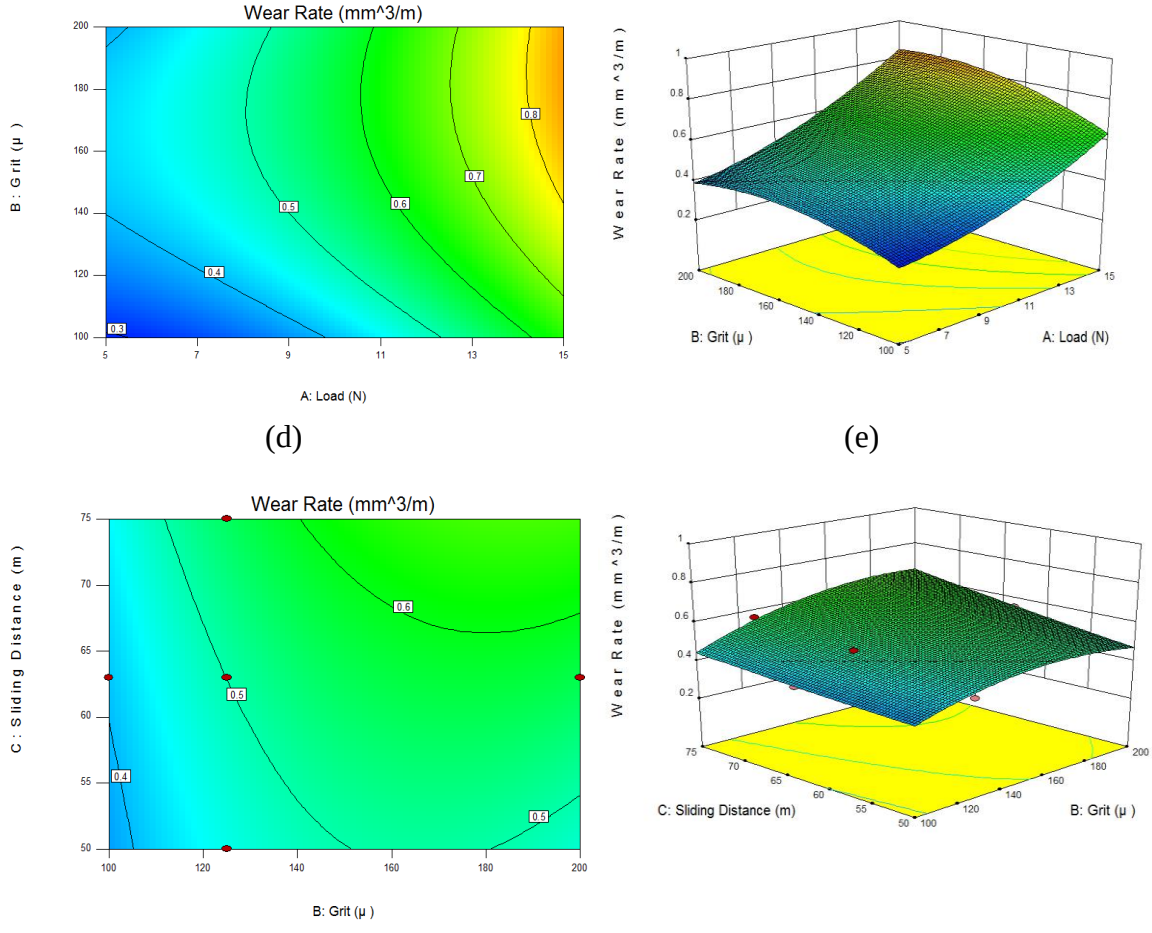

(d) (e)

Figure 6.6: (a) Normal plot of residuals, (b) & (d) contour plot and (c) & (e) surface plot of Al-SiC-Gr hybrid composite in T6 heat treated condition.

6.1.7 Consolidated results of percentage contribution of factors

Table 6.8 shows the consolidated results of % contribution of factors of all the materials. The factors with - in the table indicate the insignificant terms that were observed in ANOVA analysis of materials indicated from Table 6.2-6.7. The other factors such as error and lack of fit terms were not included as these terms were observed to be almost insignificant and was neglected. It was evident that the load applied and grit size was first and second dominant factors respectively in the abrasive wear of the materials. The former parameter % contribution lies in the range of 77-85% and the latter one contribution lies in the 9-20% range. Interestingly, it was noticed that for graphatized hybrid composites the grit size contribution was found to be near to 12-14%. This indicates the effect of grit size on hybrid composites was lower when compared to matrix alloy and SiC reinforced composites. This could be due to lubricating action of graphite present in the hybrid composites (Ted Guo *et al.*, 2000, Riahi *et al.*, 2001).

Table 6.8: Consolidated results of % contribution of factors

Material (condition)	**Factors**								
	A	**B**	**C**	**AB**	**AC**	**BC**	**A^2**	**B^2**	**C^2**
Al 6082 alloy (AC)	77.1	19.4	0.8	3.2	-	-	1.7	-	-
Al 6082 alloy (T6)	80.3	16.5	1.3	1.3	-	-	0.8	-	-
Al 6082-10%SiC (AC)	79.5	16.5	1.0	4.3	-	-	1.2	0.8	-
Al 6082-10%SiC (T6)	85.3	11.7	2.3	0.2	0.1	-	-	0.6	-
Al 6082-5%SiC-5%Gr (AC)	79.2	14.4	2.1	3.5	-	-	1.6	1.1	-
Al 6082-5%SiC-5%Gr (T6)	79.5	12.3	2.5	1.1	-	1.2	1.4	1.1	-

6.2 Regression equations of two body abrasive wear of materials

The Table 6.9 shows the regression equations of alloy and its composite materials in both cast and T6 conditions. The Eq. (6.1) to (6.6) represent the regression equations of the materials. From the regression equations, it was noticed that the coefficients of significant terms like load, grit, sliding distance, load and grit interaction were positive in sign. This indicates these terms contribute positively to wear behavior. The constant term decreased from 1.08504 to 0.890434 for matrix material, 0.975607 to 0.724129 for Al 6082-SiC composites and 0.923662 to 0.554463 for Al 6082-SiC-Gr composites. The numerical coefficients of load was almost same for matrix alloy but it decreased from 0.289186 to 0.258 for Al 6082-SiC composites and 0.294275 to 0.201349 for Al 6082-SiC-Gr composites. The coefficients of grit was found to be slightly decreased from 0.14465 to 0.134233 for matrix alloy, 0.131070 to 0.095111 for Al 6082-SiC composites and 0.116313

to 0.076160 for Al 6082-SiC-Gr composites. The coefficients of sliding distance slightly increased 0.02967 to 0.038096 for matrix alloy, 0.033069 to 0.042192 for Al 6082-SiC composites and 0.048276 to 0.061977 for Al 6082-SiC-Gr composites. The coefficients of interaction term of load and grit decreased from 0.06360 to 0.041210 for matrix alloy, 0.072644 to 0.012624 for Al 6082-SiC composites and 0.090024 to 0.028869 Al 6082-SiC-Gr composites. These trends were observed when the coefficients were compared in cast condition with T6 condition of the same material.

Table 6.9: Regression equations of the materials in as cast and T6 condition.

Material		Regression Model
As cast condition	**Al 6082 alloy**	Wear rate = 1.085 +0.2904*load+0.1447*grit+0.0297 *sliding dist+0.0636*load*grit-0.0852*load^2 ----------(6.1)
	Al 6082-10% SiC composite	Wear rate = 0.9756+0.2892*load+0.1311*grit+0.0331*sliding dist+0.0726*load*grit-0.0692*load^2-0.0794*grit^2 ----------(6.2)
	Al 6082-5% SiC-5%Gr hybrid composite	Wear rate = 0.9237 + 0.2943 * load + 0.1163 * grit + 0.0483* sliding dist + 0.09* load * grit-0.0833* load^2-0.0951* grit^2 ----------(6.3)
T6 heat treated condition	**Al 6082 alloy**	Wear rate = 0.8904 + 0.2976 * load + 0.1342 * grit + 0.0381 * sliding dist+0.0412* load*grit-0.0565* load^2 ----------(6.4)
	Al 6082-10% SiC composite	Wear rate = 0.7241 + 0.258 * load + 0.0951 * grit + 0.0422 * sliding dist + 0.0126 * load * grit + 0.0078 * load * sliding dist-0.0586*grit^2 ----------(6.5)
	Al 6082-5% SiC-5%Gr hybrid composite	Wear rate = 0.5545+0.2013*load+0.0762* grit+0.062* sliding dist+0.0289*load*grit+ 0.029976 * grit * sliding dist+0.0597* load^2-0.0715* grit^2 ----------(6.6)

In as cast condition, the constant term decreased from 1.085 to 0.9756 and to 0.9237 for alloy to Al 6082-SiC and Al 6082-SiC-Gr composites respectively. In T6 condition, the similar trend was observed for the constant coefficient term. In as cast condition, the load coefficient term decreased was observed to be almost same around 0.29 when considered from matrix alloy to Al 6082-SiC to Al 6082-SiC-Gr composites. But in T6 condition it decreased from 0.2976 to 0.258 and 0.2013 for alloy to Al 6082-SiC and Al 6082-SiC-Gr composites respectively. In as cast condition, the grit coefficient term slightly decreased from 0.1447 to 0.1311 and 0.1163 for alloy to Al 6082-SiC and Al 6082-SiC-Gr composites respectively. But in T6 condition it decreased from 0.1342 to 0.0951 and 0.0762 for alloy to Al 6082-SiC and Al 6082-SiC-Gr composites respectively. In as cast condition, the

sliding distance coefficient term slightly increased from 0.0297 to 0.0331 and 0.0483 for alloy to Al 6082-SiC and Al 6082-SiC-Gr composites respectively. In T6 condition also, the similar trend was observed for this coefficient term. In as cast condition, the load and grit interaction coefficient term slightly increased from 0.0636 to 0.0726 and 0.09 for Al 6082-SiC and Al 6082-SiC-Gr composites respectively whereas this interaction coefficient term slightly decreased from 0.0412 to 0.0126 and 0.0289 for Al 6082-SiC and Al 6082-SiC-Gr composites respectively. The other coefficients that were observed to be partial significance and insignificant were neglected; however the coefficients of all significant terms were represented in regression equations. Table 6.10 shows the adequacy of the developed regression equations of the materials. It was noticed that the error percentage of actual and predicted values of wear rates were found to be below 10%.

Table 6.10: Adequacy of the developed regression equations of the materials

Material (condition)	Load (N)	Grit Size (μm)	Sliding Distance (m)	Wear rate (mm^3/m)		Error (%)
				Actual	Predicted	
Al 6082 alloy (AC)	5	100	63	0.6099	0.5919	2.94
	10	200	50	1.1943	1.1792	1.26
	10	100	75	0.9778	0.9492	2.91
Al 6082 alloy (T6)	5	100	63	0.4550	0.4261	6.34
	10	200	50	0.9770	0.9462	3.15
	10	100	75	0.7858	0.7539	4.05
Al 6082-10% SiC composite (AC)	5	100	63	0.4989	0.4793	3.91
	10	200	50	1.0350	0.9852	4.80
	10	100	75	0.8299	0.7892	4.90
Al 6082-10% SiC composite(T6)	5	100	63	0.3402	0.3319	2.42
	10	200	50	0.7312	0.7075	3.23
	10	100	75	0.6421	0.6016	6.30
Al 6082-5% SiC-5%Gr hybrid composite (AC)	5	100	63	0.4389	0.4246	3.26
	10	200	50	0.8956	0.8767	2.10
	10	100	75	0.7659	0.7407	3.29
Al 6082-5% SiC-5%Gr hybrid composite (T6)	5	100	63	0.3006	0.2941	2.18
	10	200	50	0.4892	0.4735	3.22
	10	100	75	0.4803	0.4451	7.32

Mondal *et al*., (1998) investigated on the two body abrasive wear behaviour of Al-10% wt. Al_2O_3 composite through factorial design approach in statistical analysis. The wear rate was expressed in terms of coded values of abrasive grit size and applied load by regression equation. From the generated equation it was understood that the load applied

was higher compared to abrasive size. Sahin *et al*., (2003) studied on the abrasive wear of Al 2011-5%SiC_p composites using linear factorial approach. The wear tests were conducted on SiC and Al_2O_3 abrasive media emery paper separately by using pin on disc machine, where emery papers were bonded over the disc. The wear rate has been demonstrated through established regression equations in terms of applied load, sliding distance and abrasive particle size. The values obtained from the equations were compared with experimental results. It was reported that the wear rate increased as applied load, sliding distance and abrasive size increases when tested on SiC_p emery paper. Among these parameters, it was noticed that the abrasive size was the highest contributing factor. The mixed or combined effects of the interaction of the variables were also noticed. Later Kok *et al*., (2011) has studied on the abrasive wear behaviour of Al_2O_3 reinforced Al-MMCs on SiC emery paper using statistical analysis. The orthogonal array, S/N ratio and ANOVA were employed to find out the optimal testing parameters. The developed regression equation was used for comparison of the model prediction with experimental results. The average error between experimental and predicted was found to be around 10.25%. Mandal *et al*., (2012) investigated on the mathematical modelling of wear characteristics of Al 6061/ SiC_p composite using response surface methodology. The regression models were developed to understand the nature of the contribution in wear process. The final mathematical model was reported with significant terms. Similarly Radhika *et al*., (2012) has reported on the wear behaviour of Gr and Al_2O_3 reinforced hybrid Al-MMCs. The wear models generated though Taguchi and ANOVA techniques were found to be adequate.

In the present case, from the ANOVA, it was revealed that applied load, grit size, sliding distance, interaction of applied load and grit size and square terms of load are the main significant factors contributing in the abrasive wear of the chosen materials in present set of experiments. The applied load was first dominant factor for all the materials, i.e. contribution was ranging from 77- 85%. The other significant individual dominant factors were grit size with 11-20% and sliding distance with 1-3%. The regression models of materials reveal that coefficients of load, grit size and load-grit size interaction terms were found to be almost same, decreased and increased from alloy to hybrid composites respectively in cast condition. But in T6 condition the coefficients of load, grit size and load-grit size interaction terms were in decreasing mode. The adequacy of the developed regression models i.e. the error percentage of actual and predicted values of wear rates were noticed to be below 10%.

CHAPTER-7

CONCLUSIONS AND SCOPE FOR FURTHER STUDY

In this chapter, the conclusions and scope for further investigation of this study was briefly reported.

7.1 Conclusions

The overall summary and conclusions that were drawn from the present study are as follows:

1) The Al 6082-10%SiC (Al-SiC) composites and Al 6082-5%SiC-5%Gr (Al-SiC-Gr) hybrid composites were prepared using stir casting technique i.e. through liquid metallurgy route.
2) The microstructural survey of alloy and composites were carried out. It was noticed that reinforcements present in composite materials had the good interface bonding with the matrix material.
3) The morphological survey of SiC type abrasive grit size emery papers indicate the grit particles are oriented in random directions. It was noted that each individual grit particle will have different rake angle during cutting action and ploughing action of abrasive wear process.
4) The density of Al-SiC-Gr hybrid composite and Al-SiC composite was observed to be 2.74 g/cc and 2.79 g/cc respectively. The density of hybrid composite was reduced due to the lesser density of graphite reinforcement compared to matrix material.
5) The hardness and ultimate tensile strength of the composites increased with addition of reinforcements. The reduction of hardness and ultimate tensile strength was observed due to addition of graphite to matrix material. It was observed due to graphite eases movement of grains along slip planes leading to more material deformation.
6) The two body abrasive wear tests of Al 6082 alloy, Al 6082-10%SiC composites and Al 6082-5%SiC-5%Gr hybrid composites were done at applied loads of 5-15N, sliding distance of 50-75m and 100-200µm grit size emery papers.

7) In as cast condition, at higher conditions of applied load, grit size and sliding distance, the improvement of wear rate of Al-SiC and Al-SiC-Gr was 11.6% and 16.4% respectively. But in T6 condition, the improvement in wear rate was 22.9% and 27% for Al-SiC and Al-SiC-Gr composites respectively. The wear resistance further improved because of intermetallic precipitates formed during aging process and stronger bond between reinforcement and matrix material.

8) The wear rate of pin was lower for finer grits and lower loads, this was due to reduction in acting applied pressure leading to decrease in material removal ability.

9) At higher conditions of grit particle size and applied load, the penetration depth would be more and even it can cause intense damage to the surface of the material.

10) The effect of sliding distance was found to have partial significance for all the materials when compared to other parameters.

11) The combination of hard SiC and soft graphite reinforcements found to beneficial due to restriction of plastic flow by SiC reinforcement and formation of film by graphite reinforcement in abrasive wear process. The graphite film layer acts as a self-lubricant in Al-SiC-Gr hybrid composites. The presence of graphite reinforcement was found to beneficial/advantageous in reducing the wear.

12) The power law and quadratic equations were developed to understand any non-linear wear characteristics existed in the materials. A change in wear mechanism was observed at 125 μm abrasive grit size. The values of R^2 were observed in the range of 0.97 and 0.99.

13) In cast condition of materials, it was noticed that the exponent in power law equations was increasing from alloy to hybrid composites tested on 125μm and 200 μm abrasive grit sizes respectively. But when tested on 100 μm abrasive grit size, the exponent component was found to be decreasing.

14) In T6 condition of materials, the exponent in power law equations was decreasing from alloy to hybrid composites tested on 125 μm and 200 μm abrasive grit sizes respectively. But when tested on 100 μm abrasive grit size, the exponent component was found to be increasing.

15) The wear coefficients of all the materials decreased, increased and almost linear with increase in applied load, abrasive grit size and sliding distance respectively.

It was noticed that wear coefficients of hybrid composite decreased when compared to matrix alloy.

16) At 75m sliding distance, the wear coefficients of Al 6082-SiC-Gr hybrid composites was 0.495 X 10^{-3} at lower applied load and grit size in as cast condition; 0.460 X 10^{-3} at higher applied load and grit size in as cast condition; 0.411 x 10^{-3} at lower applied load and grit size in T6 heat treated condition; 0.426 X 10^{-3} at higher applied load and grit size in T6 heat treated condition.

17) The wear depth of all the materials increased with increase in applied load, abrasive grit size and sliding distance respectively in both the conditions. It was noticed that wear depth of hybrid composite reduced with respect to matrix alloy.

18) At higher conditions of applied load, grit size and sliding distance, the reduction of wear depth with respect to matrix alloy was around 11.4% and 16.2% for Al-SiC and Al-SiC-Gr respectively in cast condition; 15.3% and 27% for Al-SiC and Al-SiC-Gr respectively in T6 heat treated condition.

19) The effect of applied load and grit size on wear rate mechanism had a direct influence and their significance was also observed and compared through SEM analysis of worn surfaces of pin samples, emery papers and wear debris. The worn surfaces analysis was carried out to understand the possible wear mechanisms involved during abrasive process of different materials.

20) The analysis on worn surfaces of pin samples revealed shallower grooves and lower damaged portions of composites in graphitized composites when compared to matrix alloy and un-graphitized composites. Lesser fragmentation was observed in case hybrid composites compared to Al-SiC composite and matrix alloy material. It was evident that the damaged portions of composites found to due to plastic flow restriction.

21) The worn surface of emery papers indicate the abrasive grit particle blunting, fracture, tip off in some areas and debris over the emery paper formed during abrasion process. These phenomenon depend on the amount of stress levels between pin surface and grit particle of emery paper. The grit particle tip off depends on the bond strength at the interface of grit particle and emery paper. At higher loads, the severity of particle fracture and tip off was expected to be more.

22) At higher applied loads and grit size, the debris of wear tested alloy pin contained discontinuous chips and grit particles that were debonded from the emery paper along with grit particle fracture; whereas in the debris of wear tested hybrid composite pin contained discontinuous chips and fractured grit particles.

23) The abrasive grit on the emery paper could interact with the pin surface at either positive or negative or zero rake angles. Based on the type of interaction on the surface, material removal from pin surface takes place and the strength and deterioration of the abrasive grit takes place i.e. blunting, fracture and tip off.

24) The wear mechanisms for the matrix alloy basically noted to be micro-level ploughing, cutting, fracture and fatigue.

25) The wear of Al-SiC composites would have fractured SiC particulates, if debonded or fractured. It creates a cavity/pit in the matrix material and the fractured ones would act as abraders, promoting three body abrasion. If the SiC reinforcement remain intact with matrix, it arrests the material plastic flow caused due to abrasive grits.

26) The wear of Al-SiC-Gr hybrid composites would have self-lubricating layer due to graphite reinforcement along with fractured SiC particulates. This lubricant effect will lead to lesser surface deterioration, leading to wear reduction.

27) The ANOVA revealed that applied load, grit size, sliding distance, interaction of applied load and grit size and square terms of load are the main significant factors contributing in the abrasive wear of the chosen materials in present set of experiments.

28) The major dominant factor was applied load for all the materials, contribution ranging from 77% to 85%. The other significant individual dominant factors were grit size with 11-20% and sliding distance with 1-3%.

29) The regression equations of materials reveal that coefficients of load, grit size and load-grit size interaction terms were found to be almost same, decreased and increased from alloy to hybrid composites respectively in cast condition. In T6 condition, the coefficients of load, grit size and load-grit size interaction terms were in decreasing mode.

30) The adequacy of the developed regression equations of the materials was found. It was noticed that the error percentage of actual and predicted values of wear rates were found to be below 10%.

7.2 Scope for further study

The microstructural and two body abrasive wear properties of hybrid composites was evaluated in as cast and T6 conditions. However, it was felt that additional work may be undertaken in this system to generate a more comprehensive knowledge on hybrid Al-MMCs. Therefore the scope of suggested future work is as follows:

- The effect of test parameters such as sliding speed, time duration etc on wear performance can be used for extension of this study
- The effect of counter surface parameters such as grit size, other type emery paper etc on abrasive wear properties can also further investigated.
- The effect of cryogenic treatment on wear behavior can also studied and compared.
- Sub-surface deformation studies can be done.
- Other types of wear such as fretting wear, adhesive wear, and three body abrasive wear etc can also studied.
- Further, this study can be extended in various type of lubricating conditions with varied parameters.

REFERENCES

Acilar M., Gul F., Effect of applied load, sliding distance and oxidation on the dry sliding wear behaviour of Al-10Si/SiCp composites produced by vacuum infiltration technique Materials & Design 2004, 25(7), pp. 209-217.

Alpas A.T., Embury J.D., Sliding and abrasive wear behaviour of an aluminium (2014) - SiC particle reinforced composite, Scripta Materialia, 1990, 24, pp. 931-935.

Al-Rubaie K.S., Yoshimura H.N., de Mello, J.-D.-B Two body abrasive wear of Al-SiC composites, Wear 1999, 233-235, pp. 444-454.

Archard J., Contact and rubbing of flat surfaces, Journal of Applied Physics, 24(8)1953, pp. 981-988.

Axen N., Alahelisten A., Jacobson S., Abrasive wear of alumina fibre-reinforced alumina Wear, 1994, 173, pp. 95-104.

Aziz M.A., Mahmoud T.S., Zaki Z.I., Gaafer, Heat treatment and wear characteristics of Al_2O_3 and TiC particulate reinforced AA6063 Al alloy hybrid composites, ASME Journal of Tribology, 2006, 128, pp. 891-894.

Banerji A., Prasad S.V., Surappa M.K., Rohatgi P.K., Abrasive wear of cast aluminium alloy- zircon particle composites, Wear 1982, 82, pp. 141-151.

Basavarajappa S., Chandramohan G. Dry sliding wear behaviour of hybrid metal matrix composites, Material Science 2005:11 (3) pp. 253-257.

Bharat Bhushan, Introduction to Tribology, 2nd Edition, John Wiley & Sons, Ltd., 2013

Canakci A., Arslan F., Abrasive wear behaviour of B_4C particle reinforced Al2024 MMCs, International Journal of Advanced Manufacturing Technology, 63 (5) 2012, pp 785-795.

Canakci A, Ozsahin S, Varol T, Prediction of Effect of Reinforcement Size and Volume Fraction on the Abrasive Wear Behavior of AA2014/B4Cp MMCs Using Artificial Neural Network, Arabian J Sci Eng (2014) 39, pp. 6351–6361.

Chawla N., Chawla K. K., Metal matrix composites, Springer, 2006.

Clyne T.W., Comprehensive Composite Materials, Vol. 3, MMC, 2000.

Das S., Mondal D. P., Sawla S., Ramakrishnan N., Synergic effect of reinforcement and heat treatment on the two body abrasive wear of an Al–Si alloy under varying loads and abrasive sizes, Wear 2008, 264(1), pp. 47-59.

Deuis, R.L., Subramanian, C. and Yellup, J.M., Abrasive wear of aluminium composites - a review. Wear, 1996, 201(1), pp.132-144.

Garcia-Cordovilla C., Narciso J., Louis E., Abrasive wear resistance of aluminium alloy/ ceramic composites Wear, 1996, 192 pp. 170-177.

Hamblin M.G., Stachowiak G.W., Description of abrasive particle shape and its relation to two-body abrasive wear, Tribology Transactions, 1996, 39 (4), 803-810.

Hashim J., Looney L., Hashmi M.S.J., Metal matrix composites: production by the stir casting method, Journal of Materials Processing Technology, 1999, 92–93, pp. 1–7.

Hosking F.M., Portillo F.F., Wunderlin R., Merhabian R., Composites of aluminium alloys: Fabrication and wear behaviour, Journal of Materials Science, 1982, 17, pp. 477-498.

Huei-Long, L., Wun-Hwa, L. and Chan, S.L.I., Abrasive wear of powder metallurgy Al alloy 6061-SiC particle composites. Wear, 1992, 159(2), pp.223-231.

Johnson R.W., A study of the pickup of abrasive particles during abrasion of annealed aluminium on silicon carbide abrasive, Wear 1970, 16, pp. 351–358.

Kaczmar J.W., Pietrzak K., Włosinski W., The production and application of metal matrix composite materials, Journal of materials processing technology 2000, 106, pp. 58–67.

Kok M., Computational investigation of testing parameters effects on the abrasive wear behavior of Al_2O_3 particle reinfoeced MMCs using statistical analysis, Intternational Journal of Advanced Manufacturing Technology, 2011, 52, pp. 207-213.

Larsen-Basse J., Some effects of specimen size on abrasive wear, Wear, 1972, 19, pp. 27–35.

Lin S.J, Liu S.K., Effect of aging on abrasion rate in an Al-Zn-Mg-SiC composite, Wear 1988, 121, pp. 1–14.

Lloyd D.J., Particle reinforced aluminium and magnesium matrix composites, International Material Review 1994, 39 (1), pp. 1–23.

Miracle D.B., Metal matrix composites – From science to technological significance, Composites Science and Technology 2005, 65, pp. 2526–2540.

Mondal D.P., Das S., Jha A.K., Yegneswaran A.H., Abrasive wear of Al alloy-Al_2O_3 particle composite: a study on the combined effect of load and size of abrasive, Wear, 1998, 223(1-2), pp. 131-138.

Mondal D.P., Das S., High stress abrasive wear behaviour of aluminium hard particle composites: Effect of experimental parameters, particle size and volume fraction, Tribology International 2006, 39 pp.470–478

Mandal N., Roy H., Murmu N.C., Mukhopadhyay S.K., Mathematical modelling of wear characteristics of 6061 Al-alloy-SiCp composite using response surface methodology, Journal of materials engineering and performance, 2012, 21(1), pp. 17-24.

Murray M. J., Mutton P. J., Watson J.D., Abrasive wear mechanisms in steels, Journal of Lubrication Technology-ASME, 1982, 104, pp. 9-16.

Norton R. L., Machine Design- An integrated approach, Pearson Education, 2nd Edition, 2009.

Pramila Bai B.N., Ramasesh B.S., Surappa M.K., Dry sliding wear of A356-Al-SiCp composites, Wear 1992, 157, pp. 295–304.

Prasad S.V., Asthana, R. Aluminium metal-matrix composites for automotive applications: Tribology considerations, Tribology Letters 2004:17 (3), pp. 445-453.

Prasad S.V., Rohatgi P.K., Tribological properties of Al alloy particle composites, Journal of Metals, 1987, 39(11), pp.22-26.

Rabinowicz E., Friction and Wear of Materials, John Wiley & Sons, Inc., New York, 1995.

Radhika N., Subramanian R., Venkat Prasat S. and Anandavel B., Dry sliding wear behaviour of aluminium/alumina/graphite hybrid metal matrix composites, Industrial Lubrication and Tribology, 2012, 64(6), pp.359-366.

Rahimipour M.R., Tofigh A.A., Mazahery A., Shabani M.O., Strategic developments to improve the optimization performance with efficient optimum solution and produce high wear resistance aluminium–copper alloy matrix composites, Neural Computing & Applications 2014, 24, pp. 1531–1538.

Rao R.N., Das S., Effect of sliding distance on the wear and friction behaviour of as cast and heat treated Al-SiCp composites, Materials & Design 2011, 32, pp. 3051-3058.

Rao R.N., Das S., Mondal D.P., Dixit G., Effect of heat treatment on the sliding wear behaviour of aluminium alloy (Al-Zn-Mg) hard particle composite, Tribology International 2010, 43, pp. 330-339.

Rao R.N., Das S., Wear coefficient and reliability of sliding wear test procedure for high strength aluminium alloy and composite, Materials & Design 2010, 31(7), pp. 3227-3233.

Rawal R.S., Metal matrix composites for space applications, Journal of Materials science 2001, 14.

Riahi, A. R., Alpas, A. T., The role of tribo-layers on the sliding wear behavior of graphitic aluminum matrix composites. Wear 2001, 251, pp. 1396-1407.

Rohatgi P.K., Pai B.C., Panda S.C, Preparation of cast alumina-silica particulate composites, Journal of materials science, 1979, 14 (10), pp. 2277-2283.

Sahin Y, Wear behaviour of aluminium alloy and its composites reinforced by SiC particles using statistical analysis, Materials & Design 2003, 24, pp. 95–103.

Sahin Y, Özdin K., A model for the abrasive wear behaviour of aluminium based composites, Materials & Design 2008, 29, pp. 728–733.

Sanninno A.P., Rack H.J., Dry sliding wear of discontinuously reinforced aluminium composites, Wear, 1995, 189, pp. 1-19.

Sato A., Mehrabian R., Aluminum matrix composites: Fabrication and properties, Metallic Transactions, 7B, 1976, pp. 443-450.

Sawla S., Das S., Combined effect of reinforcement and heat treatment on the two body abrasive wear of aluminium alloy and aluminium particle composites, Wear 2004, 257(5), pp. 555-561.

Seah K.W.H., Sharma S.C., Girish B.M., Mechanical Properties of cast ZA-27/graphite particulate composites, Materials & Design 1995, 16, pp. 271-275.

Simon C. Tung, Yong Huang, Modelling of abrasive wear in a piston ring and engine cylinder bore system, Tribology Transactions, 2004, 47, pp. 17-22.

Singh M., Prasad B.K., Mondal D.P., Jha A.K., Worn surface, dry sliding wear behaviour of an aluminium alloy- granite particle composite, Tribology International, 2001, 34, pp. 557-567.

Song W.Q., Krauklis P., Mouritz A.P., Bandyopadhyay S., The effect of thermal ageing on the abrasive wear behavior of age-hardening 2014 Al/SiC and 6061 Al/SiC, Wear 1995, 185, pp. 125-130.

Stachowiak G. W., Batchelor A.W., Engineering Tribology, Butterworth-Heinemann publications, 4th Edition, 2013.

Surappa M.K., Microstructure evolution during solidification of DRMMCs (Discontinuously Reinforced Metal Matrix Composites): state of art., Journal of Materials Processing Technology 1997, 63, pp. 325-333.

Suresh S., Moorthi N.S.V., Vettivel S.C., Selvakumar N., Mechanical behavior and wear prediction of stir cast Al-TiB_2 composites using response surface methodology, Materials & Design 2014, 59, pp.383-396.

Suresha S., Sridhara B.K., Wear characteristics of hybrid aluminium matrix composites reinforced with graphite and silicon carbide particulates, Composites Science and Technology 2010:70 (11) pp 1652–1659.

Ted Guo M.L., Tsao C.Y.A., Tribological behaviour of self-lubricating aluminium-SiC-graphite hybrid composites synthesized by the semi-solid powder densification method, Composites Science and Technology, 2000, 60 (1) pp. 65–74.

Torralba J. M., Da Costa C. E., Velasco F., P/M aluminum matrix composites: an overview. Journal of Materials Processing Technology, 2003, 133(1), pp. 203-206.

Totten G.E., Mackenzie D.S., Handbook of Aluminium, Marcel Dekker Inc., ISBN: 978-0-8247-0896-2, 2003.

Turenne S., Caron S., Weiss O., Masounave J., Fabrication of Particulate Reinforced Metal Composites, ASM International 1990, pp. 271–276.

Wang A., Rack H.J., Abrasive wear of silicon carbide particulate- and whisker- reinforced 7091 aluminium matrix composites Wear, 1991, 146, pp. 337-348.

Wang A.G., Hutchings I.M., Wear of alumina fiber aluminium metal matrix composites by two-body abrasion, Materials Science & Technology, 5 (1989), pp. 71–76

Wilson S., Ball A., Tribology of Composite Materials, ASM (1990), pp. 103.

Yigezu B.S., Jha P.K., Mahapatra M.M., Effect of sliding distance, applied load and weight percentage of reinforcement on the abrasive wear properties of in situ synthesized Al-12%Si/TiC composites Tribology Transactions, 2013, 56, pp. 546-554.

Yılmaz O., Buytoz S., Abrasive wear of Al_2O_3-reinforced aluminium-based MMCs. Composites Science and Technology 61, 2001, pp. 2381-2392.

Zongyi M., Jing B., Yuxiong L., Hongwei S., Yinxuan G., Abrasive wear of discontinuous SiC reinforced aluminium alloy composites, Wear 1991, 148, pp. 287–293.

Zum Gahr K.-H., Wear by hard particles, Tribology International 31 (1998) pp. 587-596.

Zhang Z.F., Zhang L., Mai Y.W., Subsurface damage of ceramic particulate reinforced Al–Li alloy composite induced by scratching at an elevated temperature, Materials Science and Engineering A, 242 (1998) pp. 304–307.

Zhang Z.F., Zhang L., Mai Y.W., Modelling study wear of steel/Al_2O_3-Al particulate composite system, Wear 211 (1997) pp. 147-150.

Zhang Z.F., Zhang L., Mai Y.W., Evaluation of critical wear transition loads of MMCs by rule based fuzzy modelling, Tribology Letters 2 (1996) pp. 89-97

Zhang Z.F., Zhang L., Mai Y.W., The running-in wear of a steel/SiCp-Al composite system, Wear 194 (1996) pp. 38-43

Zhang Z.F., Zhang L., Mai Y.W., Wear of ceramic particle-reinforced metal-matrix composites Part I: Wear mechanisms, Journal of Materials Science 30 (1995) pp. 1961-1966

Zhang Z.F., Zhang L., Mai Y.W., Wear of ceramic particle-reinforced metal-matrix composites Part II: A model of adhesive wear, Journal of Materials Science 30 (1995) pp. 1967 1971

Zhang Z.F., Zhang L., Mai Y.W., Particle effects on friction and wear of aluminium matrix composites, Journal of Materials Science 30 (1995) pp. 5999-6004

Zhang L., Yan C., Single-Point Scratching of 6061 A1-MMCs, Applied Composite Materials 1 (1995) pp. 431-447

LIST OF PUBLICATIONS

The publications based on the present research work was classified into journals and conferences attended.

Publications in Web of Science Journals

1. N.Ch. Kaushik, R.N. Rao, The effect of wear parameters and heat treatment on two body abrasive wear of Al–SiC–Gr hybrid composites, ELSEVIER**,** Tribology International, ISSN: 0301-679X, Vol. 96, 184-190, 2016. (Impact Factor: 2.26)

2. N.Ch. Kaushik, R.N. Rao, Effect of grit size on two body abrasive wear of Al 6082 hybrid composites produced by stir casting method, ELSEVIER, Tribology International, ISSN: 0301-679X, Vol. 102, 52-60, 2016. (Impact Factor: 2.26)

3. N.Ch. Kaushik, R.N. Rao, Effect of applied load and grit size on wear coefficients of Al 6082–SiC–Gr hybrid composites under two body abrasion, ELSEVIER**,** Tribology International ISSN: 0301-679X, Vol. 103, pp. 298-308, 2016. (Impact Factor: 2.26)

4. N.Ch. Kaushik, R.N. Rao, Two body abrasive wear of Al-Mg-Si hybrid composites: Effect of Load & Sliding distance, Materials science (Medžiagotyra), ISSN: 1392–1320, Accepted, Vol 22(4) pp. 491-494, 2016. (Impact Factor: 0.43)

5. N.Ch. Kaushik, R.N. Rao, Influence of applied load on abrasive wear depth of hybrid Gr/SiC/Al-Mg-Si composites in two body condition, Journal of Tribology-Transactions of ASME, ISSN: 0742-4787 (Accepted for publication, In press, 2017). (Impact Factor: 1.24)

6. N.Ch. Kaushik, R.N. Rao, Effect of applied pressure on high stress abrasive wear behavior of hybrid Al-Mg-Si composites, IMechE Part J: Journal of Engineering Tribology, SAGE Publications, ISSN: 1350-6501, (Accepted for publication, In press, 2017). (Impact Factor: 0.91)

7. N.Ch. Kaushik, R.N. Rao, High stress abrasive wear behaviour of Al-Mg-Si hybrid composites using regression analysis, Industrial Lubrication and Tribology, EMERALD Publications, (Accepted for publication, In press, 2017). (Impact Factor: 0.4)

8. N.Ch. Kaushik, R.N. Rao, Abrasive grit size effect on wear depth of stir cast hybrid Al-Mg-Si composites at high stress condition, IMechE Part J: Journal of Engineering Tribology, SAGE Publications, ISSN: 1350-6501 (Under Review)

9. N.Ch. Kaushik, R.N. Rao, Material removal mechanism of hybrid Grp/SiCp/Al-Mg-Si composites during high stress abrasive wear condition, (Under communication).

10. N.Ch. Kaushik, R.N. Rao, The influence of graphite and SiC particulate reinforcements on abrasive wear of hybrid Al-Mg-Si composites tested in high stress condition, Journal of Composite Materials, SAGE Publications, ISSN: 0021-9983 (Under Review).

Papers presented in National and International conferences

1. N.Ch. Kaushik, R.N. Rao, Liquid state processed Aluminium Metal Matrix Composites: Strength, Weakness, Opportunities and Threats NCRAME-2014, JNTUK-Vizianagaram, India, March 22-23, 2014.

2. N.Ch. Kaushik, R.N. Rao, Two body abrasive wear of Al-Mg-Si hybrid composites ICAD&M-2014, NIT- Tiruchirappalli, Tamil Nadu, India, December 5-7, 2014.

3. N.Ch. Kaushik, R.N. Rao, A Charan Reddy, Prasad Mahajan, Effect of applied pressure on two body abrasive wear of as cast Al-Mg-Si hybrid composites, Tribology: Energy, Environment and Efficiency, CSIR-AMPRI, Bhopal, India, January 21-23, 2016.

4. N.Ch. Kaushik, R.N. Rao, Effect of load & grit size on high stress abrasive wear of Al-Mg-Si hybrid composites, TMS 2016, Nashville, USA, Febraury14-18, 2016.

5. N.Ch. Kaushik, R.N. Rao, Development of two body abrasive wear models of Al 6082 hybrid composites using statistical analysis, National Tribology Conference, IIT (BHU), Varanasi, India, December 8-10, 2016.

6. N.Ch. Kaushik, R.N. Rao, Influence of sliding distance on wear depth of hybrid Al 6082-SiC-Gr composites under high stress abrasion, ITS-IFToMM 2017 & K-TIS 2017, Jeju, South Korea, March 19-22, 2017. (Accepted)

BIO-DATA

Personal Information:

Name : N.Ch. Kaushik
Father's name : N.Ch. Krishnama Charyulu
Gender : Male
Date of Birth/Age : 14-02-1989/ 28yrs

Educational Qualifications:

Sl. No	*Degree / Course*	*Discipline / Area/ Specialization*	*Name of Institute / University*	*Year*	*Division, % or CGPA*
1.	Ph.D	Mechanical Engineering	National Institute of Technology-Warangal, Telangana, India.	July'12 to till date (Thesis submitted)	
2.	M.Tech	Materials Technology (Mechanical Engg)	National Institute of Technology-Warangal, Telangana, India.	2010-12	1st (7.99/10)
3.	B.Tech	Mechanical Engineering	V.R. Siddhartha Engg College, Vijayawada, Andhra Pradesh, India.	2006-10	1st (73.6%)
4.	Intermediate	Mathematics, Physics & Chemistry.	Gautam Junior college, Vijayawada, Andhra Pradesh, India.	2004-06	1st- (89.4%)
5.	S.S.C	Mathematics, Science & Social studies.	Siva Sivani Public School, Visakhapatnam, Andhra Pradesh, India.	2004	1st- (84.1%)

Present position: PhD Research Scholar, Department of Mechanical Engineering, National Institute of Technology-Warangal, India-506004.

Research Interests:

- Composites, Tribology, Surface coatings and Mechanical behavior of materials

Publications:

- Journals: 04 (Published) + 03 (Accepted for publication) + 03 (Under review)
- Conference: 08 (International Conferences**)** + 11 (National Conferences)

Memberships:

- Life time member of Tribology Society of India (Affliated to International Tribology Council, U.K.)- LM # 5193
- Life time member of Indian Institute of Scientific Heritage, Trivandrum, India

Other Certifications:

- National Cadet Corps "B" & "C", Appreciation Certificate issued by "Indian Red Cross Society".

Correspondence Address:
N.Ch. Kaushik (PhD Research Scholar),
C/o Dr. R. Narasimha Rao, Assc. Professor
Department of Mechanical Engineering,
National Institute of Technology, Warangal, Telangana, India-506 004.

Residential Address:
N.Ch. Kaushik
S/o N.Ch. Krishnama Charyulu,
Qr. No: NH3-C/110, Vindhyanagar, NTPC Vindhyachal, Sidhi District, Madhya Pradesh, India-486 885.